FROM ACETYLENES TO METAL ACETYLIDE COMPLEXES: CARBON-RICH STRUCTURES FOR MOLECULAR ELECTRONICS

MARIE-CHRISTINE OERTHEL

Durham University

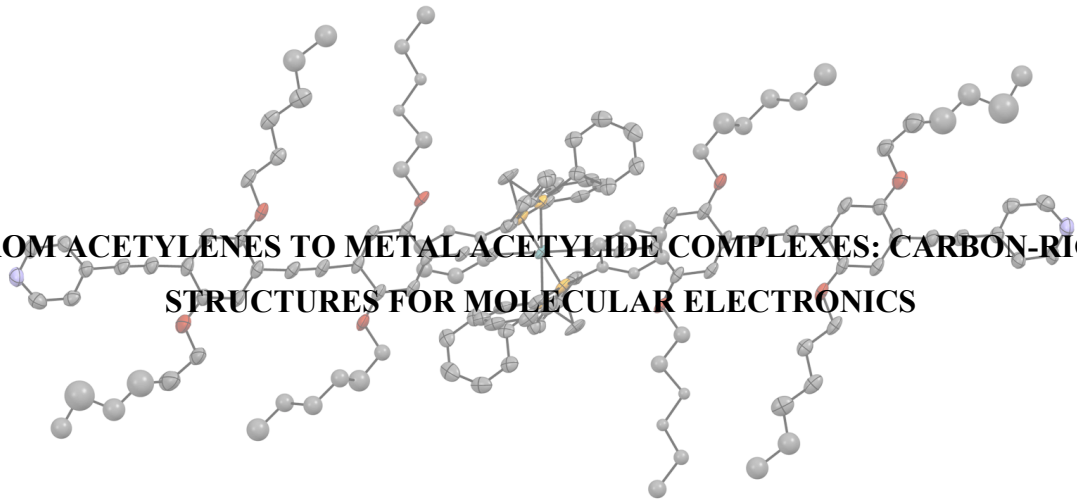

FROM ACETYLENES TO METAL ACETYLIDE COMPLEXES: CARBON-RICH STRUCTURES FOR MOLECULAR ELECTRONICS

OERTHEL Marie-Christine

S^{t} Cuthbert College

Department of Chemistry

Durham University

A Thesis Submitted for the Degree of Doctor of Philosophy at Durham University

December 2014

STATEMENT OF COPYRIGHT

DECLARATION

The work described in this thesis was carried out in the Department of Chemistry at Durham University between October 2011 and December 2014. All the work was carried out by the author unless otherwise stated and has not previously been submitted for a degree at this or any other university.

TABLE OF CONTENTS

I. Abstract VII

II. Acknowledgements IX

III. Publications XI

IV. List of Abbreviations XII

Chapter 1. Introduction to Molecular Electronics 1

1.1. A brief history of molecular electronics 1

1.2. From the design of molecular wires to their evaluation 5

1.2.1. Methods used for the molecule conductivity measurement 5

1.2.1.1. Principles 5

1.2.1.2. Scanning Probe Microscopy (SPM) 6

1.2.1.2.1. Scanning Tunneling Microscope – Break Junction (STM-BJ) 6

1.2.1.2.2. STM-based *I(s)* technique 7

1.2.1.2.3. Conductive Probe – Atomic Force Microscopy (CP-AFM) 8

1.2.2.3. Non-SPM techniques 9

1.2.2.3.1. Mechanically Controlled Break Junctions (MCBJ) 9

1.2.2.3.2. Crossed-wire 9

1.3. Molecular wires 10

1.4. Metal-Molecule contacts 12

1.4.1. Anchoring groups 12

1.4.2. Contact resistance 13

1.5. Metal-organic molecules in molecular junction 13

1.5.1. The effect of the metal on the conductance 14

1.5.2. Gating properties of the metal-organic molecules 21

1.6. References 29

Chapter 2. Oligoynes and arylynes **35**

2.1. Abstract 35

2.2. Introduction 35

2.3. All-carbon bridged bimetallic complexes as models for molecular wires 37

2.4. Synthesis of pyridyl end-capped oligoynes 39

2.5. Trimethylsilyl ethynyl: a new and interesting anchor group 41

2.6. Synthesis of the trimethylsilyl-oligoynes 45

2.7. Molecular structures 47

2.8. Synthesis of the arylynes 49

2.9. Spectroscopy 50

2.9.1. Electronic absorbance 50

2.10. Scanning Tunneling Microscope (STM) measurements 52

2.10.1. Pyridyl-oligoynes 52

2.10.2. Trimethylsilyl-oligoynes 53

2.10.3. Arylynes 55

2.11. Conclusion 56

2.12. Experimental 57

2.12.1. STM setup (Liverpool University) 57

2.12.2. General conditions for the syntheses 57

2.12.3. Oligoynes 58

2.12.4. Arylynes 63

2.13. References 64

Chapter 3. Synthesis of buta-1,3-diynyl ruthenium complexes 72

3.1. Abstract 72

3.2. Introduction 73

3.3. Synthesis of the ruthenium buta-1,3-diynyl complexes 74

3.4. Molecular structures 80

3.5. Electrochemistry 86

3.6. Spectroelectrochemistry 91

3.7. Quantum chemical calculations 96

3.8. Conclusion 101

3.9. Experimental 102

3.9.1. General conditions 102

3.10. References 111

Chapter 4. Syntheses, structures and electronic properties of organometallic molecular wires **119**

4.1. Abstract 119

4.2. Introduction 120

4.3. Synthesis of the platinum complexes via $Cu^{(I)}$ catalysed trans-metallation 121

4.4. Synthesis of the metal-OPE compounds via "on complex" Sonogashira cross-coupling reactions 123

4.5. Exploration of the binding mode through the phenyl ancillary ligand 126

4.5.1. Synthetic consideration 126

4.6. Molecular structures 127

4.7. Optical spectroscopies and electrochemical measurements 132

4.7.1. Optical spectroscopy of **30** and **33** versus OAE5 132

4.7.2. Electrochemical measurements 133

4.7.2.1. Cyclic voltammetry 133

4.7.2.2. Spectroelectrochemistry 135

4.8. Single molecule *I(s)* conductance measurements 138

4.8.1. Single molecule measurements of the organometallic molecules with TMSE linkers 139

4.8.2. Single molecule measurements of the organometallic molecules with pyridyl linkers 143

4.8.3. Single molecule measurement of the compound **39** 145

4.9. Quantum chemical modelling 146

4.10. Conclusion 150

4.11. Experimental 152

4.11.1. General conditions 152

4.11.2. Computational methods 167

4.12. References 169

Chapter 5. Carbon rich bis-terpyridine molecules **174**

5.1. Abstract 174

5.2. Introduction 175

5.3. Synthetic consideration 177

5.3.1. 4'-phenyl-2,2':6',2"-terpyridine derivatives 178

5.3.2. 2,2':6',2"-terpyridine derivatives 180

5.4. Electrochemical measurements 187

5.5. Molecular structures 188

5.6. Conclusion 190

5.7. Experimental 191

5.7.1. General conditions 191

5.8. References 197

Appendix A and Appendix B 200

I. ABSTRACT

Electronics technology is moving so fast that an alternative for the "top-down" approach (lithography on silicon wafer) has to be found. Moore described in the now famous relationship the exponential growth of the number of transistors on a single chip that has become known as "Moore's Law", but this rate of progress has nearly reached its physical limits. As a chemist, the molecular scale is the smallest scale that can be manipulated in order to design more specific components. For this reason, the "bottom-up" approach is under rigorous investigation in chemistry and physics. Moreover, organometallic chemistry is increasingly employed for the synthesis of molecules for molecular electronics due to the versatile optoelectronic and structural properties offered by this class of compound (*see* section 1.5.).

In this thesis, syntheses starting from simple but important carbon-rich organic building blocks to afford complex organometallic molecules are developed. The focus is on carbon-rich molecules such as oligoynes and oligo(phenyleneethynylene) derivatives due their high conjugation giving them good conduction properties.

The preparation of oligoynes with trimethylsilylethynyl and pyridyl linkers and their preliminary single molecule conductivity data are presented in Chapter 2. In this work, a new, simple synthesis of the 1,10-bis(trimethylsilyl)penta-1,3,5,7,9-yne from cross-coupling reactions of 1,6-bis(triphenylphosphinegold)hexa-1,3,5-triyne with 1-iodo-2-trimethylsilylacetylene is developed, which was extended for the synthesis of oligoynes bearing pyridyl termini.

"On complex" synthesis on Ru(II) butadiynyl molecules containing different aryl groups from electrodonating groups (-C_6H_4OMe-4; *N,N*-bis(4-methoxyphenyl)4-phenylamine), electroneutral (C_6H_4Me-4), anchoring groups (2,3-dihydrobenzo[*b*]thiophene (DHBT); C_5H_4N) to electrowithdrawing groups (C_6H_4CN-4) is discussed in Chapter 3. Moreover, elaboration and (spectro)electrochemistry of bimetallic complexes with oligoynes and arylyne bridges are reported and supported by DFT calculations.

Oligo(phenyleneethynylene) metal complexes with various anchoring groups (pyridyl, thioanisole) and a different metal core (Pt and Ru) is explored in Chapter 4, in order to study the influence of the metal together with the linkers on the conductance. Single

molecule conductance measurements and (spectro)electrochemistry together with DFT calculations are described.

Finally, an investigation around the coordinating ligand, 2,2':6',2"-terpyridine (tpy), and opening new properties such as storage behaviour due to its specific geometry is discussed in Chapter 5. In this last chapter, the preparation of Ru(II) and Fe(II) tpy along with the electrochemical data are reported.

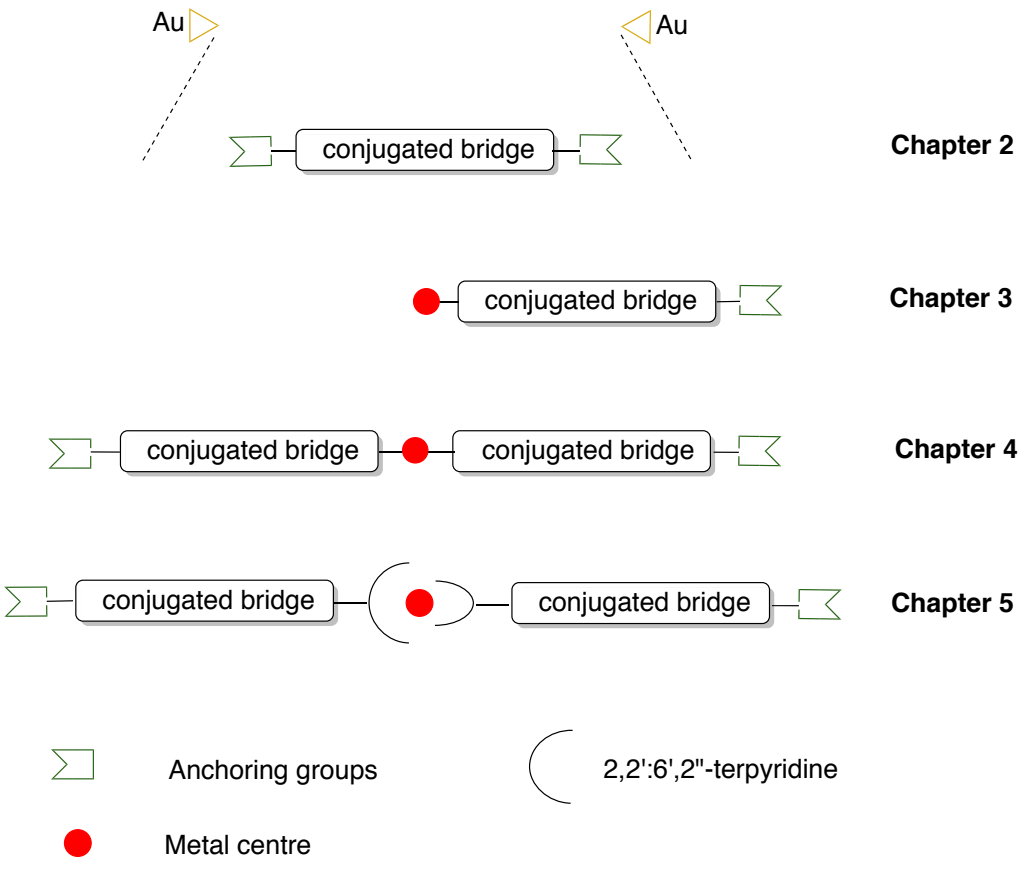

Scheme I-1. *Schematic representation of the synthesis stages in the thesis.*

II. ACKNOWLEDGEMENTS

First of all, I would like to thank my supervisors, Prof. Martin R. Bryce and Prof. Paul J. Low for giving me the opportunity to do my PhD, for their support and for their help throughout this period. Moreover, I am really grateful for the time spent in Australia in Prof. Paul Low's laboratory and for all the conferences that I have been involved around the world.

I would like obviously to thank as well all my colleagues especially Santi for his support, happiness and help but also Ross for his terpyridine advices, José for the good atmosphere in the lab, Sam, Soeren, Josef, Byron, Helen, Ian, Dan, Luke, Mat, Luke and Murat.

Thank you to Dr Dmitry Yufit for the crystal structures and the NMR team for their help. I would like to thank the collaborators without whom the thesis would not have been completed, Dr Mark Fox for the DFT calculations of the ruthenium butadiynyl; Colin Lambert's student, Oday Al-Owaedi for the DFT calculations of the metal-OPE in junction and Richard Nichols' postdoctoral researcher David Costa Milan for the STM measurements.

I also would like to thank a lot the people who surrounded me during the PhD period and especially my flatmate Bansri for her listening skill and great time spent together in Durham but also the chemists-friends, Mickaële, Martina, Alex, Valentina, Fanny….

To finish, I would like to thank my family and my boyfriend to be here every time that I needed them and encourage me to finish my PhD when the time was hard. Without you, I would not have been that far!

To my dear brother and godfather…

III. PUBLICATIONS

The following papers are based on work described in this thesis:

M.-C. Oerthel, D.S. Yufit, J.A.K. Howard, M.A. Fox, M.R. Bryce, P.J. Low. **Syntheses and Structures of Buta-1,3-Diynyl Complexes from "On Complex" Cross-Coupling Reactions**. *Accepted. DOI: 10.1021/om501186c*

M.-C. Oerthel, D. Costa-Milan, O. Al-Owaedi, D.S. Yufit, J.A.K. Howard, S.J. Higgins, R.J. Nichols, C.J. Lambert, M.R. Bryce, P.J. Low. **Syntheses, Structures and Electronic Properties of Organometallic Molecular Wires Derived from "On Complex" Cross-Coupling Reactions.** *Manuscript in preparation*

IV. LIST OF ABBREVIATIONS

AFM: Atomic Force Microscope

ASAP: Atmospheric Solids Analysis Probe

BMPA: N,N-bis(4-methoxyphenyl)-4-phenylamine

$CaSO_4$: Calcium sulfate

Cp: Cyclopentadiene

CP-AFM: Conductive Probe-AFM

DFT: Density Functional Theory

DHBT: 2,3-dihydrobenzo[b]thiophene

Dppe: 1,2-bis(diphenylphosphino)ethane

E: potential

E_F: Fermi level

EC-STS: Electrochemically-Scanning Tunneling Spectroscopy

EC-MCBJ: Electrochemically-Mechanically Controlled Break Junction

Et_2O: Diethylether

EtOAc: Ethyl acetate

FET: Field-Effect Transistor

G: conductance

HOMO-LUMO: Highest Occupied Molecular Orbital-Lowest Unoccupied Molecular Orbital

HR-MS: High Resolution-Mass Spectrometry

$HNEt_2$: Diethylamine

HN^iPr_2: Diisopropylamine

IBM: International Business Machines

I_0: Tunneling current

I_p: Peak current

IR: Infrared

I-V: Current-Voltage

MCBJ: Mechanically Controlled Break Junction

ME: Molecular Electronics

MeCN: Acetonitrile

MeOH: Methanol

MLCT: Metal to Ligand Charge Transfer

MS: Mass Spectrometry

$NaPF_6$: Sodium hexafluorophosphate

$NaBPh_4$: Sodium tetraphenylborate

NaOH: Sodium hydroxide

NDR: Negative Differential Resistance

NEt_3: Triethylamine

NIR: Near Infrared

NMR: Nuclear Magnetic Resonance

OAE: Oligo(aryleneethynylene)

OPE: Oligo(phenyleneethynylene)

OPI: Oligo(phenyleneimine)

OPV: Oligo(phenylenevinylene)

OTTLE: Optically Transparent Thin Layer Electrode

Py: 4-pyridyl

RT: Room temperature

SEC: Spectroelectrochemistry

SMe: Thiomethyl

SPM: Scanning Probe Microscope

STM: Scanning Tunneling Microscope

STM-BJ: Scanning Tunneling Microscope-Break Junction

STM-*I(s)*: Scanning Tunneling Microscope Current(distance)

tBu: Tert-butyl

TBAF: Tetrabutylammonium fluoride

TCB: Trichlorobenzene

TCNE: Tetracyanoethylene

TCNQ: Tetracyanoquinodimethane

TES: Triethylsilyl

THF: Tetrahydrofuran

$TlBF_4$: Thallium tetrafluoroborate

TMEDA: Tetramethylethylenediamine

TMS: Trimethylsilyl

TMSA: Trimethylsilylacetylene

TMSB: Trimethylsilylbutadiyne

TMSE: Trimethylsilylethynyl

Tpy: 2,2':6',2"-terpyridine

TIPS: Triisopropylsilyl

TIPSA: Triisopropylsilylacetylene

TTF: Tetrathiafulvalene

U_t: Tunneling voltage

UV-Vis: Ultraviolet-Visible

ν: scan rate

s: sharp

m: medium

b: broad

vs: very sharp

CHAPTER 1. INTRODUCTION TO MOLECULAR ELECTRONICS

1.1. A brief history of molecular electronics

In the early part of the 20th century, the key concepts of contemporary electronics began to emerge with the development of the transcontinental telephone in 1915 by AT&T Bell. At this time, the amplification of the signal essential to keep the sound level even, was effected by vacuum tubes or "audions". The simple example of the vacuum tube device is the diode, where the electrons created with the thermionic effect at a source, pass to another electrode through a filament inside a cylindrical glass filled with vacuum. With the introduction of a third electrode (grid) the diode vacuum tube serves as an amplifier, also called triode. The grid is situated between the two electrodes and helps tuning the flow of electrons coming from the source. Later, judging that the vacuum tube could be improved, workers at the AT&T Bell laboratories, particularly John Bardeen and Walter Brattain, invented the first solid state transistor made of germanium in 1947. Later, in 1958, Jack Kilby developed the first integrated circuit, ten years after the discovery of the bipolar junction transistor. Subsequently, the junction transistor gave way to field-effect transistors (FETs) in 1961 (Figure 1-1).

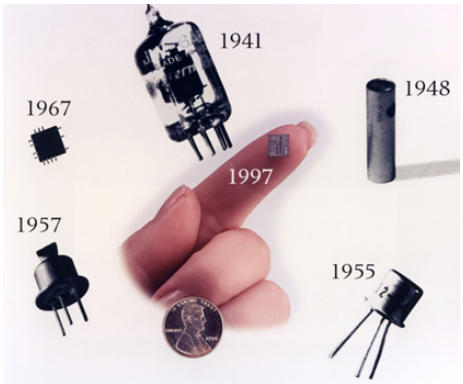

Figure 1-1. *Miniaturization of the transistor.*[1]

In 1965, Gordon Moore, one of the Intel co-founders who worked at that time for Fairchild Semiconductor, made the observations that are now embodied in the famous "Moore's Law" expression. Moore noted that the number of transistors on an integrated circuit had approximately doubled every 2 years. He suggested that with foreseeable advances in technology, this trend may continue 'until about 1975'. His observation

proved to be more than prophetic, and this rate of progress has been adopted by the semiconductor industry as an economic and technological driver (Figure 1-2). Nowadays, commercial devices contain transistors with 22 nm half-pitch (Haswell chip) and the next generation Broadwell processor (Core M) featuring 14 nm transistors, 30% thinner and 50% smaller than the Haswell chip is near to manufacture. However, these latest generation chip sets were delayed by problems in achieving the necessary device yield, and are only projected to reach the market late in 2014 or early 2015. The on-going problems with this next generation of chipset highlight concerns with maintaining the rate of device miniaturisation. The recognition of these issues by the semiconductor industry has resulted in the re-writing of Moore's Law to state that from 2013 component density will double every 3 years. Even with this slow down, the size of critical components will, inexorably, reach the engineering limits of the solid state, which leaves a place for single molecule engineering to fill a critical gap in future electronics technologies.

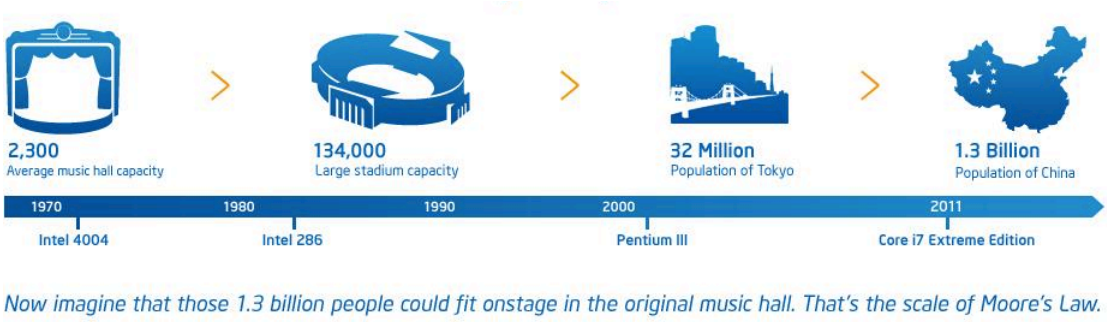

Figure 1-2. *Moore's Law representation: if transistors in a microprocessor were people from reference.*[2]

Molecular Electronics (ME) can be broadly described as the use of single molecules or layers of molecules to perform the functions of electronic components such as wires, transistors, capacitors and resistors. Research in ME is motivated not only by academic curiosity and the fundamental challenges presented in the fields of chemistry, physics and engineering, but also by the growing challenges confronting the development of semiconductor-based electronics. The first notions of ME were made as early as 1956 when Arthur von Hippel, a German physicist, suggested the "bottom up" approach as a new technique to design new materials.

Instead of taking prefabricated materials and trying to devise engineering applications consistent with their macroscopic properties, one builds materials from their atoms and molecules for the purpose at hand… (Von Hippel, 1956)[3]

The name "molecular electronics" was then used for the first time during the conference organized by the US Air Force for the scientists, engineers from military and private laboratories. At that time, Colonel C.H. Lewis, director of Electronics at the Air Research and Development Command raised the need of a breakthrough in electronics:

… Once we can correlate electronics property phenomena with the chemical, physical, structural, and molecular properties of matter, we should be able to tailor material with predetermined characteristics. We call this more exact process of constructing materials with predetermined electrical characteristics MOLECULAR ELECTRONICS. (Lewis, 1958)[3]

After this conference, a program between the Westinghouse company and the US Air Force was born with a goal of finding an alternative to the integrated circuit. The notion of "molecular electronics" reappeared at the end of 1960 when the Langmuir-Blodgett films were revisited for the study of nascent ME devices by Hans Kuhn in the University of Göttingen.[4] This technique was revolutionary at this time because it allowed the preparation of well-ordered mono-layers of molecules on an electrode surface. Whilst in principle greatly simplifying measurements of conductivity through monolayers of molecules, requiring only the attachment of a second 'top' electrode to complete the metal | molecule | metal junction, the fabrication of the 'top' electrode on a molecular film has proven to be far from straight-forward.

In the late 1970, Ari Aviram and Mark Ratner from IBM described in a theoretical paper "Molecular Rectifiers"[5] the properties of a single organic molecule that would provide elementary function for ME. It was proposed that the donor-acceptor molecule (Chart 1-1) would act as a molecular rectifier and so could be used as a diode in a circuit. The acceptor moiety, tetracyanoquinodimethane (TCNQ) is connected to the donor moiety, tetrathiafulvalene (TTF) by a saturated (non-conjugated) bridge. Following from Aviram and Ratner's seminal disclosure of a rectifier design, a variety of molecular wires, resistors and switches have been explored by different groups, and the concept of molecules as components for electronics has been the subject of several reviews.[6-9]

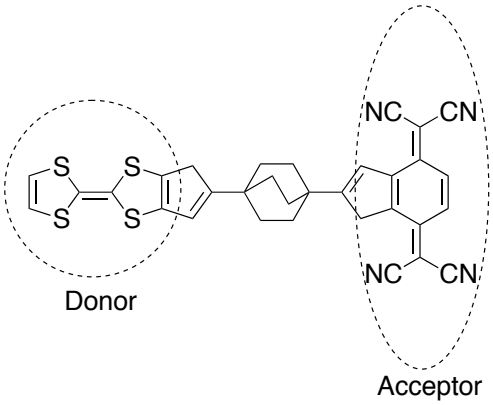

Chart 1-1. *A molecular rectifier proposed by Aviram and Ratner.*

In 1981 the invention of the Scanning Tunnelling Microscope (STM) by two physicists from IBM, Gerd Binnig and Heinrich Rohrer, gave a great boost in this area, given that molecules could be now imaged and manipulated. After Binning and Rohrer received the Physics Nobel Prize in 1986 for this work, Binnig, together with C. Quate and C. Gerber developed the Atomic Force Microscope (AFM).[10,11] The AFM is able to scan and contour of the surface in order to draw an atomic profile. Whilst STM based methods feature prominently in contemporary molecular electronics research, alternative methods such as the Mechanically Controlled Break Junction (MCBJ) or crossed-wire technique patented in 2003 by Bratovski et al.[12] are also important to the development of the area. Some of these are described in more detail below.

The challenges involved in the design, synthesis and testing of molecules for ME applications has ensured continued activity from different disciplines including biology, chemistry, physics, material science and electrical engineering. Achievements in the assembly of molecules in order to incorporate them in functional electronic devices were designated as the breakthrough of the year 2001 in the journal *Science.*[13] In an echo of the first expression of the concepts by Von Hippel, this technique is so called the "bottom-up" approach, in contrast to the current "top down" approach which permits the etching of small features on silicon wafers (lithography technique).

1.2. From the design of molecular wires to their evaluation

An advantage of working at the molecular scale is the tight control of the chemical and physical properties of molecules within a small, identifiable structure in order to make more efficient electronic devices. Whilst many intrinsic molecular properties can be established from solution based measurements, the manipulation of a single molecule within a molecular junction offers unique insights into trans-molecule electron transfer mechanisms relevant to the exploitation of molecules in a device.

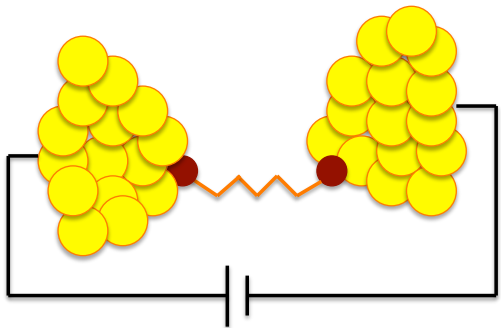

Scheme 1-1. *Schematic representation of a molecular wire sandwiched between two gold electrodes (molecule in orange and anchor groups in red).*

1.2.1. Methods used for the molecule conductivity measurement

1.2.1.1. Principles

The electronic property of a molecule (or few molecules) can be measured and analysed by incorporating the molecule(s) into a junction with two (typically metal) electrodes. A bias is applied across the two electrodes and the resulting conductance across the metal|molecule|metal junction is measured. Various adaptations of the general technique include the STM-Break Junction (STM-BJ) and the STM-*I(s)* methods, conducting Probe AFM (CP-AFM) as well as non-scanning probe methods such as crossed wire junctions and the MCBJ.

1.2.1.2. Scanning Probe Microscopy (SPM)

Scanning probe microscopy is a general term that is used to describe all of the microscopy methods that involve the use of a physical probe to scan and analyse a sample, often achieving molecular or atomic resolution. Whilst Atomic Force Microscopy (AFM) can be used to provide topological information from a surface, the incorporation of a conducting probe tip allows electrical information to also be collected, typically from thin films. However, for electrical characterisation of single molecules, Scanning Tunneling Microscopy (STM) based methods are more commonly used.

1.2.1.2.1. Scanning Tunneling Microscope – Break Junction (STM-BJ)

The in situ break junction was introduced by Xu and Tao in 2003.[14] The molecular junction is made by pushing the gold tip into the gold substrate to create a metal-metal contact (Figure 1-3 left, I). At that stage, the conductance recorded is due to the metallic contact. The tip is pulled away from the substrate to withdraw a metallic filament, the conductance of which can be shown to be a multiple of the quantum of conductance (G_0) (Figure 1-3 right, II) and decreases until the quantum conductance G_0 for a single Au-Au contact is reached. The filament eventually breaks to leave two extremely sharp electrode tips, and the metallic conductance falls to zero (Figure 1-3 right, IV). If the experiment is conducted in the presence of molecules in solution, on occasions one or more molecules will be trapped between the tip and the substrate (Figure 1-3 right, III). The conductance of the resulting molecular junction is $< 1\ G_0$, but > 0, which establishes that the metal-metal contact is replaced by metal-molecule-metal junction (Figure 1-3 left, III). The conductance then falls to 0 when the tip is pulled further than the length of the molecule (Figure 1-3 left, IV) and the molecular junction is broken.

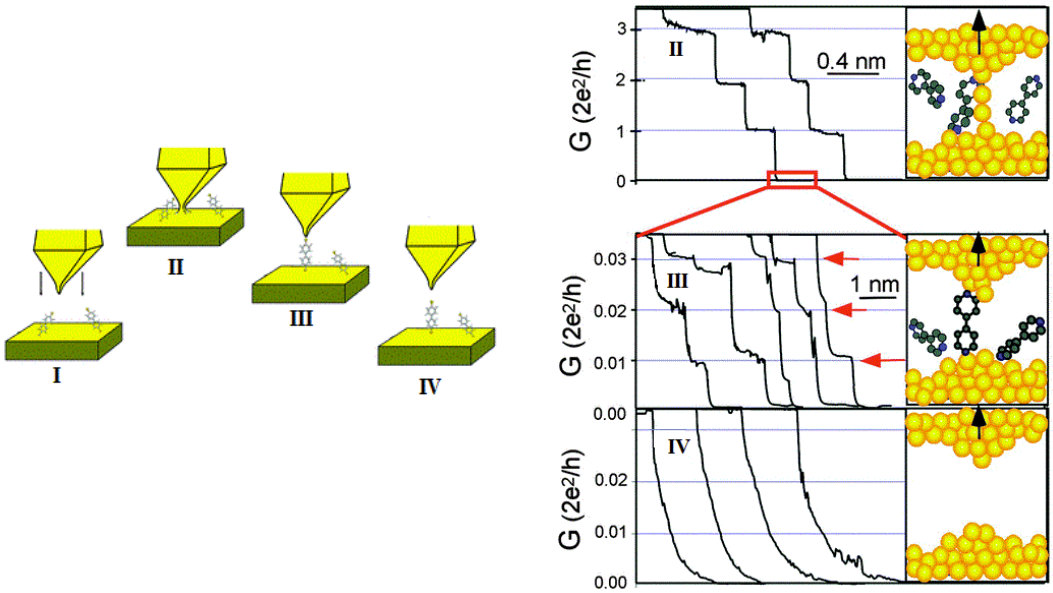

Figure 1-3. *Different steps required for the STM-break junction (left) from reference*[15] *and typical histograms observed (right) from reference.*[14]

1.2.1.2.2. STM-based *I(s)* technique

The *I(s)* technique (I = current, s = distance)[16] is comparable to the STM-BJ because the molecular junction is made between a tip and a substrate (Figure 1-4). The only difference is that in the *I(s)* technique there is no contact between the substrate and the tip. The tip is brought close to the substrate and withdrawn before metallic contact is reached, and the tunnelling current is measured during the tip retraction. The substrate is covered with a low surface density of target molecules (Figure 1-4, I). On occasion, a molecule is trapped between the electrodes to give the same sort of molecular junction as described above for the STM-BJ (Figure 1-4, II and III). On further retraction, the separation of the tip and the substrate exceeds the molecular length and the current falls back rapidly to 0 (Figure 1-4, IV). This means that whilst the STM-BJ experiment always refreshes the electrode surfaces between each measurement, the *I(s)* measurement uses the same tip for each individual measurement. Also, the STM-BJ relies on detecting a small molecular current signature against a large metallic conductance background, whereas the molecular signatures in the *I(s)* measurement are collected against a lower tunnelling current background.

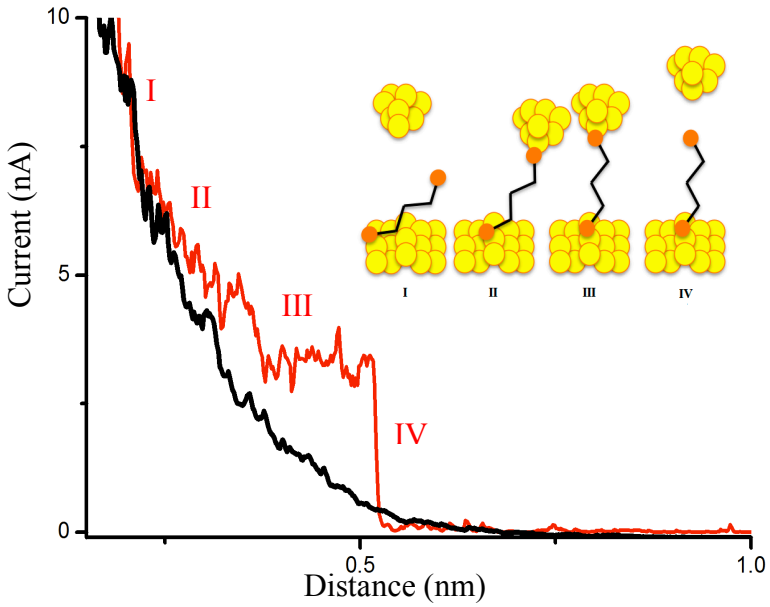

Figure 1-4. *Different steps in the STM-I(s) method with the I(s) curves (with presence of molecule in red; in absence of the molecule in black).*

1.2.1.2.3. Conductive Probe-Atomic Force Microscopy (CP-AFM)

As a complement to the STM technique, CP-AFM[17] records the topography of the sample from the distance dependence of the force between the tip and the surface. The force is measured by the deflection of the cantilever beam, which itself is connected to the tip (Figure 1-5). In addition, current-voltage measurements can be obtained at fixed points on the surface when applying a voltage between the AFM tip and the fixed counter electrode.

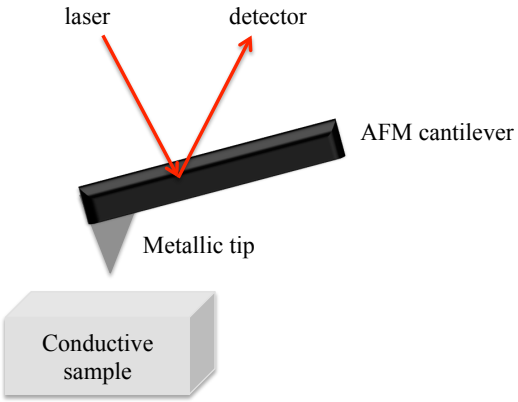

Figure 1-5. *Schematic representation of the CP-AFM technique.*

1.2.2.3. Non-SPM techniques

1.2.2.3.1. Mechanically Controlled Break Junctions (MCBJ)

MCBJ[18] is a non-SPM based method for measuring molecular conductance. The system consists of a notched gold wire, counter supports, bending beam, piezo element and a glass tube containing the solution (Figure 1-6). By bending the substrate with help of the piezo element, the gold wire breaks in much the same way as the STM-BJ. The break takes place in the solution containing the molecule of interest and the electrode tips are typically each coated with a sub-monolayer coverage of analyte molecules. The piezo controlled gap is then closed and the current followed until metallic contact is reached. Current jumps prior to metallic contact are taken as evidence for molecular conductance.

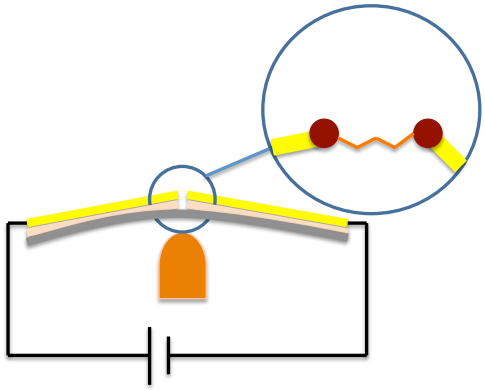

Figure 1-6. *Schematic representation of the MCBJ technique (electrodes in yellow, polymer in beige, flexible support in grey and pushing rod in orange).*

1.2.2.3.2. Crossed-wire

Another interesting method is the crossed-wire technique[19,20] (Figure 1-7) comprising two electrode wires in a crossed geometry, oriented at a right angle. The measurement is operated on a Self Assembled Monolayer (SAM) coated on the bottom electrode. Typically the area of the junction formed at the intersection of the crossed wires covers around 10^3 molecules (10 µm wire diameter). One of the wires is perpendicular to the applied magnetic field (B) and the junction is formed by carefully controlling the gap between the wires through manipulation of the Lorentz force by the slow increase of the deflection current flowing through one wire.

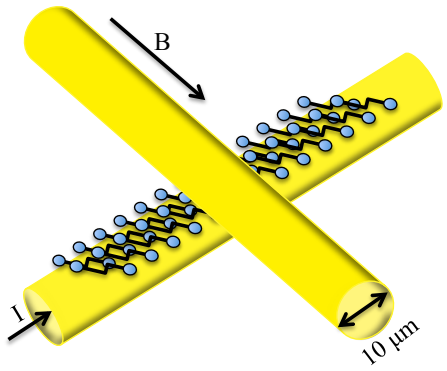

Figure 1-7. *Schematic representation of the crossed-wire method. I is the deflection current and B is the magnetic field.*

1.3. Molecular wires

A molecular wire is usually considered to be a molecule capable of promoting the efficient transport of electrons (or holes) over significant distances. Typically, molecular wires are π-conjugated organic molecules such as oligo(phenyleneethylene) (OPE), oligo(phenylenevinylene) (OPV),[21] oligophenyleneimine (OPI),[22] oligothiophene,[23] oligoynes[24,25] and oligoaryleneethylene (OAE)[26]. All these conjugated molecules have a small HOMO-LUMO gap and display significant molecular conduction. By way of example, consider the family of molecules show in Table 1-1. According to the conductivity measurements carried out with self-assembled mono-layers in a crossed-wire junction, a thiol-anchored OPV conducts three times more than a similarly contacted OPE, which itself, conducts fifteen times more than dodecanedithiol (C12) at 0.5 V (Table 1-1).[19,20] However, a noticeable point here is that the OPV molecule does not directly compare with the thiol-OPE and dodecanedithiol because the thiol linker is attached to CH_2. The methylene group is known to be insulator and even with this spacer, the conductance is increasing, which proves that the OPV is a great conductor. The difference in the conductance is consistent with the size of the HOMO-LUMO gap, 3.12 eV for the OPV, 3.51 eV for the OPE and 7.11 eV for C12, although the precise mechanism underlying conductance is more closely related to the alignment of some critical molecular orbital with the Fermi level of the metal electrodes.

Table 1-1. *Compounds with molecular structure studied by Kushmerick et al.*[19] *and the measured relative junction conductance at 0.5 V.*

Compound	Molecular structure	G
C12	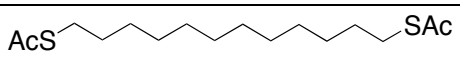	1
OPE		15
OPV	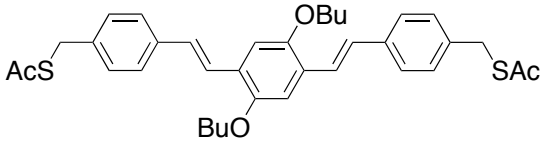	46

In a simple tunnelling regime, conductance is expected to decay exponentially with distance, L, according to the relationship $G \propto Ae^{-\beta L}$, where the conductance G decreases exponentially with the length L of the molecule with a certain decay constant β. The value of β provides a convenient parameter through which to compare the wire-like behaviour of a series of different molecular backbones.

A wide range of β-values have been reported, with those of porphyrins (β = 0.04 - 0.01 $Å^{-1}$)[27,28], OPV (0.17 A^{-1})[21] and oligoynes (β = 0.31 $Å^{-1}$)[25] being especially low. However OPE (β = 0.20 $Å^{-1}$)[29] and long OAE (β = 0.016 $Å^{-1}$)[26] molecules are among the most widely explored for molecular wire purposes because they are easier to synthesize and stable towards chemical substitution on the phenyl rings which in turn can tune the electron transport properties. For example, Xiao et al.[30] showed that the introduction of the electron withdrawing NO_2 group significantly decreases the conductance of the OPE backbone from 13 nS for **OPE3SAc** to 6 nS for **OPE3(NO_2)SAc** (Chart 1-2).

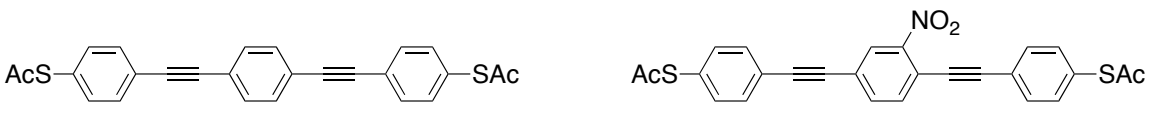

OPE3SAc **OPE3(NO_2)SAc**

Chart 1-2. *Unsubstituted OPE (**OPE3SAc**) and nitro-substituted OPE (**OPE3(NO_2)SAc**) studied by Xiao et al.*[30]

More interestingly, conductance switching has been recorded for dithiolated tetrathiafulvalene derivatives (TTFdT) by exposing the molecule to oxidizing or reducing agents.[31] The oxidized species showed a conductance higher by one order of magnitude

compared to the reduced one. The switching behaviour is due to the alternation between non-conjugated TTFdT (reduced) with a HOMO-LUMO gap of 3.7 eV and conjugated $TTF^{2+}dT$ (oxidized) with a HOMO-LUMO gap of 1.8 eV (Figure 1-8).

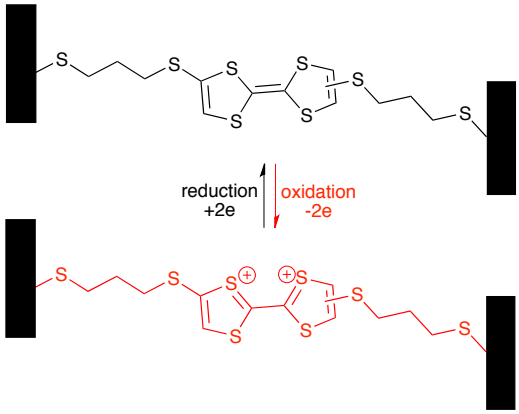

Figure 1-8. *Structure of the reduced and oxidized TTFdT studied by Liao et al.*[31]

1.4. Metal-Molecule contacts

The interaction between the electrodes (metal) and the anchor group of the molecules has considerable influence the conductance behaviour.

1.4.1. Anchoring groups

It is essential to synthesize molecules with anchoring groups in order to contact the molecule to the macroscopic electrodes. The two modes of attachment are: (i) physisorption where no covalent bonds are maintaining the molecule to the electrodes and (ii) chemisorption where the metal-molecule connection is a covalent bond.

The binding strength and the molecular orbitals through which the charges are transported are guided by the nature of the anchoring groups. Thiol (-SH) is the most used in molecular junctions[32,33] because of its strong S-Au covalent bond which gives rise to a good electronic coupling. Nevertheless, the S-Au bond can modify the surface and create different types of Au-molecule contacts. Thus, a variety of linkers have been studied such as: pyridine,[14,34,35] amine ($-NH_2$),[36] carboxylic acid (-COOH),[33] trimethylsilylethynyl ($-C{\equiv}CSiMe_3$),[37] direct Au-C contact after cleavage of $-SiMe_3$[38] or after cleavage of -

$SnMe_3$,[39] dihydrobenzothiophene,[25] diphenylphosphine (-PPh_2),[40] cyanide (-CN),[41] isocyanide (-NC),[42] methylthiol (-SMe),[43] isothiocyanate (-NCS)[44] and fullerene.[45,46]

1.4.2. Contact resistance

As mentioned in the section 1.4.1., the connections between molecule and electrodes are important to explain the junction behaviour but also the contact resistance need to be considered. The contact resistance is the result of the interfacial dipoles "Schottky barrier" created at the molecule-electrode interface where the difference of the two materials energies (molecular Gibbs energy and Fermi level E_F) is found.

1.5. Metal-organic molecules in molecular junction

Over the last 10 years there has been a growing interest around the study of organometallic molecules within molecular junctions in the search for more efficient molecular wires.[47,48] Indeed, a metal implanted into an organic core can:

- lead to different molecular conformations which may help precisely position molecular termini, introduce insulting sheaths and provide sites for molecular interconnects
- be tuned by a third gate electrode accessing different metal redox states
- permit a more modular synthetic strategy allowing the change from tunnelling to hopping as a function of molecular length to be more easily probed
- provide better electron delocalization through effective d-π fragment orbital overlaps

It was demonstrated that, depending on the molecular level (i.e. HOMO or LUMO) accessed at the Fermi level of the electrodes, redox-active metal complexes can display conduction, switching functions, negative differential resistance (NDR)[49] or Kondo effects within molecular junctions. Two principal properties of broad relevance to molecular junctions under conventional laboratory conditions, and most closely related to the topics of this thesis are developed below: the effect of the metal on the conductance and the gating properties of metal-organic molecules.

1.5.1. The effect of the metal on the conductance

Most of the organometallic complexes in the literature are reported to give a higher conductance than their parent organic molecules, a phenomenon often attributed to the better alignment between their frontier molecular orbitals and the E_F, and also because of better electron delocalization in the metal-molecule-metal assembly. Geometry constraints and conformational restrictions imposed by the metal centre on the organic backbone are also important factors in explaining the conductance results. An example is shown in Chart 1-3.[50] The I-V curve presents a resistance value which is smaller for the ruthenium(II) complex than for the N^N ligand itself, explained by the planarity of the bithiophene and bipyridine rings, forced by the complexation, versus the twisted geometries favoured by simple uncomplexed bipyridines.

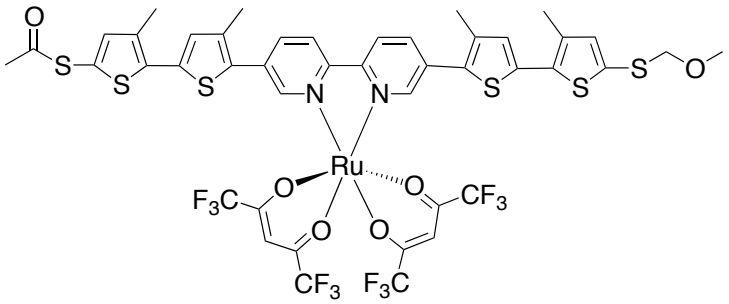

Chart 1-3. *Bipyridine ruthenium(II) complex explored by Lee et al. in a Scanning Tunneling Spectroscopy junction.*[50]

Getty et al. reported the single-molecule transport mechanisms and conductance of a ferrocene-oligophenylethynyl dithiol (Fc-OPE) against the corresponding all-organic OPE molecule (Chart 1-4).[51]

The results show that the conductance of the organic OPE molecule is at least two orders of magnitude lower than the Fc-OPE. A possible explanation has been highlighted by Density Functional Theory (DFT) calculations where a clear resonance, 30 meV above the Fermi level, is seen which is in agreement with the almost perfect transmission and the local density is conjugated throughout the entire molecule from lead to lead. In addition, coplanarity of the ring along with the scissor mode/rotation possible between the five membered rings is mentioned.

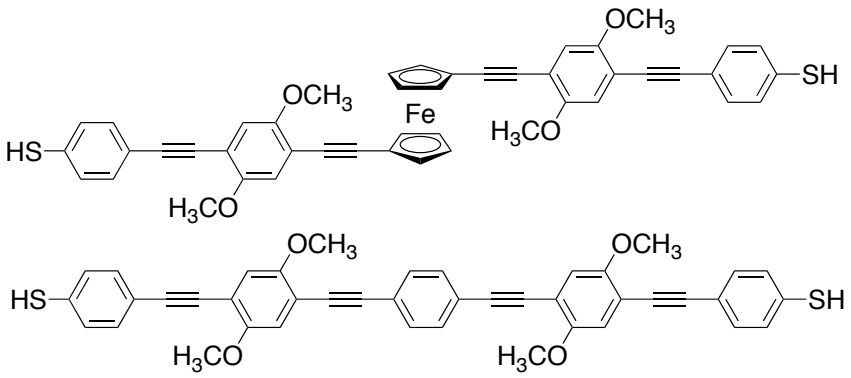

Chart 1-4. *Ferrocene molecules studied by Getty et al. in an electromigration junction.*[51]

To emphasize the favourable electronic properties of ferrocene, a series of all-organic OPEs (intramolecular N…N distances 0.98 to 5.11 nm) and their ferrocene-containing analogues (intramolecular N…N distances 1.08 to 5.14 nm) with amine anchor groups have been investigated by Lu et al. (Chart 1-5).[52]

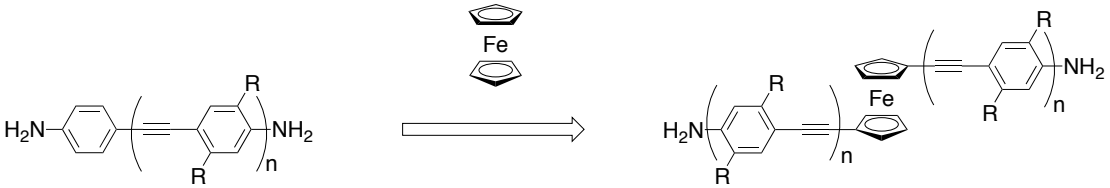

Chart 1-5. *Ferrocene molecules studied by Lu et al. in STM-BJ and CP-AFM junctions.*[52]

The authors describe enhanced conductivity for the organometallic molecules compared to the all-organic molecules, in both tunnelling and hopping conduction regimes using both STM-BJ and CP-AFM. Here, the high conductance is explained by a decrease of the LUMO level, which brings it closer to the gold E_F level. Furthermore, the difference between the conductance of the two series is found to be even bigger in the longer molecules (**OPE4** - **OPE7** and **Fc3** - **Fc7**). By comparing the two series of OPE molecules, it has been found that the incorporation of ferrocene has a larger impact on the conduction of long molecular wire due to the different transport mechanisms. Via this approach, the molecular conductance of a long molecule in the hopping regime exceeds the molecular conductance of a short one in the tunnelling regime at room temperature.

More recently, the high conductivity through organometallic wires bearing iron moieties $X(depe)_2FeC{\equiv}C\text{-}C{\equiv}CFe(depe)_2X$ (X = C_2SnMe_3; NCSe and NCS) has been highlighted by Lissel et al.[53] This work emphasises the influence of anchor groups on the molecular transport junctions, showing that the C-Au covalent bond displayed the best result (6.5×10^{-7} A at ± 1.0 V) over -N=C=Se (1.3×10^{-9} A at ± 1.0 V) and -N=C=S (1.8×10^{-10} A at ± 1.0 V). In addition, when comparing the conductance as a function of molecular length, the molecules with iron moieties have a higher conductance than poly-p-phenylene analogues.[54]

The change of transport mechanism for molecular wires with metal centres helps maintain a reasonable conductance over long distance. A series of Ru(II) bis(σ-arylacetylide)s bearing isocyanide or thioacetate linker groups, with increasing length and multiple ruthenium centres, has been studied (Chart 1-6).[55,56] SAM of the Ru(II) bis(σ-arylacetylide)s have been measured as a function of the length and temperature using CP-AFM method.

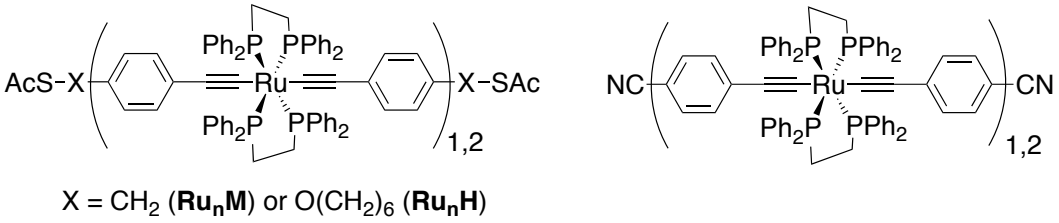

X = CH_2 (**Ru_nM**) or $O(CH_2)_6$ (**Ru_nH**)

Chart 1-6. *Ru(II) bis(σ-arylacetylide) molecules studied by Luo et al. in CP-AFM junction (left)*[56] *and by Kim et al. in CP-AFM and crossed wire junctions (right).*[55]

The measurements reveal a weak length dependence of the wire resistance β (**Ru_nM**) = 1.02 nm^{-1} and β (**Ru_nH**) = 1.64 nm^{-1} for the molecules containing the thiol groups because there is extensive delocalization of the frontier orbitals over the conjugated part of the molecule. In addition, the contact resistance of **Ru_nM** (Chart 1-6, left) is 3 orders of magnitude lower ($R_0 = 1.01 \times 10^5$ Ω) than the ruthenium wires with isocyanide linking groups ($R_0 = 4.2 \times 10^8$ Ω).

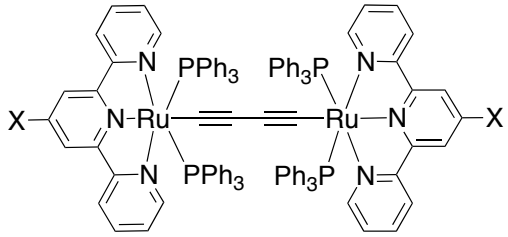

X = $C_6H_4CH_2SAc$ (**Ru1**), C_6H_4SAc (**Ru2**), $S(CH_2)_2SiMe_3$ (**Ru3**)

Chart 1-7. *Molecules studied by Wen et al. in an Electrochemically assisted-Mechanically Controllable Break Junction (EC-MCBJ).*[57]

The length dependence is remarkably low in many of these metal complex based molecular wires. Recently, EC-MCBJ measurements on a series of dinuclear ruthenium polyynediyl complexes containing a redox-active organometallic fragment $[(Phtpy)(PPh_3)_2Ru]^{2+}$ and terminated by phenylmethylene (**Ru1**), phenyl (**Ru2**) or directly connected to sulfur (**Ru3**) (Chart 1-7) have been reported.[57] Once again, these diruthenium(II) systems exhibit a higher conductance and a weaker β length dependence than OPE and OPV. The molecular conductance is an order magnitude higher (1.4×10^{-3} G_0) than the corresponding OPE (1,4-(4-$AcSC_6H_4C{\equiv}C)_2C_6H_4$) ($0.96 \times 10^{-4}$ G_0). Moreover, the terminus of the molecule also affects the molecular conductance; the molecule **Ru3** has a slightly higher conductance than **Ru2** and the molecule **Ru1** reduces the conductance by three times compared to the molecule **Ru2**. The great conductivity is due to the location of the HOMO on the Ru-C≡C-C≡C-Ru backbone with dπ(Ru) and π(C≡C-C≡C).

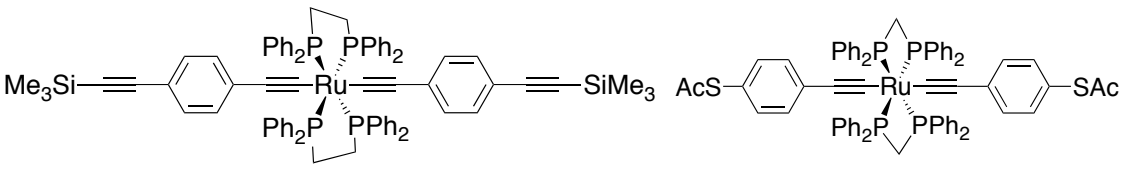

Chart 1-8. *Molecules studied by Marqués-González et al. in a STM-I(s) junction (left)*[37] *and by Liu et al. in a STM-BJ and CP-AFM junctions (right).*[58]

The positive effect on the conductance of ruthenium implanted in the π conjugated bridge is also observed by other groups. Marqués-Gonz*á*lez et al. and Liu et al. compare

the OPE and the similar organometallic molecules with the ruthenium centre (Chart 1-8) using different scanning probe microscopy techniques.[37,58] The thiol terminated OPE ruthenium(II) (Chart 1-8, right) has a better electronic decay constant and conductance ($\beta = 1.01 \pm 0.25$ Å^{-1}; $G = 19 \pm 7$ nS) than the thiol OPE ($\beta = 1.11 \pm 0.18$ Å^{-1}; $G = 3.6 \pm 2.0$ nS) thanks to a good overlap of the d-π orbitals (Figure 1-9).

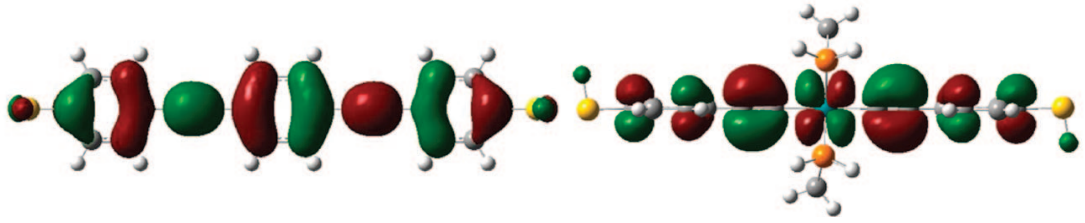

Figure 1-9. *HOMO delocalization of the thiol terminated OPE ruthenium(II) with phenyl groups replaced by hydrogen, right (Structure: Chart 1-7, right) and HOMO delocalization of the thiol terminated OPE, left from the reference.*[58]

Similarly, the trimethylsilyl-ethynyl terminated OPE ruthenium(II) complex displays higher conductance ($(5.10 \pm 0.99) \times 10^{-5}$ G_0) than the parent all-organic molecule ($(2.75 \pm 0.56) \times 10^{-5}$ G_0) with the STM-*I(s)* technique, which is in agreement with the slight shortening of the organometallic molecule and the better alignment of its HOMO with E_F of the gold electrodes.

In contrast to this nicely delocalized π-d-π ruthenium system (Figure 1-9, right), the equivalent platinum complex was described as an insulator[59] (Chart 1-9, left). Mayor et al. explain this behaviour by the pure σ character of the Pt-C(sp) bond and the unavailability of the d_{xz} and d_{yz} orbitals in the square geometry for the d-π electron delocalization.

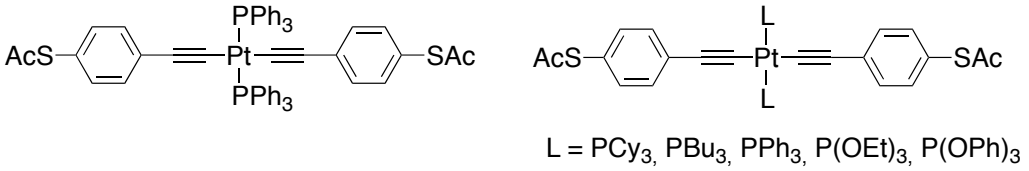

Chart 1-9. *Molecules studied by Mayor et al. in a MCBJ, left*[59] *and by Schull et al. in a crossed-wire junction, right.*[60]

Furthermore, the resistance of the platinum complex is between 5 - 50 GΩ, three orders of magnitude higher than the organic parents. Moreover, results from the work of Schull et al. who evaluated the ligand effects on the conductance, realise that the change of the phosphine ligands leads to a negligible difference in the energy of the HOMO-LUMO gap (0.08 eV) (Chart 1-9, right).[60] More importantly, the conductance of these platinum bis(arylacetylene)s is two to three times higher than the corresponding OPE, consistent with a 1.6 Å decrease in length.

The choice of the metal is important because it will direct the molecular geometry and influence the electron delocalization, but the design of the organic ligand is also essential for good conductivity. An excellent combination for long-range conductance is the Zn porphyrin connected to an ethyne based linker[61] with thiol as a binding group (Chart 1-10).

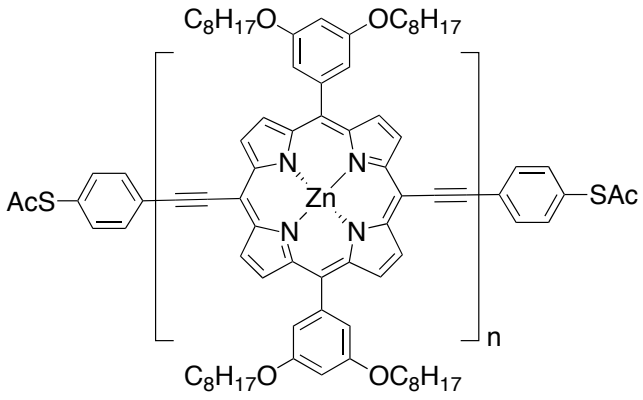

Chart 1-10. *Zn porphyrin molecules studied by Sedghi et al. in a STM-I(s) junction.*[61]

The STM-*I(s)* and *I(t)* measurements on the single molecule of the Zn porphyrin series found a very low value of β (0.04 ± 0.006 $Å^{-1}$) even lower than general π conjugated organic bridge (β = 0.1 - 0.6 $Å^{-1}$). As mentioned previously, while thiol is a good anchoring group, it generates defects on the gold surface that is why pyridine linker has been investigated instead.

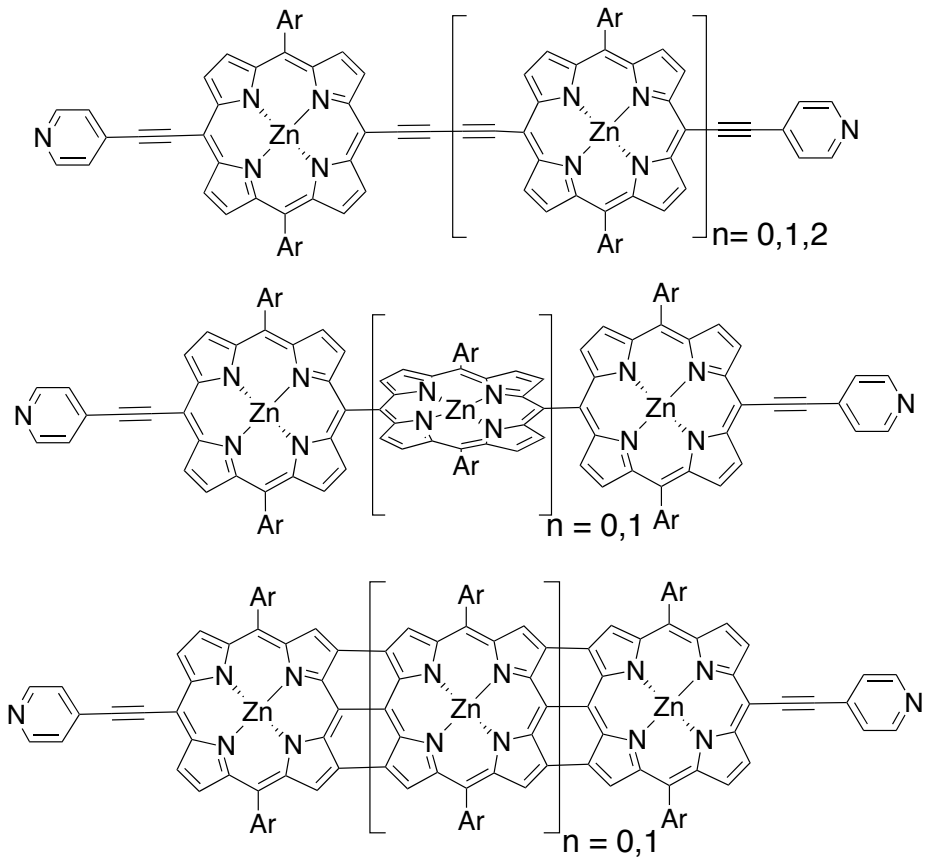

Chart 1-11. *Zn porphyrin molecules studied by Sedghi et al.*[28]

Besides, it was demonstrated that the conductance depends on the twisting angle between the Zn-porphyrin and the alkyne (Chart 1-11).[28] Predictably, the planar fused tapes mediate the charge most efficiently ($\beta = 0.019 \pm 0.001$ Å^{-1}) than the twisted molecules ($\beta = 0.11 \pm 0.01$ Å^{-1}).

Recently, the change of the conductance due to the coordination of an organic ligand with a metal reveal the importance of the molecular orbitals along with the effect of the anchor group on the charge transport.[62]

Upon the coordination of a series of phenanthroline-based molecules containing different anchoring groups (pyridine, thiol and acetylene) (**Phen1** - **Phen3**) with Cu (**Cu1** - **Cu3**) (Chart 1-12), the molecular energy level is reduced relative to E_F of the gold and then induces a change of conductance.

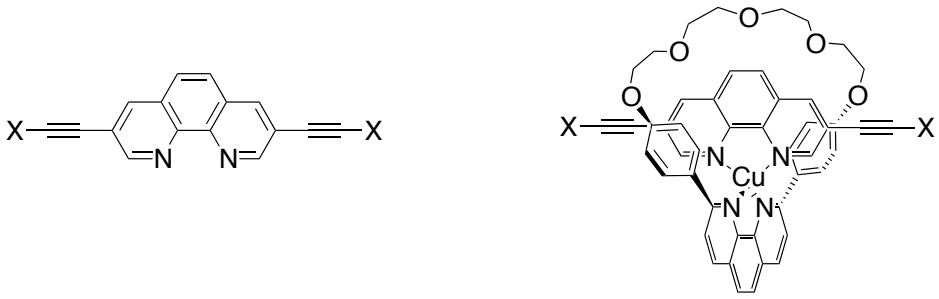

X = C_6H_4SAc (**Phen1-Cu1**), $C_6H_4C_2SiMe_3$ (**Phen2-Cu2**), C_6H_4N (**Phen3-Cu3**)

Chart 1-12. *Phenanthroline-based molecules studied by Ponce et al. in a MCBJ.*[62]

The enhancement of the conductance happens for the LUMO based anchor group (e.g. pyridine) and the decrease of the conductance is observed for the HOMO based anchor groups (e.g. thioacetate and acetylene) (Figure 1-10).

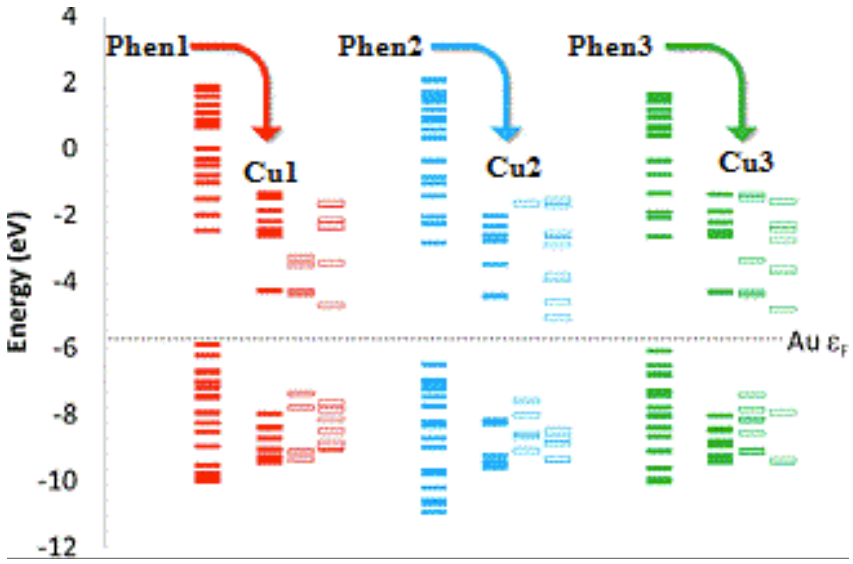

Figure 1-10. *Orbital energy level diagram before and after coordination of the phenanthroline organic bridge and Cu(I). The levels are relative to the Fermi level of the gold at - 5.53 eV from the reference.*[62]

1.5.2. Gating properties of the metal-organic molecules

This section will consider other electronic properties such as switching, Coulomb blockade or Kondo effect as a result of different spin states or redox potentials.

Redox molecules have been chosen to study switching mechanisms based on changes in molecular redox states. There are several models for the electrochemical experiments, which are performed in electrolyte with the tip and substrate bias set in relation to an additional reference electrode.

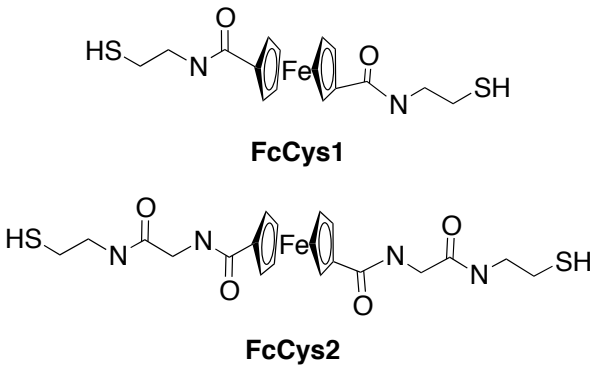

Chart 1-13. *Molecules studied by Tao et al. in an EC-STM-BJ.*[63]

Tao et al. described a ferrocene compound terminated with cysteamine as a good model for an electrochemically gated response due to the fast and reversible one electron transfer of ferrocene at gold electrodes.[63]

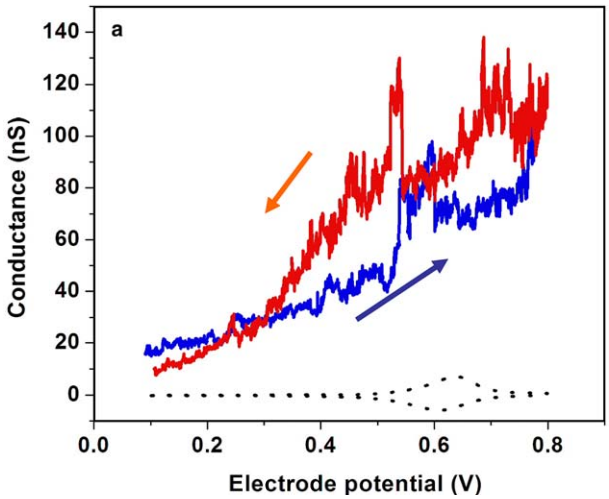

Figure 1-11. *Current recorded though **FcCys1** when the substrate potential was swept in forward and reverse directions in 0.1 M $HClO_4$ from reference.*[63]

The conductance increased by 8 - 10 times (oxidized state) compared to the reduced state when the electrochemical gate voltage is increased (Figure 1-11).

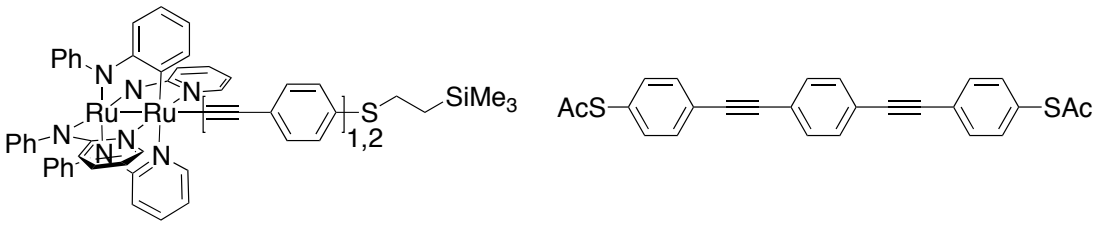

Chart 1-14. *Molecules studied by Szuchmacher Blum et al. in a STM junction.*[64]

Szuchmacher Blum et al. demonstrated that SAMs of dipyridylamine diruthenium(II) OPE complex (Chart 1-14, left) inserted in alkanethiols display a stochastic switching when contacted by STM, in accord with its low potential redox states.[64] Moreover, the introduction of the dipyridylamine diruthenium fragment lower the electronic decay constant β by 15% - 43% compared to the fully organic OPE molecule (Chart 1-14, right).

Effectively, these results indicate that the electrochemical potential can regulate the electron transport as was proved by Ricci et al. with a redox-active [Os(bipyridine)(pyridine)Cl] complex connected via a Au-S or Au-C bonds in electrochemical STS experiments (Chart 1-15).[65]

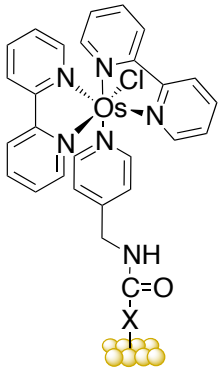

X = C_6H_4 or C_6H_4S

Chart 1-15. *[Os(bipyridine)(pyridine)Cl] molecules studied by Ricci et al. in a EC-STS junction in this work.*[65]

The bias was kept constant but the substrate electrochemical potential (E_S), set suitably away from the equilibrium redox potential of the complex (E^0), was scanned in a potential window wide enough to pass E^0. The I-V curve obtained showed current maxima at E_s - E_0

= 0.04 V for the Au-C bond and 0.1 V for the Au-S bond, which are close to E^0 of the complex.

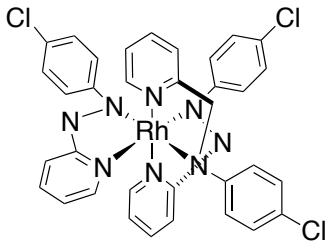

Chart 1-16. *Molecule studied by Paul et al. in an AFM junction.*[66]

Paul et al. also discovered this switching phenomenon with a film of azo anion diradical Rh(III) complexes (Chart 1-16), they recorded the I-V curve of the device in the range of + 5 V to – 5 V at scan rate = 10 mV/s with the AFM technique.[66] There was an abrupt increase of the conductance from low (OFF) to high (ON) with a threshold voltage of 2.75 V, and on the return scan, an abrupt decrease when a negative bias was applied with a threshold voltage at – 2.05 V (Figure 1-12).

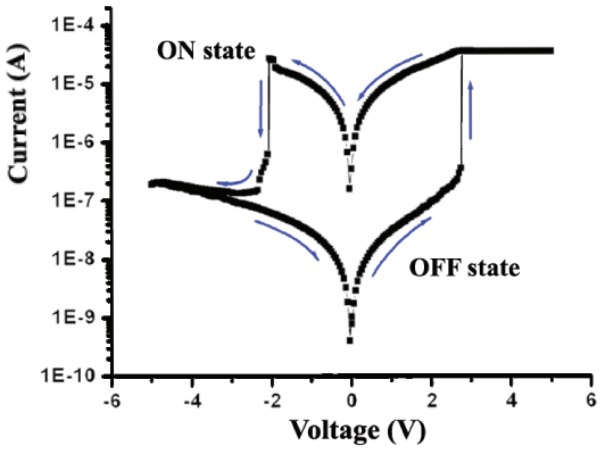

Figure 1-12. *Current-voltage of the* $[Rh^{III}(L^{\cdot-})_2(L)]CF_3SO_3$ *(2-(4-chlorophenylazo)pyridine), from reference.*[66]

Another way to switch the current is to use the bistability of a spin-crossover nanoparticle, in other words, transition from low spin to high spin. Prins et al. showed the

transition between low to high conductance with spin crossover where the change of conductance may be explained by the change in size of the molecule.[67]

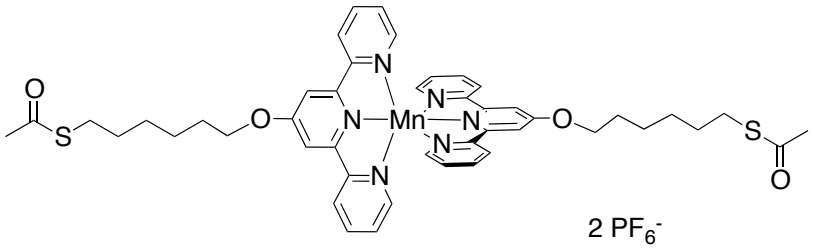

Chart 1-17. *Molecule studied by Osorio et al. in an electromigration self-breaking junction.*[68]

The same observation has been made with bis(terpyridine) Mn based complex (Chart 1-17) where a change in spin configuration leads to a suppression of current at low bias (N = 5 electrons ; S = 5/2 in its ground state N = 6 electrons; S = 0) and a lift of the spin-blockade at high bias which is found to be large enough to populate the excited states (N = 5 electrons ; S = ½ and N = 6 electrons; S = 1).[68]

The Kondo effect combined with a Coulomb blockade can be exploited: two examples with $[Co(tpy\text{-}(CH_2)_5\text{-}SH)]^{2+}$ and $[Co(tpy\text{-}SH)_2]^{2+}$ (Chart 1-18) showed the formation of distinct islands of Co^{2+} and Co^{3+} where no current is detected because the voltage is insufficient to tunnel the electrons from the electrodes to the molecule.[69]

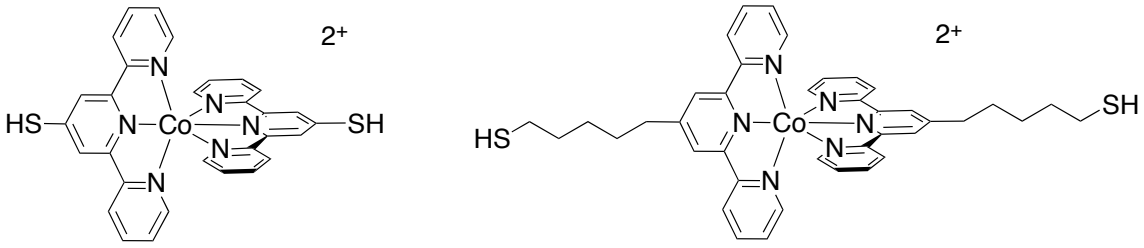

Chart 1-18. *$[Co(tpy\text{-}(CH_2)_5\text{-}SH]^{2+}$ and $[Co(tpy\text{-}SH)_2]^{2+}$ molecules studied by Nesvorny et al. in an electromigration self-breaking junction.*[69]

These two visible islands are the signatures of a single-electron transistor whose redox state can be tuned by the gate voltage. The interesting property was the observation of a Kondo effect which takes place when a strong coupling is present between the electrode

and the molecule $[Co(tpy\text{-}SH)_2]^{2+}$ (Figure 1-13). Nevertheless, the coulomb blockade behaviour can also appear when the organic ligand is not insulating, but is a metal string such as the dipyridylamine (dpa). As described by Chae et al., the preparation of a SMT (Single Molecule Transistor) with $Ni_3(dpa)_4Cl_2$ and $Cu_3(dpa)_4Cl_2$ (Chart 1-19) showed a Coulomb blockade behaviour due to the weak coupling of the molecule with the electrodes.[70]

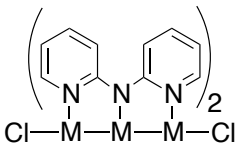

M = Cu, Ni

Chart 1-19. *Molecules studied by Chae et al. in an electromigration self-breaking junction.*[70]

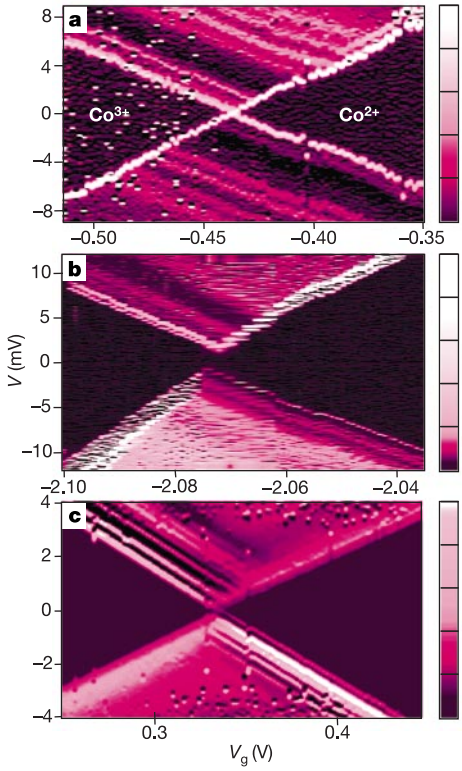

Figure 1-13. *Colour-scale plots of differential conductance (∂I/∂V) as a function of the bias voltage (V) and the gate voltage (V_g) for three different [Co(tpy-$(CH_2)_5$-SH)$_2$] single electron transistors at zero magnetic field. Black represents zero conductance and white the maximum of conductance from reference.*[69]

The metallo-terpyridine unit offers stable charge storage during redox reactions due to the metal core and the help of the insulating terpyridine ligand. For this reason, bis(terpyridine)-Fe(II) molecules (Chart 1-20) have been studied on an indium oxide (In_2O_3) nanowire FET (NW-FET).[71]

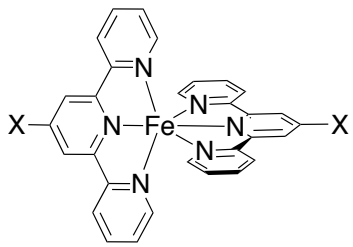

X = H, SAc, C_6H_4SAc

Chart 1-20. *Molecules studied by Li et al. in a quartz crystal microbalance junction.*[71]

When a negative voltage is applied from the silica back gate, the molecule is oxidized and displays a high conductance ("on state") and the contrary ("off state") happens when a positive voltage is set. These two states at $V_g = 0$ are the result of the hysteresis obtained in the I-V curves which suggest the exploitation of bis(terpyridine)-Fe(II) for data storage applications. The switching properties depend critically on the metal, the ligand and also on the metallic contacts. Seo et al. demonstrated that the switching voltages of M(II) $(phtpySAc)_2$ (M = Fe, Ru and Co) (Chart 1-21) shift according to the metal centre, but also according to the metal used for the conductance measurements (e.g. Au, Pt/Ir and Au/reduced graphene oxide (rGo)).[72] The switching voltages for each metal complex using a Au tip were shifted by 0.3 – 0.4 V from those in a Pt/Ir tip junction, which is equal to the energy difference between the two metals. The metallo-terpyridine containing Fe was found to be the easiest to switch with Pt/Ir metallic contacts (1.725 ± 0.025 V), then Ru (1.925 ± 0.025 V) and the hardest to switch is the Co complex (2.425 ± 0.025 V).

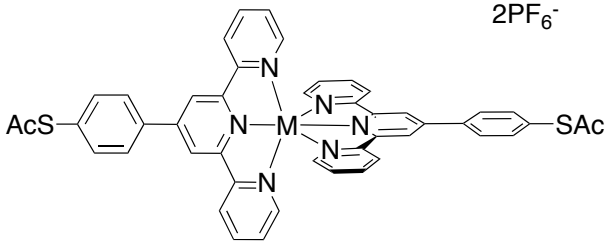

M = Fe, Ru, Co

Chart 1-21. *Molecules studied by Seo et al. in a STM junction.*[72]

As mentioned in this chapter, ME is an expanding field with a view to complementing the silicon-based electronics. Many groups are putting their effort to understand the charge transport mechanism at the molecular level in order to tightly control the properties of molecular devices. Access to different methods for measuring the current-voltage properties of a single molecule have been developed which facilitates the exploration of molecules suitable for electronics.

While a lot of organic molecules have been studied for this purpose, an increasing curiosity around the incorporation of metal centre in organic molecule has gained the scientists. In fact, the organometallic molecules give extra features in the electrical behaviour due to their redox properties, charge transport, which favours hopping mechanisms and the better electron delocalization.

For this reason, in this thesis we focussed on the synthesis of organometallic molecules bearing π-conjugated molecules and their single molecule conductance evaluation with the help of STM-*I(s)* technique.

1.6. References

(1) http://www.iact.in/iact-315-fall-2013/the-transistor/

(2) http://www.intel.it/content/www/it/it/silicon-innovations/moores-law-technology.html

(3) Choi, H.; Mody, C. C. M. *Social Studies of Science* **2009**, *39*, 11.

(4) Mann, B.; Kuhn, H. *J. Appl. Phys.* **1971**, *42*, 4398.

(5) Aviram, A.; Ratner, M. A. *Chemical Physics Letters* **1974**, *29*, 277.

(6) Carroll, R. L.; Gorman, C. B. *Angew. Chem. Int. Ed.* **2002**, 4379.

(7) Fuentes, N.; Martín-Lasanta, A.; Álvarez de Cienfuegos, L.; Ribagorda, M.; Parra, A.; Cuerva, J. M. *Nanoscale* **2011**, *3*, 4003.

(8) Coskun, A.; Spruell, J. M.; Barin, G.; Dichtel, W. R.; Flood, A. H.; Botros, Y. Y.; Stoddart, J. F. *Chem. Soc. Rev.* **2012**, *41*, 4827.

(9) Sun, L.; Diaz-Fernandez, Y. A.; Gschneidtner, T. A.; Westerlund, F.; Lara-Avila, S.; Moth-Poulsen, K. *Chem. Soc. Rev.* **2014**, *43*, 7378.

(10) Cuevas, J. C.; Scheer, E. *Molecular electronics: an introduction to theory and experiment*; World Scientific; Singapore; **2012**.

(11) Petty, M. C. *Molecular electronics: from principles to practice*; Wiley Edition; West Sussex; **2012**.

(12) Bratovski, A.; Zhang, X. - A.; Williams, R. S. Patent (US6663797) *Two crossed wires sandwiching an electrically addressable molecular specie*s; **2003**

(13) Service, R. F. *Science* **2001**, *294*, 2442.

(14) Xu, B.; Tao, N. J. *Science* **2003**, *301*, 1221.

(15) Nichols, R. J.; Haiss, W.; Higgins, S. J.; Leary, E.; Martin, S.; Bethell, D. *Phys. Chem. Chem. Phys.* **2010**, *12*, 2801.

(16) Haiss, W.; Van Zalinge, H.; Higgins, S. J.; Bethell, D.; Höbenreich, H.; Schiffrin, D. J.; Nichols, R. J. *J. Am. Chem. Soc.* **2003**, *125*, 15294.

(17) Cui, X. D. *Science* **2001**, *294*, 571.

(18) Reed, M. A. *Science* **1997**, *278*, 252.

(19) Kushmerick, J. G.; Holt, D. B.; Pollack, S. K.; Ratner, M. A.; Yang, J. C.; Schull, T. L.; Naciri, J.; Moore, M. H.; Shashidhar, R. *J. Am. Chem. Soc.* **2002**, *124*, 10654.

(20) Kushmerick, J.; Holt, D.; Yang, J.; Naciri, J.; Moore, M.; Shashidhar, R. *Phys. Rev. Lett.* **2002**, *89,* 86802.

(21) Liu, H.; Wang, N.; Zhao, J.; Guo, Y.; Yin, X.; Boey, F. Y. C.; Zhang, H. *ChemPhysChem* **2008**, *9*, 1416.

(22) Baker, S. *Science* **2008**, *320*, 1482.

(23) Xu, B. Q.; Li, X. L.; Xiao, X. Y.; Sakaguchi, H.; Tao, N. J. *Nano Lett.* **2005**, *5*, 1491.

(24) Wang, C.; Batsanov, A. S.; Bryce, M. R.; Martin, S.; Nichols, R. J.; Higgins, S. J.; García-Suárez, V. M.; Lambert, C. J. *J. Am. Chem. Soc.* **2009**, *131*, 15647.

(25) Moreno-García, P.; Gulcur, M.; Manrique, D. Z.; Pope, T.; Hong, W.; Kaliginedi, V.; Huang, C.; Batsanov, A. S.; Bryce, M. R.; Lambert, C.; Wandlowski, T. *J. Am. Chem. Soc.* **2013**, *135*, 12228.

(26) Zhao, X.; Huang, C.; Gulcur, M.; Batsanov, A. S.; Baghernejad, M.; Hong, W.; Bryce, M. R.; Wandlowski, T. *Chem. Mater.* **2013**, *25*, 4340.

(27) Sedghi, G.; García-Suárez, V. M.; Esdaile, L. J.; Anderson, H. L.; Lambert, C. J.; Martin, S.; Bethell, D.; Higgins, S. J.; Elliott, M.; Bennett, N.; Macdonald, J. E.; Nichols, R. J. *Nat. Nanotechnol.* **2011**, *6*, 517.

(28) Sedghi, G.; Esdaile, L. J.; Anderson, H. L.; Martin, S.; Bethell, D.; Higgins, S. J.; Nichols, R. J. *Adv. Mater.* **2011**, *24*, 653.

(29) Kaliginedi, V.; Moreno-García, P.; Valkenier, H.; Hong, W.; García-Suárez, V. M.; Buiter, P.; Otten, J. L. H.; Hummelen, J. C.; Lambert, C. J.; Wandlowski, T. *J. Am. Chem. Soc.* **2012**, *134*, 5262.

(30) Xiao, X.; Nagahara, L. A.; Rawlett, A. M.; Tao, N. *J. Am. Chem. Soc.* **2005**, *127*, 9235.

(31) Liao, J.; Agustsson, J. S.; Wu, S.; Schönenberger, C.; Calame, M.; Leroux, Y.; Mayor, M.; Jeannin, O.; Ran, Y.-F.; Liu, S.-X.; Decurtins, S. *Nano Lett.* **2010**, *10*, 759.

(32) Li, C.; Pobelov, I.; Wandlowski, T.; Bagrets, A.; Arnold, A.; Evers, F. *J. Am. Chem. Soc.* **2008**, *130*, 318.

(33) Chen, F.; Li, X.; Hihath, J.; Huang, Z.; Tao, N. *J. Am. Chem. Soc.* **2006**, *128*, 15874.

(34) Hong, W.; Manrique, D. Z.; Moreno-García, P.; Gulcur, M.; Mishchenko, A.; Lambert, C. J.; Bryce, M. R.; Wandlowski, T. *J. Am. Chem. Soc.* **2012**, *134*, 2292.

(35) Quek, S. Y.; Kamenetska, M.; Steigerwald, M. L.; Choi, H. J.; Louie, S. G.; Hybertsen, M. S.; Neaton, J. B.; Venkataraman, L. *Nat Nanotechnology* **2009**, *4*, 230.

(36) Tsutsui, M.; Taniguchi, M.; Kawai, T. *J. Am. Chem. Soc.* **2009**, *131*, 10552.

(37) Marqués-González, S.; Yufit, D. S.; Howard, J. A. K.; Martin, S.; Osorio, H. M.; García-Suárez, V. M.; Nichols, R. J.; Higgins, S. J.; Cea, P.; Low, P. J. *Dalton Trans.* **2013**, *42*, 338.

(38) Hong, W.; Li, H.; Liu, S.-X.; Fu, Y.; Li, J.; Kaliginedi, V.; Decurtins, S.; Wandlowski, T. *J. Am. Chem. Soc.* **2012**, *134*, 19425.

(39) Cheng, Z. L.; Skouta, R.; Vázquez, H.; Widawsky, J. R.; Schneebeli, S.; Chen, W.; Hybertsen, M. S.; Breslow, R.; Venkataraman, L. *Nat Nanotechnol* **2011**, *6*, 353.

(40) Parameswaran, R.; Widawsky, J. R.; Vázquez, H.; Park, Y. S.; Boardman, B. M.;

Nuckolls, C.; Steigerwald, M. L.; Hybertsen, M. S.; Venkataraman, L. *J. Phys. Chem. Lett.* **2010**, *1*, 2114.

(41) Zotti, L. A.; Kirchner, T.; Cuevas, J. C.; Pauly, F.; Huhn, T.; Scheer, E.; Erbe, A. *Small* **2010**, *6*, 1529.

(42) Kim, B.; Beebe, J. M.; Jun, Y.; Zhu, X. Y.; Frisbie, C. D. *J. Am. Chem. Soc.* **2006**, *128*, 4970.

(43) Park, Y. S.; Whalley, A. C.; Kamenetska, M.; Steigerwald, M. L.; Hybertsen, M. S.; Nuckolls, C.; Venkataraman, L. *J. Am. Chem. Soc.* **2007**, *129*, 15768.

(44) Ko, C.-H.; Huang, M.-J.; Fu, M.-D.; Chen, C.-H. *J. Am. Chem. Soc.* **2010**, *132*, 756.

(45) Martin, C. A.; Ding, D.; Sørensen, J. K.; Bjørnholm, T.; van Ruitenbeek, J. M.; van der Zant, H. S. J. *J. Am. Chem. Soc.* **2008**, *130*, 13198.

(46) Leary, E.; González, M. T.; van der Pol, C.; Bryce, M. R.; Filippone, S.; Martín, N.; Rubio-Bollinger, G.; Agraït, N. *Nano Lett.* **2011**, *11*, 2236.

(47) Low, P. J. *Dalton Trans.* **2005**, *17*, 2821.

(48) Rigaut, S. *Dalton Trans.* **2013**, *42*, 15859.

(49) Wassel, R. A.; Credo, G. M.; Fuierer, R. R.; Feldheim, D. L.; Gorman, C. B. *J. Am. Chem. Soc.* **2004**, *126*, 295.

(50) Lee, Y.; Yuan, S.; Sanchez, A.; Yu, L. *Chem. Commun.* **2007**, 247.

(51) Getty, S.; Engtrakul, C.; Wang, L.; Liu, R.; Ke, S.-H.; Baranger, H.; Yang, W.; Fuhrer, M.; Sita, L. *Phys. Rev. B* **2005**, *71*, 241401.

(52) Lu, Q.; Yao, C.; Wang, X.; Wang, F. *J. Phys. Chem. C* **2012**, *116*, 17853.

(53) Lissel, F.; Schwarz, F.; Blacque, O.; Riel, H.; Lörtscher, E.; Venkatesan, K.; Berke, H. *J. Am. Chem. Soc.* **2014**, *136*, 14560.

(54) Chen, W.; Widawsky, J. R.; Vázquez, H.; Schneebeli, S. T.; Hybertsen, M. S.; Breslow, R.; Venkataraman, L. *J. Am. Chem. Soc.* **2011**, *133*, 17160.

(55) Kim, B. S.; Beebe, J. M.; Olivier, C.; Rigaut, S.; Touchard, D.; Kushmerick, J. G.; Zhu, X. Y.; Frisbie, C. D. *J. Phys. Chem. C* **2007**, *111*, 7521.

(56) Luo, L.; Benameur, A.; Brignou, P.; Choi, S. H.; Rigaut, S.; Frisbie, C. D. *J. Phys. Chem. C* **2011**, *115*, 19955.

(57) Wen, H.-M.; Yang, Y.; Zhou, X.-S.; Liu, J.-Y.; Zhang, D.-B.; Chen, Z.-B.; Wang, J.-Y.; Chen, Z.-N.; Tian, Z.-Q. *Chem. Sci.* **2013**, *4*, 2471.

(58) Liu, K.; Wang, X.; Wang, F. *ACS Nano* **2008**, *2*, 2315.

(59) Mayor, M.; Hanisch, von, C.; Weber, H.; Reichert, J.; Beckmann, D. *Angew. Chem. Int. Ed.* **2002**, *41*, 1183.

(60) Schull, T. L.; Kushmerick, J. G.; Patterson, C. H.; George, C.; Moore, M. H.; Pollack, S. K.; Shashidhar, R. *J. Am. Chem. Soc.* **2003**, *125*, 3202.

(61) Sedghi, G.; Sawada, K.; Esdaile, L. J.; Hoffmann, M.; Anderson, H. L.; Bethell, D.; Haiss, W.; Higgins, S. J.; Nichols, R. J. *J. Am. Chem. Soc.* **2008**, *130*, 8582.

(62) Ponce, J.; Arroyo, C. R.; Tatay, S.; Frisenda, R.; Gaviña, P.; Aravena, D.; Ruiz, E.; van der Zant, H. S. J.; Coronado, E. *J. Am. Chem. Soc.* **2014**, *136*, 8314.

(63) Xiao, X.; Brune, D.; He, J.; Lindsay, S.; Gorman, C. B.; Tao, N. *Chemical Physics* **2006**, *326*, 138.

(64) Blum, A. S.; Ren, T.; Parish, D. A.; Trammell, S. A.; Moore, M. H.; Kushmerick, J. G.; Xu, G.-L.; Deschamps, J. R.; Pollack, S. K.; Shashidhar, R. *J. Am. Chem. Soc.* **2005**, *127*, 10010.

(65) Ricci, A. M.; Calvo, E. J.; Martin, S.; Nichols, R. J. *J. Am. Chem. Soc.* **2010**, *132*, 2494.

(66) Paul, N. D.; Rana, U.; Goswami, S.; Mondal, T. K.; Goswami, S. *J. Am. Chem. Soc.* **2012**, *134*, 6520.

(67) Prins, F.; Monrabal-Capilla, M.; Osorio, E. A.; Coronado, E.; van der Zant, H. S. J. *Adv. Mater.* **2011**, *23*, 1545.

(68) Osorio, E. A.; Moth-Poulsen, K.; van der Zant, H. S. J.; Paaske, J.; Hedegård, P.; Flensberg, K.; Bendix, J.; Bjørnholm, T. *Nano Lett.* **2010**, *10*, 105.

(69) Nesvorný, D.; Bottke, W. F., Jr; Dones, L.; Levison, H. F. *Nature* **2002**, *417*, 720.

(70) Chae, D.-H.; Berry, J. F.; Jung, S.; Cotton, F. A.; Murillo, C. A.; Yao, Z. *Nano Lett.* **2006**, *6*, 165.

(71) Li, C.; Fan, W.; Straus, D. A.; Lei, B.; Asano, S.; Zhang, D.; Han, J.; Meyyappan, M.; Zhou, C. *J. Am. Chem. Soc.* **2004**, *126*, 7750.

(72) Seo, S.; Lee, J.; Choi, S.-Y.; Lee, H. *J. Mater. Chem.* **2012**, *22*, 1868.

CHAPTER 2. OLIGOYNES AND ARYLYNES

2.1. Abstract

Cross-coupling of bis(triphenylphosphinegold) stabilised oligoynes with 4-iodo-pyridine or 4-(iodoethynyl)pyridine provides a simple synthetic route to oligoynes stabilised by pyridyl end-caps $Py(C{\equiv}C)_nPy$ (n = 3, 5; Py = 4-pyridyl), the pyridyl group being chosen as a well-known surface contacting group that promotes conduction through π* channels. The novel preparation of $Py(C{\equiv}C)_3Py$ (**4**) allows further evaluation of the effect of the length on conductance through comparison of single molecule measurements with other pyridyl end-capped oligoynes[1,2] and oligoynes based on sulfur-derived contacts that promote HOMO-based conductance.[2]

A combination of traditional tele-elimination chemistry, Cadiot-Chodkiewicz cross-coupling of iodo-oligoynes with terminal oligoynes and the gold(I) – iodo-oligoyne cross coupling reaction have yielded oligoynes $Me_3Si(C{\equiv}C)_nSiMe_3$ (n = 5 (**10**)) allowing further investigation of the trimethylsilylethynyl moiety ($Me_3SiC{\equiv}C$-) as an anchor group to gold. These studies have been augmented by single molecule conductance measurements on the arylene-interpolated derivative $Me_3SiC{\equiv}CC{\equiv}CC_6H_4C{\equiv}CC{\equiv}CSiMe_3$ (**12**). All the single molecule measurements have been performed in collaboration with Prof. Richard Nichols' group at the University of Liverpool.

2.2. Introduction

The linear chain of *n* repeating alkyne moieties in an oligoyne, $R\text{-}(C{\equiv}C)_n\text{-}R$ may be considered as an example of an 'all-carbon' bridge linking two end-capping R groups (where R = H, organic, inorganic or organometallic). The carbyne-like† all-carbon string is one of the most interesting and conceptually simple conjugated organic oligomers for ME purposes. Oligoynes contain pairs of carbons linked through alternating single and triple bonds, $–(C{\equiv}C)_n–$ which give the carbon chain a pseudo one-dimensional geometry. The sp-hybridization of the carbon atoms within the oligoyne chain, leads to a cylindrical distribution of π-electron density and extensive electronic delocalization along the chain. Considerable effort has been expended in determining the conjugation limit of oligoynes,

† carbyne is a hypothetical linear, 1-D allotrope of carbon

with current estimates suggesting ca. 22 repeat alkyne units (i.e. 44 carbon atoms) approximates the carbyne-like limit.[3] Although it is appealing to consider oligoynes as offering rigid-rod-like geometries, the low bending force constant of the –C≡C– moiety leads to an extraordinary array of curved (symmetrical or unsymmetrical bow) and sigmoidal geometries (S-shape) of these compounds in the solid state.[4] Nevertheless, the appealing structural and electronic characteristics of oligoynes have led to this class of compound attracting considerable attention as a wire-like motif initially in metal-complex models[4-7] and more recently within molecular junctions and single molecule experiments.[2,8]

However, both strategies for assessing the wire-like nature of the oligoyne chain rest on the synthesis of compounds containing long carbon chains. Synthetic pathways to long chain compounds R-(C≡C)$_n$-R are complicated by the rapidly increasing instability of both potential intermediate terminal oligoynes R-(C≡C)$_x$-H and the oligoyne products for small R groups as the sp-carbon chain elongates.[9] To resolve this problem, the addition of bulky end groups such as branched alkyl introduced first by Bohlmann (tBu-(C≡C)$_7$-tBu), then used by Jones and co-workers (tBu-(C≡C)$_{10}$-tBu)[10] and Walton et al. (tBu-(C≡C)$_{12}$-tBu and contaminated TES-(C≡C)$_{16}$-TES)[11] have been used. However, it is known that cyano end-cap groups investigated by Hirsch (NC-(C≡C)$_7$-CN),[12] aryl [3,13,14] or organometallic end-groups[6,15,16] can also be employed to stabilise oligoyne chains (Chart 2-1). In addition, odd number oligoynes from the corresponding cyclobutenediones have been synthesized by Diederich.[17] More recently, two research groups Gladysz et al.[18] and Tykwinski, Anderson et al.[19] have insulated the oligoyne with a macrocycle to give interlocked rotaxane molecules.

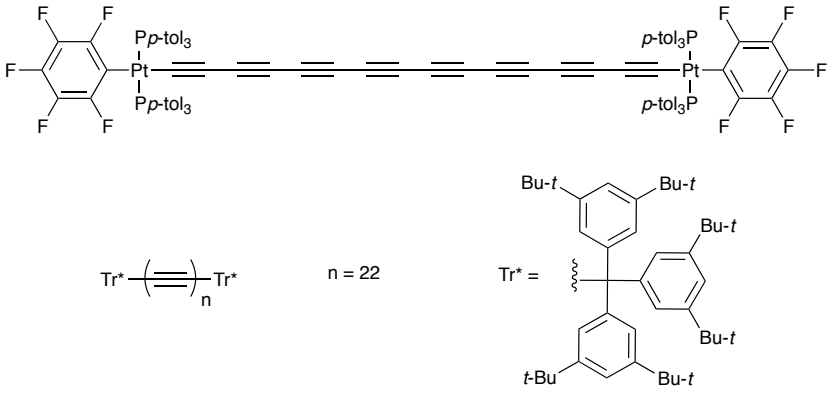

Chart 2-1. *Examples of end-capped oligoynes (top);*[6] *(bottom).*[3]

An alternative strategy to stabilise both the final oligoyne and precursors is to introduce an aryl moiety within the oligoyne core, as is the case in the oligo(arylenebutadiynylene)s,[20,21] oligo(phenyleneethynylene) (OPE)[22] or oligo(aryleneethynylene) (OAE).[23-25] These arylene modified carbon chains, which may be termed 'carbon-rich' to distinguish them from the 'all-carbon' oligoyne chains, are easier to synthesize than the oligoynes and allow the physical, chemical and electronic properties of the compounds to be further tuned via substitution on the arylene ring (Chart 2-2).[26,27] The optoelectronic properties of these OAE and OPE compounds have been widely investigated,[28] the first dialkyl substituted OPE reported by Bunz and Müllen in 1995[29] and their potential exploitation as molecular wires described by Tour, Allara and Weiss.[23,30-32]

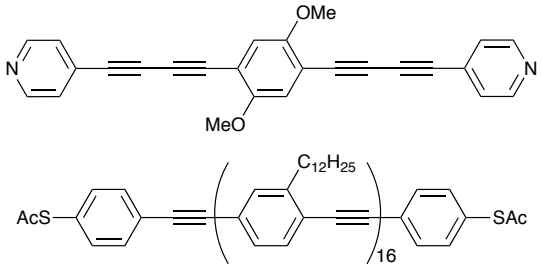

Chart 2-2. *Examples of oligoarylbutadiyne and OPE molecules from references.*[20,28]

2.3. All-carbon bridged bimetallic complexes as models for molecular wires

The use of metal centres as stabilising end-caps for the synthesis of long oligoynes opens the possibility to explore the electronic transport properties, the physical and chemical changes within the all-carbon fragment as a function of oxidation state.[33,34] Many different systems containing metal end-caps $\{ML_m\}$ and carbon chains $-(C\equiv C)_n-$ of various lengths and in different charge (redox) states x $[\{L_mM\}\{\mu\text{-}(C\equiv C)_n\}\{ML_m\}]^{x+}$ have been studied. The exceptional stability afforded by the organometallic complexes to the long-chain bimetallic products and to the intermediates $\{L_mM\}\{(C\equiv C)_{n'}\text{-}H\}$ allows growth of systems of quite impressive length.[17,35] The syntheses of these bimetallic complexes are usually straightforward by, for example, one-pot desilylation/metallation of trimethylsilyl stabilised oligoynes,[36-39] oxidative dimerization with[17,40,41] or without a lithiated intermediate[42] and cross-coupling between a phosphinegold(I) oligo-ynyl complex and a

suitable iodo alkyne.[43] Metal centres utilised as end-caps in this context, include Fe(dppe)Cp*,[44,45] Os(dppe)Cp*,[46,47] Mo(dppe)(η-C_7H_7),[48] Ru(dppx)(Cp'),[42,49,50] Re(NO)(PPh_3)Cp*,[41] Mn(MeC_5H_4)(dmpe)[51] and WI$(dppe)_2$.[52]

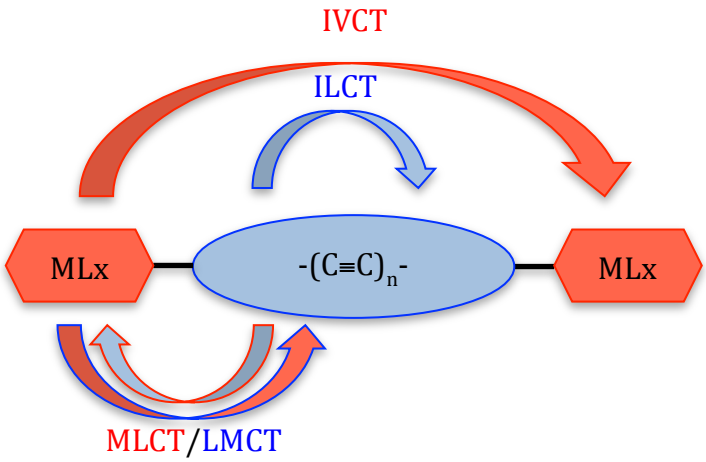

Figure 2-1. *Electronic communications envisaged in all-carbon metal systems. (IVCT: Intervalence Charge Transfer; ILCT: Inter Ligand Charge Transfer; LMCT: Ligand to Metal Charge Transfer; MLCT: Metal to Ligand Charge Transfer*).

The redox activity often associated with the bimetallic compounds, and the analysis of the optical and vibrational spectra of 'mixed-valence' complexes, made possible through the seminal work of Hush,[53] Taube,[54] Creutz,[55] Sutin,[56] Brunschwig[57] and others, allow protypical systems $\{L_nM\}(C\equiv C)_n\{M^+L_m\}$ to be used to assess the 'wire-like' properties of the all-carbon bridge (Figure 2-1). A general conclusion from the range of studies on mixed-valence complexes prepared through both chemical oxidation and spectroelectrochemical methods is that the frontier orbitals are derived from a combination of the metal d-orbitals and the orthogonal $-(C\equiv C)_n-$ π systems. The precise character therefore depends on both the geometry of the metal fragment (which influences the ordering of the metal d-orbitals – c.f. Mo(dppe)(C_7H_7)), the group (which determines the number of metal orbitals available to populate the d-π scaffold c.f. Mn$(dmpe)_2$I) and the row, which determines the metal d-orbital energy (c.f. Fe(dppe)Cp* vs Ru(dppe)Cp*). These basic principles are summarised in an elegant early fragment orbital description by Frapper and Kertesz[58] and later expanded with more detailed calculations at higher levels of theory.[33,59]

However, the study of bimetallic mixed-valence oligoyne complexes does not provide information concerning the electrical characteristics of an oligoyne in a junction as

the models neglect the contribution to the overall transmission from the surface contact to the molecule via the anchor group. For coherent tunnelling through a single channel metal | molecule | metal junction, conductance G may be represented in the Landauer formalism $G = \frac{2e^2}{h} \cdot \Gamma_L \cdot \Gamma_B \cdot \Gamma_R$ (where e is the electron charge, h is Planck's constant and Γ_L, Γ_B and Γ_R are the transmission coefficient of the left contact, the molecular bridge and the right contact, respectively; more detailed descriptions of the entire junction beyond the one-electron/single-channel view are beyond the scope of this introduction.

Therefore, in order to develop a more accurate description of the molecular characteristics of the –(C≡C)$_n$– fragment which extends beyond mixed-valence models, attention has been turned to oligoynes R-(C≡C)$_n$-R in which the R groups serve not only to provide kinetic stability to the all-carbon fragment, but also as anchor groups allowing studies within a molecular junction.

2.4. Synthesis of pyridyl end-capped oligoynes

The pyridine moiety is established as an effective anchor group in single molecule conductance studies[1,60-62] giving rise to LUMO-based conductance channels, allowing comparison with sulfur based anchors (thiolates, thioethers) which promote HOMO-based conductance channels. In addition, pyridine promotes high hit ratios of molecular junction formation during *I(s)*/STM-BJ measurements.[1]

Within the family of bis(pyridine) compounds Py-(C≡C)$_n$-Py (Py = 4-pyridyl) the compounds n = 0,[60] 1 (**1**), 2 (**2**), 4 (**3**),[1,62] (Chart 2-3) have been studied in various STM-based junctions.

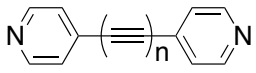

1 n = 1
2 n = 2
3 n = 4

Chart 2-3. *Series of pyridyl end-capped oligoynes reported previously.*[1]

Previously, the even numbered pyridyl oligoynes have been successfully synthesized[63] but only one odd numbered oligoyne has been reported (**1**) (Chart 2-3),[64] primarily due to the synthetic complexity encountered for uneven numbered oligoynes. Thus, the effort here is focussed on the synthesis of pyridyl oligoynes with n = 3 (**4**) and n = 5 (**5**) in order to complete the extended series. Whilst the Cu(I) oxidative Glaser-Hay[65] and Sonogashira dimerizations readily afford even numbered pyridyl oligoynes, this route is not applicable for odd-number of alkyne moieties, e.g. bis(pyridyl) triyne **4** and bis(pyridyl) pentayne **5**.

A straightforward route to **4** from the oligo-ynyl gold(I) complex (Ph_3P)Au-C≡CC≡CC≡C-Au(PPh_3) (**6**) and 4-iodopyridine in the presence of catalytic amount of palladium and copper has been developed here (Scheme 2-1). The oligo-ynyl gold(I) **6** was prepared from the bis(trimethylsilyl)hexatriyne (**8**) (*see* Scheme 2-2) via a one pot desilylation/metallation with an excess of sodium hydroxide (NaOH) and 1.9 equivalents of AuCl(PPh_3) in methanol. The final product was easily obtained after a simple filtration of the mixture giving a pale yellow solid. The yield of this reaction was found to be better after 2 days (96%) compared to 4 h (33%) at room temperature. The identity of compound **6** was confirmed by elemental analysis, X-ray crystallography, mass spectrometry (MS), infrared (IR) and nuclear magnetic resonance (NMR) spectroscopies. ^{1}H NMR and ^{13}C NMR were not that helpful because the oligoyne bridge was not distinguishable, but the ^{31}P NMR spectrum showed a shift from the starting material AuCl(PPh_3) (33.2 ppm) to **6** (41.2 ppm). Moreover, MALDI-TOF MS showed a major peak at 990.0 corresponding to the molecular mass of **6** and crystals suitable for X-ray diffraction were grown from $CDCl_3$. Concerning the bis(pyridyl) triyne **4**, the reaction between **6** and 4-iodopyridine in tetrahydrofuran (THF) in the presence of Pd(PPh_3)$_4$ (5 mol%) and CuI (10 mol%) at room temperature gave 46% of the pure product **4** after column chromatography. The compound **4** was also characterized by IR, MS and NMR spectroscopy. The protons of the pyridine moiety were detected as two doublets at δ_H 8.61 and 7.37 ppm and the ^{13}C NMR showed the quaternary carbons at δ_C 77.9, 76.2, 67.3 ppm. Moreover, no elemental analysis was obtained due to the potential instability of the triyne but high-resolution mass spectrometry confirmed that the compound **4** was synthesized.

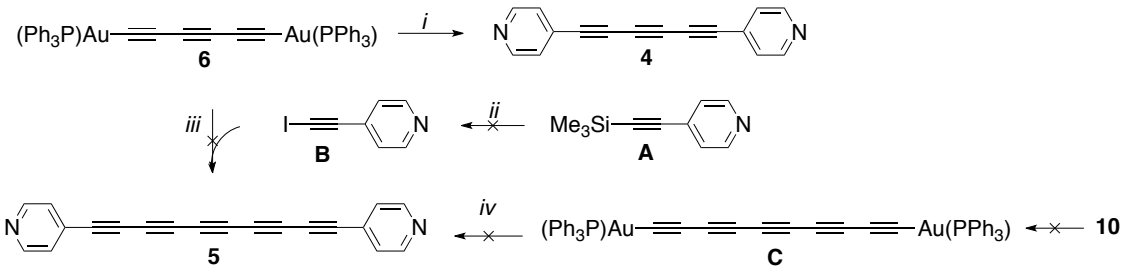

Scheme 2-1. *Attempted synthetic routes for the formation of the pyridyl end-capped oligoynes. (i) 4-iodopyridine, Pd(PPh$_3$)$_4$, CuI in THF, rt, overnight, 46%; (ii) NaHCO$_3$ (4.5 eq), I$_2$ (4.5 eq) in MeOH or MeLi.LiBr, I$_2$ in Et$_2$O; (iii) Pd(PPh$_3$)$_4$, CuI in THF; (iv) 4-iodopyridine, Pd(PPh$_3$)$_4$, CuI in THF.*

Guided by this successful result, two different synthetic routes were attempted to obtain the pentayne **5** (Scheme 2-1). An initial target was 4-iodoethynylpyridine (**B**) from a one-pot desilylation/iodination or lithiation/iodination of 4-trimethylsilylethynylpyridine (**A**) (routes ii) avoiding the preparation of 4-ethynylpyridine due to its instability. The next step would be the reaction between the 4-iodoethynylpyridine and (PPh$_3$)Au-CC≡CC≡C≡C-Au(PPh$_3$) **6** (route iii). However, the formation of **B**, from either the lithiated or deprotected intermediate (route ii), was unfruitful because the starting material did not react. Another route was proposed where the trimethylsilyl end-capped pentayne **10** (described later in this chapter) could react with AuCl(PPh$_3$) to make the pentaynyl gold(I) complex (PPh$_3$)Au-C≡CC≡CC≡CC≡CC≡C-Au(PPh$_3$) (**C**) which could give compound **5** after addition of 4-iodopyridine (route iv). Unfortunately, this approach was unsuccessful because no trace of the pentaynyl gold(I) complex was found.

2.5. Trimethylsilyl ethynyl: a new and interesting anchor group

The trimethylsilyl ethynyl moiety (TMSE) (Me$_3$SiC≡C-) has attracted recent attention as a surface binding group in molecular electronics.[66,67] As noted in the introduction, the molecule-metal interaction has a significant effect on the conductance of single molecules.[62] The usual anchoring groups are thiol (SH)[68,69] or pyridine (C$_5$H$_4$N)[60] due to their good affinity with the gold electrode and their high junction formation probability.[8] The strength of the thiolate-gold bond is close to that of the gold-gold bond.[70]

However, thiolates also give rise to a range of Au-S-molecule conformations in which the sulfur atom resides in contact atop, as a bridge or in hollow sites of the Au surface.[71,72] Similarly, experimental data on the oligoynes Py-(C≡C)$_n$-Py (**1**, **2**, **3**) suggest different contact modes (Figure 2-2) as a result of the position of the pyridine on the surface. Either pyridine uses the nitrogen lone pair to make contact with the gold, denoted A contact (both pyridyl nitrogen atoms adsorbed atop on a flat gold terrace), or the pyridine binds to gold via the ring π electrons, denoted B and C contacts (one or both pyridyl group are located alongside a gold surface adatom).[1] There is interest, therefore, in alternative anchor groups which have fewer adsorption configurations, thereby simplifying the conductance histogram, or even displaying a single conductance value.

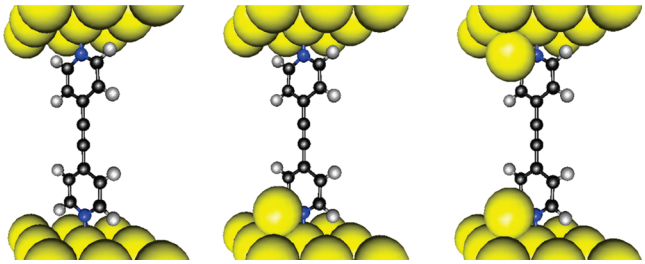

Figure 2-2. *Illustration of the different metal | molecule | metal configurations for molecule n =**1** in chart 1-1: A, B, C (from left to right) from reference.*[1]

In this context the novel TMSE linker gives a similar conductance value (1.2×10^{-5} G_0) to the A-type conductance mode of standard linkers.[73] The clean and well-resolved single molecule conductance is the signature of a single binding mode (C contact) induced by the steric bulk of the SiMe$_3$-C≡C- group limiting the accessible surface binding sites.[67] The narrow and sharp conductance peaks allow the measure of the conductance shift with greater certainty.

Recently, Hong et al.[74] reported that a terminal trimethylsilyl (TMS) moiety could be cleaved in situ with tetrabutylammonium fluoride (TBAF) to create Au-C σ-bonded OPE-based junctions (Figure 2-3). However, traces of electrolyte ions TBA^+ and F^- are detected around the noise level at $\approx 10^{-6}$ G_0. In this example, the acetylide R-C≡C$^-$, bonds directly to the gold surface. The use of terminal acetylenes, R-C≡CH, as a linker has also been

explored for Langmuir-Blodgett films and the conductance values compare with the usual linkers.[75]

Is it necessary to deprotect TMS in situ to do the conductance measurements? Osorio et al. prepared metal-molecule-gold nanoparticle assemblies using the Langmuir-Blodgett technique with OPEs containing a terminal carboxylate to bind the gold surface (at the bottom) and a terminal alkyne to interact with the gold nanoparticles (on top). Their I-V results from the CP-AFM technique proves that the Au-C σ-bond is robust and makes reliable top-contacts.[76] However, most of the OPE and oligoynes are more stable and more soluble with the TMS protecting group than the unprotected analogues.

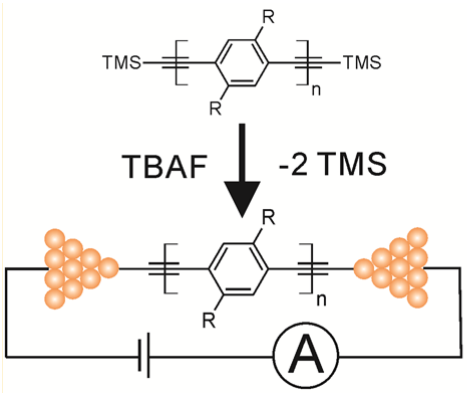

Figure 2-3. *Formation of the Au-C junction formation after deprotection in situ.*[74]

STM images of SAM of molecules containing the $Me_3SiC{\equiv}C$- end group on a gold surface[66,77] (Figure 2-4) show an interesting lateral repeat distance with hexagonal geometry, suggesting that the TMSE moiety stands upright on the gold. The silicon atom and the trimethyl groups appear to be important in the chemisorption because molecules having C instead of Si, or ^{i}Pr instead of CH_3, do not self-assemble on gold. The nature of the TMSE/gold interaction is not fully known, but it is assumed that the Si is activated by the electron-withdrawing C≡C unit and then reacts with the electron-donating Au to give a pentacoordinate complex.[66,77] Nevertheless, studies with TMSE contacted OPE and related organometallic complexes have demonstrated clean conductance profiles, encouraging further examination of this class of molecule.

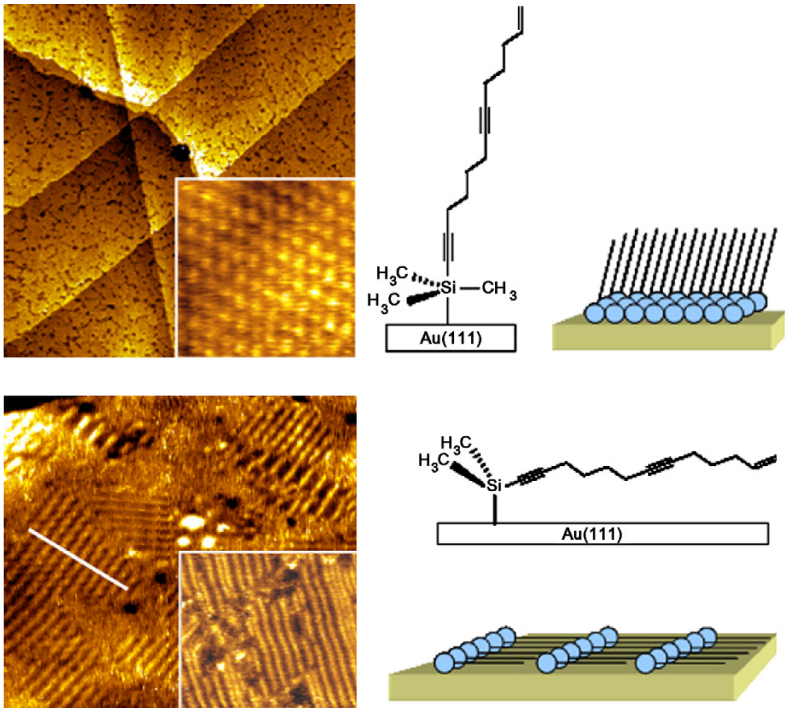

Figure 2-4. *STM image of a SAM of molecule containing $SiMe_3$-C≡C- (top right) and molecule containing $SiHMe_2$-C≡C- (bottom right). Schematic representation of the molecule absorbed on the gold surface (left) from reference.*[66]

Recently, new on-going computational and experimental work in collaboration with the groups of J. Ferrer (University of Oviedo), C. Lambert (University of Lancaster), R. Nichols (University of Liverpool) has revealed the key points of the TMSE│Au contact within molecular junction.[77] It was demonstrated that there is no significant re-arrangement of the local silicon geometry which seems to rule out the initial proposal of the five coordinate silicon. Indeed, the new calculations indicate a more subtle molecule-substrate interaction where the silicon centre stays in a tetrahedral configuration. In this configuration the methyl groups are oriented so that the silicon atom is as close as possible to the gold pyramid, i.e. the space between two methyl groups is directed towards the pyramid and close to it (Figure 2-5, a). Here, the contacts are made by a charge transfer interaction between the gold substrate and the silicon atom. Another position of TMSE is found where the methyl groups are in contact with the gold surface leading to a displacement of silicon from the surface and then generating a lower conductance (Figure 2-5, b). These findings are in excellent agreement with the data obtained by Fichou et al.

from SAMs of TMSE functionalised unsaturated hydrocarbons on flat gold substrates.[66,78-80]

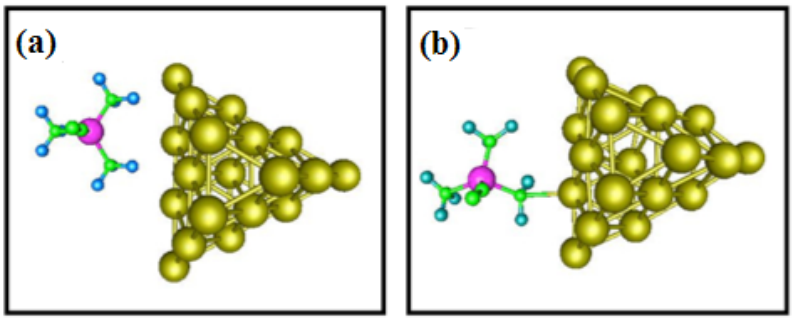

Figure 2-5. *A top view of the interaction between the -C≡CSiMe$_3$ group and the pyramid for the C contact (a) and the very poorly conductive configuration (b). Blue, green, magenta and yellow atoms represent hydrogen, carbon, silicon and gold atoms, respectively. Only the gold atoms of the pyramid are shown and not the underlying gold terrace.*

2.6. Synthesis of the trimethylsilyl-oligoynes

A series of oligoynes containing TMSE (Me$_3$SiC≡C-) as both end-cap and surface binding group have been explored (Chart 2-4).

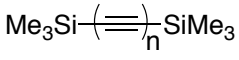

7 n = 2
8 n = 3
9 n = 4
10 n = 5

Chart 2-4. *Trimethylsilyl-oligoynes studied in this work.*

The oligoyne n = 2 (**7**) was purchased from commercial sources, whilst oligoynes **8 – 10** were synthesized using one of a number of different methods. Compound **8** was obtained from a procedure developed by Diederich.[12] A Hay coupling[65] of two molecules of propargyl alcohol gave the hexa-2,4-diyne-1,6-diol (**D**) which was tosylated to yield the intermediate hexa-2,4-diyne-1,6-diyl bis(4-methylbenzenesulfonate) (**E**). The next step involves a series of deprotonation and tele-eliminations in the presence of chlorotrimethylsilane (SiClMe$_3$) to give the target compound **8**.

For compound **9**, our synthetic route was different than those from the literature where a range of reactions from Hay coupling of the 4-trimethylsilylbuta-1,3-diyne[81] to a coupling between the 1,4-diiodobuta-1,3-diyne and trimethylsilyltin complex[81,82] were reported. The oligoyne **9** was prepared in very good yield (92%) from a hybrid Sonogashira reaction between 1-iodo-4-trimethylsilylbuta-1,3-diyne (**G**) and 4-trimethylsilylbuta-1,3-diyne (**F**) (Scheme 2-2). The terminal alkyne **F** was synthesized from the monodeprotection of **7** with MeLi·LiBr in dry ether, and protonated by ammonium chloride.[83] The iodinated compound **G** was formed from the same mono-lithiation of $Me_3Si\text{-}C{\equiv}CC{\equiv}C\text{-}SiMe_3$ followed by trapping with I_2. Here, the synthetic route chosen is safer because it does not use tin acetylides and the yield is better (92%) compared to the one from the literature (59%). The reaction was carried out overnight, at room temperature and the pure product **9** was obtained as a grey solid after column chromatography. Elemental analysis, NMR, MS and IR spectroscopies confirm the presence of the product **9.** ^{13}C NMR displayed the four quaternary carbons at δ_C 88.0, 87.8, 62.2, 62.1 ppm, the methyl from $SiMe_3$ at -0.6 along with the peak at 2044 cm^{-1} in the IR and MS (ASAP) with twice the molecular weight.

Finally, the longest oligoyne **10** was prepared from the intermediate 1,6-bis-triphenylphosphinegold-hexa-1,3,5-triyne **6** which allowed the carbon chain to be extended from n = 3 to n = 5 via a trans-metallation in presence of catalytic amount of palladium (5 mol%), copper (10 mol%) and 2 equivalents of the commercial 1-iodo-2-(trimethylsilyl)acetylene (Scheme 2-2). Although this trans-metallation route was not described before for the elaboration of oligoynes, it had been applied for the formation of oligo-ynyl carbon tricobalt clusters[84] and ruthenium complexes.[43,85] The reaction needed 20 h for completion and column chromatography gave **10** as a brown oil which was kept in the freezer to avoid its decomposition. The detection of the five carbons at δ_C 88.6, 87.7, 62.6, 62.2, 61.2 ppm in the ^{13}C NMR, the peak at 2027 cm^{-1} in the IR and the molecular peak at 266.0940 for $C_{16}H_{18}{}^{18}Si_2$ in HR-MS (ASAP) prove the formation of the oligoyne **10**. The yield was reasonable (38%) and although lower than that from the literature (61%) our synthetic route used, did not require any special precaution, in contrast with the one reported by DeCicco et al. for the manipulation of the diiodopolyyne and the tin-acetylides.[82]

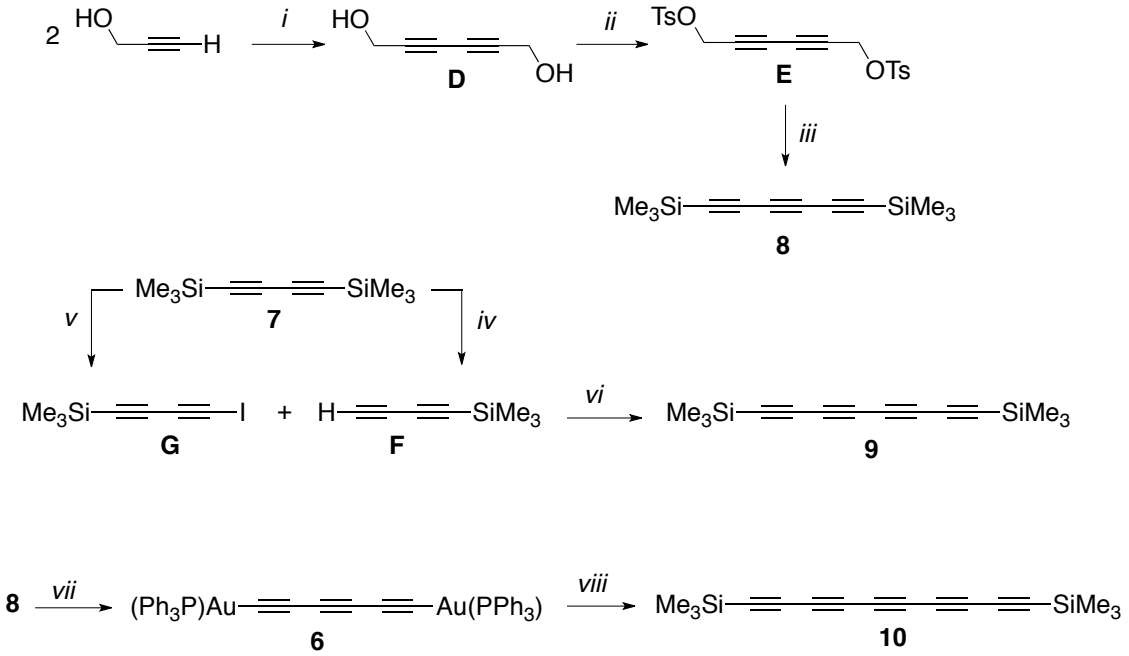

Scheme 2-2. *Synthetic routes for the trimethylsilyl end capped oligoynes. (i) TMEDA, CuCl, O_2 in acetone, rt, 3 h, 45%; (ii) 4-toluenesulfonyl chloride (2.2 eq), KOH in THF, rt, 2 h, 64%; (iii) $SiMe_3Cl$, n-BuLi (3.3 eq) in THF, -78 °C, 3 h, 25%; (iv) a. MeLi.LiBr in Et_2O, overnight, rt. b. NH_4Cl, 76% (v) a. MeLi.LiBr, rt, 4 h. b. I_2, rt, 22%; (vi) $Pd(PPh_3)_4$, CuI in Et_3N, rt, overnight, 92%; (vii) $AuCl(PPh_3)$, NaOH in MeOH, rt, 42 h, 96%; (viii) 1-iodo-2-(trimethylsilyl)acetylene, $Pd(PPh_3)_4$, CuI in THF, rt, 20 h, 38%.*

2.7. Molecular structures

Single crystals suitable for X-ray diffraction analysis were obtained for **6** (Figure 2-6). The compound **6** adopts a bow shape (P1-Au1-C1: 175.12° (15); C1-C2-C3: 175.9° (6)) and more interestingly the crystal packing is dictated by a bond between two adjacent gold atoms from two different molecules (Au-Au: 3.078 Å). This phenomenon is frequently found in molecules containing Au. The aurophilicity denominates the chemical bonding between two-coordinate gold(I) centres and the Au-Au distance is around 3.0 Å, significantly less than the sum of two van de Waals radii (3.7 Å).[86] This kind of Au-Au short intermolecular interactions is common with Au bearing phenylphosphine groups as ancillary ligands.[87,88] The PR_3 ligands open up the Au 5d shell which increase the stability and enhance the aurophilic interaction.[89]

a

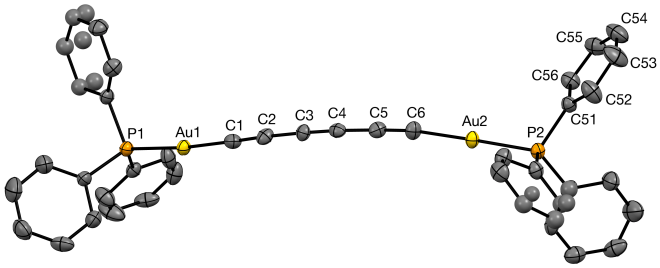

b

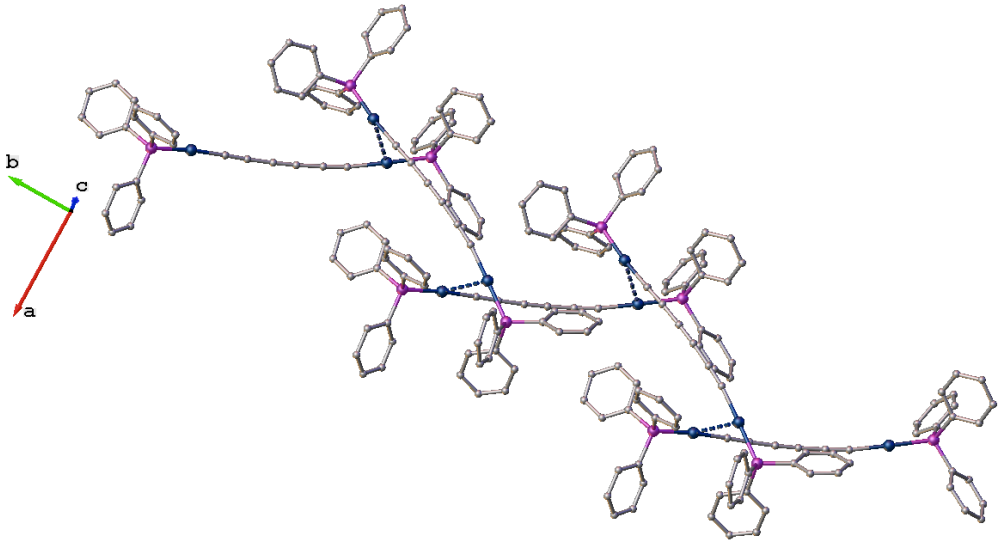

Figure 2-6. *X-ray molecular structure (a) and crystal packing diagram (b) of (PPh$_3$)Au-C≡CC≡CC≡C-Au(PPh$_3$)* ***6****.*

In **6** the bond lengths alternate from triple (C1-C2, C3-C4: 1.211(7) Å) to single (C2-C3, C4-C5: 1.371(7) Å) and are comparable with those of other of oligoynes.[3,4,8] The Au-P length (2.2784 (12) Å) is within the range of the one recorded in the literature (2.271 (1) Å).[85]

2.8. Synthesis of the arylynes

This section concerns the preparation of arylynes featuring -C≡C-$SiMe_3$ termini. The principal aim is to evaluate the influence of the phenyl ring inside an oligoyne core on the conductance. The phenyl ring can extend the conjugation of the oligoyne but also can disrupt it by rotation out of the oligoyne plane. Thus, molecules **11** and **12** (Chart 2-5) were synthesized from Sonogashira reactions[90] between the 1,4-diiodobenzene and trimethylsilylacetylene (TMSA), and between the 1,4-diiodobenzene and 4-trimethylsilylbuta-1,3-diyne, respectively, in good yields (80 and 92%).

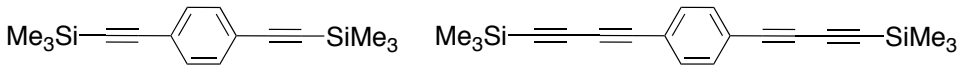

11 **12**

Chart 2-5. *Molecular structure of the arylynes **11** and **12**.*

The route chosen for the preparation of **12** is 2-steps shorter than the literature method where a free carbenoid intermediate undergoes a rearrangement to give the alkyne.[91] The carbenoid is the tetrabromide **H** (Chart 2-6) which reacts with 2.4 equivalents of n-BuLi to form **12**.

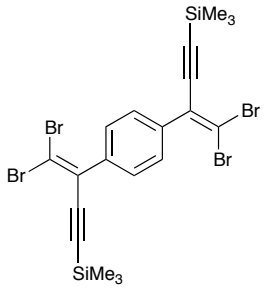

Chart 2-6. *Molecule **H** from reference.*[91]

The reaction was completed after just 2 h at room temperature and the pure compound **12**, obtained after filtration through a short silica pad, was analysed by IR, NMR and HR-MS.

2.9. Spectroscopy

2.9.1. Electronic absorbance

The UV-Vis electronic absorption spectra of oligoynes are a good tool for their characterization, giving information on the conjugation of the compound and the nature of the electronic transitions.

Table 2-1. *UV/Vis spectroscopic data (λ_{max}) for the TMS-(C≡C)$_n$-TMS, n = 2,3,4,5 in hexane solution.*

TMS-(C≡C)$_n$-TMS	λ_{max} (nm)	E_g (eV)
2 (**7**)	211	5.7
3 (**8**)	224	5.4
4 (**9**)	249	4.9
5 (**10**)	273	4.4

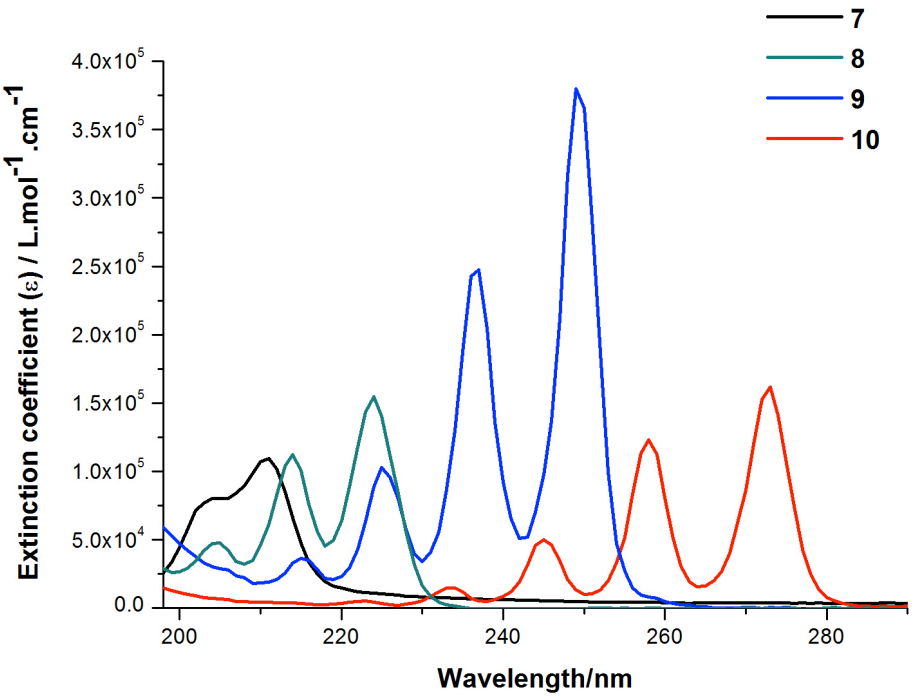

Figure 2-7. *UV-Vis spectra of the series TMS-(C≡C)$_n$-TMS; n = 2 (**7**), 3 (**8**), 4 (**9**), 5 (**10**) in hexane solution.*

The signature of the vibronic bands from the oligoynes series is in accord with their degree of conjugation (Figure 2-7). The spacing between the optical vibronic bands ($\Delta\nu$ = 1508 cm^{-1} to 2460 cm^{-1}) shows the expected vibrational band ν(C≡C). Moreover, a trend can be easily distinguished where the longest oligoyne displays a higher λ_{max} and the shortest oligoyne has the smallest λ_{max} (Table 2-1) which suggests that the HOMO-LUMO gap is reduced when the length of the oligoynes increases. The more conjugation there is, the more intense and red-shifted is the λ_{max} value. These results are in complete accord with similar oligoynes. [9,92] The value of λ_{max} (> 200 nm) is the result of promotion of electrons from the ground state π (HOMO) to the excited state π^* (LUMO).[93]

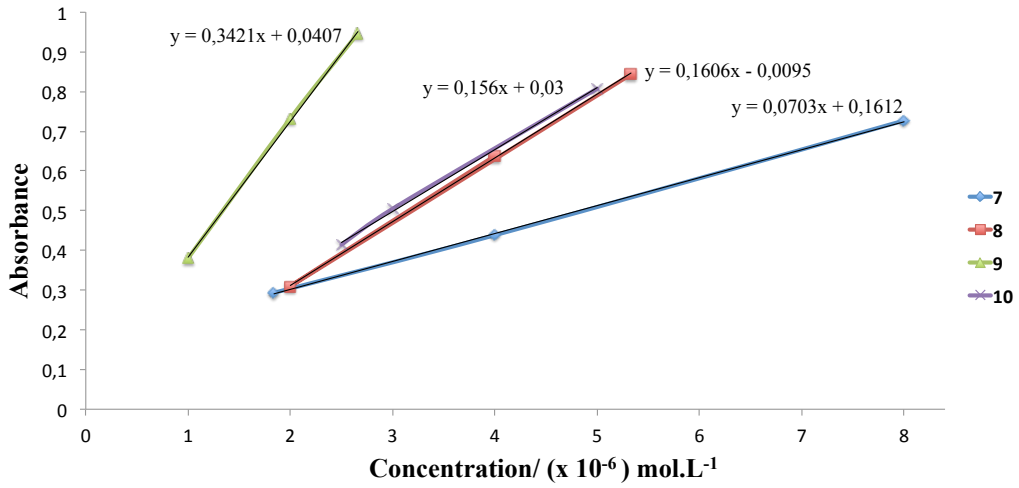

Figure 2-8. *Absorbance as a function of the concentration for the molecules 7 – **10** in hexane solution.*

Plots of the absorbance against the concentration of the series of trimethylsilyl-oligoynes (**7 - 10**) are recorded (Figure 2-8) and confirm the Beer-Lambert law where the absorbance follows a linear function with the extinction coefficient (ε) as the gradient of the line. The extinction coefficient increases with the length until it reaches n = 5 (**10**).

2.10. Scanning Tunneling Microscope (STM) measurements

Oligoynes have been explored experimentally as molecular wires.[1,2,8] Wang et al. pointed out the weak length dependence of the oligoynes on the conductance ($\beta = 0.6 \pm 0.3$ nm^{-1}),[1] essential for wiring purpose. A subsequent study on the same series using both STM-BJ and MCBJ gave a significantly different β value of 2.2 ± 0.2 nm^{-1} for the high-conductance peaks.[2] The wire-like behaviour has been confirmed by DFT calculations on the relaxed geometries of thiol capped oligoynes in a junction[94] which also demonstrate little dependence of the molecule length on conductance, along with the unchanged conductance under different bias. More recently, these results have been supported by theoretical calculations in Lambert's group.[95]

The *I*(*s*) technique developed by the Liverpool team[96,97] was used to measure the single molecule conductances of **4** and **7** - **10** using the procedures and conditions described in the Appendix A.

2.10.1. Pyridyl-oligoynes

Single molecule measurements have been carried out on the compound **4** (Py-$(C{\equiv}C)_3$-Py) which is a missing member of the homologous series of pyridyl-oligoynes studied previously.[1] STM using the *I(s)* technique was chosen for this measurement and revealed little difference between Py-$(C{\equiv}C)_4$-Py **3** ($0.51 \pm 0.11 \times 10^{-4}$ G_0) collected using STM-BJ, and **4** (4 ± 0.82 nS or $0.51 \pm 0.10 \times 10^{-4}$ G_0) (Figure 2-9). The break-off distance of 1.64 nm is not far from the length of the molecular model (N…N distance 1.54 nm) with the Au-N distances (ca. 0.21 nm), which shows that the molecule should be more or less perpendicular to the electrodes surfaces. This result can be attributed either to the charge transport which goes from tunnelling (**4** Py-$(C{\equiv}C)_3$-Py) to hopping (**3** Py-$(C{\equiv}C)_4$-Py), or to the method used knowing that STM-*I(s)* is softer. Despite the proximity between the two values, the conductance measurement is in agreement with those done previously which is reassuring for the experiment reproducibility.

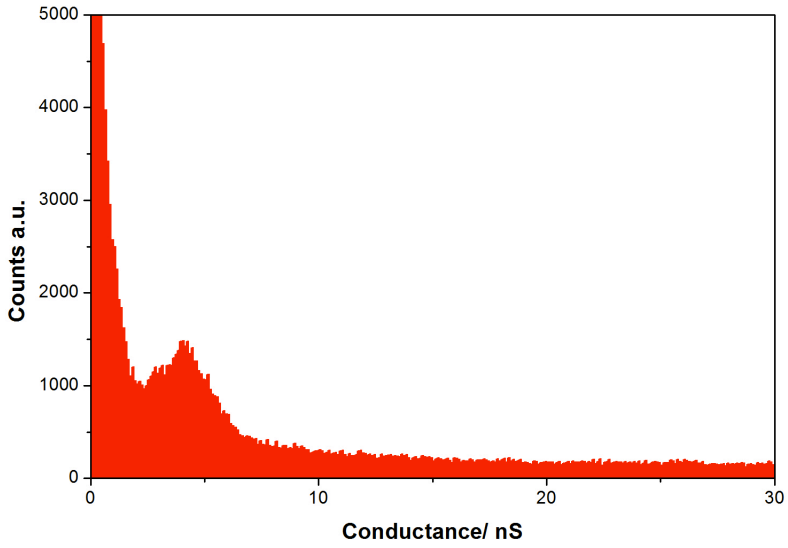

Figure 2-9. *Conductance histograms of **4** in mesitylene derived from the I(s) measurement (U_t = 0.6 V; I_0 =30 nA) with a conductance value (G = 4 ± 0.82 nS) and break-off distance of 1.64 nm.*

2.10.2. Trimethylsilyl-oligoynes

At this stage, the question that drives the project is "Do the oligoynes bearing -C≡C-$SiMe_3$ anchoring group display a low attenuation factor as reported previously in the literature for the series of pyridyl-oligoynes?"[1,8] In addition to this curiosity, the -C≡C-$SiMe_3$ terminus gave more reproducible conductance features due to the limited binding modes, which is a considerable advantage over the pyridyl anchoring group.

Single molecule measurements using the *I(s)* technique were used to explore the length dependence of the trimethylsilyl ethynyl contacted oligoynes and to compare the results with those from the pyridyl-oligoyne series. The conductance histograms (Figure 2-10) for compounds **7** - **10** (n = 2, n = 3, n = 4 and n = 5) show a clear single conductance value, in accord with the limited binding sites of the -C≡C-$SiMe_3$ linker on the gold surface.

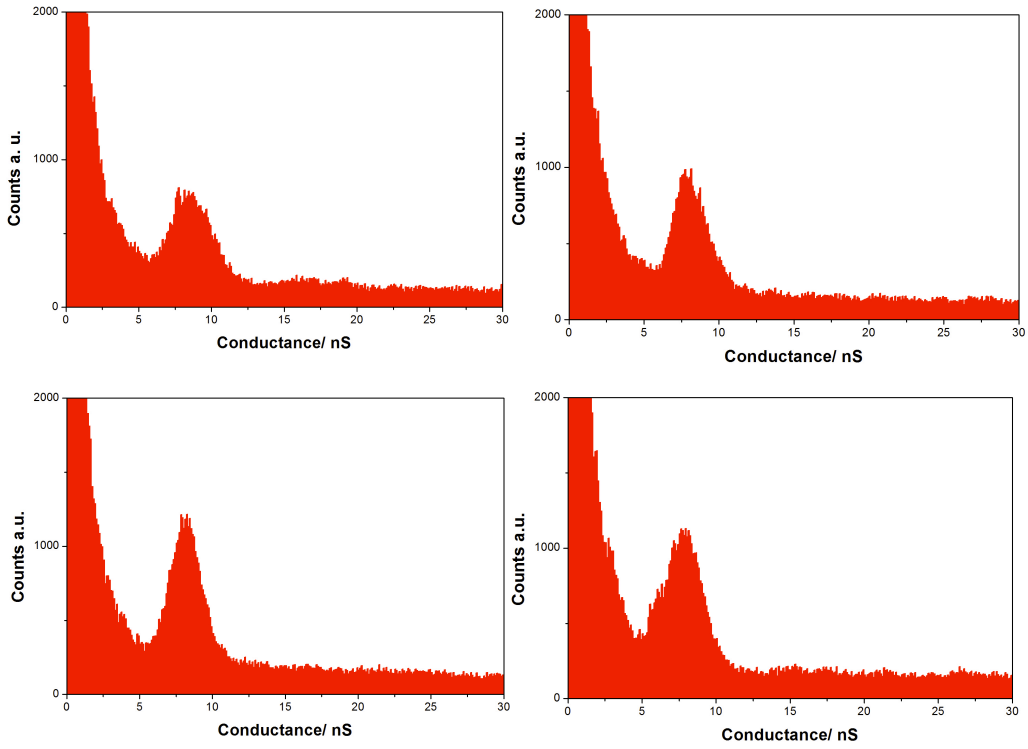

Figure 2-10. *I(s) conductance histograms of the compounds* ***7*** *-* ***10*** *in trichlorobenzene (TCB) (U_t = 0.6 V; I_0 = 30 nA).*

Table 2-2 *Summary of the conductance studies of compounds* ***7*** *-* ***10*** *obtained by the I(s) method in TCB based on ≥ 10000 individual traces.*

Compound	**Molecular length** *Si···Si d(nm)**	**Break-off Distance (nm)**	**Conductance (10^{-5} G_0)** *I(s) method in TCB*
7 *(n = 2)*	~ 0.74	1.20	11 ± 1.77
8 *(n = 3)*	~ 0.98	1.45	10.8 ± 1.37
9 *(n = 4)*	~ 1.22	1.65	1.05 ± 1.37
10 *(n = 5)*	~ 1.46	1.90	9.95 ± 1.61

**MM2 energy minimization*

The conductance values are almost independent of the molecule length and the conductance values of ca. 9.95 × 10^{-5} G_0 - 11 × 10^{-5} G_0 are comparable with the pyridyl-oligoynes (5 × 10^{-5} G_0 - 2 × 10^{-5} G_0)[1]. In addition, the attenuation coefficient, which represents the electronic coupling for a specific family of molecules, can be extracted and

is found to be low (β = 0.15 nm^{-1}) (Figure 2-11) and even lower than the initial literature value for the pyridyl-oligoynes (i.e. 0.6 ± 0.3 nm^{-1}).

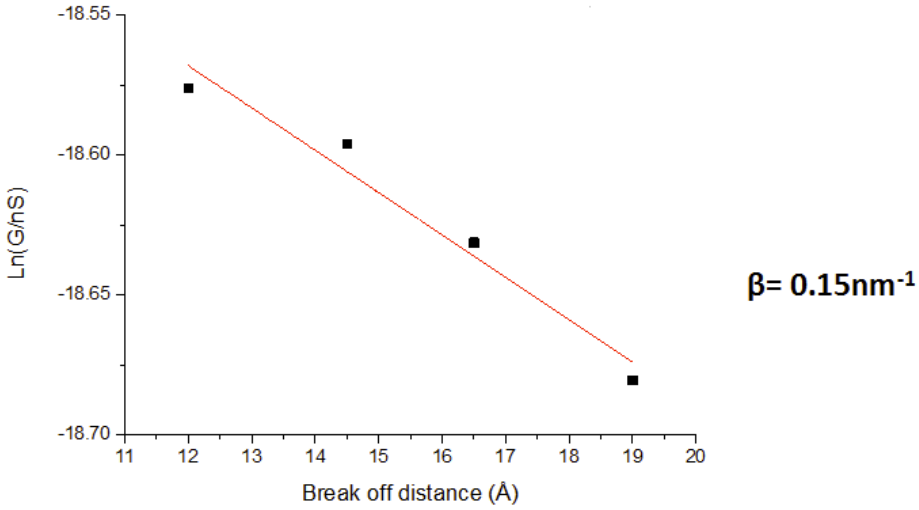

Figure 2-11. *Plot of Ln(G) versus the break-off distance with β value as the slope.*

2.10.3. Arylynes

While the single molecule measurement of the compound **11** is still under investigation, the compound **12** has been measured with the *I(s)* technique.

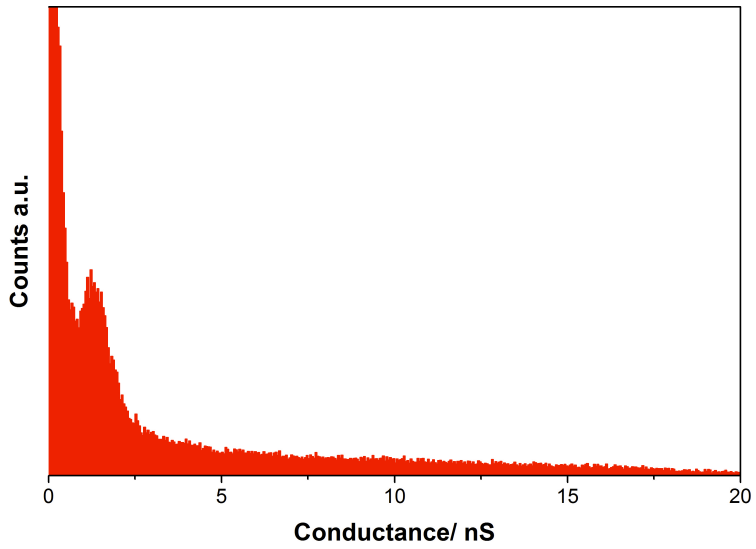

Figure 2-12. *Conductance histograms of **12** in mesitylene derived from the I(s) measurement (U_t = 0.6 V; I_0 = 10 nA) with a conductance value (G = 1.28 ± 0.26 nS) and break-off distance of 1.41 nm.*

A conductance decrease is observed from oligoynes to arylynes. In fact, the comparison of the conductance values for the butayne **9** (5.2 nS; preliminary result using *I(s)* technique in mesitylene) and the corresponding arylyne **12** (phenyl inserted in the backbone) (1.28 nS ± 0.26 nS) are remarkable. The lower conductance value for **12** can be explained by the conductance pathway disruption due to rotation of the phenyl out of the oligoyne plane but also because the conjugation between the oligoyne and the phenyl moieties is not fully delocalized.

2.11. Conclusion

Series of trimethylsilyl-oligoynes have been synthesized via new synthetic strategies such as the cross-coupling between the oligoynyl-gold and 1-iodo-2-(trimethylsilyl)acetylene to give the pentayne **10**. This new route was used in the elaboration of the 1,6-di(pyridine-4-yl)hexa-1,3,5-triyne **4**, important for the completion of the former pyridyl-oligoynes series.[1,2] Highlight has been done on the emerging TMSE anchoring group because of its single conductance value coming from the low contact (C-type), in agreement with its bulkiness. In addition, single molecule measurements on the oligoynes with TMSE linker suggest almost no conductance dependence on the length of these molecule that give an attenuation coefficient $\beta = 0.15$ nm^{-1}, in complete agreement with theory and previous experimental work. The addition of the phenyl in the oligoyne core (**12**) results to a decrease of the conductance compared to the oligoynes which can be explained by the disruption of the conjugation. Finally, on-going STM-BJ and *I(s)* experiments are being performed on the compounds **7** - **10** in mesitylene in order to confirm the low β value obtained.

2.12. Experimental

2.12.1. STM setup (Liverpool University)

A general setup of the STM using *I(s)* technique is described in the Appendix A.

2.12.2. General conditions for the syntheses

All reactions were carried out in oven-dried glassware under oxygen-free argon atmosphere (apart for the preparation of **D**). NEt_3 was purified by distillation from $CaSO_4$, other reaction solvents were purified and dried using Innovative Technology SPS-400 and if necessary degassed before use. $AuCl(PPh_3)$ was prepared following a previous method.[98] Other reagents were purchased commercially and used as received or prepared by variations on literature methods as described below. NMR spectra were recorded in deuterated solvent solutions on Bruker Avance 400 MHz and Varian VNMRS 700 MHz spectrometers and referenced against residual protio-solvent resonances after nuclei ($CHCl_3$: ^{1}H 7.26 ppm, ^{13}C 77.00 ppm; $(CD_3)_2CO$: ^{1}H 2.05 ppm, ^{13}C 29.84 and 206.26 ppm) or H_3PO_4 (^{31}P). In the NMR assignment, the phenyl rings associated with the PPh_3 are denoted Ph and Ar indicates any arylene group.

Mass spectra were measured on a Waters Xevo OtoFMs with an Atmospheric Solids Analysis Probe (ASAP). Electron ionization mass spectra were recorded on a Thermoquest Trace or Thermo-Finnigan DSQ. Infrared spectra were recorded on a Thermo 6700 spectrometer CH_2Cl_2 solution in a cell fitted CaF_2 windows. Elemental analyses were performed on a CE-400 Elemental Analyzer. UV spectra were recorded on a Thermo Scientific evolution 220 UV-Vis spectrophotometer. Single-crystal X-ray data were collected at 120(2) K on a Bruker SMART CCD 6000 (fine-focus sealed tube, graphite-monochromator).

2.12.3. Oligoynes

HC≡CC≡CSiMe$_3$; F[99]

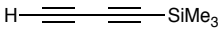

To an oven dried Schlenk flask containing dry Et_2O (200 mL), 1,4-bis(trimethylsilyl)buta-1,3-diyne (10.0 g, 51.4 mmol) and MeLi·LiBr (1.5 M in Et_2O) (34.3 mL, 51.4 mmol) was added. The reaction mixture was stirred overnight until the tan-brown solution became black. The solution of the lithiated intermediate was poured into a saturated aqueous solution of NH_4Cl in order to be quenched. The aqueous layer was separated, extracted with ether (2 × 100 mL) and the combined organic parts were extracted with water (100 mL) and brine (100 mL). The ether solution, dried over $MgSO_4$, was evaporated to dryness to give an orange liquid, which was purified by distillation (20 mbar, 40 °C) yielding **F** as a yellow liquid. Yield: 2.7 g, 76%. ^{1}H NMR (400 MHz, $CDCl_3$): δ 2.11 (s, 1H, *H*-C≡), 0.20 (s, 9H, Si*Me$_3$*) ppm. ^{13}C {^{1}H} NMR (101 MHz, $CDCl_3$): δ 87.4, 84.7, 68.3, 66.6 (*C*≡), -0.6 (Si*Me$_3$*) ppm. NMR data were in agreement with the literature.[99]

IC≡CC≡CSiMe$_3$; G[15]

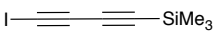

1,4-bis(trimethylsilyl)-1,3-butadiyne (0.90 g, 4.60 mmol) was dissolved in dry Et_2O (20 mL). MeLi·LiBr (1.5 M in Et_2O) (3.80 mL, 5.70 mmol) was added and the mixture was stirred at room temperature for 4 h. Iodine (1.50 g, 5.70 mmol) was added in portions until the brown color of the solution was stable and persistent. Sodium bisulfite saturated aqueous solution ($NaHSO_3$) (20 mL) was added to the mixture and the Et_2O layer was separated, and dried over $MgSO_4$. The solvent was removed under vacuum to give a brownish-colored oil, which was purified on a silica column. Elution with hexane gave a yellow oil which crystallized in air. Yield: 0.26 g, 22%. ^{1}H NMR (400 MHz, $CDCl_3$): δ 0.19 (s, 9H, Si*Me$_3$*) ppm. ^{13}C {^{1}H} NMR (101 MHz, $CDCl_3$): δ 88.7, 83.2, 78.9 (*C*≡), -0.5 (Si*Me$_3$*), -1.2 (I*C*≡) ppm. NMR data were in agreement with the literature.[15]

$HOH_2CC{\equiv}CC{\equiv}CCH_2OH$; D[12,81]

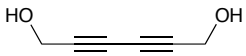

1) A 150 mL two-necked round-bottomed flask was charged with freshly distilled *N,N,N',N'*-tetramethylethylenediamine (TMEDA) (1.25 mL, 8.80 mmol) and CuCl (2.50 g, 20.5 mmol) in acetone (75 mL). The reaction mixture was stirred for 30 minutes under argon and the solid was allowed to settle, leaving a clear deep-blue solution of the CuCl-TMEDA catalyst used for the oxidative coupling reaction.

2) A 500 mL four-necked round-bottomed flask, equipped with a thermometer, gas inlet, condenser and a rubber septum was charged with a mixture of acetone (150 mL) and propargyl alcohol (14.5 mL, 250 mmol). The reaction mixture was stirred with a stream of oxygen for 30 minutes. The blue supernatant from the CuCl-TMEDA solution was added in 5 mL portions into the reaction vessel while the temperature of the reaction was kept constant at 30 °C; if necessary the reaction flask was cooled by an external bath.After the addition of the catalyst was completed, the reaction mixture was stirred for 3 h at room temperature whilst maintaining the stream of O_2 leading to a green solution with a yellowish precipitate. The solvent was removed under vacuo and the residue was dissolved in EtOAc (100 mL) and extracted with 3 M HCl (75 mL). The aqueous part was extracted a second time with EtOAc (100 mL) and the combined organic phases washed with brine (100 mL), separated and dried over $MgSO_4$. The solvent was removed by evaporation to give an off-white solid. Yield: 6.20 g, 45%. ^{1}H NMR (400 MHz, $(CD_3)_2CO$): δ 4.40 (br s, 2H, O-*H*), 4.27 (s, 4H, CH_2) ppm. ^{13}C {^{1}H} NMR (101 MHz, $(CD_3)_2CO$): δ 79.5, 69.0 (*C*≡), 50.8 (*C*H_2) ppm. NMR data were in agreement with the literature.[12]

$TsOH_2CC{\equiv}CC{\equiv}CCH_2OTs$; E[12]

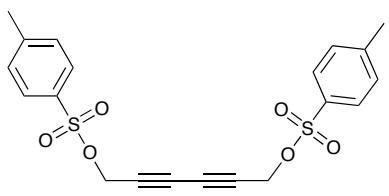

To a 250 mL round-bottomed flask charged with dry THF (120 mL) and **D** (5.0 g, 45 mmol) at - 30°C, was added 4-toluenesulfonyl chloride (TsCl) (18.8 g, 99 mmol). The

reaction mixture was stirred for 15 minutes before adding KOH (5.8 g, 104 mmol) aqueous solution (18 mL) in 1 mL portions. The yellow-orange solution was stirred for 2 h at -30 °C and for 2 h at room temperature until the solution changed to a deep-red colour. The suspension was poured into ice-water (400 mL) to give a glutinous brown precipitate which was filtered and washed with MeOH (200 mL) yielding a pink solid. Yield: 12.28 g, 64%. ^{1}H NMR (400 MHz, $CDCl_3$): δ 7.79 (d, J = 7.8 Hz, 4H, Ar), 7.36 (d, J = 7.8 Hz, 4H, Ar), 4.73 (s, 4H, C*H*$_2$), 2.45 (s, 6H, C*H*$_3$) ppm. ^{13}C {^{1}H} NMR (101 MHz, $CDCl_3$): δ 145.5, 132.6, 129.9, 128.1(*C*$_{Ar}$), 72.2, 71.9 (*C*≡), 57.4 (*C*H_2); 21.7 (*C*H_3) ppm. NMR data were in agreement with the literature.[12]

1,6-Bis(trimethylsilyl)hexa-1,3,5-triyne; 8[81]

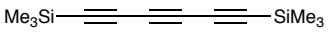

A 250 mL three-necked round-bottomed flask equipped with a dropping funnel, a rubber septum and a stopper was charged with dry and degassed THF (125 mL) and **E** (7.5 g, 18 mmol). The solution was stirred at – 78 °C and chlorotrimethylsilane ($SiMe_3Cl$) (9.7 g, 11.3 mL, 89 mmol), n-BuLi (2.5 M in hexane) (24 mL, 60 mmol) were added dropwise over 30 minutes. After 3 h stirring at - 78 °C, the reaction mixture was warmed to - 20 °C in order to add the NH_4Cl saturated aqueous solution (200 mL). The yellow solution was poured into the separating funnel and the combined organic layers washed with brine to give an orange solution which was dried over $MgSO_4$. The solvent was removed under reduced pressure and purified on a silica gel column eluted with hexane. The product was obtained as the first yellow band and was dried to yield an oil which solidified on standing. Yield: 1.0 g, 25%. ^{1}H NMR (400 MHz, $CDCl_3$): δ 0.20 (s, 18H, Si*Me*$_3$) ppm. ^{13}C {^{1}H} NMR (101 MHz, $CDCl_3$): δ 87.9, 87.4, 61.9 (*C*≡), -0.5 (Si*Me*$_3$) ppm. The NMR data were consistent with the literature.[81]

1,8-Bis(trimethylsilyl)-1,3,5,7-octatetrayne; 9 (Modified procedure[82])

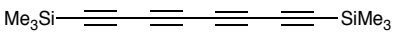

A Schlenk flask was charged with **G** (0.10 g, 0.40 mmol), **F** (90.0 μL, 0.07 g, 0.60 mmol), $Pd(PPh_3)_4$ (6.8 mg, 0.06 mmol) and CuI (1 mg, 0.06 mmol) in a degassed solution of NEt_3 (10 mL). The yellow solution was stirred overnight at room temperature, under argon. The mixture was purified on a silica gel column eluted with hexane to give the product as a yellow oil, which crystallized in air on standing. Yield: 0.09 g, 92%. ^{1}H NMR (400 MHz, $CDCl_3$): δ 0.20 (s, 18H, $SiMe_3$) ppm. ^{13}C {^{1}H} NMR (700 MHz, $CDCl_3$): δ 88.0, 87.8, 62.2, 62.1 (*C*≡), -0.6 ($SiMe_3$) ppm. MS (ASAP$^+$; *m/z*): 484.2 [2 M]$^+$. Anal. Calcd. for $C_{14}H_{18}Si_2$: C, 69.35; H, 7.48; found C, 69.25; H, 7.56. IR (CH_2Cl_2): ν(C≡C-$SiMe_3$) 2044 (s); 2150, 2016 cm^{-1}. The NMR data are constituent with the literature.[82]

(PPh_3)Au-C≡CC≡CC≡C-Au(PPh_3); 6

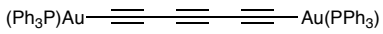

A 250 mL two-necked round-bottomed flask was charged with 1,6-bis(trimethylsilyl)hexa-1,3,5-triyne **8** (0.22 g, 1.0 mmol), $AuCl(PPh_3)$ (0.94 g, 1.9 mmol) and NaOH (0.78 g, 20 mmol) dissolved in MeOH (150 mL). The reaction mixture was stirred at room temperature for 42 h. The bright yellow suspension was filtered and the solvent was removed under vacuum to give a pale yellow solid. Yield: 0.95 g, 96%. Crystals suitable for X-ray diffraction were obtained by evaporation of a deuterated chloroform solution. ^{1}H NMR (400 MHz, $CDCl_3$): δ 7.52 - 7.41 (m, 30H, Ph) ppm. ^{31}P{^{1}H} NMR (400 MHz, $CDCl_3$): 41.2 ppm. ^{13}C {^{1}H} NMR (101 MHz, $CDCl_3$): δ 134.2 (d, J = 13.8 Hz, Ph), 131.6 (Ph), 129.7 (Ph), 129.1 (d, J = 11.4 Hz, Ph), the other quaternary ^{13}C are not seen. MS (MALDI-TOF; *m/z*): 990.0 [M]$^+$. HR-ESI$^+$-MS: *m/z* calcd for $C_{42}H_{30}P_2{}^{197}Au_2H$ 991.1257; found 991.1232. Calcd. for $C_{42}H_{30}Au_2P_2$: C, 50.93; H, 3.05; found C, 50.82; H, 2.97. IR (CH_2Cl_2): ν(C≡C-Au) 2112 (br); 2691 (s) cm^{-1}. Crystal data for **6**: $C_{42}H_{30}Au_2P_2$, M = 990.53, monoclinic, space group C2/c, *a* = 33.5370(10) Å, *b* = 14.2261(7) Å, *c* = 24.0838(8) Å, *β* = 134.018(2) °, *U* = 8263.0(5) Å^3, F(000) = 3760, Z = 8, D_C = 1.592 mg/mm^3, μ = 7.196 mm^{-1}; 58717 reflections were

collected , yielding 9975 unique data (R_{merg} = 0.0997). Final $wR_2(F^2)$ = 0.0491 for all data (409 refined parameters), conventional R_1 (F) = 0.0326 with I ≥ 2σ, GOF = 0.961.

1,10-Bis(trimethylsilyl)-1,3,5,7,9-decapentayne; 10 (Modified procedure[82])

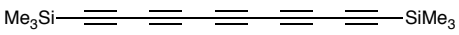

To a solution of degassed THF (90 mL) was added **6** (0.90 g, 0.91 mmol), 1-iodo-2-(trimethylsilyl)acetylene (52 mg, 0.28 mL, 1.82 mmol), $Pd(PPh_3)_4$ (52 mg, 0.04 mmol) and CuI (17 mg, 0.09 mmol). The solution was stirred at room temperature for 20 h under argon, dried and then the reaction mixture purified on a silica gel column eluted with hexane. The first band was collected giving a yellow solution, which was dried to yield a brown oil. Yield: 92 mg, 38%. ^{1}H NMR (400 MHz, $CDCl_3$): δ 0.21 (s, 18H, Si*Me$_3$*) ppm. ^{13}C {^{1}H} NMR (101 MHz, $CDCl_3$): δ 88.6, 87.7, 62.6, 62.2, 61.2 (*C*≡), -0.6 (Si*Me$_3$*) ppm. MS (ASAP$^+$; m/z): 266.1 $[M]^+$. HR-(ASAP$^+$)-MS m/z: calcd for $C_{16}H_{18}{}^{28}Si_2$ 266.0947; found 266.0940. IR (CH_2Cl_2): ν(C≡C-$SiMe_3$) 2027 (s); 2102 (s). The NMR data were constituent with the literature.[82]

1,6-Di(pyridin-4-yl)hexa-1,3,5-triyne; 4

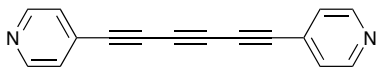

To a solution of degassed THF (5 mL) was added **6** (500 mg, 0.5 mmol), 4-iodopyridine (31.5 mg, 0.15 mmol), $Pd(PPh_3)_4$ (3 mg, 0.002 mmol) and CuI (1 mg, 0.005 mmol). The yellow solution was stirred for 2 days at room temperature, dried and purified on silica gel column eluted with CH_2Cl_2:acetone (2:1 v/v) to give an off-white fluffy solid. Yield: 52 mg, 46%. ^{1}H NMR (400 MHz, $CDCl_3$): δ 8.61 (d, J = 5.9 Hz, 4H, Ar), 7.37 (d, J = 5.9 Hz, 4H, Ar) ppm. ^{13}C {^{1}H} NMR (101 MHz, $CDCl_3$): δ 149.9, 128.9, 126.3 (C_{Ar}), 77.9, 76.2, 67.3 (*C*≡) ppm. MS (ASAP$^+$; m/z): 229.06 $[M + H]^+$. HR-(ASAP$^+$)-MS m/z: Calcd for $C_{16}H_8N_2$ 228.0687; found 228.0698. IR (CH_2Cl_2): ν(C≡C) 2186 (s); 2691 (s) cm^{-1}.

2.12.4 Arylynes

1,4-Bis(2-trimethylsilylethynyl)benzene; 11[100]

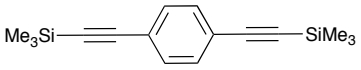

A Schlenk flask charged with trimethylsilylacetylene (314 mg, 0.45 mL, 3.2 mmol), 1,4-diiodobenzene (500 mg, 1.50 mmol), $Pd(PPh_3)_4$ (86 mg, 0.07 mmol) and CuI (28 mg, 0.15 mmol) in degassed NEt_3 (25 mL) was stirred overnight at room temperature. The black solution was evaporated to dryness in vacuo and purified on a silica gel plug eluted with hexane. The solvent was removed to give white flakes. Yield: 320 mg, 80%. ^{1}H NMR (400 MHz, $CDCl_3$): δ 7.38 (s, 4H, Ar); 0.24 (s, 18H, Si*Me*$_3$) ppm. ^{13}C NMR {^{1}H} (101 MHz, $CDCl_3$): δ 131.7, 123.1 (C_{Ar}), 104.5, 96.3 (C≡); -0.1 (Si*Me*$_3$) ppm. The NMR data were consistent with the literature.[100]

1,4-Bis(4-trimethylsilyl-1,3-butadiynyl)benzene; 12 (Modified procedure [91])

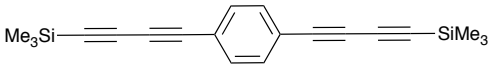

A 100 mL two-necked round-bottomed flask charged with **F** (730 mg, 900 μL, 6 mmol), 1,4-diiodobenzene (0.99 g, 3 mmol), $Pd(PPh_3)_4$ (0.17 g, 0.15 mmmol) and CuI (57 mg, 0.3 mmol) in degassed NEt_3 (50 mL) was stirred under argon at room temperature for 2 h. The mixture was evaporated to dryness in vacuo and purified on a short silica gel pad eluted with hexane to give **12** as a fluffy white solid. Yield: 0.88 g, 92%. ^{1}H NMR (400 MHz, $CDCl_3$): δ 7.41 (s, 4H, Ar); 0.23 (s, 18H, Si*Me*$_3$) ppm. ^{13}C NMR {^{1}H} (101 MHz, $CDCl_3$): δ 132.6, 122.3 (C_{Ar}); 92.4, 87.5, 76.7, 75.9 (C≡); -0.5 (Si*Me*$_3$) ppm. MS (ASAP$^+$) m/z: 318.1 $[M]^+$. HR-(ASAP$^+$)-MS m/z: calcd for $C_{20}H_{22}Si_2$ 318.1260; found 318.1259. The NMR data were consistent with the literature.[91]

2.13. References

(1) Wang, C.; Batsanov, A. S.; Bryce, M. R.; Martin, S.; Nichols, R. J.; Higgins, S. J.; García-Suárez, V. M.; Lambert, C. J. *J. Am. Chem. Soc.* **2009**, *131*, 15647.

(2) Moreno-García, P.; Gulcur, M.; Manrique, D. Z.; Pope, T.; Hong, W.; Kaliginedi, V.; Huang, C.; Batsanov, A. S.; Bryce, M. R.; Lambert, C.; Wandlowski, T. *J. Am. Chem. Soc.* **2013**, *135*, 12228.

(3) Chalifoux, W. A.; Tykwinski, R. R. *Nature Chemistry* **2010**, *2*, 967.

(4) Szafert, S.; A, G. J. *Chem. Rev.* **2006**, *106*, PR1.

(5) Meyer, W. E.; Amoroso, A. J.; Horn, C. R.; Jaeger, M.; A, G. J. *Organometallics* **2001**, *20*, 1115.

(6) Mohr, W.; Stahl, J.; Hampel, F.; A, G. J. *Chem. Eur. J.* **2003**, *9*, 3324.

(7) Paul, F.; Lapinte, C. *Coordination Chemistry Reviews* **1998**, *178*, 431.

(8) Gulcur, M.; Moreno-García, P.; Zhao, X.; Baghernejad, M.; Batsanov, A. S.; Hong, W.; Bryce, M. R.; Wandlowski, T. *Chem. Eur. J.* **2014**, *20*, 4653.

(9) Eisler, S.; Slepkov, A. D.; Elliott, E.; Luu, T.; McDonald, R.; Hegmann, F. A.; Tykwinski, R. R. *J. Am. Chem. Soc.* **2005**, *127*, 2666.

(10) Jones, E. R. H.; Lee, H. H.; Whiting, M. C. *J. Chem. Soc.* **1960**, 3483.

(11) Johnson, T.; Walton, D. *Tetrahedron* **1972**, *28*, 5221.

(12) Grösser, T.; Hirsch, A. *Angew. Chem. Int. Ed. Engl.* **1993**, *32*, 1340.

(13) Pålsson, L.-O.; Wang, C.; Batsanov, A. S.; King, S. M.; Beeby, A.; Monkman, A. P.; Bryce, M. R. *Chem. Eur. J.* **2010**, *16*, 1470.

(14) Wang, C.; Batsanov, A. S.; West, K.; Bryce, M. R. *Org. Lett.* **2008**, *10*, 3069.

(15) Nakamura, K.; Fujimoto, T.; Takara, S.; Sugiura, K.-I.; Miyasaka, H.; Ishii, T.; Yamashita, M.; Sakata, Y. *Chem. Lett.* **2003**, *32*, 694.

(16) Dembinski, R.; Bartik, T.; Bartik, B.; Jaeger, M.; Gladysz, J. A. *J. Am. Chem. Soc.* **2000**, *122*, 810.

(17) Rubin, Y.; Lin, S. S.; Knobler, C. B.; Anthony, J.; Boldi, A. M.; Diederich, F. *J. Am. Chem. Soc.* **1991**, 6943.

(18) Weisbach, N.; Baranová, Z.; Gauthier, S.; Reibenspies, J. H.; Gladysz, J. A. *Chem. Commun.* **2012**, *48*, 7562.

(19) Movsisyan, L. D.; Kondratuk, D. V.; Franz, M.; Thompson, A. L.; Tykwinski, R. R.; Anderson, H. L. *Org. Lett.* **2012**, *14*, 3424.

(20) West, K.; Wang, C.; Batsanov, A. S.; Bryce, M. R. *Org. Biomol. Chem.* **2008**, *6*, 1934.

(21) Lin, V. S. Y.; Radu, D. R.; Han, M.-K.; Deng, W.; Kuroki, S.; Shanks, B. H.; Pruski, M. *J. Am. Chem. Soc.* **2002**, *124*, 9040.

(22) Jenny, N. M.; Mayor, M.; Eaton, T. R. *Eur. J. Org. Chem.* **2011**, *26*, 4965.

(23) Tour, J. M. *Chem. Rev.* **1996**, *96*, 537.

(24) Bunz, U. H. F. *Chem. Rev.* **2000**, *100*, 1605.

(25) Zhao, X.; Huang, C.; Gulcur, M.; Batsanov, A. S.; Baghernejad, M.; Hong, W.; Bryce, M. R.; Wandlowski, T. *Chem. Mater.* **2013**, *25*, 4340.

(26) Xiao, X.; Nagahara, L. A.; Rawlett, A. M.; Tao, N. *J. Am. Chem. Soc.* **2005**, *127*, 9235.

(27) Wei, Z.; Li, T.; Jennum, K.; Santella, M.; Bovet, N.; Hu, W.; Nielsen, M. B.; Bjørnholm, T.; Solomon, G. C.; Laursen, B. W.; Nørgaard, K. *Langmuir* **2012**, *28*, 4016.

(28) Tour, J. M. *Acc. Chem. Res.* **2000**, *33*, 791.

(29) Francke, V.; Mangel, T.; Müllen, K. *Macromolecules* **1998**, *31*, 2447.

(30) Bumm, L. A.; Arnold, J. J.; Cygan, M. T.; Dunbar, T. D.; Burgin, T. P.; Jones, L., II; Allara, D. L.; Tour, J. M.; Weiss, P. S. *Science* **1996**, *271*, 1705.

(31) Schumm, J. F.; Pearson, D. L.; Tour, J. M. *Angew. Chem. Int. Ed. Engl.* **1994**, *33*, 1360.

(32) Huang, S.; Tour, J. M. *J. Am. Chem. Soc.* **1999**, *121*, 4908.

(33) Costuas, K.; Rigaut, S. *Dalton Trans.* **2011**, *40*, 5643.

(34) Bruce, M. I.; Low, P. J. *Advances in Organometallic Chemistry* **2004**, *50*, 179.

(35) Rigaut, S.; Perruchon, J.; Le Pichon, L.; Touchard, D.; Dixneuf, P. H. *Journal of Organometallic Chemistry* **2003**, *670*, 37.

(36) Bruce, M. I.; Hall, B. C.; Kelly, B. D.; Low, P. J.; Skelton, B. W.; White, A. H. *J. Chem. Soc., Dalton Trans.* **1999**, *21*, 3719.

(37) Bruce, M. I.; Kelly, B. D.; Skelton, B. W.; White, A. H. *Journal of Organometallic Chemistry* **2000**, *604*, 150.

(38) Fox, M. A.; Le Guennic, B.; Roberts, R. L.; Brue, D. A.; Yufit, D. S.; Howard, J. A. K.; Manca, G.; Halet, J.-F.; Hartl, F.; Low, P. J. *J. Am. Chem. Soc.* **2011**, *133*, 18433.

(39) Khairul, W. M.; Fox, M. A.; Schauer, P. A.; Yufit, D. S.; Albesa-Jové, D.; Howard, J. A. K.; Low, P. J. *Dalton Trans.* **2010**, *39*, 11605.

(40) Weng, W.; Bartik, T.; Johnson, M. T.; Arif, A. M.; Gladysz, J. A. *Organometallics* **1995**, *14*, 889.

(41) Brady, M.; Weng, W.; Zhou, Y.; Seyler, J. W.; Amoroso, A. J.; Arif, A. M.; Böhme, M.; Frenking, G.; Gladysz, J. A. *J. Am. Chem. Soc.* **1997**, *119*, 775.

(42) Bruce, M. I.; Ellis, B. G.; Low, P. J.; Skelton, B. W.; White, A. H. *Organometallics* **2003**, *22*, 3184.

(43) Antonova, A. B.; Bruce, M. I.; Ellis, B. G.; Gaudio, M.; Humphrey, P. A.; Jevric,

M.; Melino, G.; Nicholson, B. K.; Perkins, G. J.; Skelton, B. W.; Stapleton, B.; White, A. H.; Zaitseva, N. N. *Chem. Commun.* **2004**, *8*, 960.

(44) Le Narvor, N.; Toupet, L.; Lapinte, C. *J. Am. Chem. Soc.* **1995**, *117*, 7129.

(45) Guillemot, M.; Toupet, L.; Lapinte, C. *Organometallics* **1998**, *17*, 1928.

(46) Bruce, M. I.; Costuas, K.; Davin, T.; Halet, J.-F.; Kramarczuk, K. A.; Low, P. J.; Nicholson, B. K.; Perkins, G. J.; Roberts, R. L.; Skelton, B. W.; Smith, M. E.; White, A. H. *Dalton Trans.* **2007**, *46*, 5387.

(47) Bruce, M. I.; Kramarczuk, K. A.; Skelton, B. W.; White, A. H. *Journal of Organometallic Chemistry* **2010**, *695*, 469.

(48) Fitzgerald, E. C.; Brown, N. J.; Edge, R.; Helliwell, M.; Roberts, H. N.; Tuna, F.; Beeby, A.; Collison, D.; Low, P. J.; Whiteley, M. W. *Organometallics* **2012**, *31*, 157.

(49) Bruce, M. I.; Low, P. J.; Costuas, K.; Halet, J.-F.; Best, S. P.; Heath, G. A. *J. Am. Chem. Soc.* **2000**, *122*, 1949.

(50) Gao, L.-B.; Zhang, L.-Y.; Shi, L.-X.; Chen, Z.-N. *Organometallics* **2005**, *24*, 1678.

(51) Bruce, M. I.; Costuas, K.; Ellis, B. G.; Halet, J.-F.; Low, P. J.; Moubaraki, B.; Murray, K. S.; Ouddaï, N.; Perkins, G. J.; Skelton, B. W.; White, A. H. *Organometallics* **2007**, *26*, 3735.

(52) Semenov, S. N.; Blacque, O.; Fox, T.; Venkatesan, K.; Berke, H. *J. Am. Chem. Soc.* **2010**, *132*, 3115.

(53) Reimers, J. P.; Hush, N. S. *Chemical Physics* **1989**, *134*, 323.

(54) Taube, H.; Richardson, D. E. *Coordination Chemistry Reviews* **1984**, *60*, 107.

(55) Creutz, C.; Taube, H. *J. Am. Chem. Soc.* **1973**, *95*, 1086.

(56) Marcus, R. A.; Sutin, N. *Comments on inorganic chemistry* **1986**, *5*, 119.

(57) Brunschwig, B. S.; Creutz, C.; Sutin, N. *Chem. Soc. Rev.* **2002**, *31*, 168.

(58) Frapper, G.; Kertesz, M. *Inorg. Chem.* **1993**, *32*, 732.

(59) Re, N.; Sgamellotti, A.; Floriani, C. *J. Chem. Soc., Dalton Trans.* **1998**, *15*, 2521.

(60) Xu, B.; Tao, N. J. *Science* **2003**, *301*, 1221.

(61) Kamenetska, M.; Quek, S. Y.; Whalley, A. C.; Steigerwald, M. L.; Choi, H. J.; Louie, S. G.; Nuckolls, C.; Hybertsen, M. S.; Neaton, J. B.; Venkataraman, L. *J. Am. Chem. Soc.* **2010**, *132*, 6817.

(62) Hong, W.; Manrique, D. Z.; Moreno-García, P.; Gulcur, M.; Mishchenko, A.; Lambert, C. J.; Bryce, M. R.; Wandlowski, T. *J. Am. Chem. Soc.* **2012**, *134*, 2292.

(63) Lee, C. K. Y.; Groneman, J. L.; Turner, P.; Rendina, L. M.; Harding, M. M. *Tetrahedron* **2006**, *62*, 4870–4878.

(64) Champness, N. R.; Khlobystov, A. N.; Majuga, A. G.; Schröder, M.; Zyk, N. V. *Tetrahedron Letters* **1999**, *40*, 5413.

(65) Hay, A. *J. Org. Chem.* **1962**, *27*, 3320.

(66) Katsonis, N.; Marchenko, A.; Fichou, D.; Barrett, N. *Surface Science* **2008**, *602*, 9.

(67) Marqués-González, S.; Yufit, D. S.; Howard, J. A. K.; Martin, S.; Osorio, H. M.; García-Suárez, V. M.; Nichols, R. J.; Higgins, S. J.; Cea, P.; Low, P. J. *Dalton Trans.* **2013**, *42*, 338.

(68) Ashwell, G. J.; Urasinska, B.; Wang, C.; Bryce, M. R.; Grace, I.; Lambert, C. J. *Chem. Commun.* **2006**, *45*, 4706.

(69) Basch, H.; Ratner, M. A. *J. Chem. Phys.* **2004**, *120*, 5771.

(70) Krüger, D.; Fuchs, H.; Rousseau, R.; Marx, D.; Parrinello, M. *Phys. Rev. Lett.* **2002**, *89*, 186402.

(71) Ulrich, J.; Esrail, D.; Pontius, W.; Venkataraman, L.; Millar, D.; Doerrer, L. H. *J.*

Phys. Chem. B **2006**, *110*, 2462.

(72) Basch, H.; Cohen, R.; Ratner, M. A. *Nano Lett.* **2005**, *5*, 1668.

(73) Pera, G.; Martin, S.; Ballesteros, L. M.; Hope, A. J.; Low, P. J.; Nichols, R. J.; Cea, P. *Chem. Eur. J.* **2010**, *16*, 13398.

(74) Hong, W.; Li, H.; Liu, S.-X.; Fu, Y.; Li, J.; Kaliginedi, V.; Decurtins, S.; Wandlowski, T. *J. Am. Chem. Soc.* **2012**, *134*, 19425.

(75) Ballesteros, L. M.; Martin, S.; Momblona, C.; Marqués-González, S.; López, M. C.; Nichols, R. J.; Low, P. J.; Cea, P. *J. Phys. Chem. C* **2012**, *116*, 9142.

(76) Osorio, H. M.; Cea, P.; Ballesteros, L. M.; Gascón, I.; Marqués-González, S.; Nichols, R. J.; Pérez-Murano, F.; Low, P. J.; Martin, S. *Journal of Materials Chemistry C* **2014**, *2*, 7348.

(77) Ferrer, J.; Garcia-Suarez, C.; Lambert, C.; Nichols, R. J. *Private communication*

(78) Katsonis, N.; Marchenko, A.; Taillemite, S.; Fichou, D.; Chouraqui, G.; Aubert, C.; Malacria, M. *Chem. Eur. J.* **2003**, *9*, 2574.

(79) Petrov, E. G.; Marchenko, A.; Kapitanchuk, O. L.; Katsonis, N.; Fichou, D. *Molecular Crystals and Liquid Crystals* **2014**, *589*, 3.

(80) Nion, A.; Katsonis, N.; Marchenko, A.; Aubert, C.; Fichou, D. *New J. Chem.* **2013**, *37*, 2261.

(81) Gao, K.; Goroff, N. S. *J. Am. Chem. Soc.* **2000**, *122*, 9320.

(82) DeCicco, R. C.; Black, A.; Li, L.; Goroff, N. S. *Eur. J. Org. Chem.* **2012**, *25*, 4699.

(83) Fiandanese, V.; Bottalico, D.; Marchese, G.; Punzi, A. *Tetrahedron Letters* **2003**, *44*, 9087.

(84) Antonova, A. B.; Bruce, M. I.; Humphrey, P. A.; Gaudio, M.; Nicholson, B. K.; Scoleri, N.; Skelton, B. W.; White, A. H.; Zaitseva, N. N. *Journal of*

Organometallic Chemistry **2006**, *691*, 4694.

(85) Bruce, M. I.; Büschel, S.; Cole, M. L.; Scoleri, N.; Skelton, B. W.; White, A. H.; Zaitseva, N. N. *Inorganica Chimica Acta* **2012**, *382*, 6.

(86) Schmidbaur, H., *Gold Bulletin* **2000**, *33*, 3.

(87) Bruce, M. I.; Duffy, D. N. *Aust J Chem* **1986**, *39*, 1697.

(88) Li, D.; Hong, X.; Che, C.-M.; Lo, W.-C.; Peng, S.-M. *J. Chem. Soc., Dalton Trans.* **1993**, 2929.

(89) *Gold chemistry: Application and Future direction in the Life Sciences*; Mohr, F., Ed.; Wiley-VCH; Weinheim; **2009**.

(90) Sonogashira, K.; Tohda, Y.; Hagihara, N. *Tetrahedron Letters* **1975**, *50*, 4467.

(91) Shi Shun, A. L. K.; Chernick, E. T.; Eisler, S.; Tykwinski, R. R. *J. Org. Chem.* **2003**, *68*, 1339.

(92) Tykwinski, R. R.; Chalifoux, W.; Eisler, S.; Lucotti, A.; Tommasini, M.; Fazzi, D.; Del Zoppo, M.; Zerbi, G. *Pure Appl. Chem.* **2010**, *82*, 891.

(93) Slepkov, A. D.; Hegmann, F. A.; Eisler, S.; Elliott, E.; Tykwinski, R. R. *J. Chem. Phys.* **2004**, *120*, 6807.

(94) Crljen, Ž.; Baranović, G. *Phys. Rev. Lett.* **2007**, *98*, 116801.

(95) Al-Backri, A.; Zólyomi, V.; Lambert, C. J. *J. Chem. Phys.* **2014**, *140*, 104306.

(96) Haiss, W.; Van Zalinge, H.; Higgins, S. J.; Bethell, D.; Höbenreich, H.; Schiffrin, D. J.; Nichols, R. J. *J. Am. Chem. Soc.* **2003**, *125*, 15294.

(97) Nichols, R. J.; Haiss, W.; Higgins, S. J.; Leary, E.; Martin, S.; Bethell, D. *Phys. Chem. Chem. Phys.* **2010**, *12*, 2801.

(98) Zalesskiy, S. S.; Sedykh, A. E.; Kashin, A. S.; Ananikov, V. P. *J. Am. Chem. Soc.* **2013**, *135*, 3550.

(99) Bruce, M. I.; Low, P. J.; Werth, A.; Skelton, B. W.; White, A. H. *J. Chem. Soc., Dalton Trans.* **1996**, *8*, 1551.

(100) Liu, K.; Wang, X.; Wang, F. *ACS Nano* **2008**, *2*, 2315.

CHAPTER 3. SYNTHESIS OF BUTA-1,3-DIYNYL RUTHENIUM COMPLEXES

3.1. Abstract

The buta-1,3-diynyl complexes Ru(C≡CC≡CAr)(PPh_3)$_2$Cp (Ar = C_6H_4CN-4 (**15**), C_6H_4Me-4 (**16**), C_6H_4OMe-4 (**17**), DHBT (**18**), C_5H_4N (**19**), BMPA (**20**)) were synthesised by a straightforward Pd(PPh_3)$_4$/CuI co-catalysed cross-coupling reaction of Ru(C≡CC≡CH)(PPh_3)$_2$Cp (**14**) with aryl iodides, Ar-I (Ar = C_6H_4CN-4; C_6H_4Me-4; C_6H_4OMe-4; 2,3-dihydrobenzo[*b*]thiophene (DHBT); C_5H_4N; *N,N*-bis(4-methoxyphenyl)-4-phenylamine (BMPA)) in diisopropylamine (HN^iPr_2) solution and under inert atmosphere. This route allows the rapid preparation of a range of ruthenium(II) complexes of arylbuta-1,3-diynyl ligands without necessitating the prior synthesis of the individual buta-1,3-diynes as ligand precursors. In addition, the bimetallic derivative {Ru(PPh_3)$_2$Cp}$_2$(μ-C≡CC≡C-1,4-C_6H_4-C≡CC≡C) (**21**) was prepared from cross-coupling of **14** with half an equivalent of 1,4-diiodobenzene. The homo-coupling of **14** in the presence of atmospheric oxygen gave the octa-1,3,5,7-tetrayndiyl complex {Ru(PPh_3)$_2$Cp}$_2$(μ-C≡CC≡CC≡CC≡C) (**22**). Further reaction of **16** with tetracyanoethene (TCNE) gave the tetracyanobutadienylethynyl derivative Ru{C≡CC[=C(CN)$_2$]C(C_6H_4Me-4)=C(CN)$_2$}(PPh_3)$_2$Cp (**23**).

The molecular structures of seven complexes (**15**, **16**, **18**, **20**, **21**, **22** and **23**) have been determined by single crystal X-ray diffraction. Electrochemical properties are discussed for all of the complexes described here, and spectroelectrochemical studies (UV-Vis-NIR and IR) for the octatetraynyl ruthenium **22**, reveal chemical complications, likely intermolecular dimerization, on the time scale of the spectroelectrochemical experiments. In light of the chemical reactivity of [**21**]$^{n+}$ and [**22**]$^{n+}$, quantum chemical calculations of **21** and **22** have been carried out to establish the bonding patterns in the carbon chains and changes occurring during step-wise oxidation of the complexes.

CHAPTER 3

3.2. Introduction

As discussed in Chapter 2, metal fragments have been widely used for the stabilization of otherwise reactive oligoynes. Metal oligoynyl $M\{(C\equiv C)_nH\}L_x$ species have attracted significant interest over several decades, serving as scaffolds for the assembly of bi-[1-12] and poly-metallic[12,13,17-26] complexes, and as models and building blocks for metallomacrocycles,[18,19,27-29] and metallo-polymers.[30,31] Detailed studies of the underlying electronic structure of this family of complexes have used a variety of computational and spectroscopic methods, often with a view to modelling the behaviour of these prototypical molecular wires.[22,32,33] The terminal C≡CH moiety in oligoynyl complexes $M\{(C\equiv C)_{n-1}C\equiv CH\}L_x$ offers a convenient entry point for the preparation of a wide range of oligoynyl derivatives; however, the functionalization reactions of $-(C\equiv C)_{n-1}C\equiv CH$ ligands are largely based on deprotonation and subsequent trapping with various electrophiles,[7,24,34-37] including metal complex electrophiles.[13,14,38]

To the best of our knowledge, the use of the Sonogashira cross-coupling reaction as a tool to prepare substituted derivatives of buta-1,3-diynyl complexes was first demonstrated in reactions of $W(C\equiv CC\equiv CH)(CO)_3Cp$ with iodoaromatics.[39] However, despite further successful demonstrations of this 'chemistry on the complex' concept to functionalize[40-44] or extend[45-48] metal-alkynyl ligands through homo or cross-coupling protocols, the use of cross-coupling reactions to functionalize metal complexes[56] has been largely overlooked for the preparation of more functional metal alkynyl complexes. More conventional strategies involving the metallation of pre-formed alkynes and (oligo)ynes of general form $H(C\equiv C)_nC\equiv CR$ or $Me_3Si(C\equiv C)_nC\equiv CR$[57,58-61] have been preferred. Indeed, $Ru(C\equiv CC\equiv CC_6H_5)(PPh_3)_2Cp$ has been synthesised in two steps where $RuCl(PPh_3)_2Cp$ reacted with 4-trimethylsilylbutadiynylbenzene, deprotected in-situ with the presence of potassium fluoride (KF) in methanol (Scheme 3-1).[62]

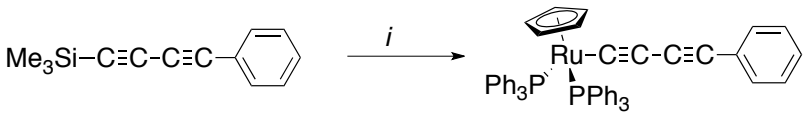

Scheme 3-1. *Preparation of the ruthenium complex $Ru(C\equiv CC\equiv CC_6H_5)(PPh_3)_2Cp$.[62] (i) $RuCl(PPh_3)_2Cp$, KF in MeOH.*

Here, with the aim of simplifying the preparation of buta-1,3-diynyl derivatives by developing a more modular synthetic route, Sonogashira-style cross-coupling reactions have been exploited for the preparation of a range of ruthenium buta-1,3-diynyl complexes from a common $Ru(C{\equiv}CC{\equiv}CH)(PPh_3)_2Cp$ platform. This strategy avoids the preparation of the different diyne ligands for each complex, providing rapid access to a range of complexes with various aryl-substituted buta-1,3-diynyl ligands.

3.3. Synthesis of the ruthenium buta-1,3-diynyl complexes

The reaction between $RuCl(PPh_3)_2Cp$ and trimethylsilylbutadiyne (TMSB) leads to the complex $Ru(C{\equiv}CC{\equiv}CSiMe_3)(PPh_3)_2Cp$ (**13**) with the help of an abstracting agent sodium tetraphenylborate ($NaBPh_4$) in a basic solution (NEt_3/THF) to deprotonate the vinylidene/ethynylvinylidene intermediate (Scheme 3-2).[34,63-65]

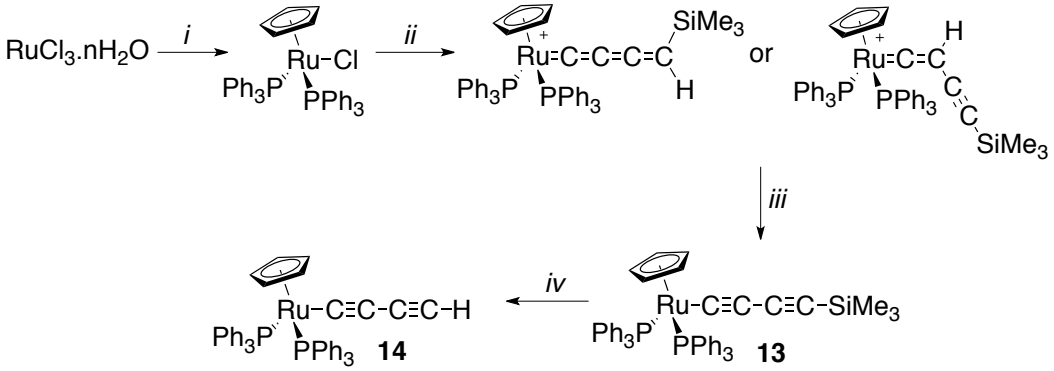

Scheme 3-2. *Synthesis of the platform ruthenium(II) compound **14**. (i) Cyclopentadiene, PPh_3 in EtOH, reflux, 4 h;(ii) TMSB, $NaBPh_4$ in NEt_3/THF, 50 °C, overnight; (iii) Deprotonation with NEt_3, 88%; (iv) TBAF in THF, rt, overnight, 53%.*

Subsequently, fluoride induced desilylation of **13** affords the terminal buta-1,3-diyl complex $Ru(C{\equiv}CC{\equiv}CH)(PPh_3)_2Cp$ (**14**),[19] which was chosen as a test-bed for Sonogashira cross-coupling reactions with a wider range of aryl iodides than explored previously on the $W(C{\equiv}CC{\equiv}CH)(CO)_3Cp$ platform (Scheme 3-3).[15]

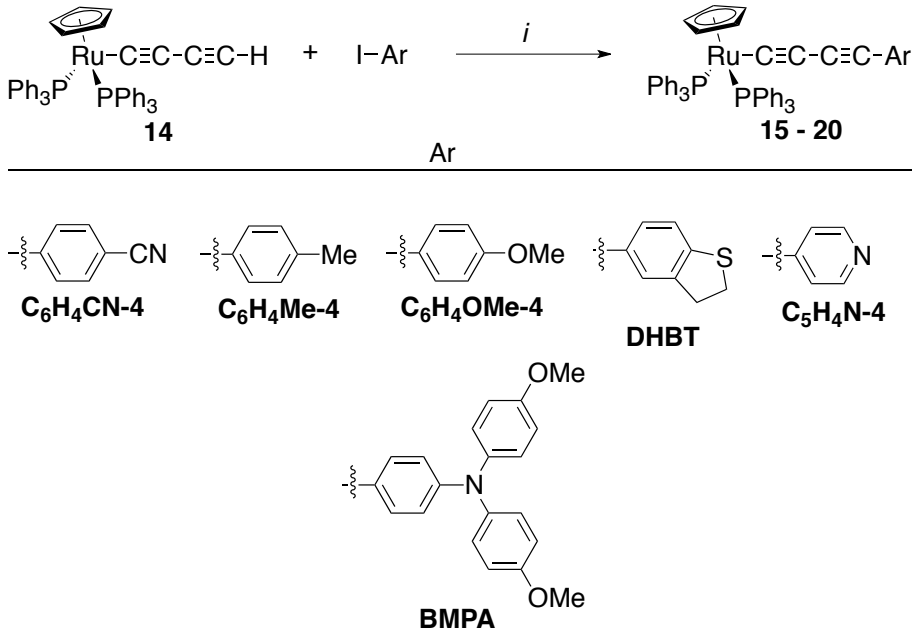

Scheme 3-3. *The Sonogashira cross-coupling reactions of **14** with aryl iodides yielding **15 – 20**; (i) 5 mol% $Pd(PPh_3)_4$, 10 mol% CuI in HN^iPr_2, 90 °C.*

Reaction of **14** with the aryl iodides in HN^iPr_2 co-catalyzed by a simple $Pd(PPh_3)_4$ (5 mol%)/CuI (10 mol%) mixture gave the substituted buta-1,3-diynyl complexes $Ru(C{\equiv}CC{\equiv}CAr)(PPh_3)_2Cp$ **15** - **20** in moderate (**15**, 47%; **17**, 59%; **18**, 54%; **19**, 60%; **20**, 29%) to good (**16**, 87%) yields. These examples illustrate the versatility of the 'chemistry-on-complex' strategy, with buta-1,3-diynyl complexes derived from aryl iodides featuring electron-withdrawing (**C_6H_4CN-4**), electro-neutral (**C_6H_4Me-4**), electron-donating (**C_6H_4OMe-4**, **BMPA**) or metal surface contacting (**DHBT**, **C_5H_4N**) properties being obtained.

Similarly reaction of **14** with one-half equivalent of 1,4-diiodobenzene gave the bimetallic bis(buta-1,4-diynyl) complex $\{Ru(PPh_3)_2Cp\}_2(\mu\text{-}C{\equiv}CC{\equiv}C\text{-}1,4\text{-}C_6H_4C{\equiv}CC{\equiv}C)$ (**21**) in 67% yield (Scheme 3-4).

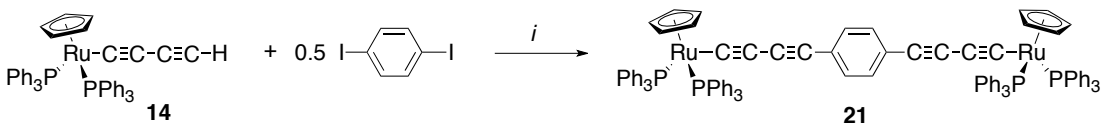

Scheme 3-4. *Synthesis of the bimetallic complex $\{Ru(PPh_3)_2Cp\}_2(\mu\text{-}C{\equiv}CC{\equiv}C\text{-}1,4\text{-}C_6H_4C{\equiv}CC{\equiv}C)$ **21**. (i) 5 mol% $Pd(PPh_3)_4$, 10 mol% CuI in HN^iPr_2, 90°C, 2 h, 67%.*

All the products were obtained in good purity as precipitates from the reaction mixtures and, where necessary, further purification was achieved by column chromatography and/or crystallisation. Identification of the products was readily achieved through a combination of IR, ^{1}H, ^{13}C and ^{31}P NMR spectroscopies, MALDI-TOF, high-resolution ES MS and elemental analysis. Solutions of the buta-1,3-diynyl complexes for spectroscopy and crystallisation were treated with small aliquots of NEt_3 to prevent formation of the analogous butatrienylidenes from adventitious protons and subsequent decomposition.[66-68] The phosphine ligands were detected in the ^{31}P NMR spectra as singlets in the narrow range 48.2 (**15**) - 49.3 (**20**) ppm, whilst the cyclopentadiene (Cp) ligands were detected in the ^{1}H spectra between 4.31 - 4.38 ppm. The C_α carbon was only detected in the ^{13}C NMR spectra of **15**, **16**, **17**, **21** and **22**, as a characteristic triplet (J_{CP} = ca. 25 Hz) (Figure 3-1). In all cases the buta-1,3-diynyl ligand gave rise to a two-band ν(C≡CC≡CAr) pattern in the IR spectra, with absorptions near 2160 and 2020 cm^{-1} that can be approximated as the local oscillations of the C≡CAr and Ru-C≡C fragments, respectively. These typical IR features, which compare with the ν(C≡CC≡CH) and ν(≡C-H) bands at 1971, 2112 and 3301 cm^{-1}, respectively, were also useful markers through which to assess the progress and completion of the reactions (Figure 3-2). In each case the MALDI-TOF spectrum contained the molecular ion, together with a fragment ion derived from loss of PPh_3 in some cases.

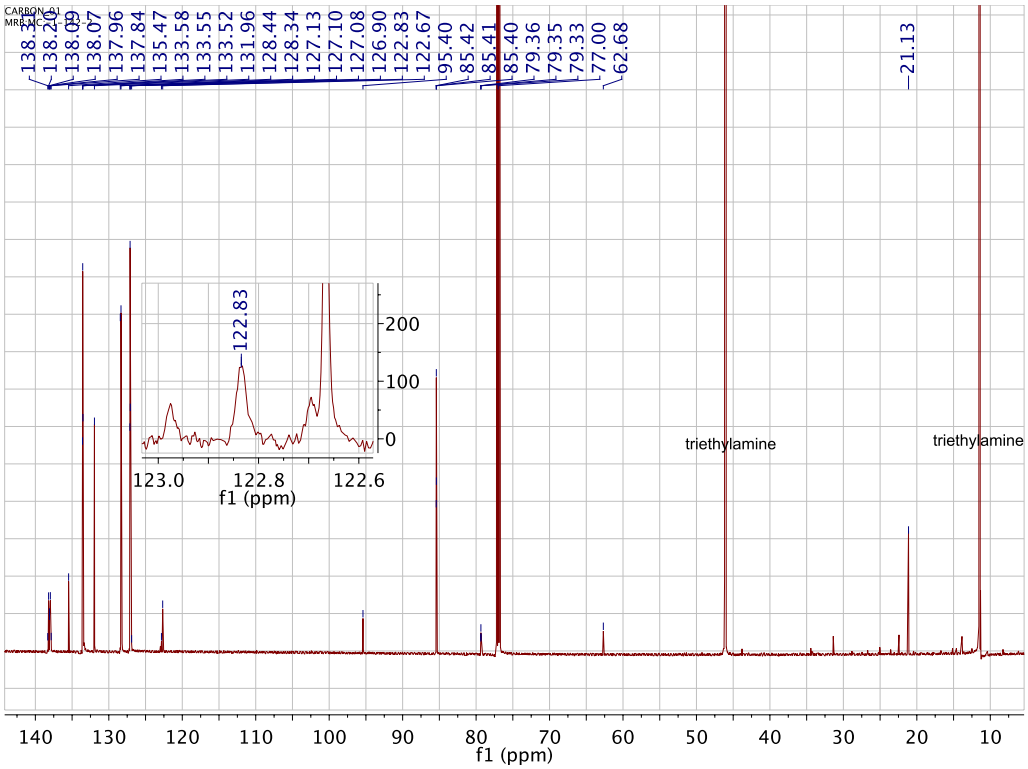

Figure 3-1. *Example of a ^{13}C NMR spectrum (compound **16**) when the Cα is visible (inset expansion).*

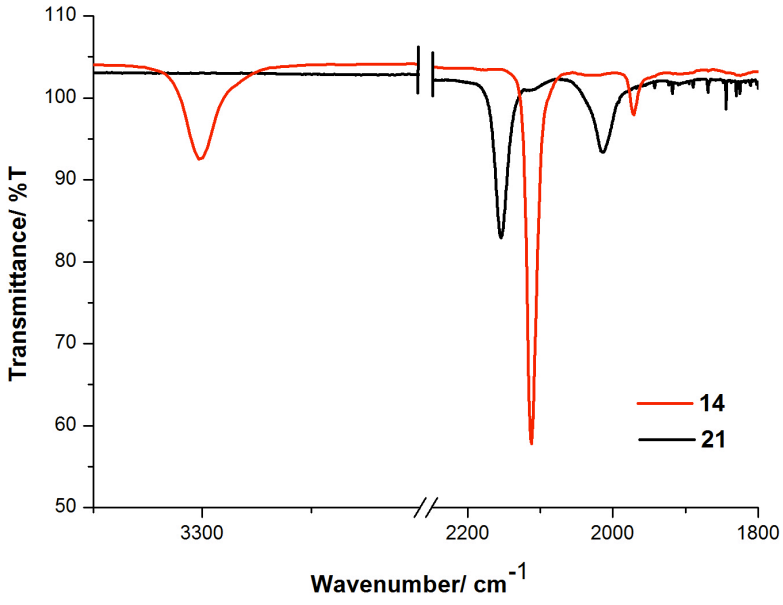

Figure 3-2. *IR monitoring of the Sonogashira reaction of **14** with 1,4-diiodobenzene to give the bimetallic compound **21**.*

Although most commonly used as a cross-coupling methodology, it is well-known that the Sonogashira cycle can be intercepted by oxidants to promote homo-coupling of the terminal alkyne,[15,16,40,41,69-71] and use of Sonogashira-like conditions in the presence of a strategic oxidant is emerging as a viable alternative to the Glaser-Hay type methods of 1,3-diyne synthesis.[71] The reaction of **14** with catalytic $Pd(PPh_3)_4$/CuI in HN^iPr_2 in an open flask proceeded rapidly to give the homo-coupled octa-1,3,5,7-tetrayndiyl complex $\{Ru(PPh_3)_2Cp\}_2(\mu\text{-}C{\equiv}CC{\equiv}CC{\equiv}CC{\equiv}C)$ (**22**, 55%). Complex **22**[73] and the closely related buta-1,3-diyndiyl $\{Ru(PPh_3)_2Cp\}_2(\mu\text{-}C{\equiv}CC{\equiv}C)$ and hexa-1,3,5-triyndiyl $\{Ru(PPh_3)_2Cp\}_2(\mu\text{-}C{\equiv}CC{\equiv}CC{\equiv}C)$[62] and octa-1,3,5,7-butyndiyl $\{Ru(PPh_3)_2Cp\}_2(\mu\text{-}C{\equiv}CC{\equiv}CC{\equiv}CC{\equiv}C)$ complexes have previously been prepared from desilylation/metallation reactions of the appropriate di-, tri- or tetra-yne $Me_3Si\text{-}(C{\equiv}C)_n\text{-}SiMe_3$ with $RuCl(PPh_3)_2Cp$ in presence of KF (Scheme 3-5). Other octa-1,3,5,7-tetrayndiyl complexes have been prepared from oxidative Hay or Glaser style homo-coupling of buta-1,3-diynyl complexes.[2,42,43,46,48,74-77] The approach described here is a complementary and highly convenient route to these systems.

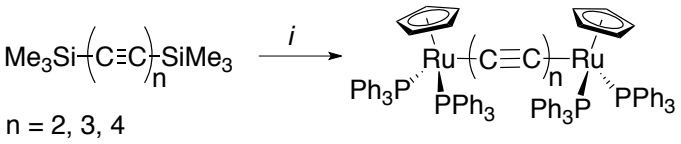

Scheme 3-5. *Desilylation/Metallation reaction for the preparation of oligoynyl ruthenium complexes. (i) 2 eq. $RuCl(PPh_3)_2Cp$, 2 eq. KF in MeOH.*

The protonation reactions of **16** were attempted as a route to the analogous cumulene complexes (e.g. Scheme 3-6), but without success. Addition of electrophiles (HBF_4; MeI) at low temperature (-78 ºC) caused solutions to turn to a characteristic red colour. However, the instability of the cumulene did not allow any analysis. Attempts at trapping the cumulene by addition of nucleophiles such as diphenylamine, diethylamine and N-(phenylmethylene)-benzenamine were also unsuccessful with extensive decomposition precluding isolation and analysis of the products. However, in keeping with the acid-base relationship between the buta-1,3-diynyl (Ru-C≡CC≡CR) and putative butatrienylidene (Ru^+=C=C=C=C(H)R), addition of sodium methoxide (NaOMe) to the red solutions gave the buta-1,3-diynyl starting material.

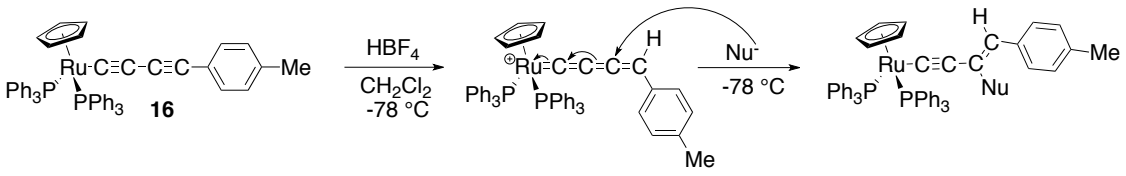

Scheme 3-6. *Synthetic routes envisaged for the formation of the cumulene.*

The putative butatrienylidene might be failing to react smoothly with nucleophiles on steric grounds. Therefore, a test reaction between **16** and TCNE was conducted (Scheme 3-7). The pseudo-[2+2] cycloaddition with organo-transition metal compounds and TCNE is well known.[47-49,78-80] The reaction evolves the anion radical of TCNE as intermediate before the formation of the cyclobutenyl via the zwitterion and finally, a ring opening to give **23**.[81] The reaction was instant and after 3 h at room temperature, the yellow solution of **16** turned dark red, which suggested that the cumulene is not easy to isolate probably due to its instability in solution. The identity of **23** was established by ^{1}H NMR, ^{13}C NMR, mass spectrometry and single crystal X-ray structure. The mass of the molecule (958.0 $[M]^{+}$) was detected with MALDI-TOF method, the carbons of C≡N are in the range of δ_C 112.4 - 116.2 ppm, the C≡C carbons are at δ_C 82.1 and 81.2 ppm and the protons of Cp are at δ_H 4.60 ppm, which is more downfield than the ruthenium buta-1,3-diynyl **15** - **20**. These data are in complete agreement with similar compounds reported in the literature.[62,73]

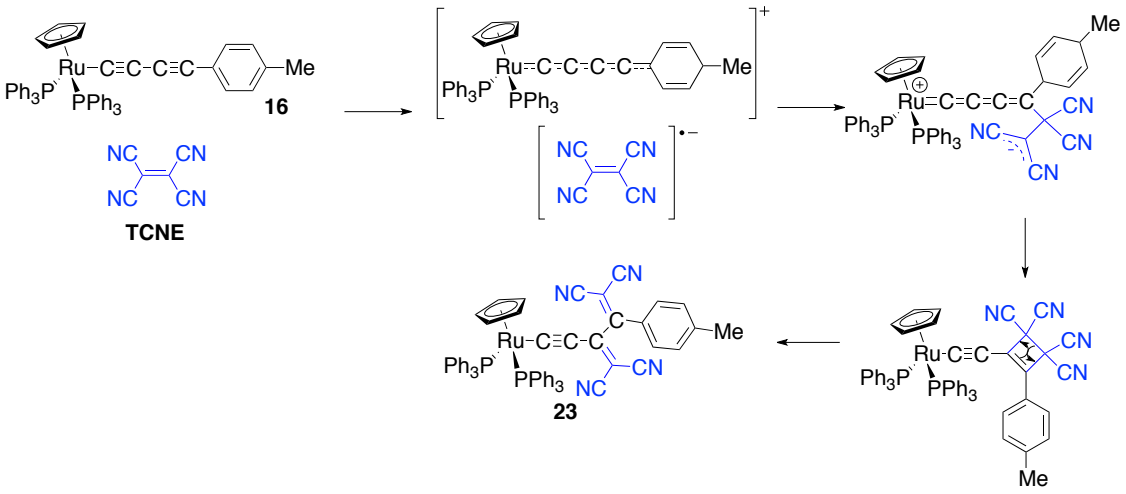

Scheme 3-7. *Reaction of **16** with TCNE.*

3.4. Molecular Structures

Single crystals suitable for X-ray diffraction analysis were obtained for the buta-1,3-diynyl complexes **15**, **16**, **18**, **20**, bimetallic complexes **21** (as a *mono*-CH_2Cl_2 solvate) and **22** (as a *bis*-CH_2Cl_2 solvate) and compound **23**; the structure of **22** as the chloroform solvate has been reported recently by Bruce and colleagues.[82] Plots of these molecules are given in Figures 3-3 – 3-9 and selected bond lengths and angles are summarized in Table 3-1. The diynyl complexes **15** (Figure 3-3), **16** (Figure 3-4), **18** (Figure 3-5) and **20** (Figure 3-6) featuring the $Ru(PPh_3)_2Cp$ fragment display bond lengths associated with both the diynyl ligand and the metallic half-sandwich moiety that barely differ from the few other examples of $Ru(C{\equiv}CC{\equiv}CR)(PPh_3)_2Cp$ compounds reported to date: (R = $SiMe_3$,[19] $C(Ph)CBr_2$,[61] Ph,[62] and CN[83]). Thus, the ruthenium center has the usual pseudo-octahedral geometry, with bond lengths and angles in the ranges: Ru-P 2.278(14) - 2.342(2) Å and P(1)-Ru-P(2) 96.42(8) - 101.388(8)°, P(1,2)-Ru-C(1) 88.37(6) - 92.24(5)°. The Ru-C(1) lengths fall between 1.9843(19) Å (**15**) and 2.002(3) Å (**16**) which compares with the 1.986(4) - 1.99(1) Å range found in previous examples. For the diynyl chain, the bond lengths display the expected pattern of short-long alternation: C(1)-C(2) 1.205(7) - 1.233(13) Å; C(2)-C(3) 1.346(14) - 1.380(4) Å; C(3)-C(4) 1.168(14) - 1.216(4) Å; and the chain is essentially linear, with angles: Ru-C(1)-C(2) 172.76(17) - 175.6(3)°; C(1)-C(2)-C(3) 170.3(12) - 178.6(2)°.

The formation of the compound **23** (Figure 3-9) was confirmed by the crystal structure in which the carbon chain from C(3)-C(4) is disordered with a twisting effect of the moiety $CC[{=}C(CN)_2]CTol{=}C(CN)_2$. A closely related molecular structure without disorder, $Ru\{C{\equiv}CC[{=}C(CN)_2]CPh{=}C(CN)_2\}(PPh_3)_2Cp$ from the literature was chosen for comparison.[62] The Ru-C(1) bond is longer in compound **23** (1.9843(19) Å) than the literature compound (1.947(8) Å) and the other bond lengths are slightly shorter: Ru-P(1) 2.2936(5) Å; Ru-P(2) 2.2915(5) Å than those from the literature compound: Ru-P(1) 2.305(5) Å; Ru-P(2) 2.299(5)) Å. All the bond lengths are in the same range for the compounds **15**, **16**, **18** and **20** with a noticeable shortening for Ru-C(1) 1.931(4) Å. In addition, the bond lengths of C≡N (1.144(3)) are comparable with those from the literature (1.11(1) - 1.15(1) Å).

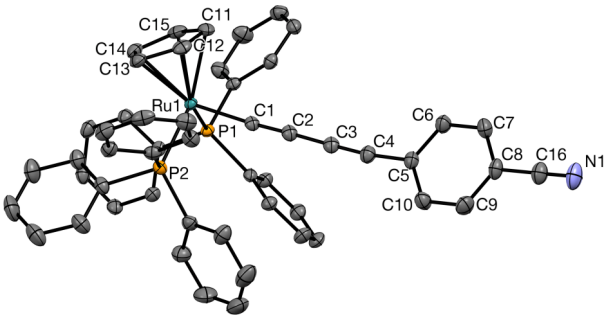

Figure 3-3. *Molecular structure of **15** showing the atom labelling scheme. In this and all subsequent plots, thermal ellipsoids are plotted at 50% and hydrogen atoms have been omitted for clarity.*

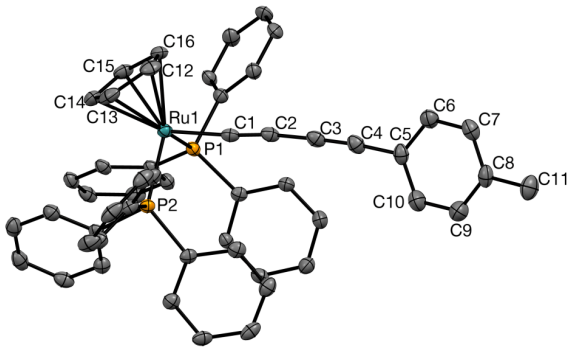

Figure 3-4. *Molecular structure of **16**.*

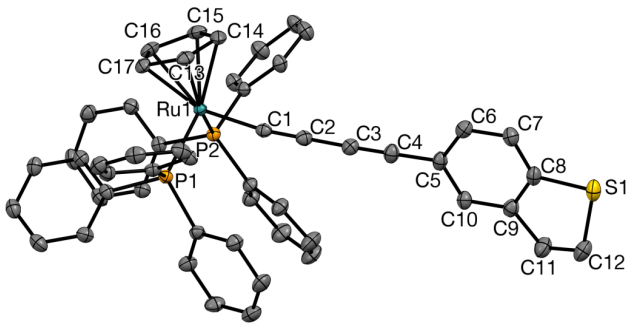

Figure 3-5. *Molecular structure of **18**.*

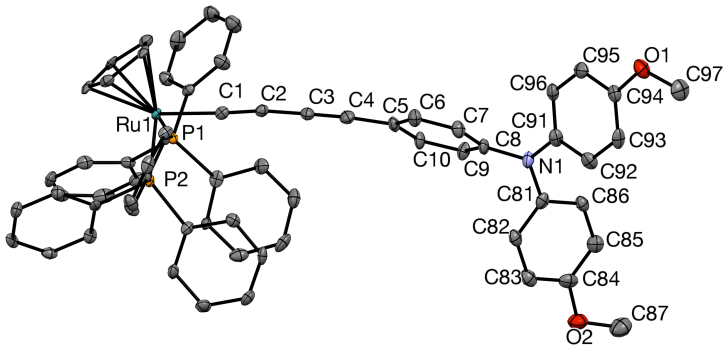

Figure 3-6. *Molecular structure of **20**. Solvent molecules have been omitted for clarity.*

Table 3-1. *Selected crystallographically determined bond lengths (Å) and angles (º) for complexes **15**, **16**, **18**, **20**, **21**, **22** and **23** and related data from the DFT optimized (B3LYP/3-21G*/CPCM-CH_2Cl_2) geometries (**15´**, **21´** and **22´**).*

Bond lengths (Å)	**15**	**15´**	**16**	**18**	**20**
Ru-P(1)	2.2936(5)	2.3366	2.2884(8)	2.2844(5)	2.2785(14)
Ru-P(2)	2.2915(5)	2.3315	2.3001(7)	2.3088(5)	2.2969(14)
Ru-C(1)	1.984(2)	1.9783	2.002(3)	1.9947(19)	1.999(5)
C(1)-C(2)	1.221(3)	1.2420	1.214(4)	1.226(3)	1.205(7)
C(2)-C(3)	1.371(3)	1.3485	1.380(4)	1.373(3)	1.377(7)
C(3)-C(4)	1.204(3)	1.2255	1.216(4)	1.211(3)	1.206(7)
C(4)-C(5)/C(4)-C(4´)	1.430(3)	1.4139	1.429(4)	1.431(3)	1.435(8)
Angles (°)					
P(1)-Ru-P(2)	101.39(2)	102.63	98.89(3)	97.44(2)	99.37(5)
P(1)-Ru-C(1)	90.67(5)	90.96	89.89(9)	92.24(5)	85.90(15)
P(2)-Ru-C(1)	88.37(6)	88.24	91.77(8)	91.85(5)	91.75(15)
Ru-C(1)-C(2)	175.0(2)	175.10	175.6(3)	172.8(2)	174.8(5)
C(1)-C(2)-C(3)	178.6(2)	179.21	173.5(3)	174.9(2)	172.0(6)
C(2)-C(3)-C(4)	178.3(2)	177.9(3)	177.9(3)	178.2(2)	179.2(6)
C(3)-C(4)-C(5)/C(3)-C(4)-C(4´)	173.4(2)	173.6(3)	173.6(3)	179.4(2)	173.2(6)

Table 3-1. *(Continued).*

21	**21´**	**22**	**22**[82]	**22´**	**23**
2.342(2)	2.3324, 2.3344	2.298(2)	2.305(2)	2.3432, 2.3432	2.2936(5)
2.306(3)	2.3245, 2.3233	2.282(2)	2.291(2)	2.3404, 2.3314	2.2915(6)
1.965(10)	1.9855, 1.9860	1.976(5)	1.963(6)	1.9822, 1.9841	1.9843(19)
1.233(13)	1.2406, 1.2407	1.229(7)	1.237(7)	1.2440, 1.2445	1.221(3)
1.346(14)	1.3519, 1.3519	1.362(8)	1.370(8)	1.3445, 1.3444	1.371(3)
1.168(14)	1.2250, 1.2250	1.220(7)	1.197(7)	1.2345, 1.2346	1.204(3)
1.476(16)	1.4174, 1.4175	1.358(11)	1.385(12)	1.3395	1.430(3)
96.42(8)	101.07, 101.23	100.27(5)	98.74(4)	101.95, 100.35	101.388(18)
93.9(3)	91.07, 91.46	86.49(15)	87.2(1)	88.35, 92.20	90.67(5)
90.1(3)	91.13, 90.71	94.12(16)	93.5(1)	92.07, 89.76	88.37(6)
172.8(8)	173.91, 173.86	168.5(5)	174.6(4)	173.17, 175.94	175.02(17)
170.3(12)	178.95, 179.03	170.3(6)	173.6(5)	178.35, 178.76	178.6(2)
176.2(12)	179.24, 179.87	175.0(6)	176.7(5)	178.97, 179.08	178.3(2)
177.2(13)	179.11, 179.35	179.8(8)	178.3(7)	179.05	173.4(2)

In the solid state, the bimetallic complexes **21** and **22** adopt a *trans*-conformation of the Cp rings. The torsion angle C(0)-Ru-C(5)-C(6) is 172.88° (C(0) is the centroid of the Cp ring) suggesting that, at least in the structure adopted in the solid state, the d_{yz} and d_{xz} orbitals of the Ru atom are able to participate in the conjugation along the carbon-rich bridging ligand. The octa-1,3,5,7-tetrayn-1,8-diyl ligand in **22** displays the sigmoidal distortions from linearity often observed for extended carbon chain complexes.[82,84] In **21** the Ru-C(1) distance (1.965(10) Å) is the shortest in the series, and arguably shorter than the Ru-C_α bond found in the related hexa-1,3,5-triyne-1,6-diyl complex [{Ru(PPh_3)$_2$Cp}$_2$(μ-C≡CC≡CC≡C)] (2.001(6) Å),[62] and in **22**•2CH_2Cl_2, but equal to that found in **22**•4$CHCl_3$ (1.963(6) Å).[82] However, it does seem that the octa-1,3,5,7-tetrayn-1,8-diyl chain in **22** displays a less pronounced long-short alternation than in the diynyl complexes **15 - 20** and **21**, which supports a degree of extended delocalization along the molecular backbone.

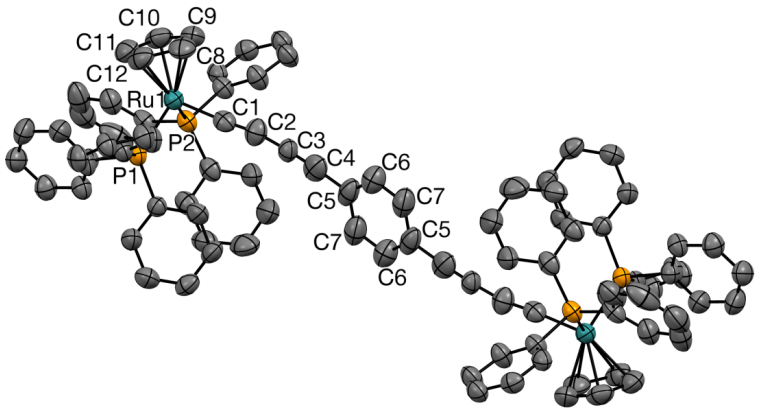

Figure 3-7. *Molecular structure of **21**. Solvent molecules have been omitted for clarity.*

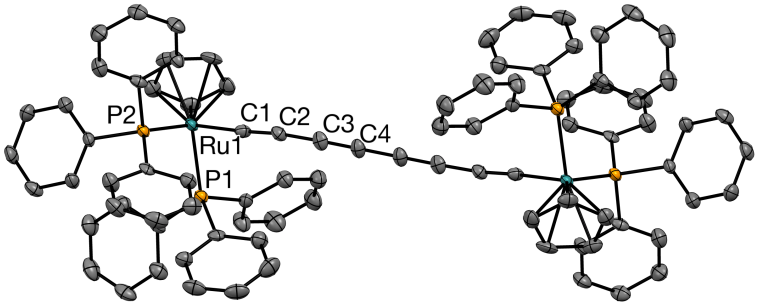

Figure 3-8. *Molecular structure of **22**. Solvent molecules have been omitted for clarity.*

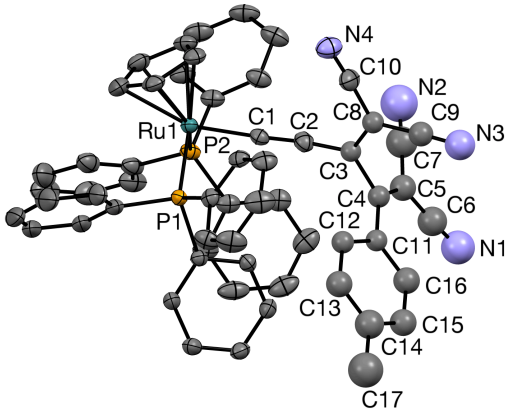

Figure 3-9. *Molecular structure of **23**. The disorder has been omitted for clarity.*

3.5. Electrochemistry

The monometallic complexes **15** – **20** each give an oxidation wave that is electrochemically reversible, supported by the observation of a linear dependence of the peak current (i_p) vs $\nu^{1/2}$ (Figure 3-11), but chemically irreversible, with peak potentials that vary between 0.01 V - 0.22 V (Table 3-2) and exhibit a trend in accord with the electronic character of the aryl substituent: Ru(C≡CC≡C-C_6H_4N(C_6H_4OMe-4)$_2$(PPh_3)$_2$Cp **20** < Ru(C≡CC≡CC_6H_4OMe-4)(PPh_3)$_2$Cp **17** < Ru(C≡CC≡CC_6H_4Me-4)(PPh_3)$_2$Cp **16** < Ru(C≡CC≡CDHBT)(PPh_3)$_2$Cp **18** < Ru(C≡CC≡CC_6H_4CN-4)(PPh_3)$_2$Cp **15** < Ru(C≡CC≡CC_5H_4N)(PPh_3)$_2$Cp **19** (Figure 3-10). Indeed, the electrochemical reversibility is explained by the rate of the mass transport being lower than the rate of the electron transfer. The irreversibility of similar diynyl complexes is known,[19] and is likely due to intermolecular coupling of the generated diynyl radicals.[58,85]

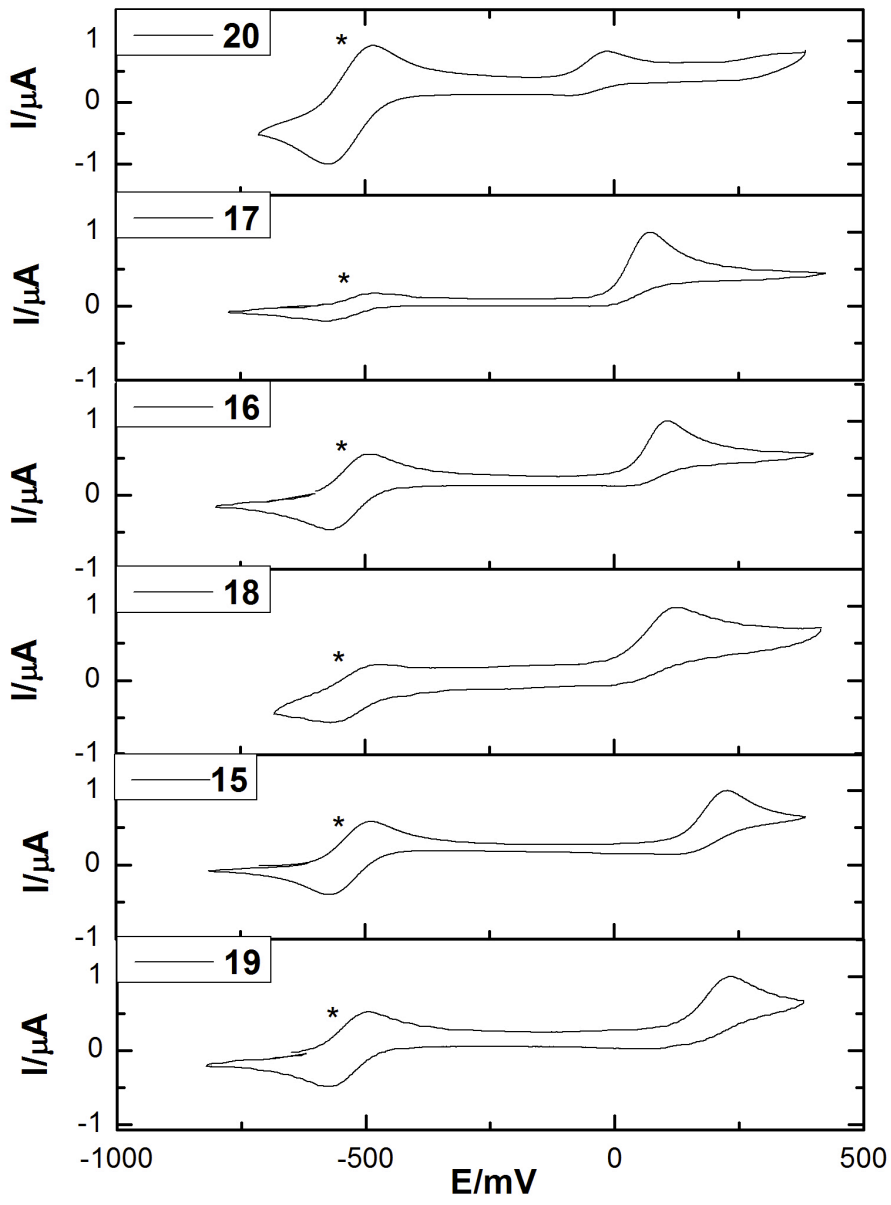

Figure 3-10. *Cyclic voltammograms of the compounds **15 - 20**. Experimental conditions are given in Table 3-2. Internal decamethylferrocene reference is represented by an asterisk.*

Table 3-2. *Electrochemical data of the Ru(C≡CC≡C-Ar)(PPh$_3$)$_2$Cp derivatives **15**, **16**, **17**, **18**, **19** and **20** [a] listed in order of increasing peak potential.*

Compounds	E_{pa}
Ru(C≡CC≡C-C$_6$H$_4$N(C$_6$H$_4$OMe-4)$_2$(PPh$_3$)$_2$Cp **20**	- 0.01
Ru(C≡CC≡CC$_6$H$_4$OMe-4)(PPh$_3$)$_2$Cp **17**	0.06
Ru(C≡CC≡CC$_6$H$_4$Me-4)(PPh$_3$)$_2$Cp **16**	0.09
Ru(C≡CC≡CDHBT)(PPh$_3$)$_2$Cp **18**	0.11
Ru(C≡CC≡CC$_6$H$_4$CN-4)(PPh$_3$)$_2$Cp **15**	0.21
Ru(C≡CC≡CC$_5$H$_4$N)(PPh$_3$)$_2$Cp **19**	0.22

[a] *E_{pa} (anodic peak potential, V) vs. ferrocene/ferrocenium ($FeCp_2$/$[FeCp_2]^+$) (CH_2Cl_2, 0.1 M NBu_4PF_6, Pt dot working electrode). Data reported against an internal decamethylferrocene/ decamethylferrocenium ($FeCp^*_2$/$[FeCp^*_2]^+$) standard. Under these conditions $FeCp^*_2$/$[FeCp^*_2]^+$ = - 0.53 V vs $FeCp_2$/$[FeCp_2]^+$.*

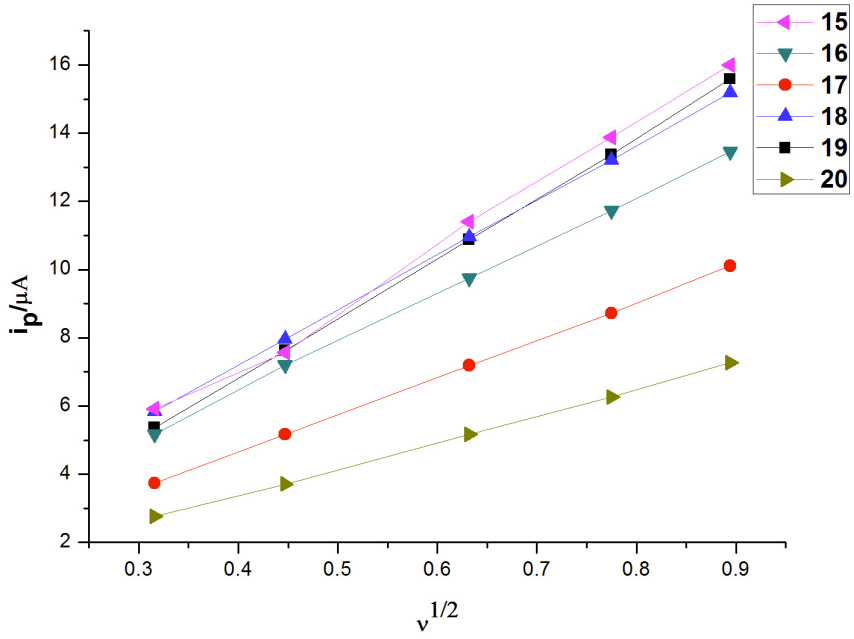

Figure 3-11. *Graphical representation of the peak current (i_p) versus $\nu^{1/2}$ for compounds **15** - **20**.*

Table 3-3. *Electrochemical data of the bimetallic complexes **21** and **22**.*

Compounds	E_{pa} (1)	E_{pa} (2)	E_{pa} (3)	E_{pa} (4)
$\{Ru(PPh_3)_2Cp\}_2(\mu\text{-}C{\equiv}CC{\equiv}CC_6H_5C{\equiv}CC{\equiv}C)$ **21**	0.04	0.24		
$\{Ru(PPh_3)_2Cp\}_2(\mu\text{-}C{\equiv}CC{\equiv}CC{\equiv}CC{\equiv}C)$ **22**	-0.16[b]	0.15	0.61	0.82
$\{Ru(PPh_3)_2Cp\}_2(\mu\text{-}C{\equiv}CC{\equiv}C)$[85]	-0.68 [b]	-0.04[b]	0.59[b]	

[a]*E_{pa} (anodic peak potential, V) vs. ferrocene/ferrocenium ($FeCp_2/[FeCp_2]^+$) (CH_2Cl_2, 0.1 M NBu_4PF_6, Pt dot working electrode). Data reported against an internal decamethylferrocene/ decamethylferrocenium ($FeCp^*_2/[FeCp^*_2]^+$) standard. Under these conditions $FeCp^*_2/[FeCp^*_2]^+$ = - 0.53 V vs $FeCp_2/[FeCp_2]^+$;* [b]*Reversible process $E_{1/2}$.*

Two electrochemically reversible, but chemically irreversible, oxidation waves are observed in the cyclic voltammogram of the bis(buta-1,3-diynyl) complex **21** (Figure 3-12). Thus, whilst the peak potential was independent of scan rate, and peak currents were linear vs $\nu^{1/2}$, the initially formed dication was chemically reactive, as evidenced by the appearance of a new reduction wave at - 0.15 V on the return scan. The chemical stability of $[\mathbf{21}]^+$ did not improve at lower temperatures (ambient to - 30 °C) and chemical complications were still apparent at ν = 800 $mV.s^{-1}$. The chemical instability of this bis(buta-1,3-diynyl) complex is entirely consistent with the limited chemical stability of **15** - **20**, and other related systems reported elsewhere.[85]

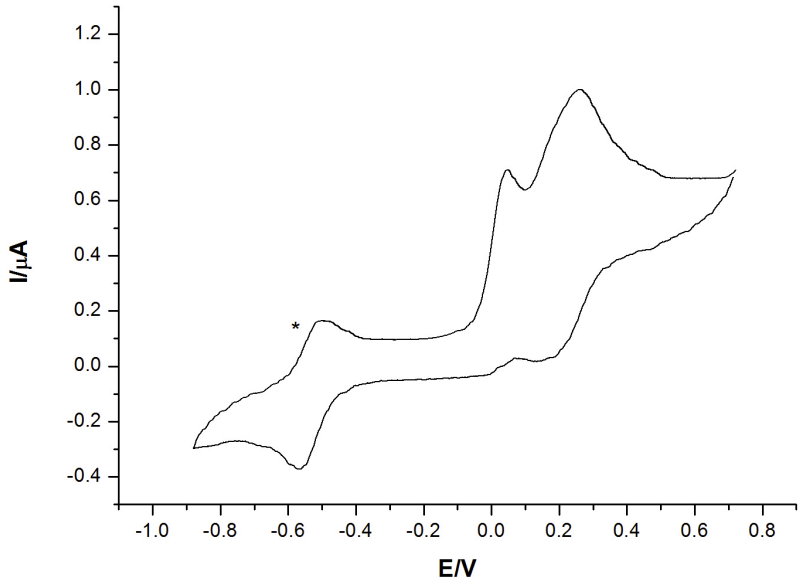

Figure 3-12. *Cyclic voltammogram of **21**. Experimental conditions are given in Table 3-3. Internal decamethylferrocene reference is represented by an asterisk.*

In contrast to these buta-1,3-diynyl derivatives, the bimetallic octatetrayndiyl complex **22** displays one fully reversible oxidation wave (ip_f/ip_r = 0.98, ΔE_p = 74 mV which is comparable with the internal decamethylferrocene reference) and three subsequent, irreversible processes (Figure 3-13). These four processes correspond well to the four oxidation processes described for the analogous buta-1,3-diyndiyl (-C≡CC≡C-) complex $\{Ru(PPh_3)_2Cp\}_2(\mu\text{-}C{\equiv}CC{\equiv}C)$ (Table 3-3).[86,87] In the case of $\{Ru(PPh_3)_2Cp\}_2(\mu\text{-}C{\equiv}CC{\equiv}C)$, the first three redox processes at least are chemically reversible. As a consequence of the reversibility of the bimetallic complex **22**, spectroelectrochemical studies have been explored. In addition, quantum chemical calculations on compounds **21** and **22** have been used to support and demonstrate the progressive shift in the character of the carbon chain from buta-1,3-diyndiyl (-C≡CC≡C-) through butatrienylidene (=C=C=C=) towards butynediylidide (≡CC≡CC≡).

The closely related hexatriyndiyl complex $\{Ru(dppe)_2Cp\}_2(\mu\text{-}C{\equiv}CC{\equiv}CC{\equiv}C)$ exhibits three redox processes in the potential window explored, the first two of which were reversible, the third being only partially chemically reversible.[60] However, in contrast to the C_4 example, in which $[\{Ru(PPh_3)_2Cp\}_2(\mu\text{-}C{\equiv}CC{\equiv}C)]^+$ is sufficiently kinetically and thermodynamically stable to be isolated,[86,87] the more exposed C_6 chain in $[\{Ru(dppe)_2Cp\}_2(\mu\text{-}C{\equiv}CC{\equiv}CC{\equiv}C)]^+$ undergoes an intermolecular coupling reaction on

timescales longer than the voltammetric measurement at temperatures above – 10 °C. The product is an unusual dimeric complex featuring a cyclobutene motif formed by coupling between $C_\alpha \equiv C_\beta$ of one molecule with $C_\gamma \equiv C_\delta$ of another.[59] This contrasting reactivity prompted further spectroelectrochemical investigation of the first electrochemically reversible process observed for **22**, leading to $[\mathbf{22}]^+$.

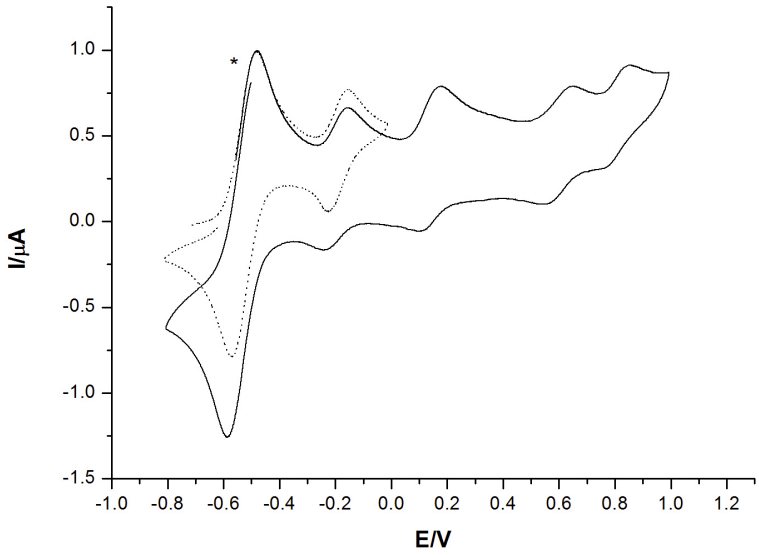

Figure 3-13. *Cyclic voltammogram of **22** with the first reversible oxidation wave (dashed line). Experimental conditions are given in Table 3-3. Internal decamethylferrocene reference is represented by an asterisk.*

3.6. Spectroelectrochemistry

The investigation of the electronic structures of the carbon-rich metal complexes upon oxidation or reduction provides information for future elaboration of new molecules as molecular wires. Spectroelectrochemistry (SEC) characterises which part of the systems is involved during the electrochemical event and so unveils the electronic changes. The method uses an OTTLE (Optically Transparent Thin Layer Electrode) cell where spectra are recorded while the electrochemical reaction takes place in situ. The cell contains optical windows together with Pt working (WE), auxiliary electrodes (CE) and Ag reference electrode (RE)[88] (Figure 3-14).

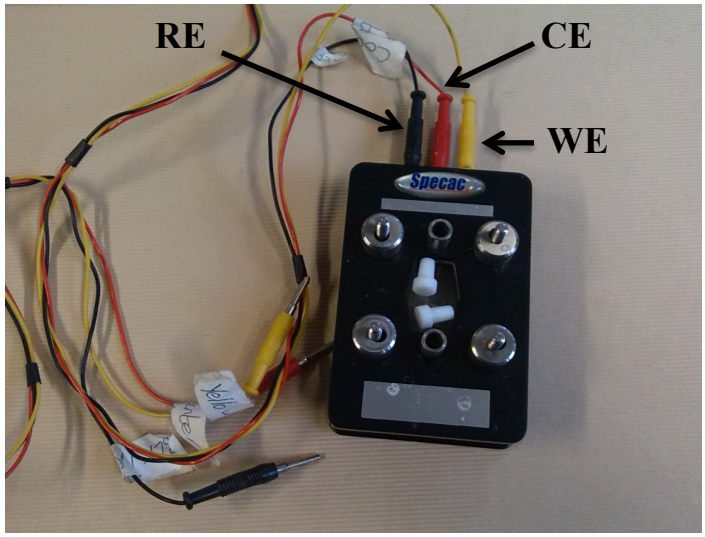

Figure 3-14. *OTTLE cell.*

Previous theoretical calculations of oligoynyl bimetallic complexes demonstrate that in general, oxidation results in depopulation of an orbital that has contributions from all atoms in the M-C_n-M chain, the precise contributions of which are modulated according to the nature of the metal and the length of the molecule.[89,90] These calculations are supported by SEC UV-Vis, DFT calculations and bond length evolution of crystal structures, showing that there is a clear contribution of the carbon bridge upon the oxidation in the complex (C_5Me_5)(dppe)-Fe(C≡CC≡C)Ru(dppe)(C_5Me_5).[10] This contribution is now widely described as an example of ligand redox "non-innocent" behaviour in organometallic complexes.[33] This behaviour arising from the carbon bridge was supported by M.I. Bruce et al. where theoretical calculations along with the SEC of the complex $\{Ru(PPh_3)_2Cp\}_2(\mu$-C≡CC≡C) agreed on the gradual depopulation of the frontier orbitals situated on the carbon bridge leading to a more cumulenic character (Figure 3-15 left). This phenomenon is explained by the HOMO being the out-of-phase combination of the metal with the π-C_n systems, where the M-C_α, C_β-C_γ, C_δ-C_ε… are the anti-bonding orbitals. Another interesting observation is the similarity of the IR data between the ruthenium complexes and the osmium complexes, but also the difference noticed between these spectroscopic data and those from the iron. The conclusion is that the frontier orbitals are more situated

on the metal in the case of lighter metal (eg. iron) than heavier metal (eg. ruthenium, osmium).

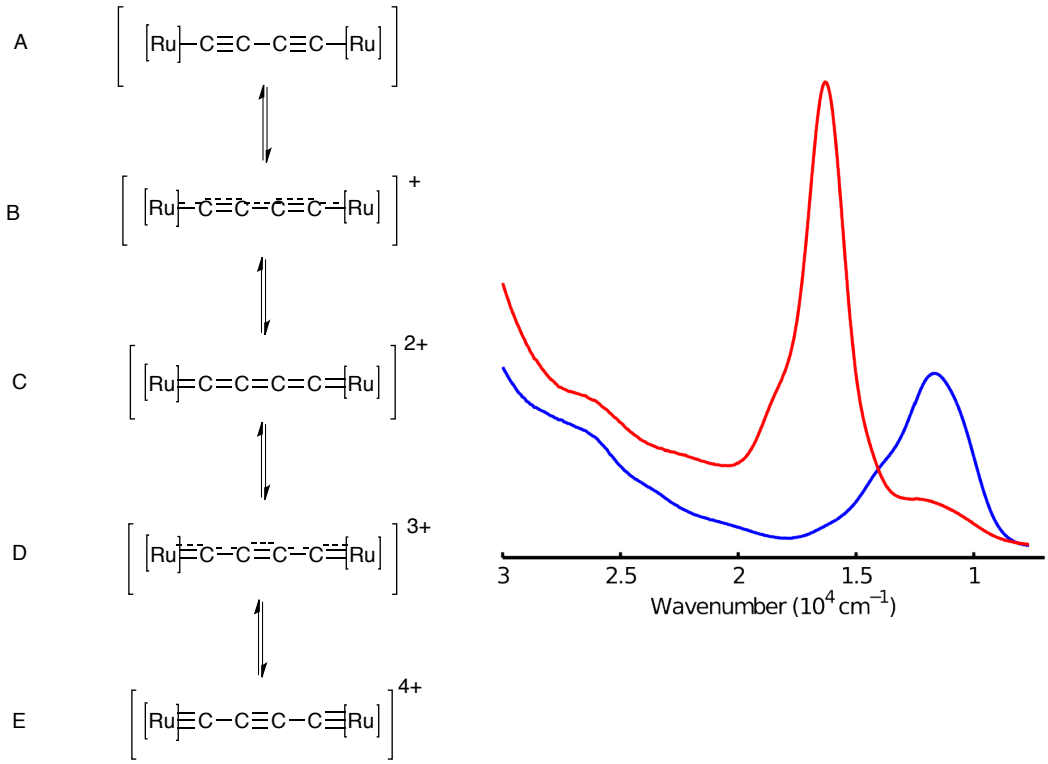

Figure 3-15. *Cumulenic character of the oxidized species [{Ru(PPh$_3$)$_2$Cp}$_2$(μ-C≡CC≡C)]$^{n+}$ (left); UV-Vis-NIR (right) spectroscopic evolution of [{Ru(PPh$_3$)$_2$Cp}$_2$(μ-C≡CC≡C)]$^{n+}$ (n=1 in blue; n=2 in red) from reference.*[86]

More recently, the observation of an additional shoulder in the Near-Infrared region (NIR) at higher energy for the bimetallic compound [{Ru(PPh$_3$)$_2$Cp}$_2$(μ-C≡CC≡C)]$^+$ led to a reinvestigation of the band shape (Figure 3-15 right).[86] Thus, DFT calculations performed on various conformers observed crystallographically predicted that three conformations had an absorption around 11600 cm^{-1} which was ascribed to a π-π* transition. However, one of the conformations (perp) displayed another less intense excitation at 13982 cm^{-1} for a MLCT transition and explained the shoulder in the NIR region.

Compound **22** was studied in a Hartl-style OTTLE cell in 0.1 M NBu$_4$PF$_6$/CH$_2$Cl$_2$ solution at ambient temperature. The characteristic ν(C≡C) bands of **22** were observed at 2107 and 1955 cm^{-1} (Figure 3-16). On oxidation of **22** to [**22**]•$^+$ the spectrum evolved to a more complex series of ν(CC) bands between 2059 - 1862 with clear maxima at 2059 s,

2039 s, 1953 m, and 1862 vs cm^{-1}. However, back reduction failed to completely recover the original spectrum of **22** suggesting an electrochemical process on the longer timescale of the electrolysis, albeit low volume, required for the spectroelectrochemical method.

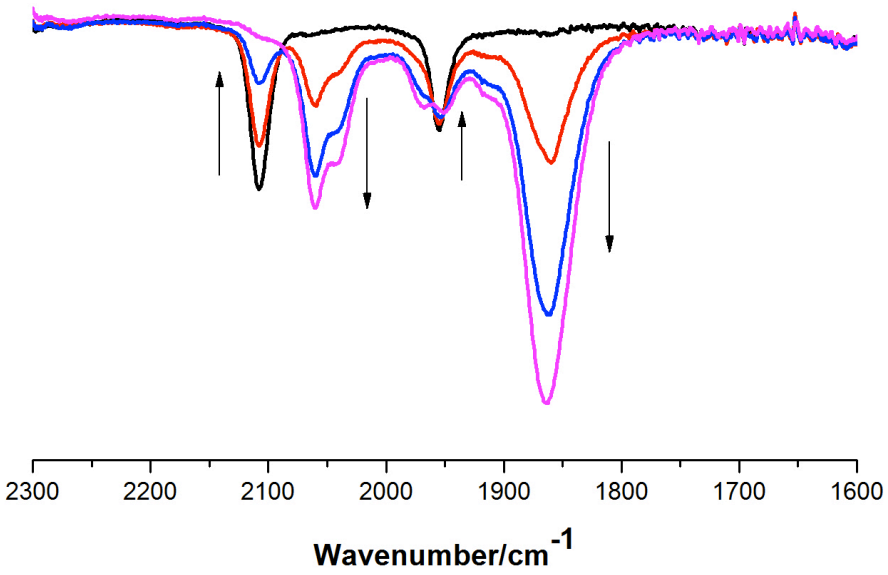

Figure 3-16. *The IR spectra collected in a spectroelectrochemical cell during oxidation of* ***22*** *(0.1 M NBu_4PF_6 /CH_2Cl_2).*

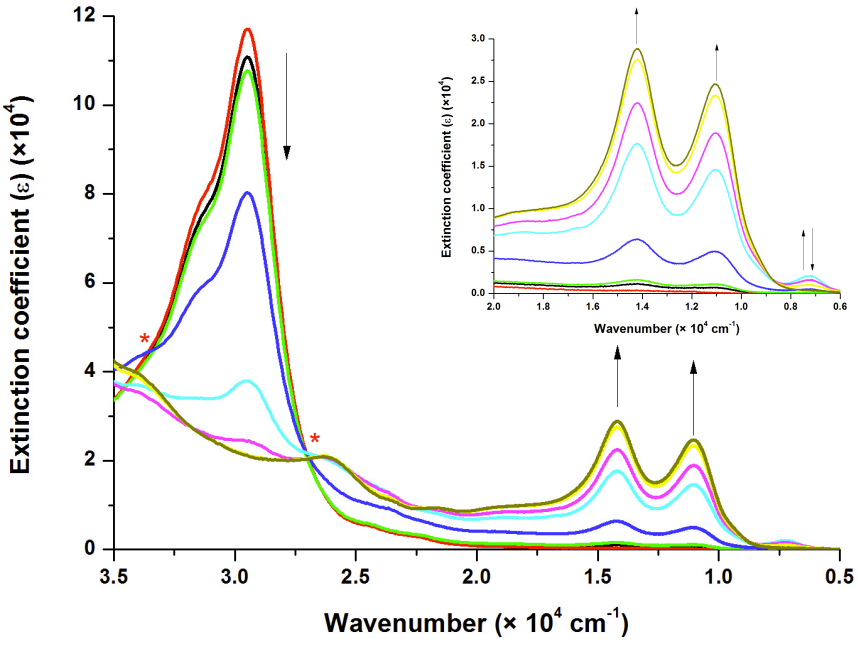

Figure 3-17. *The UV-Vis-NIR spectra collected in a spectroelectrochemical cell during oxidation of* ***22*** *(0.1 M NBu_4PF_6 /CH_2Cl_2). Isosbestic points are marked with asterisk.*

To supplement the information given in the NIR-IR region, the oxidation of **22** was explored in the UV-vis-NIR region (Figure 3-17). Upon one-electron oxidation, the spectra display a loss of the intense UV band at 29793 cm^{-1} and the appearance of new features in the NIR region at 7500 cm^{-1}, which grew and decayed during the earlier stages of the electrolysis, and at 11048 and 14280 cm^{-1}, which continued to grow throughout the experiment. Again, back-reduction failed to regenerate **22**, but more surprisingly the bands at 11049 and 14280 cm^{-1} kept increasing before disappearing, confirming the electrochemical process taking place in the initial stages of the spectroelectrochemical experiment. Although we have not identified the product ultimately formed on oxidation of **22**, the transient band observed at 7500 cm^{-1} likely arises from the initial oxidation product [**22**]$\bullet^{+}$, whilst the relatively intense, persistent features observed at the later stages at 11048 and 14280 cm^{-1} are similar to those in the absorption spectrum of {*cyclo*-C([Ru])C(CCCC[Ru])C(CC]Ru]C(CC[Ru])}$^{2+}$ (12060, 16640 cm^{-1}, [Ru] = Ru(dppe)Cp) (Figure 3-18).[60]

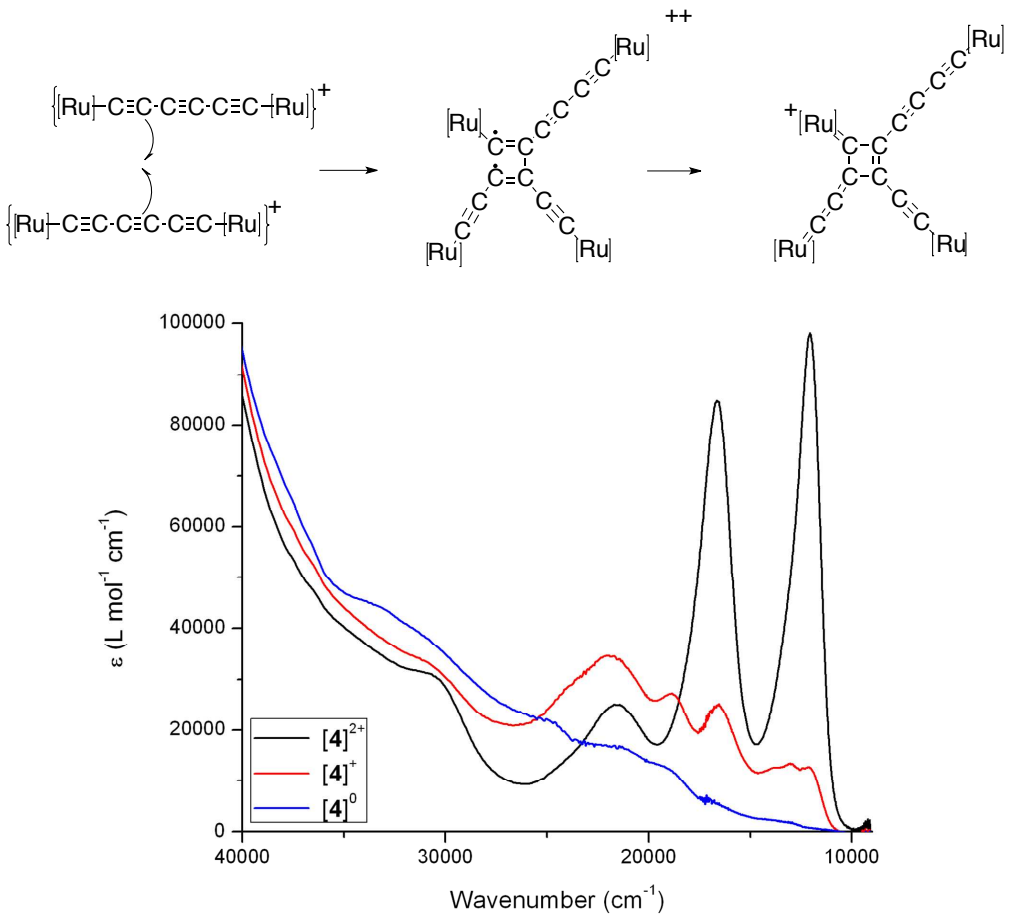

Figure 3-18. Proposed mechanism for the self-coupling of *[{Ru(PPh$_3$)$_2$Cp}$_2$(μ-C≡CC≡CC≡C)]$^{+}$ (top)*; *UV-Vis spectra of the reduction cycle of [{Ru(PPh$_3$)$_2$Cp}$_2$(μ-C≡CC≡CC≡C)]$^{n+}$ (n = 2 black, n = 1 red and n = 0 blue) (bottom) from reference.*[60]

Indeed, two isosbestic points are distinguishable from the UV-Vis-NIR, the crossing between light blue and pink curves and between dark blue and green curves (Figure 3-17). It therefore appears probable that the initial oxidation of **22** give the radical cation $[\mathbf{22}]^+$ which is followed by a cyclodimerization process analogous to that observed for $[\{Ru(dppe)Cp\}_2(\mu\text{-}C{\equiv}CC{\equiv}CC{\equiv}C)]^+$ (Scheme 3-19).

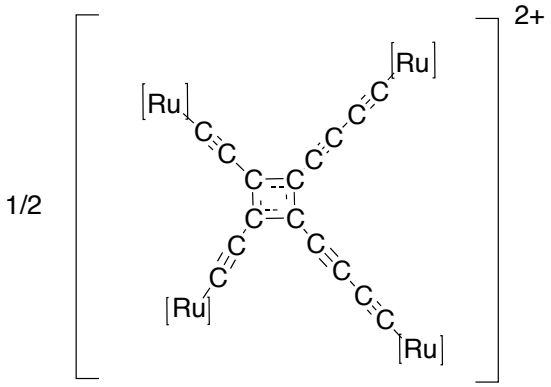

Figure 3-19. Possible dimerization of the compound $[\mathbf{22}]^+$.

3.7. Quantum chemical calculations

The electronic structure of monometallic oligoynyl[57,91,92] and bimetallic oligoyndiyl[32,33,86,93,94] complexes has been explored in detail over the last 20 years at increasingly sophisticated levels of theory.

Here, hybrid-DFT calculations (B3LYP/3-21G*/CPCM-CH_2Cl_2) spectroscopy[95] were carried out by Dr Mark Fox and Prof Paul Low on the compounds **21** and **22** to investigate the influence of the interpolated phenylene ring on the electronic structure along with **15** as a monometallic example for comparison. Each system was fully optimized without symmetry constraints, with frequency calculations indicating each structure to be a true minimum. The resulting computational systems are denoted **21´** and **22´** to distinguish them from the synthesised complexes (Figure 3-20).

Each bimetallic structure adopts mutual *trans*-arrangement of the Cp rings and in the case of **21´** the phenylene ring essentially bisects the P-Ru-P angles at each metal (Cp(0)-Ru(1)-C(5)-C(7): 172.9° (**21**); 165.26 (**21´**); Cp(0) is the centroid of the Cp ring. The selected

bond lengths and angles for **15´**, **21´** and **22´** summarized in Table 3-5 enable comparison with the crystallographically determined structures. The majority of experimental bond lengths are reproduced well with differences of < 0.02 Å. The most significant deviations arise from the Ru-P distances in **22**, which are over-estimated by 0.04 - 0.06 Å, and the ± 0.06 Å difference between the calculated C(3)-C(4) and C(4)-C(5) distances in **21´** and the values obtained from the relatively low precision crystallographic structure. Nevertheless, deviations of this magnitude are not uncommon for calculations of organometallic complexes and the overall level of agreement is more than satisfactory.

The electronic structures of **21´** (Table 3-4) and **22´** (Table 3-5) were also examined, and give features that are broadly as expected for half-sandwich alkynyl-derivatives.[95,96,97] Thus, in each case the HOMO and HOMO-1 have dπ/π character along the Ru-C≡C-…-C≡C-Ru backbone, with the usual nodal planes between the formally singly-bonded atoms (Figure 3-20).

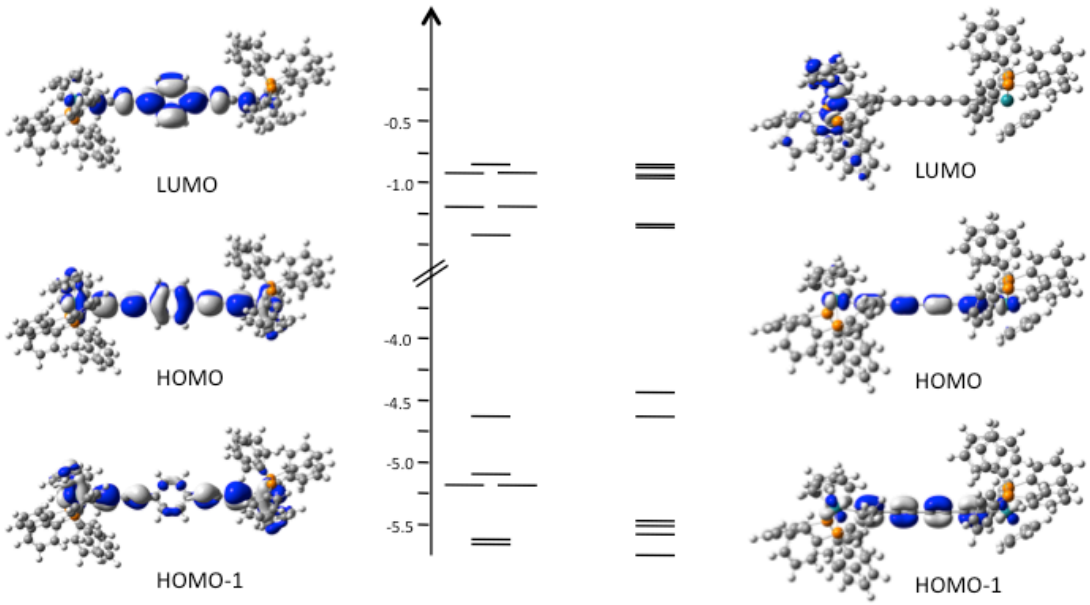

Figure 3-20. MO diagrams of **21'** (left) and **22'** (right) and plots of key frontier molecular orbitals (plotted with contour value ±0.02 $(e/bohr^3)^{1/2}$).

These filled frontier orbitals are well separated from the LUMO and LUMO+1 ($\Delta E_{HOMO-LUMO}$: 3.31 eV (**21´**), 3.20 eV (**22´**)) which in **22´** are essentially degenerate and largely located on the $Ru(PPh_3)_2Cp$ fragments. However, at this level of theory, in **21´** the LUMO is bis(buta-1,3-diynyl)benzene π* orbital in character, with the degenerate $Ru(PPh_3)_2Cp$

metal-ligand anti-bonding orbitals forming the LUMO+1 and LUMO+2 and lying ca. 0.1 eV above the LUMO.

Whilst the dπ/π-type HOMO of **21´** is delocalized extensively along the entire length of the RuC≡CC≡CC_6H_4C≡CC≡CRu chain (ca. 14% Ru, 48% C_4, 15% C_6H_4), the planar phenylene moiety breaks the conjugation in the orthogonal HOMO–1 (ca. 38% Ru, 40% C_4, 4% C_6H_4), and gives a substantial HOMO to HOMO-1 gap of ca. 0.5 eV. In contrast, the cylindrical symmetry of the all-carbon chain in **22´** results in a more similar composition and energy of the HOMO (- 4.46 eV; 27% Ru, 62% C_8) and HOMO-1 (- 4.64 eV; 27% Ru, 67% C_8). The presence of one (**21´**) or two (**22´**) occupied orbitals in the frontier region is consistent with the observation of two (**21´**) or four (**22´**) oxidation processes in these complexes. In addition, the lower lying HOMO **21´**, which arises from the significant carbon character of this orbital, is consistent with the more positive redox potentials (Table 3-3) observed for the first and second processes of **21´** relative to **22´**.

Table 3-4. *Orbital energies (eV) and composition (%) for selected frontier orbitals of **21'**.*

MO		eV	Cp1	$PPh_3$1	Ru1	Cα1	Cβ1	Cγ1	Cδ1	C_6H_4	Cδ2	Cχ2	Cβ2	Cα2	Ru2	$PPh_3$2	Cp2
405	L+5	-0.81	4	76	10	1	0	0	0	0	0	0	0	0	1	8	0
404	L+4	-0.85	1	98	1	0	0	0	0	0	0	0	0	0	0	0	0
403	L+3	-0.85	0	0	0	0	0	0	0	0	0	0	0	0	1	98	1
402	L+2	-1.23	0	0	0	0	0	0	0	0	0	0	0	0	32	54	14
401	L+1	-1.23	14	54	32	0	0	0	0	0	0	0	0	0	0	0	0
400	LUMO	-1.33	1	1	2	8	0	11	3	49	3	11	0	8	2	1	1
399	HOMO	-4.64	3	3	12	5	8	4	7	15	7	4	8	5	12	3	3
398	H-1	-5.14	5	4	20	3	10	1	7	4	6	1	9	3	18	4	5
397	H-2	-5.2	1	1	6	1	3	0	2	2	11	2	15	6	40	5	5
396	H-3	-5.2	5	5	40	6	15	2	11	2	2	0	3	1	7	1	1
395	H-4	-5.61	19	16	34	5	4	1	4	1	1	0	1	1	6	3	4
394	H-5	-5.62	4	3	6	1	1	0	1	1	4	1	5	5	33	16	19

Table 3-5. *Orbital energies (eV) and composition (%) for selected frontier orbitals of **22′**.*

MO		eV	Cp1	$PPh_3$1	Ru1	Cα1	Cβ1	Cχ1	Cδ1	Cδ2	Cχ2	Cβ2	Cα2	Ru2	$PPh_3$2	Cp2
385	L+5	-0.81	2	31	6	7	0	8	4	4	8	0	7	6	13	3
384	L+4	-0.82	2	60	9	4	0	4	2	2	4	0	3	2	6	1
383	L+3	-0.88	1	68	2	3	0	3	2	2	3	0	3	3	8	1
382	L+2	-0.9	0	3	0	1	0	1	1	1	1	0	1	6	82	2
381	L+1	-1.25	0	0	0	0	0	0	0	0	0	0	0	34	52	15
380	LUMO	-1.26	15	53	32	0	0	0	0	0	0	0	0	0	0	0
379	HOMO	-4.46	3	3	13	8	8	7	7	8	7	9	8	14	3	3
378	H-1	-4.64	1	1	14	9	8	8	8	8	9	8	9	13	1	1
377	H-2	-5.44	7	6	21	0	8	1	4	4	1	8	0	25	6	8
376	H-3	-5.46	13	10	34	1	2	0	1	1	0	3	1	21	6	7
375	H-4	-5.56	10	7	18	2	1	1	1	1	1	1	2	27	14	17
374	H-5	-5.88	4	7	28	1	8	0	4	4	0	8	1	23	6	4

3.8. Conclusion

We have demonstrated that the availability of stable terminal buta-1,3-diynyl complexes makes Sonogashira cross-coupling protocols an appealing entry point for the preparation of a wide range of substituted buta-1,3-diynyl compounds, thereby avoiding the preparation of buta-1,3-diyne ligand precursors. The process is suitable for the preparation of 'simple' buta-1,3-diynyl complexes, i.e. those bearing relatively chemically and functionally complex substituents, which are chemically and functionally rather sensitive, such as 2,3-dihydrobenzo[*b*]thiophene (**18**) and pyridine (**19**), and more elaborate bis(diynyl) complexes such as **21**. Facile homo-coupling of $Ru(C{\equiv}CC{\equiv}CH)(PPh_3)_2Cp$ in the presence of Pd(II)/Cu(I) co-catalysts and air as an oxidant affords the octa-1,3,5,7-tetra-1,8-diyl complex **20**. Whilst the chemical reactivity of $[\mathbf{21}]^+$ and $[\mathbf{22}]^+$ prevented detailed analysis of these compounds by spectroelectrochemical methods, DFT calculations have been used to indicate the greater organic character in the frontier orbitals of **21´** relative to **22´**, which is consistent with the trends in electrochemical properties. The work described here therefore extends the 'chemistry on the complex' approach to the preparation of complex organometallic compounds, and further illustrates the facile synthetic routes that may be developed using this strategy.

CHAPTER 3

3.9. Experimental

3.9.1. General conditions

All reactions were carried out in oven-dried glassware under oxygen-free argon atmosphere using standard Schlenk techniques. HN^iPr_2 was purified by distillation from KOH and NEt_3 were purified by distillation from $CaSO_4$, other reaction solvents were purified and dried using Innovative Technology SPS-400 and degassed before use. The compound $Ru(C{\equiv}CC{\equiv}CH)(PPh_3)_2Cp$[19] was prepared following the literature method. DHBT was prepared by Dr Murat Gulcur using the literature route.[98] Other reagents were purchased commercially and used as received. NMR spectra were recorded in deuterated solvent solutions on Bruker Avance 400 MHz and Varian VNMRS 700 MHz spectrometers and referenced against residual protio-solvent resonances after nuclei ($CHCl_3$: ^1H 7.26 ppm, ^{13}C 77.00 ppm and CH_2Cl_2: ^1H 5.32 ppm, ^{13}C 53.84 ppm) and H_3PO_4 (^{31}P). In the NMR assignment, the phenyl ring associated with PPh_3 are denoted Ph and Ar indicates any arylene group belonging to the alkynyl ligands.

Matrix-assisted laser desorption ionization (MALDI) mass spectra were recorded using an Autoflex II TOF/TOF mass spectrometer with a 337 nm laser. Electron ionisation mass spectra were recorded on a Thermoquest Trace or a Thermo-Finnigan DSQ. Infrared spectra were recorded on a Thermo 6700 spectrometer from CH_2Cl_2 solution in a cell fitted with CaF_2 windows. UV-Vis spectra were recorded on a Cary 5000 Series UV-Vis-NIR spectrophotometer. Electrochemical analyses were recorded using a BAS CV50W electrochemical analyzer fitted with a three-electrode system consisting of a Pt disk as working electrode, auxiliary and reference electrode from solution in CH_2Cl_2 containing 0.1 M NBu_4PF_6. Elemental analyses were performed on a CE-400 Elemental Analyzer. Single-crystal X-ray data were collected at 120(2) K on a Bruker SMART CCD 6000 (fine-focus sealed tube, graphite-monochromator).

General procedure for the preparation of the butadiynyl ruthenium (II) complexes ***15, 16, 17, 18, 19, 20****:* In a Schlenk flask, a mixture of Ru(C≡CC≡CH)$(PPh_3)_2$Cp (**14**), 1.5 equivalent of the appropriate iodoaryl, 5 mol% $Pd(PPh_3)_4$ and 10 mol% CuI was added to a solution of degassed HN^iPr_2 (1 mL/mmol). The reaction mixture was heated to 90 °C for 2 h and cooled to room temperature. The resulting precipitate was collected by filtration, washed with cold hexane, dried, and washed with cold MeOH to give the final compound.

Ru(C≡CC≡C-C_6H_4CN-4)$(PPh_3)_2$Cp; 15

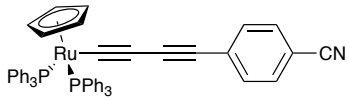

From **14** (100 mg, 0.135 mmol) and isolated as a honey-yellow colored solid. Yield: 53 mg, 47%. Single crystals suitable for X-ray diffraction were grown by slow diffusion of methanol into a CH_2Cl_2 solution containing 5% NEt_3. ^{1}H NMR (400 MHz, $CDCl_3$): δ 7.43 (ABq, J = 8.2 Hz, 4H, Ar), 7.37 - 7.35 (m, 12H, Ph), 7.21 - 7.19 (m, 6H, Ph), 7.12 - 7.10 (m, 12H, Ph), 4.33 (s, 5H, Cp) ppm. ^{31}P $\{^1H\}$ NMR (162 MHz, $CDCl_3$): δ 48.2 (s) ppm. $^{13}C\{^1H\}$ NMR (700 MHz, $CDCl_3$): δ 138.1 - 137.8 (m, Ph_i), 134.1 (t, J = 24.7 Hz, C_α), 133.6 (t, J = 4.9 Hz, Ph_o), 132.6 (HC_{Ar}), 131.6 (C_{Ar}), 131.5 (HC_{Ar}), 128.7 (Ph_p), 127.4 (t, J = 4.6 Hz, Ph_m), 119.3 (C≡N), 108.2 (C_{Ar}), 96.0 (C_β), 85.9 (Cp), 85.7 (C_γ), 61.8 (C_δ) ppm. IR (CH_2Cl_2): ν(C≡CC≡C) 2147 (s); 2017 (m) cm^{-1}. MS (MALDI-TOF; *m/z*): 579.2 $[M-PPh_3]^+$, 841 $[M]^+$, 719 $[Ru(CO)(PPh_3)_2Cp]^+$. HR-ESI$^+$-MS: *m/z* calcd for $C_{52}H_{40}NP_2{}^{96}Ru$ 836.1712; found 836.1737. Crystal data for **15**: $C_{52}H_{40}NP_2{}^{96}Ru$, M = 840.85, monoclinic, space group P2/c, *a* = 14.2477(6) Å, *b* = 16.6875(8) Å, *c* = 17.3130(8) Å, β = 90.515(1) °, *U* = 4116.1(3) Å^3, F(000) = 1728, Z = 4, D_C = 1.357 mg/mm^3, μ = 0.496 mm^{-1}; 64895 reflections were collected , yielding 10431 unique data (R_{merg} = 0.0691). Final $wR_2(F^2)$ = 0.0818 for all data (505 refined parameters), conventional $R_1(F)$ = 0.0330 for 7972 reflections with I ≥ 2σ, GOF = 1.007.

CHAPTER 3

Ru(C≡CC≡C-$C_6H_4CH_3$-4)(PPh_3)$_2$Cp; 16

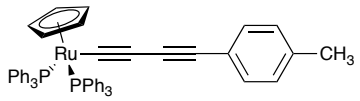

From **14** (40 mg, 0.054 mmol) to give a yellow solid. Yield: 39 mg, 87%. Single crystals suitable for X-ray diffraction were grown by slow diffusion of methanol into a CH_2Cl_2 solution containing 5% NEt_3. ^{1}H NMR (400 MHz, $CDCl_3$): δ 7.44 - 7.39 (m, 12H, Ph); 7.34 - 7.32 (m, 2H, Ar); 7.24 - 7.20 (m, 6H, Ph); 7.15 - 7.11 (m, 12H, Ph); 7.06 - 7.04 (m, 2H, Ar); 4.33 (s, 5H, Cp); 2.32 (s, 3H, C*H*$_3$) ppm. ^{31}P{^{1}H} NMR (162 MHz, $CDCl_3$): δ 48.4 (s) ppm. ^{13}C{^{1}H} NMR (700 MHz, $CDCl_3$): δ 138.3 - 137.8 (m, Ph_i), 135.5 (C_{Ar}), 133.6 (t, J = 5.1 Hz, Ph_o), 132.0 (HC_{Ar}), 128.4, 128.3 (HC_{Ar} or Ph_p), 127.1 (t, J = 4.6 Hz, Ph_m), 122.8 (t, J = 24.9 Hz, C_α), 122.7 (C_{Ar}), 95.4 (C_β), 85.4 (Cp), 79.3 (C_γ), 62.7 (C_δ), 21.1 (*C*H$_3$) ppm. IR (CH_2Cl_2): ν(C≡CC≡C) 2159 (s); 2021 (m) cm^{-1}. MS (MALDI-TOF; *m/z*): 568.2 [M-PPh_3]$^+$, 830.0 [M]$^+$. HR-ESI$^+$-MS: *m/z* calcd for $C_{52}H_{42}P_2{}^{96}Ru$ 824.1838; found 824.1862. Anal. Calcd for $C_{52}H_{42}P_2Ru$: C, 75.26; H, 5.10. Found: C, 75.17; H, 5.05. Crystal data for **16**: $C_{52}H_{42}P_2{}^{96}Ru$, M = 829.87, monoclinic, space group $P2_1/n$, *a* = 12.9342(9) Å, *b* = 23.3662(17) Å, *c* = 13.3100(10) Å, β = 98.512(2) °, *U* = 3978.3(5) Å^3, F(000) = 1712, Z = 4, D_C = 1.386 mg/mm^3, μ = 0.511mm^{-1}; 45590 reflections were collected , yielding 9605 unique data (R_{merg} = 0.0997). Final *w*$R_2(F^2)$ = 0.0413 for all data (497 refined parameters), conventional $R_1(F)$ = 0.0413 for 5906 reflections with I ≥ 2σ, GOF = 0.961.

Ru(C≡CC≡C-C_6H_4OMe-4)(PPh_3)$_2$Cp; 17

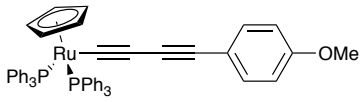

From **14** (40 mg, 0.054 mmol) to give a yellow solid. Yield: 27 mg, 59%. ^{1}H NMR (400 MHz, $CDCl_3$): δ 7.43 - 7.40 (m, 12H, Ph), 7.37 (d, J = 8.6 Hz, 2H, Ar), 7.24 - 7.20 (m, 6H, Ph), 7.15 - 7.11 (m, 12H, Ph), 6.79 (d, J = 8.6 Hz, 2H, Ar), 4.33 (s, 5H, Cp), 3.80 (s, 3H, O*Me*) ppm. ^{31}P{^{1}H} NMR (162 MHz, $CDCl_3$): δ 49.1 (s) ppm. ^{13}C{^{1}H} NMR (600 MHz, $CDCl_3$): δ 158.0 (C_{Ar}-OMe), 138.6 - 137.9 (m, Ph_i), 133.7 (t, J = 5.1 Hz, Ph_o), 133.5 (HC_{Ar}), 128.5 (Ph_p), 127.3 (t, J = 4.7 Hz, Ph_m), 122.9 (t, J = 25.0 Hz, C_α), 118.1 (C_{Ar}),

113.6 (HC_{Ar}), 95.4 (C_β), 85.6 (Cp), 78.7 (C_γ), 62.4 (C_δ), 55.1 (O-CH$_3$). IR (CH_2Cl_2): ν(C≡CC≡C) 2160 (s); 2021 (m) cm^{-1}. MS (MALDI-TOF; *m/z*): 584.1 [M-PPh$_3$]$^+$, 846.1 [M]$^+$. HR-ESI$^+$-MS: *m/z* calcd for $C_{52}H_{42}OP_2{}^{96}Ru$ 840.1787; found 840.1828. Anal. Calcd for $C_{52}H_{42}OP_2Ru$•0.5 CH_2Cl_2: C, 70.98; H, 4.88. Found: C, 71.45; H, 4.31.

Ru(C≡C-C≡C-DHBT)(PPh$_3$)$_2$Cp; 18

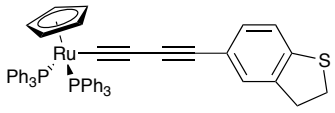

From **14** (40 mg, 0.054 mmol) to give a mustard-colored solid. Yield: 25 mg, 54%. Single crystals suitable for X-ray diffraction were grown by slow diffusion of methanol into a CH_2Cl_2 solution containing 5% NEt_3. ^{1}H NMR (400 MHz, $CDCl_3$): δ 7.42 - 7.39 (m, 12H, Ph), 7.23 - 7.19 (m, 8H, Ph + Ar), 7.13 - 7.09 (m, 12H, Ph), 7.05 (d, J =8.0 Hz, 1H, Ar), 4.32 (s, 5H, Cp), 3.35 - 3.31 (m, 2H, CH_2), 3.24 - 3.20 (m, 2H, CH_2) ppm. ^{31}P {^{1}H} NMR (162 MHz, $CDCl_3$): δ 49.3 (s) ppm. ^{13}C{^{1}H} NMR (700 MHz, $CDCl_3$): δ 139.8 (C_{Ar}), 139.3 (C_{Ar}), 138.3 - 138.1 (m, Ph$_i$), 133.7 (t, J = 4.9 Hz, Ph$_o$), 131.5 (HC_{Ar}), 128.5 (Ph$_p$), 128.0 (HC_{Ar}), 127.3 (t, J = 4.6 Hz, Ph$_m$), 121.6 (C_{Ar}), 121.5 (HC_{Ar}), 95.5 (C_β), 85.6 (Cp), 79.7 (C_γ), 62.7 (C_δ), 35.9 (CH$_2$), 33.4 (CH$_2$) ppm, the C_α peak was not visible. IR (CH_2Cl_2): ν(C≡CC≡C) 2156 (s); 2015 (m) cm^{-1}. MS (MALDI-TOF; *m/z*): 875.2 [M + H]$^+$, 719.1 [Ru(CO)(PPh$_3$)$_2$Cp]$^+$. HR-ESI$^+$-MS: *m/z* calcd for $C_{53}H_{42}P_2S^{96}Ru$ 868.1558; found 868.1597. Calcd for $C_{53}H_{42}P_2RuS$•0.75 CH_2Cl_2: C, 68.85; H, 4.89. Found: C, 68.75; H, 4.89. Crystal data for **18**: $C_{52}H_{42}P_2S^{96}Ru$, M = 873.94, monoclinic, space group P2$_1$/n, *a* = 11.2014(7) Å, *b* = 16.3616(11) Å, *c* = 22.0949(14) Å, β = 90.675(2) °, *U* = 4049.1(5) Å^3, F(000) = 1800, Z = 4, D_C = 1.434 mg/mm^3, μ = 0.556 mm^{-1}; 66387 reflections were collected , yielding 10767 unique data (R_{merg} = 0.0420). Final $wR_2(F^2)$ = 0.0423 for all data (682 refined parameters), conventional $R_1(F)$ = 0.0315 for 8977 reflections with I ≥ 2σ, GOF = 1.065.

CHAPTER 3

Ru(C≡CC≡C-C_5H_4N)(PPh_3)$_2$Cp; 19

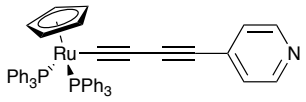

From **14** (50 mg, 0.067 mmol) to give a yellow powder. Yield: 33 mg, 60%. ^{1}H NMR (400 MHz, CD_2Cl_2): δ 8.40 (d, J = 6.1 Hz, 2H, Ar), 7.39 - 7.36 (m, 12H, Ph), 7.29 - 7.27 (m, 6H, Ph), 7.22 (d, J = 6.1 Hz, 2H, Ar), 7.18 - 7.15 (m, 12H, Ph), 4.38 (s, 5H, Cp) ppm. ^{31}P{^{1}H} NMR (162 MHz, $CDCl_3$): δ 48.8 (s) ppm. ^{13}C{^{1}H} NMR (600 MHz, $CDCl_3$): δ 149.0 (HC_{Ar}), 138.2 - 137.8 (m, Ph_i), 134.5 (C_{Ar}), 133.6 (t, J = 5.0 Hz, Ph_o), 128.7 (Ph_p), 127.3 (t, J = 5.0 Hz, Ph_m), 126.4 (HC_{Ar}), 95.7 (C_β), 85.9 (Cp), 85.7 (C_γ), 60.4 (C_δ), the C_α was not visible. IR (CH_2Cl_2): ν(C≡CC≡C) 2150 (s); 2006 (m) cm^{-1}. MS (MALDI-TOF; *m/z*): 817.1 [M]$^+$. HR-ESI$^+$-MS: *m/z* calcd for $C_{50}H_{40}NP_2{}^{96}Ru$ 812.1712; found 812.1740.

N,N-Bis-4-methoxyphenylamine (Modified procedure[99])

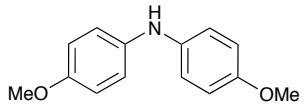

To an oven dried two necked flask was added in dry toluene (50 mL), p-anisidine (2.5 g, 20 mmol), 4-iodoanisole (5.1 g, 22 mmol), 0.5 mol% tris-(dibenzylideneacetone)palladium ($Pd_2(dba)_3$) (90 mg, 0.10 mmol), 2.5 mol% 1,1'-bis(diphenylphosphino)ferrocene (Xphos) (110 mg, 0.23 mmol) and sodium tert-butoxide (Na^{t}OBu) (5.4 g, 56 mmol). The reaction mixture was heated at 110°C overnight. The brown suspension was dried and the residue was purified on a silica chromatography column using hexane/acetone (9.5:0.5 v/v). The first band was the remaining 4-iodoanisole and the second band was the product, obtained as a yellowish solid. Yield: 2.12 g, 46%. ^{1}H NMR (400 MHz, DMSO-d_6): δ 7.52 (s, 1H, N*H*), 6.94 - 6.89 (m, 4H, Ar), 6.83 - 6.78 (m, 4H, Ar), 3.68 (s, 6H, C*H*$_3$) ppm. ^{13}C NMR {^{1}H} (400 MHz, DMSO-d_6): δ 152.8 (O-C_{Ar}), 128.0 (C_{Ar}), 118.0, 114.5 (HC_{Ar}), 55.2 (*C*H$_3$) ppm. The data were consistent with the literature.[99]

N,N-Di(4-methoxyphenyl)-4-phenylamine (Modified procedure[99])

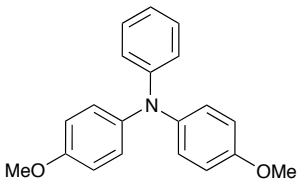

A solution of dry and degassed toluene (20 mL), N,N-bis-4-methoxyphenylamine (1g, 4.4 mmol), bromobenzene (753 mg, 4.8 mmol), $Pd_2(dba)_3$ (40 mg, 0.04 mmol), Xphos (63 mg, 0.13 mmol) and Na^{t}Bu (1.18 g, 12.3 mmol) was heated at 110 °C for 24 h. The resulting solution was dried and the mixture was purified on a silica chromatography column using hexane/EtOAc as eluent (10:1 v/v) to give an off-white solid. Yield: 926 mg, 69%. ^{1}H NMR (400 MHz, DMSO-d_6): δ 7.20 - 7.14 (m, 2H, Ar), 7.01 - 6.96 (m, 4H, Ar), 6.92 - 6.87 (m, 4H, Ar), 6.83 (tt, J = 7.3, 1.1 Hz, 1H, Ar), 6.79 - 6.76 (m, 2H, Ar), 3.73 (s, 6H, C*H*$_3$). The NMR data are consistent with the literature.[99]

N,N-Bis(4-methoxyphenyl)-4-iodophenylamine (Modified procedure[99])

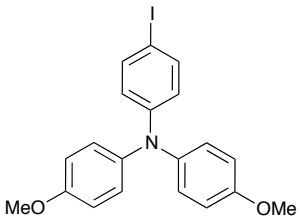

To a solution of EtOH (20 mL) and N,N-di(4-methoxyphenyl)-4-phenylamine (500 mg, 1.6 mmol) was added periodic acid (73 mg, 0.32 mmol) and iodine (162 mg, 0.64 mmol). The reaction mixture was stirred at reflux temperature overnight and then concentrated. The impure product was purified on a silica chromatography column using CH_2Cl_2/hexane as eluent (5:5 v/v) to give a sticky oil which was recrystallized in hot ethanol to form white crystals. Yield: 250 mg, 36%. ^{1}H NMR (400 MHz, $CDCl_3$): δ 7.41 - 7.39 (m, 2H, Ar), 7.04 - 7.02 (m, 4H, Ar), 6.82 (pseudo-d, 4H, Ar), 6.68 - 6.66 (m, 2H, Ar), 3.79 (s, 6H, C*H*$_3$). The NMR data are consistent with the literature.[99]

Ru(C≡CC≡C-$C_6H_4N(C_6H_4OMe$-4)$_2(PPh_3)_2Cp$; 20

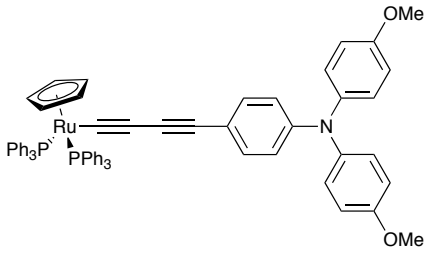

From **14** (80 mg, 0.11 mmol) to give a mustard-colored solid. The solution was heated at 90 °C for 48 h and purified on a neutral alumina column eluted by CH_2Cl_2/hexane (1:1 v/v) and the yellow solution was dried to give a mustard solid. Yield: 33 mg, 29%. Single crystals suitable for X-ray diffraction were grown by slow diffusion of diethyl ether into a CH_2Cl_2 solution containing 5% NEt_3. ^{1}H NMR (400 MHz, $CDCl_3$): δ 7.42 - 7.39 (m, 12H, Ph), 7.23 (pseudo-d, 2H, Ar), 7.21 - 7.19 (m, 6H, Ph), 7.12 - 7.10 (m, 12H, Ph), 7.02 (pseudo-d, 4H, Ar), 6.81 - 6.79 (m, 6H, Ar), 4.31 (s, 5H, Cp), 3.78 (s, 6H, C*H*$_3$) ppm. ^{31}P $\{^1$H$\}$ NMR (162 MHz, $CDCl_3$): δ 49.3 (2P) ppm. ^{13}C NMR $\{^1$H$\}$ (700 MHz, $CDCl_3$): δ 155.7 (C_{Ar}-OCH_3), 146.8 (C_{Ar}-N), 140.8 (C_{Ar}), 138.4 - 138.2 (m, Ph_i), 133.8 (t, J = 5.0 Hz, Ph_o), 133.0 (HC_{Ar}), 128.5 (Ph_p), 127.3 (t, J = 4.6 Hz, Ph_m), 126.4 (HC_{Ar}), 120.3 (HC_{Ar}), 117.5 (C_{Ar}), 114.6 (HC_{Ar}), 95.7 (C_β), 85.6 (Cp), 79.0 (C_γ), 63.1 (C_δ), 55.4 (O*C*H$_3$) ppm, the C_α was not visible. IR (CH_2Cl_2): ν(C≡CC≡C) 2156 (s); 2022 (m) cm^{-1}. MS (MALDI-TOF; *m/z*): 719.1 $[Ru(CO)(PPh_3)_2Cp]^+$, 1043.2 $[M]^+$. HR-ESI$^+$-MS: *m/z* calcd for $C_{65}H_{53}NO_2P_2{}^{96}Ru$ 1037.2629; found 1037.2628. Crystal data for **20**: $C_{65}H_{53}NO_2P_2{}^{96}Ru{\cdot}CH_2Cl_2$, M = 1128.02, triclinic, space group P-1, *a* = 11.1066(11) Å, *b* = 13.9775(14) Å, *c* = 17.0724(17) Å, β = 87.161(3) °, *U* = 2628.7(5) Å^3, F(000) = 1164, Z = 2, D_C = 1.425 mg/mm^3, μ = 0.509 mm^{-1}; 33955 reflections were collected , yielding 11986 unique data (R_{merg} = 0.0420). Final $wR_2(F^2)$ = 0.1849 for all data (669 refined parameters), conventional $R_1(F)$ = 0.0800 with I ≥ 2σ, GOF = 1.065.

$\{Ru(PPh_3)_2Cp\}_2$(μ-C≡C-C≡CC_6H_4C≡C-C≡C); 21

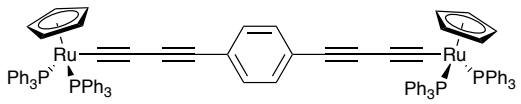

A solution of Ru(C≡CC≡CH)$(PPh_3)_2Cp$ (**14**) (100 mg, 0.135 mmol), 1,4-diiodobenzene (23 mg, 0.067 mmol), $Pd(PPh_3)_4$ (7 mg, 0.006 mmol) and CuI (2 mg, 0.012 mmol) in

HN^iPr_2 (10 mL) was stirred for 2 h at room temperature before being heated at reflux for 2 h. The solvent was removed, and the residue purified on a neutral alumina column eluted with CH_2Cl_2:NEt_3 (95:5 v/v). The main yellow band was collected and a gold-brown solid was obtained upon addition of methanol (5 mL). Yield: 70 mg, 67%. Single crystals suitable for X-ray diffraction were grown by slow diffusion of diethyl ether into a CH_2Cl_2 solution containing 5% NEt_3. ^1H NMR (400 MHz, $CDCl_3$): δ 7.44 - 7.33 (m, 24H, Ph), 7.30 (s, 4H, Ar), 7.25 - 7.21 (m, 12H, Ph), 7.15 - 7.12 (m, 24H, Ph), 4.34 (s, 10H, Cp) ppm. $^{31}P\{^1H\}$ NMR (162 MHz, $CDCl_3$): δ 48.4 (s) ppm. $^{13}C\{^1H\}$ NMR (700 MHz, $CDCl_3$): δ 138.3 - 138.1 (Ph_i), 133.7 (t, (J = 5.0 Hz), Ph_o), 131.8 (HC_{Ar}), 128.5 (Ph_p), 127.3 (t, (J = 4.7 Hz), Ph_m), 125.7 (t, (J = 23.0 Hz), C_α), 123.4 (C_{Ar}), 95.9 (C_β), 85.6 (Cp), 81.8 (C_γ), 63.4 (C_δ). IR (CH_2Cl_2): ν(C≡CC≡C) 2155 (s); 2016 (m) cm^{-1}. MS (MALDI-TOF; *m/z*): 1554.0 $[M]^+$. HR-ESI^+-MS: *m/z* calcd for $C_{96}H_{74}P_4Ru_2$ 1554.2871; found: 1554.2665. Crystal data for **21**: $C_{96}H_{74}P_4{}^{96}Ru_2 \cdot CH_2Cl_2$, M = 1638.50, monoclinic, space group $P2_1/c$, a = 16.693(7) Å, b = 11.384(4) Å, c = 21.646(9) Å, β = 98.678(5) °, U = 4066(3) $Å^3$, F(000) = 1680, Z = 2, D_C = 1.338 mg/mm^3, μ = 0.563 mm^{-1}; 20671 reflections were collected , yielding 6114 unique data (R_{merg} = 0.0929). Final $wR_2(F^2)$ = 0.2575 for all data (487 refined parameters), conventional $R_1(F)$ = 0.0800 for 3957 reflections with I ≥ 2σ, GOF = 1.024.

{Ru(PPh$_3$)$_2$Cp}$_2$(μ-C≡CC≡CC≡CC≡C); 22[73]

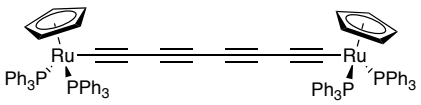

An open flask was charged with a solution of Ru(C≡CC≡CH)(PPh_3)$_2$Cp (**14**) (100 mg, 0.135 mmol), Pd(PPh_3)$_4$ (6.8 mg, 0.006 mmol) and an excess of CuI (8 mg) in HN^iPr_2 (8 mL). The mixture was stirred at room temperature for 1 h after which time the solution had turned yellow in color and a brown precipitate had formed. The solvent was removed and the residue purified on a neutral alumina column eluted by CH_2Cl_2/5% NEt_3. After precipitation from hexane a bright yellow solid was obtained. Yield: 55 mg, 55%. ^1H NMR (400 MHz, CD_2Cl_2): δ 7.42 - 7.38 (m, 24H, Ph), 7.24 - 7.21 (m, 12H, Ph), 7.15 - 7.11 (m, 24H, Ph), 4.31 (s, 10H, Cp) ppm. $^{31}P\{^1H\}$ NMR (162 MHz, $CDCl_3$): δ 48.9 (s) ppm. $^{13}C\{^1H\}$ NMR (600 MHz, CD_2Cl_2): δ 138.9 - 138.3 (Ph_i), 134.1 (t, J = 5.0 Hz, Ph_o), 129.2

(Ph_p), 127.8 (t, J = 4.6 Hz, Ph_m), 119.6 (t, J = 24.9 Hz, C_α), 96.7 (C_β), 86.4 (Cp), 62.6 (C_γ), 51.7 (C_δ). IR (CH_2Cl_2): ν((C≡C)$_4$) 2107 (s); 1955 (m) cm^{-1}. MS^+ (MALDI-TOF; *m/z*): 954.1 $[M\text{-}2PPh_3]^+$, 1216.1 $[M\text{-}PPh_3]^+$, 1478 $[M]^+$. HR-ESI^+-MS: *m/z* calcd for $C_{90}H_{70}P_4Ru_2$ 1478.2556; found 1478.2368. Calcd for $C_{91}H_{70}P_4Ru_2 \bullet 0.5CH_2Cl_2$: C, 71.51; H, 4.71. Found: C, 71.85; H, 4.80. Crystal data for **22**: $C_{90}H_{70}P_4{}^{96}Ru_2 \cdot 2CH_2Cl_2$, M = 1647.33, triclinic, space group P1, *a* = 8.8692(4) Å, *b* = 12.6858(5) Å, *c* = 17.6885(7) Å, β = 96.49(2) °, *U* = 1895.25(14) $Å^3$, F(000) = 842, Z = 1, D_C = 1.443 mg/mm^3, μ = 0.672 mm^{-1}; 32488 reflections were collected , yielding 8724 unique data (R_{merg} = 0.1696). Final $wR_2(F^2)$ = 0.1745 for all data (464 refined parameters), conventional $R_1(F)$ = 0.0753 for 5362 reflections with I ≥ 2σ, GOF = 0.991.

Ru{C≡CC[=C(CN)$_2$]CC$_6$H$_4$Me=C(CN)$_2$}(PPh$_3$)$_2$Cp; 23

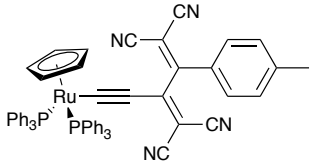

To an oven dried Schlenk flask was added degassed THF (3 mL), Ru(C≡CC≡C-$C_6H_5CH_3$-4)(PPh_3)$_2$Cp (**16**) (30 mg, 0.04 mmol) and TCNE (15 mg, 0.12 mmol). The reaction was stirred for 3 h at room temperature. The mixture was purified on a neutral alumina chromatography column using CH_2Cl_2/5%NEt_3 as eluent to give a red solid. Yield: 25 mg, 65%. X-ray quality crystals were grown by slow diffusion in CH_2Cl_2/hexane/5% NEt_3. ^1H NMR (400 MHz, $CDCl_3$): δ 7.31 - 7.27 (m, 6H, Ph), 7.25 - 7.19 (m, 14H, Ph + Ar), 7.14 - 7.10 (m, 12H, Ph), 6.94 - 6.91 (m, 2H, Ar), 4.60 (s, 5H, Cp), 2.29 (s, 3H, C*H$_3$*) ppm. $^{31}P\{^1H\}$ NMR (162 MHz, $CDCl_3$): δ 49.0 (s) ppm ^{13}C NMR $\{^1H\}$ (400 MHz, $CDCl_3$): δ 168.7 (C=*C*(CN_2)), 146.8 (C=*C*(CN_2)), 144.6 (*C*=C(CN_2)), 136.8 (m, Ph_i), 133.5 (t, J = 5.2 Hz, Ph_o), 130.7 (C_{Ar}), 129.7 (HC_{Ar}), 129.5 (Ph_p), 129.4 (*C*=C(CN_2)), 129.0, 127.8 (t, J = 4.9 Hz, Ph_m), 116.2, 114.8, 113.2, 112.4 (*C*≡N), 88.9 (Cp), 82.1, 81.2 (*C*≡), 21.8 (*C*H_3) ppm. MS (MALDI-TOF; *m/z*): 958.0 $[M]^+$. Crystal data for **23**: $C_{58}H_{42}N_4P_2{}^{96}Ru \cdot 0.5C_6H_{14} \cdot 0.2CH_2Cl_2$, M = 1018.04, monoclinic, space group $P2_1/n$, *a* = 16.4919(9) Å, *b* = 17.3216(9) Å, *c* = 19.0144(10) Å, β = 101.266(2) °, *U* = 5327.1(5) $Å^3$, F(000) = 2102, Z = 4, D_C = 1.269 mg/mm^3, μ = 0.416 mm^{-1}; 79974 reflections were collected , yielding 13482 unique data (R_{merg} = 0.0431). Final $wR_2(F^2)$ = 0.1900 for all data (584 refined parameters), conventional $R_1(F)$ = 0.0692 with I ≥ 2σ, GOF = 0.991.

3.10. References

(1) Akita, M.; Chung, M.-C.; Sakurai, A.; Shuichiro, S.; Terada, M.; Tanaka, M.; Moro-oka, Y. *Organometallics* **1997**, *16*, 4882.

(2) Mohr, W.; Stahl, J.; Hampel, F.; Gladysz, J.A. *Chem. Eur. J.* **2003**, *9*, 3324.

(3) Owen, G. R.; Stahl, J.; Hampel, F.; Gladysz, J.A. *Organometallics* **2004**, *23*, 5889.

(4) Stahl, J.; Bohling, J. C.; Peters, T. B.; de Quadras, L.; Gladysz, J. A. *Pure Appl. Chem.* **2008**, *80*, 459.

(5) Bruce, M. I.; Low, P. J.; Ke, M.; Kelly, B. D.; Skelton, B. W.; Smith, M. E.; White, A. H.; Witton, N. B. *Aust J Chem* **2001**, *54*, 453.

(6) Bruce, M. I.; Jevric, M.; Skelton, B. W.; Smith, M. E.; White, A. H.; Zaitseva, N. N. *Journal of Organometallic Chemistry* **2006**, *691*, 361.

(7) Bruce, M. I.; Scoleri, N.; Skelton, B. W. *Journal of Organometallic Chemistry* **2011**, *696*, 3473.

(8) Roberts, R. L.; Puschmann, H.; Howard, J. A. K.; Yamamoto, J. H.; Carty, A. J.; Low, P. J. *Dalton Trans.* **2003**, *6*, 1099.

(9) Paul, F.; Meyer, W. E.; Toupet, L.; Jiao, H.; Gladysz, J. A.; Lapinte, C. *J. Am. Chem. Soc.* **2000**, *122*, 9405.

(10) Bruce, M. I.; Costuas, K.; Davin, T.; Ellis, B. G.; Halet, J.-F.; Lapinte, C.; Low, P. J.; Smith, M. E.; Skelton, B. W.; Toupet, L.; White, A. H. *Organometallics* **2005**, *24*, 3864.

(11) Bartlett, M. J.; Hill, A. F.; Smith, M. K. *Organometallics* **2005**, *24*, 5795.

(12) Moreno, C.; Arnanz, A.; Delgado, S. *Inorganica Chimica Acta* **2001**, *312*, 139.

(13) Bruce, M. I.; Costuas, K.; Halet, J.-F.; Hall, B. C.; Low, P. J.; Nicholson, B. K.; Skelton, B. W.; White, A. H. *J. Chem. Soc., Dalton Trans.* **2002**, *3*, 383.

(14) de Quadras, L.; Shelton, A. H.; Kuhn, H.; Hampel, F.; Schanze, K. S.; Gladysz, J. A. *Organometallics* **2008**, *27*, 4979.

(15) Bruce, M. I.; Ke, M.; Low, P. J.; Skelton, B. W.; White, A. H. *Organometallics* **1998**, *17*, 3539.

(16) Liu, Q.; Burton, D. J. *Tetrahedron Letters* **1997**, *38*, 4371.

(17) Bruce, M. I.; Ellis, B. G.; Skelton, B. W.; White, A. H. *Journal of Organometallic Chemistry* **2000**, *607*, 137.

(18) Bruce, M. I.; Halet, J.-F.; Guennic, B. L.; Skelton, B. W.; Smith, M. E.; White, A. H. *Inorganica Chimica Acta* **2003**, *350*, 175.

(19) Bruce, M. I.; Ellis, B. G.; Gaudio, M.; Lapinte, C.; Melino, G.; Paul, F. D. R.; Skelton, B. W.; Smith, M. E.; Toupet, L.; White, A. H. *Dalton Trans.* **2004**, *10*, 1601.

(20) Bruce, M. I.; Low, P. J.; Nicholson, B. K.; Skelton, B. W.; Zaitseva, N. N.; Zhao, X.-L. *Journal of Organometallic Chemistry* **2010**, *695*, 1569.

(21) Bruce, M. I.; Büschel, S.; Cole, M. L.; Scoleri, N.; Skelton, B. W.; White, A. H.; Zaitseva, N. N. *Inorganica Chimica Acta* **2012**, *382*, 6.

(22) Bruce, M. I.; Le Guennic, B.; Scoleri, N.; Zaitseva, N. N.; Halet, J.-F. *Organometallics* **2012**, *31*, 4701.

(23) Bear, J. L.; Han, B.; Wu, Z.; Van Caemelbecke, E.; Kadish, K. M. *Inorg. Chem.* **2001**, *40*, 2275.

(24) Falloon, S. B.; Arif, A. M.; A, G. J. *Chem. Commun.* **1997**, *6*, 629.

(25) Semenov, S. N.; Taghipourian, S. F.; Blacque, O.; Fox, T.; Venkatesan, K.; Berke, H. *J. Am. Chem. Soc.* **2010**, *132*, 7584.

(26) Lissel, F.; Fox, T.; Blacque, O.; Polit, W.; Winter, R. F.; Venkatesan, K.; Berke, H. *J. Am. Chem. Soc.* **2013**, *135*, 4051.

(27) ALQaisi, S. M.; Galat, K. J.; Chai, M.; Ray, D. G.; Rinaldi, P. L.; Tessier, C. A.; Youngs, W. J. *J. Am. Chem. Soc.* **1998**, *120*, 12149.

(28) Horn, C. R.; Gladysz, J. A. *Eur. J. Inorg. Chem.* **2003**, *12*, 2211.

(29) Owen, G. R.; Hampel, F.; Gladysz, J.A. *Organometallics* **2004**, *23*, 5893.

(30) Chisholm, M. H. *Angew. Chem. Int. Ed. Engl.* **1991**, *30*, 673.

(31) Takahashi, S.; Kariya, M.; Yatake, T.; Sonogashira, K.; Hagihara, N. *Macromolecules* **1978**, *11*, 1063.

(32) Zhuravlev, F.; Gladysz, J. A. *Chem. Eur. J.* **2004**, *10*, 6510.

(33) Costuas, K.; Rigaut, S. *Dalton Trans.* **2011**, *40*, 5643.

(34) Weng, W.; Bartik, T.; Gladysz, J. A. *Angew. Chem. Int. Ed. Engl.* **1994**, *33*, 2199.

(35) Weng, W.; Bartik, T.; Brady, M.; Bartik, B.; Ramsden, J. A.; Gladysz, J. A. *J. Am. Chem. Soc.* **1995**, *117*, 11922.

(36) Bartik, T.; Weng, W.; Ramsden, J. A.; Szafert, S.; Falloon, S. B.; Arif, A. M.; Gladysz, J.A. *J. Am. Chem. Soc.* **1998**, *120*, 11071.

(37) Bruce, M. I.; Scoleri, N.; Skelton, B. W.; White, A. H. *Journal of Organometallic Chemistry* **2010**, *695*, 1561.

(38) Wong, A.; Kang, P. C. W.; Tagge, C. D.; Leon, D. R. *Organometallics* **1990**, *9*, 1992.

(39) Bruce, M. I.; Ke, M.; Low, P. J.; Skelton, B. W.; White, A. H. *Organometallics* **1998**, *17*, 3539.

(40) Denis, R.; Weyland, T.; Paul, F.; Lapinte, C. *Journal of Organometallic Chemistry* **1997**, *545-546*, 615.

(41) Le Stang, S.; Lenz, D.; Paul, F.; Lapinte, C. *Journal of Organometallic*

Chemistry **1999**, *572*, 189.

(42) Denis, R.; Toupet, L.; Paul, F.; Lapinte, C. *Organometallics* **2000**, *19*, 4240.

(43) Courmacel, J.; Le Gland, G.; Toupet, L.; Paul, F.; Lapinte, C. *Journal of Organometallic Chemistry* **2003**, *670*, 108.

(44) Hurst, E. B. S. K.; Cifuentes, M. P.; McDonagh, A. M.; Humphrey, M. G.; Samoc, M.; Luther-Davies, B.; Asselberghs, I.; Persoons, A. *Journal of Organometallic Chemistry* **2002**, *642*, 259.

(45) Brady, M.; Weng, W.; Gladysz, J.A. *J. Chem. Soc., Chem. Commun.* **1994**, *23*, 2655.

(46) Dembinski, R.; Lis, T.; Szafert, S.; Mayne, C. L.; Bartik, T.; Gladysz, J. A. *Journal of Organometallic Chemistry* **1999**, *578*, 229.

(47) Peters, T. B.; Bohling, J. C.; Arif, A. M.; Gladysz, J.A *Organometallics* **1999**, *18*, 3261.

(48) Dembinski, R.; Bartik, T.; Bartik, B.; Jaeger, M.; Gladysz, J.A. *J. Am. Chem. Soc.* **2000**, *122*, 810.

(49) Meyer, W. E.; Amoroso, A. J.; Horn, C. R.; Jaeger, M.; Gladysz, J.A.. *Organometallics* **2001**, *20*, 1115.

(50) Mohr, W.; Stahl, J.; Hampel, F.; Gladysz, J.A. *Inorg. Chem.* **2001**, *40*, 3263.

(51) Zheng, Q.; A, Gladysz, J.A. *J. Am. Chem. Soc.* **2005**, *127*, 10508.

(52) Zheng, Q.; Bohling, J. C.; Peters, T. B.; Frisch, A. C.; Hampel, F.; Gladysz, J.A. *Chem. Eur. J.* **2006**, *12*, 6486.

(53) Bruce, M. I.; Kramarczuk, K. A.; Zaitseva, N. N.; Skelton, B. W.; White, A. H. *Journal of Organometallic Chemistry* **2005**, *690*, 1549.

(54) Frapper, G.; Kertesz, M. *Inorg. Chem.* **1993**, *32*, 732.

(55) Antonova, A. B.; Bruce, M. I.; Ellis, B. G.; Gaudio, M.; Humphrey, P. A.; Jevric, M.; Melino, G.; Nicholson, B. K.; Perkins, G. J.; Skelton, B. W.; Stapleton, B.; White, A. H.; Zaitseva, N. N. *Chem. Commun.* **2004**, *8*, 960.

(56) Ren, T. *Chem. Rev.* **2008**, *108*, 4185.

(57) Gendron, F.; Burgun, A.; Skelton, B. W.; White, A. H.; Roisnel, T.; Bruce, M. I.; Halet, J.-F.; Lapinte, C.; Costuas, K. *Organometallics* **2012**, *31*, 6796.

(58) Burgun, A.; Gendron, F.; Roisnel, T.; Sinbandhit, S.; Costuas, K.; Halet, J.-F.; Bruce, M. I.; Lapinte, C. *Organometallics* **2013**, *32*, 1866.

(59) Bruce, M. I.; Costuas, K.; Gendron, F.; Halet, J.-F.; Jevric, M.; Skelton, B. W. *Organometallics* **2012**, *31*, 6555.

(60) Burgun, A.; Gendron, F.; Schauer, P. A.; Skelton, B. W.; Low, P. J.; Costuas, K.; Halet, J.-F.; Bruce, M. I.; Lapinte, C. *Organometallics* **2013**, *32*, 5015.

(61) Bruce, M. I.; Burgun, A.; Grelaud, G.; Jevric, M.; Nicholson, B. K.; Skelton, B. W.; White, A. H.; Zaitseva, N. N. *Z. Anorg. Allg. Chem* **2011**, *637*, 1334.

(62) Bruce, M. I.; Hall, B. C.; Kelly, B. D.; Low, P. J.; Skelton, B. W.; White, A. H. *J. Chem. Soc., Dalton Trans.* **1999**, *21*, 3719.

(63) Moreno, C.; Gómez, J. L.; Medina, R.-M.; Macazaga, M.-J.; Arnanz, A.; Lough, A.; Farrar, D. H.; Delgado, S. *Journal of Organometallic Chemistry* **1999**, *579*, 1.

(64) Dede, M.; Drexler, M.; Fischer, H. *Organometallics* **2007**, *26*, 4294–4299.

(65) Creati, F.; Coletti, C.; Re, N. *Organometallics* **2009**, *28*, 6603.

(66) Bruce, M. I.; Hall, B. C.; Low, P. J.; Skelton, B. W.; White, A. H. *Journal of Organometallic Chemistry* **1999**, *592*, 74.

(67) Bruce, M. I.; Hinterding, P.; Tiekink, E. R. T. *Journal of Organometallic Chemistry* **1993**, 209.

(68) Bruce, M. I.; Hinterding, P.; Low, P. J.; Skelton, B. W.; White, A. H. *J. Chem. Soc., Dalton Trans.* **1998**, 467.

(69) Nguyen, P.; uan, Z. Y.; Agocs, L.; Lesley, G.; Marder, T. B. *Inorganica Chimica Acta* **1994**, *220*, 289.

(70) Batsanov, A. S.; Collings, J. C.; Fairlamb, I. J. S.; Holland, J. P.; Howard, J. A. K.; Lin, Z.; Marder, T. B.; Parsons, A. C.; Ward, R. M.; Zhu, J. *J. Org. Chem.* **2005**, *70*, 703.

(71) Rossi, R.; Carpita, A.; Bigelli, C. *Tetrahedron Letters* **1985**, *26*, 523.

(72) Hay, A. *J. Org. Chem.* **1962**, *27*, 3320.

(73) Bruce, M. I.; Kelly, B. D.; Skelton, B. W.; White, A. H. *Journal of Organometallic Chemistry* **2000**, *604*, 150.

(74) Coat, F.; Lapinte, C. *Organometallics* **1996**, *15*, 477.

(75) Zheng, Q.; Hampel, F.; Gladysz, J.A. *Organometallics* **2004**, *23*, 5896.

(76) de Quadras, L.; Hampel, F.; Gladysz, J.A. *Dalton Trans.* **2006**, 2929.

(77) Peters, T. B.; Zeng, Q.; Stahl, J.; Bohling, J. C.; Arif, A. M.; Hampel, A. M.; Gladysz, J. A. *Journal of Organometallic Chemistry* **2002**, *641*, 53.

(78) Bruce, M. I.; Humphrey, P. A.; Snow, M. R.; Tiekink, E. R. T. *Journal of Organometallic Chemistry* **1986**, *303*, 417.

(79) Armitt, D. J.; Bruce, M. I.; Skelton, B. W.; White, A. H. *Journal of Organometallic Chemistry* **2008**, *693*, 3571.

(80) Bruce, M. I. *Aust J Chem* **2011**, *64*, 77.

(81) Bruce, M. I.; Burgun, A.; Grelaud, G.; Lapinte, C.; Skelton, B. W.; Zaitseva, N. N. *Aust J Chem* **2012**, *65*, 763.

(82) Bruce, M. I.; Cole, M. L.; Ellis, B. G.; Gaudio, M.; Nicholson, B. K.; Parker, C.

R.; Skelton, B. W.; White, A. H. *Polyhedron* **2014**, 1.DOI/10.1016/j.poly.2014.04.052

(83) Bock, S.; Eaves, S. G.; Parthey, M.; Kaupp, M.; Le Guennic, B.; Halet, J.-F.; Yufit, D. S.; Howard, J. A. K.; Low, P. J. *Dalton Trans.* **2013**, *42*, 4240.

(84) Szafert, S.; Gladysz, J.A. *Chem. Rev.* **2006**, *106*, PR1.

(85) Schauer, P. A.; Low, P. J. *Eur. J. Inorg. Chem.* **2012**, *2012*, 390.

(86) Parthey, M.; Gluyas, J. B. G.; Schauer, P. A.; Yufit, D. S.; Howard, J. A. K.; Kaupp, M.; Low, P. J. *Chem. Eur. J.* **2013**, *19*, 9780.

(87) Bruce, M. I.; Low, P. J.; Costuas, K.; Halet, J.-F.; Best, S. P.; Heath, Gladysz, J.A. *J. Am. Chem. Soc.* **2000**, *122*, 1949.

(88) Kaim, W.; Fiedler, J. *Chem. Soc. Rev.* **2009**, *38*, 3373.

(89) Akita, M.; Koike, T. *Dalton Trans.* **2008**, *27*, 3523.

(90) Bruce, M. I.; Costuas, K.; Ellis, B. G.; Halet, J.-F.; Low, P. J.; Moubaraki, B.; Murray, K. S.; Ouddaï, N.; Perkins, G. J.; Skelton, B. W.; White, A. H. *Organometallics* **2007**, *26*, 3735.

(91) Lichtenberger, D. L.; Renshaw, S. K.; Wong, A.; Tagge, C. D. *Organometallics* **1993**, *12*, 3522.

(92) Koentjoro, O. F.; Rousseau, R.; Low, P. J. *Organometallics* **2001**, *20*, 4502.

(93) Herrmann, C.; Neugebauer, J.; Gladysz, J. A.; Reiher, M. *Inorg. Chem.* **2005**, *44*, 6174.

(94) Belanzoni, P.; Re, N.; Sgamellotti, A.; Floriani, C. *J. Chem. Soc., Dalton Trans.* **1998**, 1825.

(95) Fox, M. A.; Roberts, R. L.; Khairul, W. M.; Hartl, F.; Low, P. J. *Journal of Organometallic Chemistry* **2007**, *692*, 3277.

(96) McGrady, J. E.; Lovell, T.; Stranger, R.; Humphrey, M. G. *Organometallics* **1997**, *16*, 4004.

(97) Paul, F.; Ellis, B. G.; Bruce, M. I.; Toupet, L.; Roisnel, T.; Costuas, K.; Halet, J.-F.; Lapinte, C. *Organometallics* **2006**, *25*, 649.

(98) Moreno-García, P.; Gulcur, M.; Manrique, D. Z.; Pope, T.; Hong, W.; Kaliginedi, V.; Huang, C.; Batsanov, A. S.; Bryce, M. R.; Lambert, C.; Wandlowski, T. *J. Am. Chem. Soc.* **2013**, *135*, 12228.

(99) Song, J.-L.; Amaladass, P.; Wen, S.-H.; Pasunooti, K. K.; Li, A.; Yu, Y.-L.; Wang, X.; Deng, W.-Q.; Liu, X.-W. *New J. Chem.* **2011**, *35*, 127.

CHAPTER 4. SYNTHESES, STRUCTURES AND ELECTRONIC PROPERTIES OF ORGANOMETALLIC MOLECULAR WIRES

4.1. Abstract

This chapter investigates the influence of the metal (Ru, Pt) integrated directly within the conjugated organic core (OPE, oligoyne) on the conductance of a series of molecular wires. Organometallic molecules bearing TMSE (-C≡CSiMe$_3$) and pyridyl contacting groups were prepared to permit single molecule conductance measurements. The compounds *trans*-Pt(C≡CC≡CSiMe$_3$)$_2$(PPh$_3$)$_2$ (**24**), *trans*-Pt[C≡C{1,4-C$_6$H$_2$(R)$_2$}C≡CSiMe$_3$]$_2$(PPh$_3$)$_2$ (R = H (**25**); OC$_6$H$_{13}$ (**26**)) and *trans*-Pt(C≡CC≡CC$_6$H$_4$N)$_2$(PPh$_3$)$_2$ (**27**) were synthesized from the parent organic ligands and *cis*-PtCl$_2$(PPh$_3$)$_2$. In all cases, the conductance of the organometallic compounds is enhanced relative to similarly structured all-organic molecules. Surprisingly, in contrast to design rules established for organic oligo(aryleneethynylene) based wires in which solubilizing groups have little effect on the molecular conductance, a difference in the single molecule conductance values was found between compounds **25** and **26**. With the aid of computational modeling performed by the Lancaster group, this phenomenon may be attributed to the greater destabilization of the LUMO caused by the electron-donating, solubilizing hexyloxy groups, but also the contact of the STM tip to the PPh$_3$ ancillary ligand, which is feasible when the hexyloxy protecting shell is not present.

Pyridyl and thiomethyl (-SMe) surface contacting groups have also been introduced into metalla-oligoarylene ethynylene structures (metal-OPE), specifically *trans*-M[{C≡C-C$_6$H$_2$(OR)$_2$}$_x$C≡CC$_6$H$_4$N]$_2$L$_n$ [R = C$_6$H$_{13}$; x = 1 ML$_n$ = Ru(dppe)$_2$ (**30**) Pt(PPh$_3$)$_2$ (**33**); x = 2 ML$_n$ = Ru(dppe)$_2$ (**38**)] and *trans*-M[{C≡C-C$_6$H$_2$(OR)$_2$}C≡CC$_6$H$_4$SMe]$_2$L$_n$ [R = C$_6$H$_{13}$; ML$_n$ = Ru(dppe)$_2$ (**34**) Pt(PPh$_3$)$_2$ (**35**)] through 'on complex' cross-coupling protocols. The crystallographically determined structures of **25**, **30**, **33**, **35**, **38** and the intermediate *trans*-Ru{C≡CC$_6$H$_2$(OR)$_2$C≡CH}(dppe)$_2$ **29** are reported. The effect of the metal (Pt and Ru) in these metal OPE derivatives, in combination with pyridyl anchor groups is assessed in terms of their effects on the through molecule conductivity, with single molecule current-distance (I(s)) measurements of **30** and **33** giving similar conductance values,

reflecting the dominant conductance channel through the π* orbitals promoted by the terminal pyridine contacting group. These results highlight the need to consider each component of the entire junction as part of a single ensemble in the design of materials for ME.

To further investigate the possibility of the STM tip contact through the PPh_3 ancillary ligand, compound *trans*-$Pt(PPh_3)_2\{C{\equiv}C\text{-}(4\text{-}C_6H_4{}^tBu)\}_2$ **39** has been synthesized and measured.

4.2. Introduction

Single molecule measurements of a wide variety of saturated, conjugated and redox active organic compounds have driven the development of concepts and techniques in ME.[1-3] However, metal complexes offer several potential advantages over organic compounds as components in ME devices, including redox activity at moderate potentials, ready tuning of frontier molecular orbital energy levels to better match the Fermi levels of metallic electronics, and magnetic properties.[4,5] Consequently, attention has been turned to the study of metal complexes[6-11] and carbon-rich organometallic species[12-16] within molecular junctions, as described in Chapter 1. Single molecule measurements using both organic and organometallic compounds have clearly shown that the electronic properties of the prototypical metal | molecule | metal junctions are strongly influenced by not only the chemical structure of the molecular backbone but also by the combination of the surface and contacting groups.[17-22] However, the intricacy of how these various factors combine to dictate the overall junction conductance is still not determined.

Therefore, the further study of an organometallic platform for ME now depends on molecular structures that realize electronic function beyond that of a simple wire, and which also integrate appropriate surface binding groups. To this end, instead of assembling a pre-formed ligand to the metal centre, as used for the synthesis of compounds **24** - **27**, new synthetic strategies that allow the modular assembly of metallic moieties, π-conjugated fragments and surface binding groups are now sought.

Thus, as part of a wider study of metal complexes within molecular junctions[12] we desired modular access to metal oligo(phenyleneethynylene) complexes featuring different combinations of metal centre, π-conjugated fragments and surface binding groups. The 'chemistry on the complex' approach based on the Sonogashira cross-coupling reaction, described in Chapter 3, offers potential for the construction of such systems.[23] Thus, molecules bearing pyridyl (**30**, **33** and **38**) and thiomethyl anchor groups (**34** and **35**) have been designed.

The single molecule measurements of the molecules **24** - **27**, **30**, **33** and **39** have been probed using the *I*(s) method. Interestingly, the electrical properties of **30** and **33** reveal remarkably similar conductance values, which, with the aid of computational models, can be attributed to the significant role of the LUMO (i.e. π*) system in the primary conductance channel. Moreover, a distinction between the TMSE and pyridyl anchoring groups has been made for clarity of the discussion of the conductance data. Generally, the conductance of the metal complexes was found to be higher than parent organic molecules but the influence of the solubilizing hexyloxy chains and the anchoring group on the orbital channel is significant.

4.3. Synthesis of the platinum complexes via $Cu^{(I)}$ catalyzed trans-metallation

The conditions used for the preparation of platinum bis(alkynyl) complexes from *cis*-$PtCl_2(PPh_3)_2$ and a terminal alkyne were first described by K. Sonogashira et al.[24] The first step of the reaction is a deprotonation of the terminal alkyne by a base, typically an alkyl amine such as diethylamine ($HNEt_2$) that also serves as the reaction medium, and subsequent reaction with a copper(I) halide catalyst to give a copper alkynyl species. Secondly, a trans-metallation between the copper complex and the platinum centre takes place to finally give the desired platinum acetylide, and regenerate a $Cu^{(I)}$ halide (Scheme 4-1). The formation of the platinum acetylide can be easily distinguished by ^{31}P NMR spectroscopy where the coupling constant $J_{Pt\text{-}P}$ for *trans*-platinum complexes (ca. 2000 – 2500 Hz) is smaller than that of the *cis*-$PtCl_2(PPh_3)_2$ starting material (ca. 3000 – 3500 Hz).

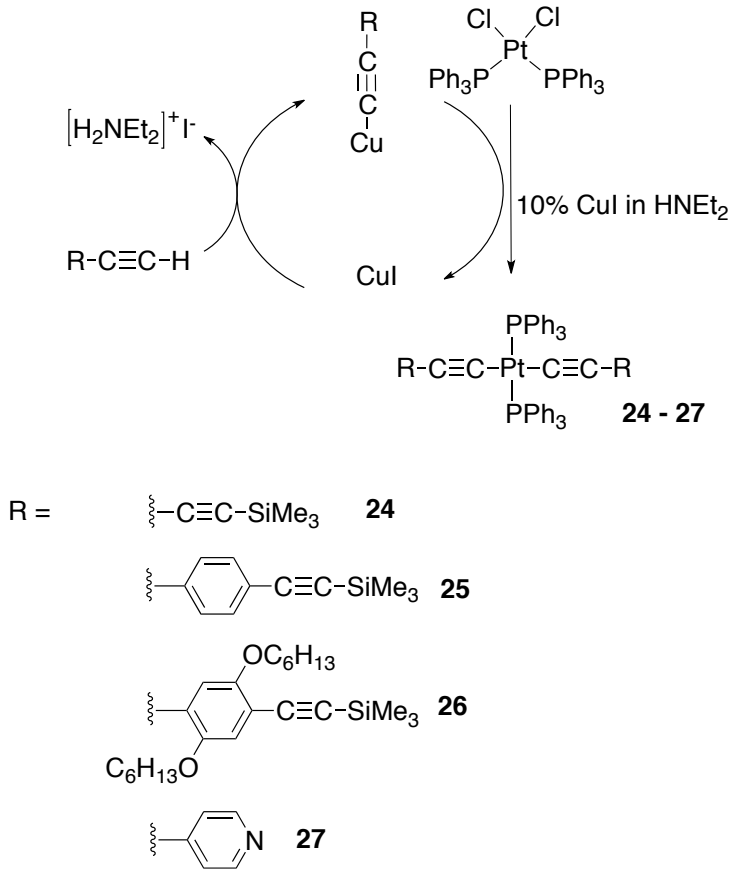

Scheme 4-1. *A general schematic of the synthetic route used for compounds **24** – **27**.*

The compounds **24** - **27** are formed from reactions at 50 °C - reflux for 2 - 16 h, and isolated as precipitates by simple filtration of the reaction mixture, followed by washing with MeOH to remove the co-precipitated alkylammonium salts ($[H_2NEt_2]^+X^-$). The synthesis of the platinum acetylide **27** required a lower reaction temperature than the compounds **24** - **26** due to the instability of 4-ethynylpyridine (50 °C overnight). The yields for these reactions are between 25% for **27** to 85% for **25**. Characterization of the organometallic complexes was achieved by the usual array of IR, ^{1}H, ^{13}C and ^{31}P NMR spectroscopies, MALDI-TOF, high-resolution ES mass spectrometries. The ^{31}P NMR spectra comprised a singlet in the region of 17.4 - 18.8 ppm with satellites arising from coupling to the NMR active isotope ^{195}Pt (33.8%). The IR spectra for each of the complexes **24** - **27** displayed the expected vibrational bands near 2100 and 2186 cm^{-1} for Pt-C≡C and C≡CR (R = C_5H_4N-4 or $SiMe_3$), respectively.

CHAPTER 4

4.4. Synthesis of the metal-OPE compounds via 'on complex' Sonogashira cross-coupling reactions

A wide range of ruthenium and platinum *trans*-bis(alkynyl) complexes featuring more complex carbon rich ligands and binding groups to permit their analysis in molecular junctions were envisaged from the introduction of surface contacting groups through the 'on complex' approach and a reactive metal-containing core structure (*see* Chapter 3).

The key organic building block **I** was prepared from hydroquinone,[25] by a Williamson ether synthesis to introduce the solubilising side chains (Scheme 4-2 (i)) before double iodination (Scheme 4-2, (ii)). Stoichiometrically controlled mono-alkynylation using TMSA under conventional Sonogashira conditions was subsequently performed (Scheme 4-2, (iii)). A second Sonogashira reaction with triisopropylsilylacetylene (TIPSA) gave the differentially substituted dialkyne (Scheme 4-2, (iv)) which could be selectively deprotected (K_2CO_3/MeOH) to give **I** (Scheme 4-2, (v)).

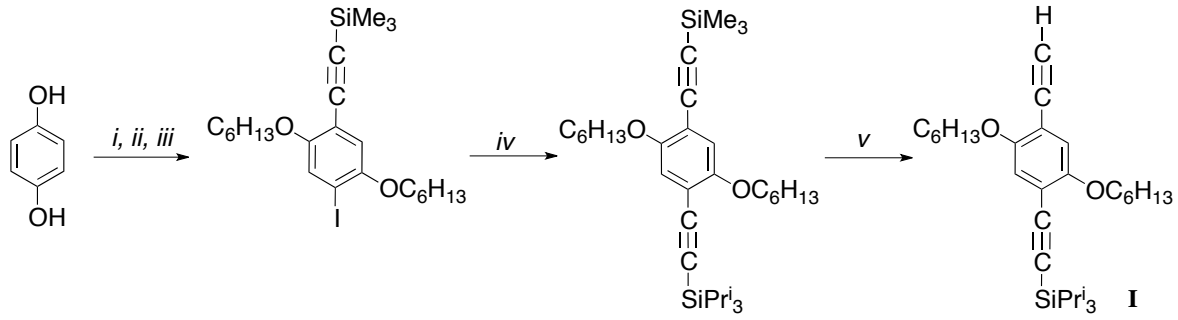

Scheme 4-2. *Preparation of **I**. (i) $C_6H_{13}Br$, KOH in EtOH, 80 °C, overnight, 51%; (ii) KIO_3, I_2, H_2SO_4/CH_3COOH, reflux, 6.5 h, 53%; (iii) TMSA (0.45 eq), 5 mol% $PdCl_2(PPh_3)_2$/5 mol% CuI in NEt_3, rt, overnight, 76%; (iv) TIPSA (0.9 eq), 5 mol% $Pd(PPh_3)_4$/5 mol% CuI in NEt_3, rt, overnight 60%; (v) K_2CO_3, THF/MeOH, rt, 2 h, 91%.*

The reactions of $[RuCl(dppe)_2]^+$ salts with terminal alkynes, HC≡CR, proceed readily to give the vinylidene complex cations $[RuCl(C{=}CHR)(dppe)_2]^+$, which can be deprotonated either in situ or after isolation to give the mono-acetylide complexes *trans*-$RuCl(C{\equiv}CR)(dppe)_2$.[26] Upon treatment with a suitable halide abstracting agent, such as sodium hexafluorophosphate ($NaPF_6$)[27,28] or thallium tetrafluoroborate ($TlBF_4$)[29] in the presence of further terminal alkyne and base, the bis(acetylide) complexes *trans*-$Ru(C{\equiv}CR)_2(dppe)_2$ are formed (Scheme 4-3).

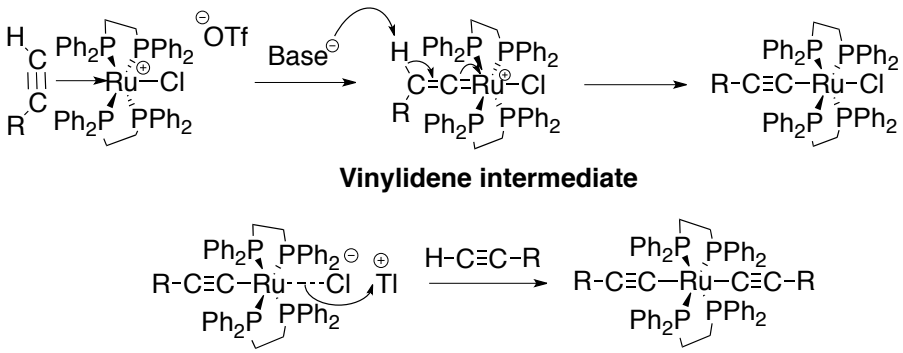

Scheme 4-3. *Formation of the bis(acetylide) complexes trans-Ru(C≡CR)$_2$(dppe)$_2$.*

In this manner, reaction of [RuCl(dppe)$_2$]OTf with 2.1 equivalents of **I** and 2 equivalents of $TlBF_4$ in CH_2Cl_2 under inert atmosphere gave **28** in 76% isolated yield (Scheme 4-4). The protecting triisopropylsilyl moieties (TIPS) were removed from **28** by treatment with tetrabutylammonium fluoride (TBAF) to give **29**, and subsequent Sonogashira coupling of **29** with 4-iodopyridine or 4-thioanisole gave the desired compounds **30** (64%) or **34** (34%), containing the pyridyl and thiomethyl contacting groups, respectively.

Group 10 alkynyl complexes are readily obtained from terminal alkynes through Cu^I-mediated trans-metallation reactions (*see* Section 4.3).[30] Treatment of *cis*-$PtCl_2(PPh_3)_2$ with 2.2 equivalents of **I** in $HNEt_2$ containing a catalytic amount of CuI gave the bis(acetylide) **31** in 73% yield. Subsequent removal of TIPS with TBAF gave **32** (93%), which was cross-coupled with 4-iodopyridine or 4-thioanisole in the usual Sonogashira fashion to give the extended linear platinum complexes **33** (30%) and **35** (17%) (Scheme 4-4).

Complexes **28 – 30**, **31 – 33** and **34**, **35** were characterized by the usual spectroscopic methods, low and high resolution mass spectrometry and elemental analysis. ^{1}H NMR resonances from the hexyloxy chains (especially from the -OCH_2- moiety), 4-ethynyl pyridine or 4-ethynyl thioanisole fragments, and terminal alkyne C≡C-H proton resonances in the case of **29** and **32**, combined with characteristic singlets in the ^{31}P NMR spectra near 52 (**28** – **30**, **34**) and 17 (**31 – 33**, **35**) ppm (the latter showing the expected satellites arising from coupling to ^{195}Pt), and the IR ν(Pt/Ru-C≡C), ν(C≡CSiPr^i_3) and ν(≡C-H) provided evidence for the proposed structures.

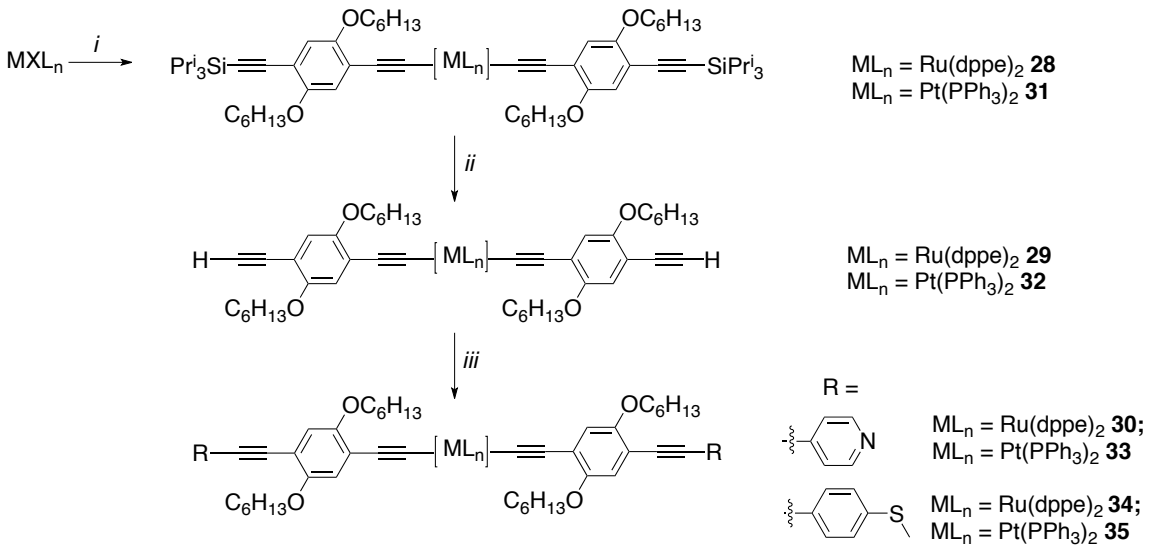

Scheme 4-4. *Preparation of **28** – **33** and **34** – **35**. (i) **I** (2.1 eq), MXL_n = [RuCl(dppe)$_2$]OTf (a) 1,8-diazabicyclo[5,4,0]undec-7-ene (DBU), CH_2Cl_2, rt, 1 h then (b) $TlBF_4$, 20 min at RT 76%; (i) **I** (2.2 eq), MXL_n = $PtCl_2(PPh_3)_2$ 10 mol% CuI in $HNEt_2$, 90 °C, 2 h, 73%; (ii) TBAF (2.4 eq), THF; (iii) 4-iodopyridine (2.3 eq) for **30** and **33** or 4-thioanisole (2.3 eq), 5 mol% $Pd(PPh_3)_4$/5 mol% CuI in HN^iPr_2.*

The same reaction procedure afforded the longer derivative **38** (Scheme 4-5). Thus, reaction of [RuCl(dppe)$_2$]OTf with 2.1 eq of the selectively protected ethynyl tolane ligand **J** gave the TIPS-protected bis(ethynyl) complex **36** (33%). Removal of the TIPS protecting groups was readily achieved upon reaction with TBAF in THF/MeOH to give **37**, which was used without further purification. The Sonogashira cross-coupling of **37** and 2 equivalents of 4-iodopyridine gave the bis(pyridyl) derivative **38** (43%) after precipitation from CH_2Cl_2/MeOH and crystals were obtained from slow diffusion in CH_2Cl_2/Et_2O. The structure was confirmed by ^{1}H, ^{31}P, ^{13}C NMR, IR spectroscopies, MALDI-TOF mass spectrometry and single crystal X-ray crystallography.

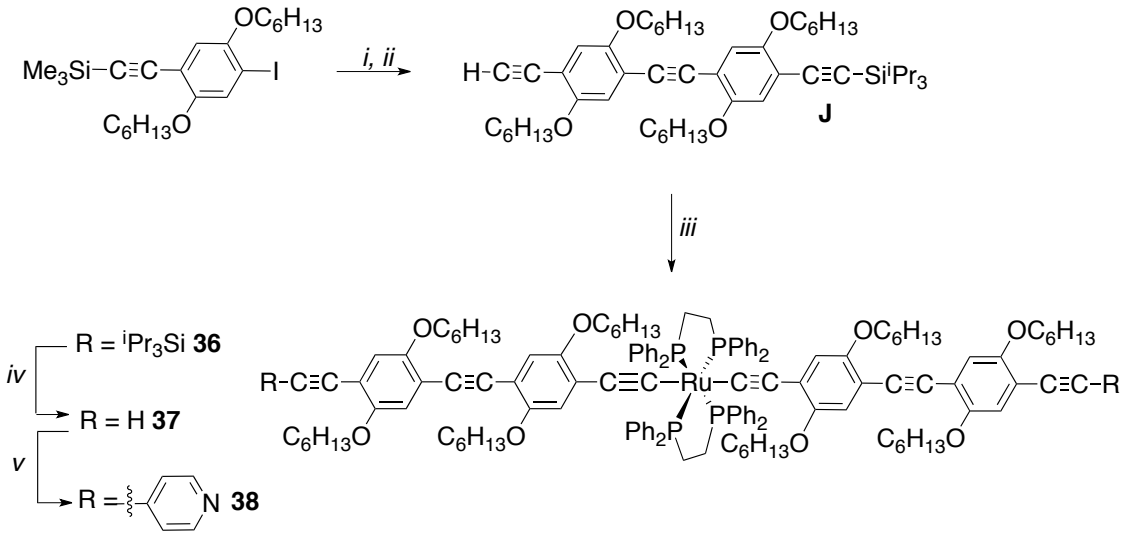

Scheme 4-5. *Preparation of **36 - 38**. (i) 10 mol% $Pd(PPh_3)_4$/10 mol% CuI, HN^iPr_2, rt, overnight, 67%; (ii) K_2CO_3 in THF/MeOH, 83%, rt, overnight; (iii) (a) $[RuCl(dppe)_2]OTf$ (0.47 eq), DBU in CH_2Cl_2, rt, 30 min then (b) $TlBF_4$, rt, 2 h, 33%; (iv) TBAF (2.5 eq) in THF, rt, overnight. v) 4-iodopyridine (2 eq), 10 mol% $Pd(PPh_3)_4$/10 mol% CuI in HN^iPr_2/THF, 100 °C, overnight, 43%.*

4.5. Exploration of binding mode through the phenyl ancillary ligand

4.5.1. Synthetic consideration

The single molecule measurements of compounds **24** and **33** gave rise to broad conductance peaks due to the different binding combinations (*see* Section 4.8.). In fact, as stated in the abstract, the molecule can bind through the phenyl ancillary ligand (PPh_3), the TMSE or pyridyl anchor groups. However, in the case of the platinum molecule **33**, (N…N distance 2.86 nm), the break-off distance of the highest conductance value is equal to 2.60 nm, suggesting another possible binding geometry which can be attributed to the gold-pyridyl on one side and PPh_3-gold on the other side or even more possible, a competition between the different contacting groups. Therefore, *trans*-$Pt(PPh_3)_2\{C{\equiv}C\text{-}(4\text{-}C_6H_4{}^tBu)\}_2$ **39** was designed in order to force the binding through the phenyl of the ancillary ligand and then, block the position of the horizontal molecule from tert-butyl phenyl (Scheme 4-6).

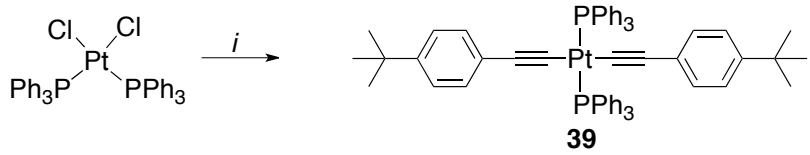

39

Scheme 4-6. *Synthesis of the molecule **39**. (i) 4-tert-butylphenylacetylene (2 eq), 10 mol% CuI in HN^{i}Pr$_2$, rt, overnight, 69%.*

The reaction gave **39** (69%) after purification by filtration of the product with the addition of MeOH to remove the salts. Complex **39** was characterized by the usual spectroscopic methods and mass spectrometry. The ^{31}P NMR spectrum shows the characteristic singlet at 18.6 ppm with the expected Pt satellites coupling constant (J_{Pt-P} = 2661.6 Hz).

4.6. Molecular Structures

Single crystals suitable for X-ray diffraction analysis were obtained for **25**, **29**, **30**, **33**, **35** and **38**. Key bond lengths and angles are summarized in Table 4-1, and representative plots of the molecules are given in Figures 4-1 – 4-6. The bond lengths of the platinum complexes **25**, **33** and **35** fall in the usual ranges[31] Pt-P(1,2) 2.296(3) - 2.310(1) Å; Pt-C(1) 1.997(2) - 2.05 (15) Å; C(1)-C(2) 1.209(3) - 1.16(2) Å. For the metalla-oligoarylene ethynylene complexes *trans*-Ru[{C≡C-$C_6H_2(OC_6H_{13})_2$}C≡CH]$_2$(dppe)$_2$ (**29**) and *trans*-Ru[{C≡C-$C_6H_2(OC_6H_{13})_2$}$_x$C≡CC_6H_4N]$_2$L$_n$ (**30** and **38**), the bond lengths fall in the usual ranges[29] Ru-P(1,2) 2.3289(4) - 2.3677(11) Å; Ru-C(1) 2.049(4) - 2.073(1) Å; C(1)-C(2) 1.127(3) - 1.221(2) Å whilst the angles span P(1)-Ru-P(1') 179.99(2) - 180.0°; P(2)-Ru-P(1') 97.82(4) - 98.21(2)°; P(2')-Ru-P(1') 81.79(2) - 82.18(4)°; C(1)-C(2)-Ru 173.99(12) - 178.24(18)° and C-O(1,2)-C 116.7(4) - 120.18(13)°. All the complexes **25**, **29**, **30**, **33**, **35** and **38** are essentially linear with angles C(1)-Ru/Pt-C(1') close or equal to 180°. Compared with **29**, the presence of the pyridyl moiety has little effect on the bond lengths along the π-conjugated ligands.

The hexyloxy chains in **29** adopt a largely extended structure with staggered methylene groups, although the chain is disordered from C(13) - C(16), and lie in the plane bisecting the ethane backbone of the dppe ligands. In contrast, for the other ruthenium complexes **30**

and **38**, whilst the O(1)-C(18)-C(23) chain adopts a similar, extended staggered conformation, the O(2)-C…-C(26) fragment is forced into a *gauche* conformation, probably due to crystal packing effects. Interestingly, the presence of the metal centers in **29**, **30**, **33** and **35** cause a generally more significant deviation from the idealised linear, planar geometries found recently in closely related oligoaryleneethynylene (OAE) compounds.[32] The metal complexes are ca. 3 - 5% shorter in length than the purely organic analogues, [**30, 33** N(1)-N(1') ≅ 28.6 Å] versus OAE with 5 aromatic units (OAE5) (Chart 4-1) [N(1)-N(1') 30.05 Å] and **38** [N(1)-N(1') 42.07 Å] versus OAE with 7 aromatic units (OAE7) (Chart 4-1) [N(1)-N(1') 43.67 Å].[32] Whilst the X-ray analysis of **38** confirms the structure and large scale features, unfortunately the relatively poor crystal quality prevents a more precise refinement and precludes detailed discussion.

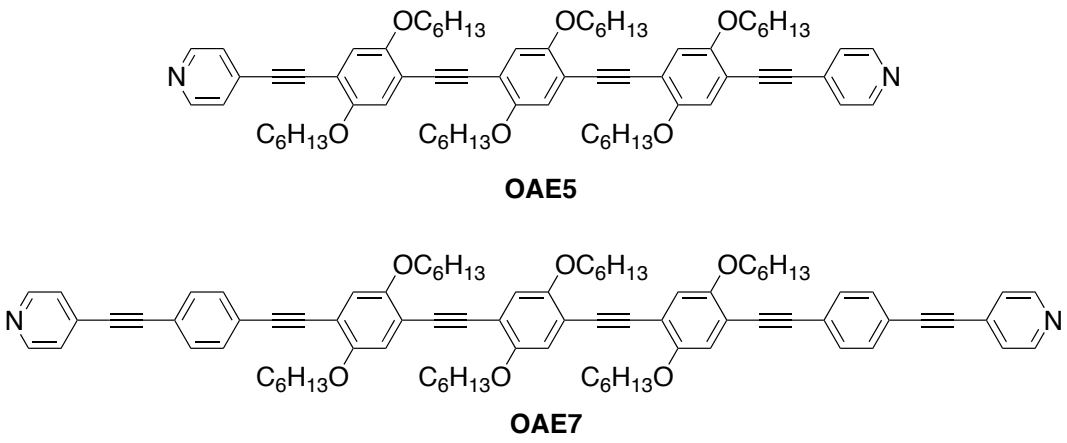

Chart 4-1. *Molecular structure of OAE5 and OAE7.*[32]

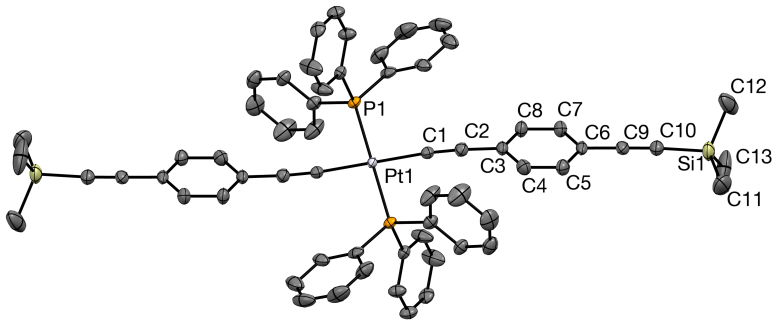

Figure 4-1. *Plot of the molecule **25** showing the atom labelling. Solvent molecules and hydrogen atoms have been omitted for clarity. In this and all subsequent plots, thermal ellipsoids are plotted at 50%.*

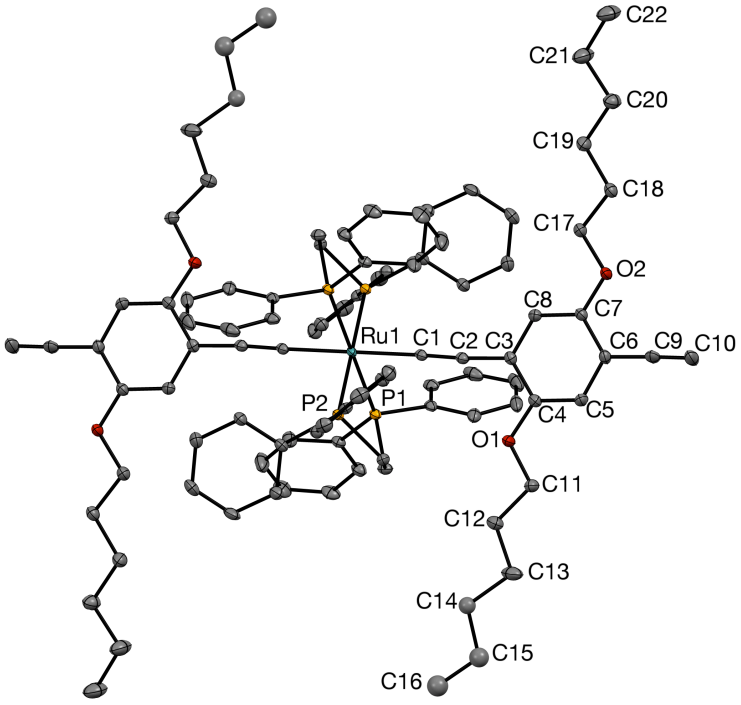

Figure 4-2. *Plot of the molecule **29**. The disorder has been omitted for clarity.*

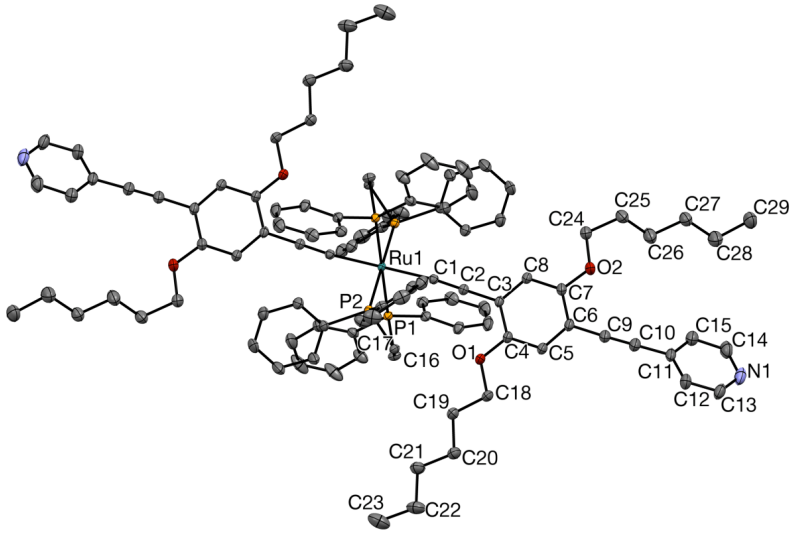

Figure 4-3. *Plot of the molecule **30**. Torsion angle C(7)-C(6)-C(11)-C(12) : 144.03°; N(1)-N(1') : 28.63 Å.*

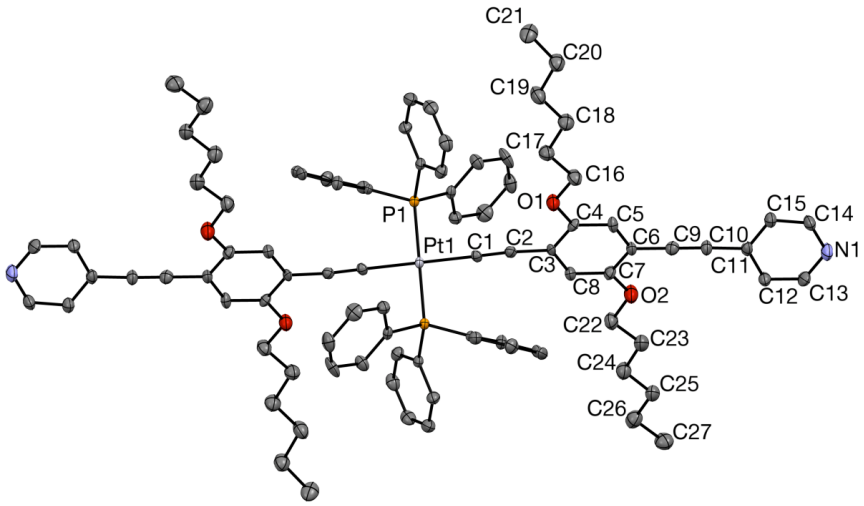

Figure 4-4. *Plot of the molecule **33**. Torsion angle C7-C6-C11-C12 164.05°; N(1)-N(1') : 28.62 Å.*

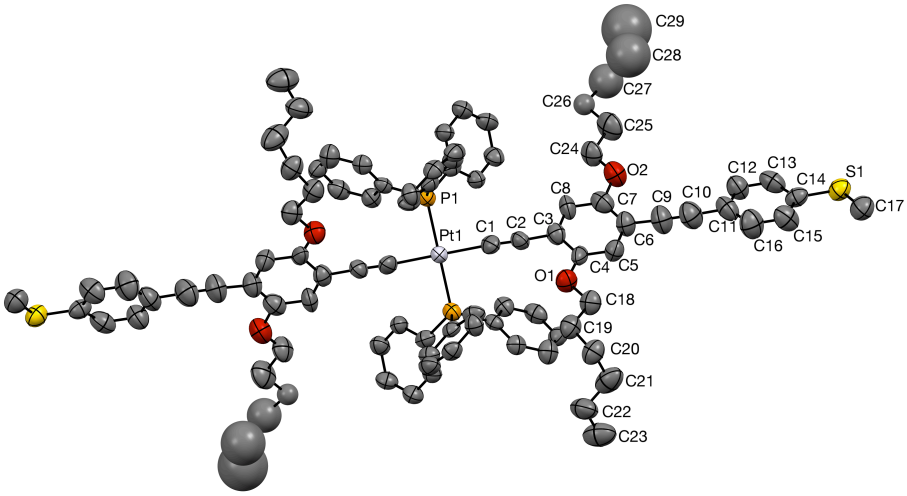

Figure 4-5. *Plot of the molecule **35**. The disorder has been omitted for clarity.*

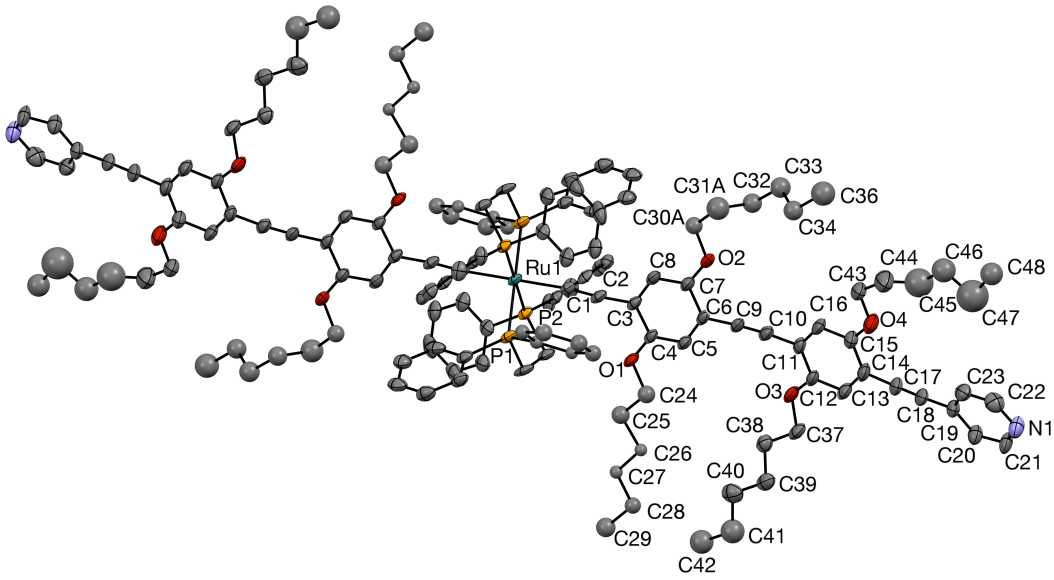

Figure 4-6. *Plot of the molecule **38**. Torsion angles C(5)-C(6)-C(11)-C(16) 167.2(6)°, C(13)-C(14)-C(19)-C(23) 161.1(6)°; N(1)-N(1') : 42.07 Å. The disorder has been omitted for clarity.*

Table 4-1. *Selected bond lengths (Å) and angles (°) for complexes **25**, **29**, **30**, **33**, **35** and **38***

	29	**30**	**38**	**25**	**33**	**35**
Bond Lengths(Å)						
Ru-P(1)/ Pt-P(1)	2.3618(5)	2.3650(4)	2.3677(11)	2.3098(6)	2.3104(11)	2.296(3)
Ru-P(2)/ Pt-P(1')	2.3348(5)	2.3289(4)	2.3346(11)	2.3098(6)	2.3104(11)	2.296(3)
Ru-C(1)/ Pt-C(1)	2.056(2)	2.0729(14)	2.049(4)	1.997(2)	2.018(4)	2.050(15)
C(1)-C(2)	1.217(3)	1.221(2)	1.217(6)	1.209(3)	1.198(6)	1.163(17)
C(2)-C(3)	1.428(3)	1.4371(19)	1.433(6)	1.438(3)	1.433(6)	1.438(16)
C(9)-C(10)	1.184(3)	1.196(2)	1.202(6)		1.202(6)	1.16(2)
Angles (°)						
P(1)-Ru-P(1')/ P(1)-Pt-P(1')	179.999(2)	179.999(16)	180.0	180.0	180.000(1)	179.16(17)
P(2)-Ru-P(1')	98.209(18)	97.873(13)	97.82(4)			
P(2')-Ru-P(1')	81.791(18)	82.126(13)	82.18(4)			
C-O(1)-C*	118.02(16)	117.94(12)	117.9(3)		116.7(4)	117.0(10)
C-O(2)-C**	116.43(15)	120.18(13)	119.3(3)		118.2(4)	117.6(10)
C(1)-C(2)-Ru/ C(2)-C(1)-Pt	178.24(18)	173.99(12)	175.0(4)	175.3(2)	178.6(4)	176.7(11)
C(1)-C(2)-C(3)	175.9(2)	173.32(15)	175.4(5)		172.2(5)	173.7(14)

For **29**: *C(4)-O(1)-C(11); **C(7)-O(2)-C(17)

For **30**: *C(4)-O(1)-C(18); **C(7)-O(2)-C(24)

For **33**: *C(4)-O(1)-C(16); **C(7)-O(2)-C(22)

For **35**: *C(4)-O(1)-C(18); **C(7)-O(2)-C(24)

For **38**: *C(4)-O(1)-C(24); **C(7)-O(2)-C(30A)

*C(12)-O(3)-C(37): 120.2 (4); **C(15)-O(4)-C(43): 118.8 (4)

4.7. Optical spectroscopies and electrochemical measurements

4.7.1. Optical spectroscopy of 30 and 33 versus OAE5

The absorption spectra of the metal-OPE molecules **30** and **33** were compared with their all-organic analogous OAE5 to assess the effective conjugation length of these metal

complexes. The spectra show a red-shift in the lowest energy absorption band for the ruthenium compound **30** and a blue shift for the platinum compound **33** compared with OAE5 (Figure 4-7). In other words, the HOMO-LUMO gap gets smaller when inserting ruthenium in the organic core, and increases when the metal is platinum. If the HOMO-LUMO gap is the only parameter in consideration, the expected conductivity should be higher in the case of the ruthenium complex and lower for the platinum complex, *vs* OAE5, which is in agreement with previous experiments.[33,34] This point is addressed in greater detail below.

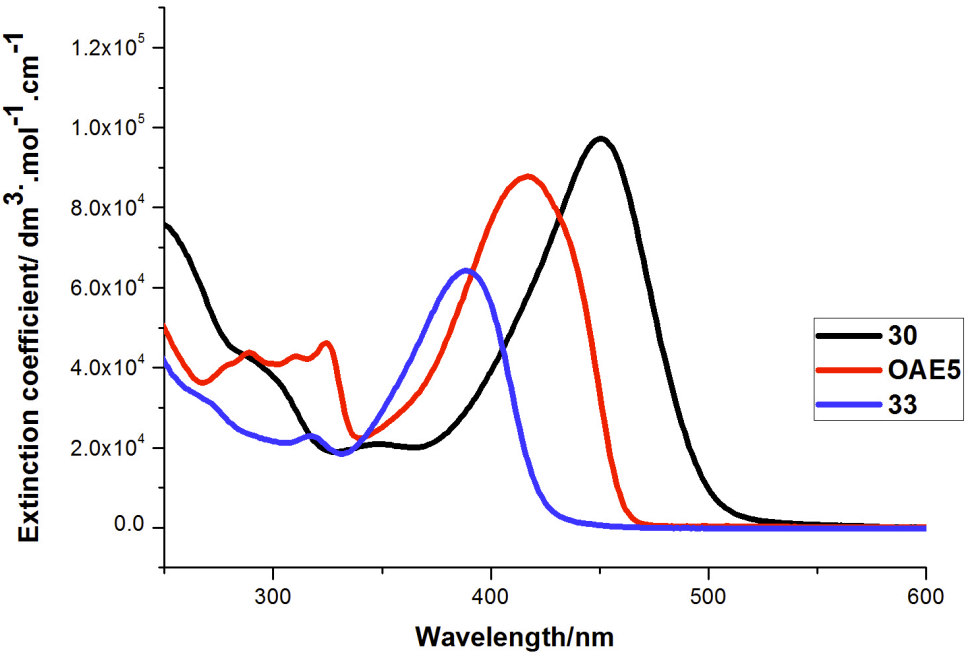

Figure 4-7. *UV-Vis spectra of the compounds **30** and **33** vs the OAE5 in dichloromethane.*

4.7.2. Electrochemical measurements

4.7.2.1. Cyclic voltammetry

The cyclic voltammetry of the pyridyl metal-OPE complexes **30** and **33** show irreversible oxidations (Figure 4-8, b and c), which are essentially ligand centred.[35] However, in contrast, the ruthenium complexes **30** and **34** display a first reversible oxidation wave ($ip_f/ip_r = 0.88$) (Figure 4-8, c), ($ip_f/ip_r = 0.90$) (Figure 4-8, d) which is comparable with the internal decamethylferrocene reference under these conditions. However, no oxidation

wave was observed for the platinum-OPE **35** which is not redox active in common solvents and within the potential range.

Table 4-2. *Electrochemical data of the pyridyl terminated metal-OPE complexes **30** and **33** versus the organic OAE5. E_{pa} vs. ferrocene/ferrocenium ($FeCp_2/[FeCp_2]^+$) (CH_2Cl_2, 0.1 M NBu_4PF_6, Pt dot working electrode). Data reported against an internal decamethylferrocene/ decamethylferrocenium ($FeCp^*_2/[FeCp^*_2]^+$) standard. Under these conditions $FeCp^*_2/[FeCp^*_2]^+$ = - 0.53 V vs $FeCp_2/[FeCp_2]^+$.* [a] *Reversible process*

Compound	E_{pa} (1)	E_{pa} (2)	E_{pa} (3)
OAE5	0.89	1.36	×
30	- 0.015[a]	0.83	×
33	0.63	0.86	1.06

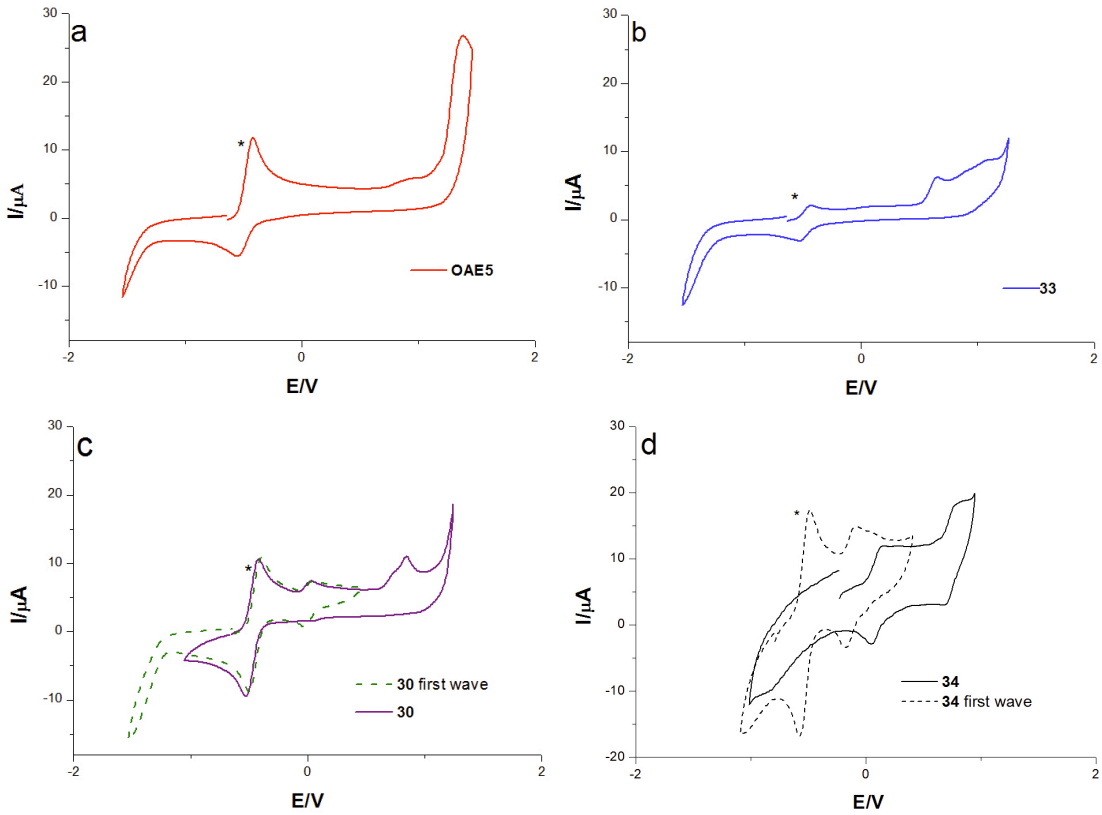

Figure 4-8. *Full cyclic voltammograms of OAE5 (a), **33** (b), **30** with its first oxidation wave (c) and **34** with its first oxidation wave (d). Experimental conditions are given in Table 4.2. The internal decamethylferrocene is shown with an asterix.*

The electrochemical data of the ruthenium complexes **30** and **34** are very similar, the first oxidation potential is lower for pyridyl molecule **30** ($E_{1/2}$ = - 0.015 V) than for thioanisole analogue **34** ($E_{1/2}$ = - 0.012 V). However, two reversible oxidation waves are visible for the compound **34** but the second oxidation wave disappeared with the addition of decamethylferrocene.

4.7.2.2. Spectroelectrochemistry

The well-behaved electrochemical response of **30** and **34** lead us to study these complexes and their oxidation products by spectroelectrochemical methods. The NIR and IR spectra of $[\mathbf{30}]^{n+}$ and $[\mathbf{34}]^{n+}$ (n = 0, 1) were recorded in 0.1 M NBu_4PF_6/CH_2Cl_2 with an OTTLE cell (Figures 4-9 - 4.10). The ruthenium coordinated ethynyl bands ν(Ru-C≡C) are near 2050 cm^{-1} for the neutral ruthenium compounds (18 e^- configuration), and shifted by ca. 150 cm^{-1} to lower wavenumber with a significant increase in intensity at 1880 ($[\mathbf{30}]^{\bullet+}$) - 1900 ($[\mathbf{34}]^{\bullet+}$) cm^{-1}. In addition, a small shift to lower wavenumber for the breathing mode of the aryl substituent is observed for the oxidized species $[\mathbf{30}]^{\bullet+}$ at 1585 cm^{-1}. Upon oxidation in the OTTLE cell, a new feature in the NIR region appears at ca. 7000 cm^{-1} for both $[\mathbf{30}]^{\bullet+}$ and $[\mathbf{34}]^{\bullet+}$.

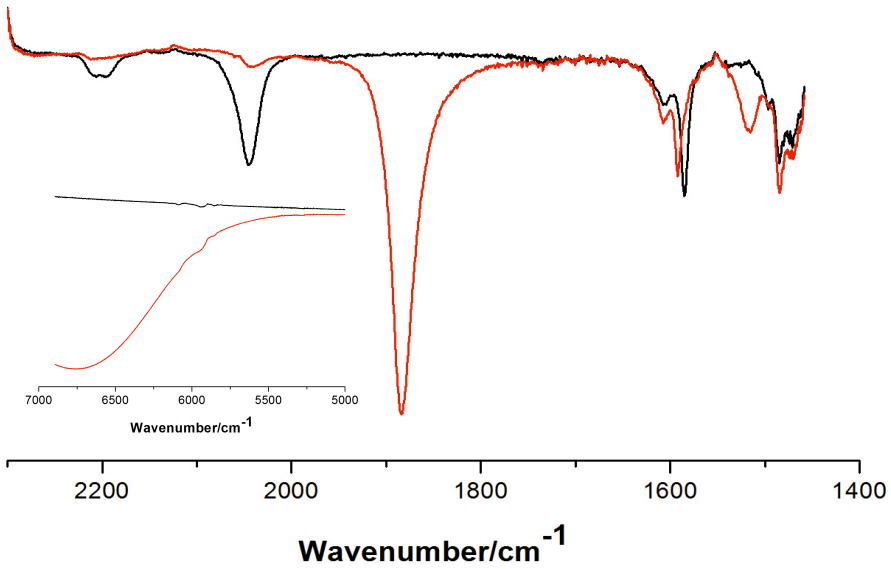

Figure 4-9. *IR spectroelectrochemistry of the compound **30** (black) and [**30**] $^{\bullet+}$(red) with NIR region in inset.*

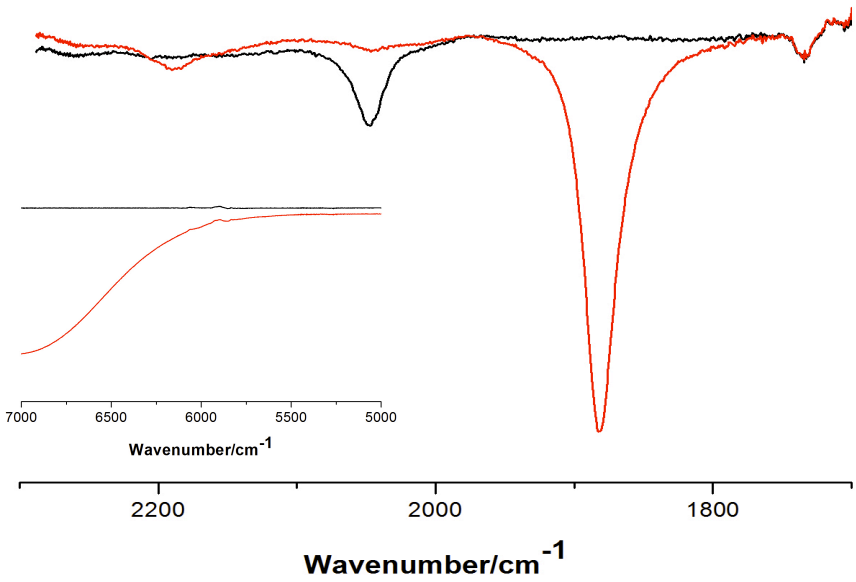

Figure 4-10. *IR spectroelectrochemistry of the compound **34** (black) and **[34]**•+ (red) with NIR region in inset.*

In the IR region of **30** and **34**, the electrochemical oxidation reveals a strong effect of the ethynyl ligand redox activity. The NIR electronic transition located at around 7000 cm^{-1} is also observed by Rigaut et al.[36] and Marqués-González et al.[29] for similar ruthenium complexes. More importantly, Marqués-González et al. reported for related symmetrical ruthenium complexes, and supported by DFT calculations, that the HOMO features have a significant electronic contribution from the entire ethynyl ligand (73 - 91% spin density contribution) whereas the SOMO has more contribution from the $Ru(dppe)_2$ centre (39 - 50% spin density contribution) (Figure 4-11, right). Besides, the electronic structure of the ruthenium complex $\{Ru(C{\equiv}CR)_2(dppe)_2\}$, which is distributed over the entire molecule with more density on the bridge, is totally different than the platinum complex $\{Pt(C{\equiv}CR)_2(dppe)_2\}$ (Figure 4-11, left). As discussed in Chapter 1, a platinum complex was described as an insulator by Mayor et al. due to its Pt-C(sp) σ character[33] and Liu et al. described an enhancement of the conductance for the analogous with the ruthenium complex.[34] This lack of π-electron conjugation can be explained by the square planar geometry adopted by the platinum complex, which leads to weakly bonding to almost non-bonding character of the d_{xy}, d_{xz}, d_{yz} and d_{z2} metal orbitals with the ligand orbitals. The insulator type behavior was emphasized by Vives et al. where the electronic coupling for the 1,4-(diferrocenyl)butadiyne oligoyne (0.036 eV) was found to be better than *trans*-bis(ferrocenylethynyl) bis(triethylphosphine)platinum (0.025 eV).[37] DFT calculations of

trans-$Pt(PPh_3)_2(C{\equiv}CMe_3TTF)_2$ highlight the poor contribution of the organometallic linker to the spin density of [*trans*-$Pt(PPh_3)_2(C{\equiv}CMe_3TTF)_2]^{\bullet+}$, in other words the SOMO (Figure 4-11, left) which explains the unresolved first oxidation of this complex.[38]

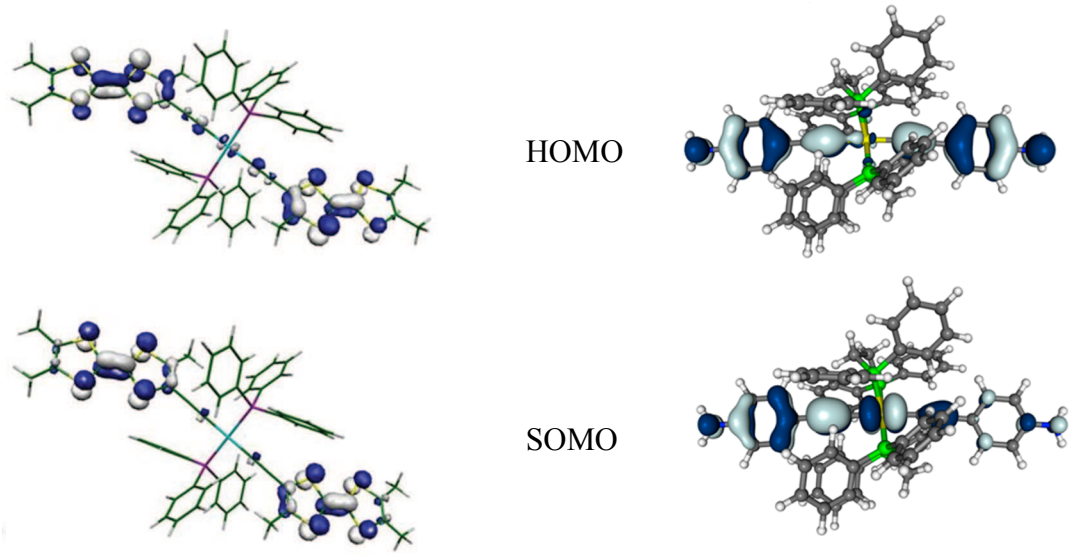

Figure 4-11. *Graphical representations for the HOMO and SOMO of trans-$Pt(PPh_3)_2(C{\equiv}CMe_3TTF)_2$ shown with a cut-off of 0.04 (e bohr^{-3})$^{1/2}$ (left)[38] and isosurface plots (± 0.03 au) of the SOMO and the HOMO for in-plane trans-$Ru(C{\equiv}CC_6H_4NH_2$-4)$_2$(dppe)$_2$ calculated at the BLYP35/COSMO(CH_2Cl_2) level (right).*[29]

4.8. Single molecule *I(s)* conductance measurements

The single molecule conductance measurements of the compounds **24**, **25**, **26**, **27**, **30** and **33** can be analysed in terms of three distinct structural features: 1) the input of the metal in the organic core; 2) the electronic nature of the bridge; and 3) the nature/contact points of the anchor groups. The results offer insights into the wire-like properties of *trans*-bis(alkynyl) metal complexes based on ruthenium[12,14,15,39,34] and platinum,[33] in a single molecule metal | molecule | metal junction, and provide a basis for the further, rational design of metal-containing molecular components for electronics.

Initial studies focused on the molecules **24** - **26**, due to the ease with which molecules bearing the terminal TMSE group can be synthesized, and the known single conductance histogram obtained in single molecule measurements with molecules bearing this contact.[12] However, balancing these attractive aspects, the TMSE binding groups generally lead to low conductance values from measurements with low hit ratios (i.e. ratio of *I*(s) curves featuring plateaus characteristic of single molecule junctions to those that show no features). For this reason, the molecules **30**, **33** and **38** with pyridyl termini have been synthesized. Indeed, the pyridyl moiety has been widely used as a surface contacting group in single molecule studies of oligoynes[40,41], tolanes[17] and OAE[32] providing a range of data for qualitative comparisons with the metal complexes described here.

Both TMSE and pyridyl series display a LUMO-based conductance. By analogy with pyridyl metal-OPE molecules **30** and **33**, and in order to verify that the electronic nature of the bridge and the influence of the metal on the conductance are not just due to a modulation of the LUMO energy level with respect to the energy Fermi level, metal-OPE complexes with thiomethyl linkers **34** and **35** have been prepared. In addition, the thiomethyl linker is attractive because it does not give any stochastic switching, leading to less noise in the conductance traces compared to thiol.[19]

The conductance of compound **39** has been analyzed to check if a phenyl ring, from the ancillary PPh_3, can bind to gold, which could be the origin of the two contacts modes found in the conductance histograms of **27** and **33**.

The *I*(*s*) technique developed by the Liverpool team[2,42] was used to measure the single molecule conductances of **24** - **27** and **30**, **33** and **39** using the procedures and conditions described in the Appendix A.

4.8.1. Single molecule measurements of the organometallic molecules with TMSE linkers (24 – 26)

The conductance histograms obtained from plateaus observed in *I*(*s*) curves are shown in Figures 4-12 and 4-13. Careful calibration of the tip-substrate distance allows an estimate of the electrode separation at which the molecular junction is broken. This value can be compared with the molecular length (obtained crystallographically in the case of **24** (1.52 nm), **25** and **26** (2.38 nm)).

In general, the conductance is found to be higher in the case of the molecules bearing TMSE (**24** - **26**) than the organic homologue which contain a phenyl ring instead of the metal, such as **12** (1.43 ± 0.43 nS; *see* chapter 2) or trimethylsilyl ethynyl terminated OPE derivatives[12] (e.g. TMSE-OPE; 2.13 ± 0.39 nS) (Chart 4-2).

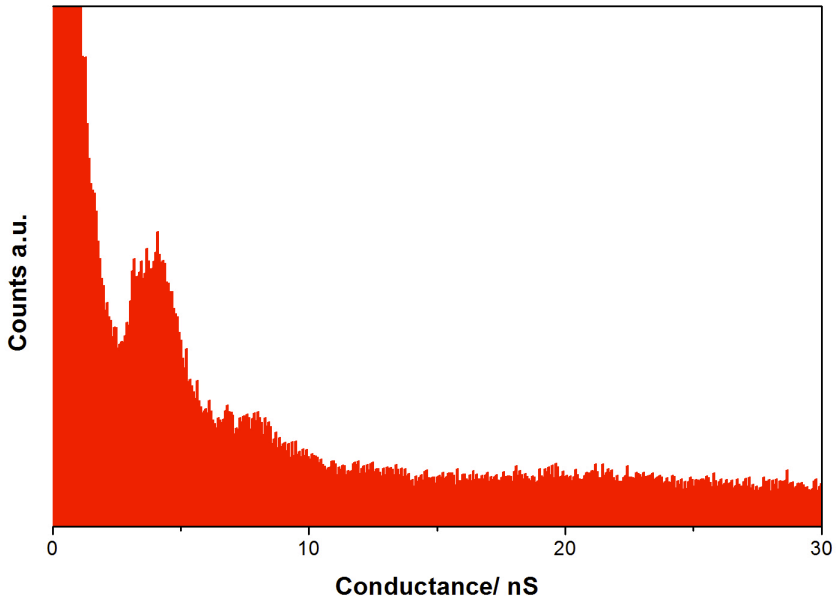

Figure 4-12. *Conductance histogram of **24** in mesitylene derived from the I(s) measurement (U_t = 0.6 V; I_0 = 20 nA) with a conductance value (G = 3.98 ± 0.66 nS and 7.91 ± 0.68 nS) and break-off distance of 1.47 nm and 1.31 nm.*

For the structurally simplest compound, *trans*-Pt(C≡CC≡CSiMe$_3$)$_2$(PPh$_3$)$_2$ (**24**) the conductance histogram reveals two apparent peaks, consistent with two distinct binding motifs. The most pronounced peak at 3.98 nS (break-off distance 1.47 nm) is assigned to the A-type contacts formed by attachment of the molecule to the gold STM tip and the substrate surface through the TMSE and phenyl moieties. The break-off distance associated with this peak does not agree with the molecular length from the crystal structure (Si…Si = 1.52 nm)[43] but fits more with the contacts through TMSE and PPh$_3$ (1.27 nm). The higher conductance peak at 7.91 nS (break-off distance 1.31 nm) is associated with a shorter contact length which might be in agreement with the PPh$_3$…PPh$_3$ distance from the crystal structure of **24** (1.15 nm). The attachment of STM tips to internal regions of molecules has been demonstrated elsewhere and the position of contact used to tune molecular conductance. In the present case, the contact to the phenyl rings of the supporting PPh$_3$ ligands appears a possible explanation which is developed further in the studies described below.

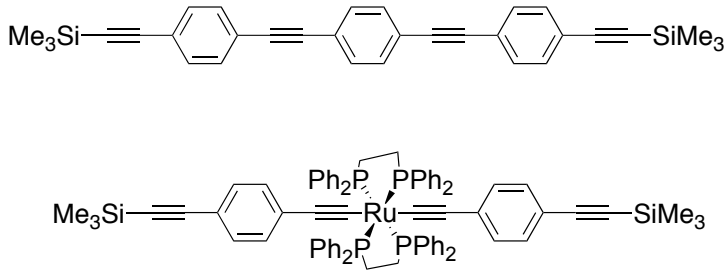

Chart 4-2. *Molecules studied by Marqués-González et al.*[29]

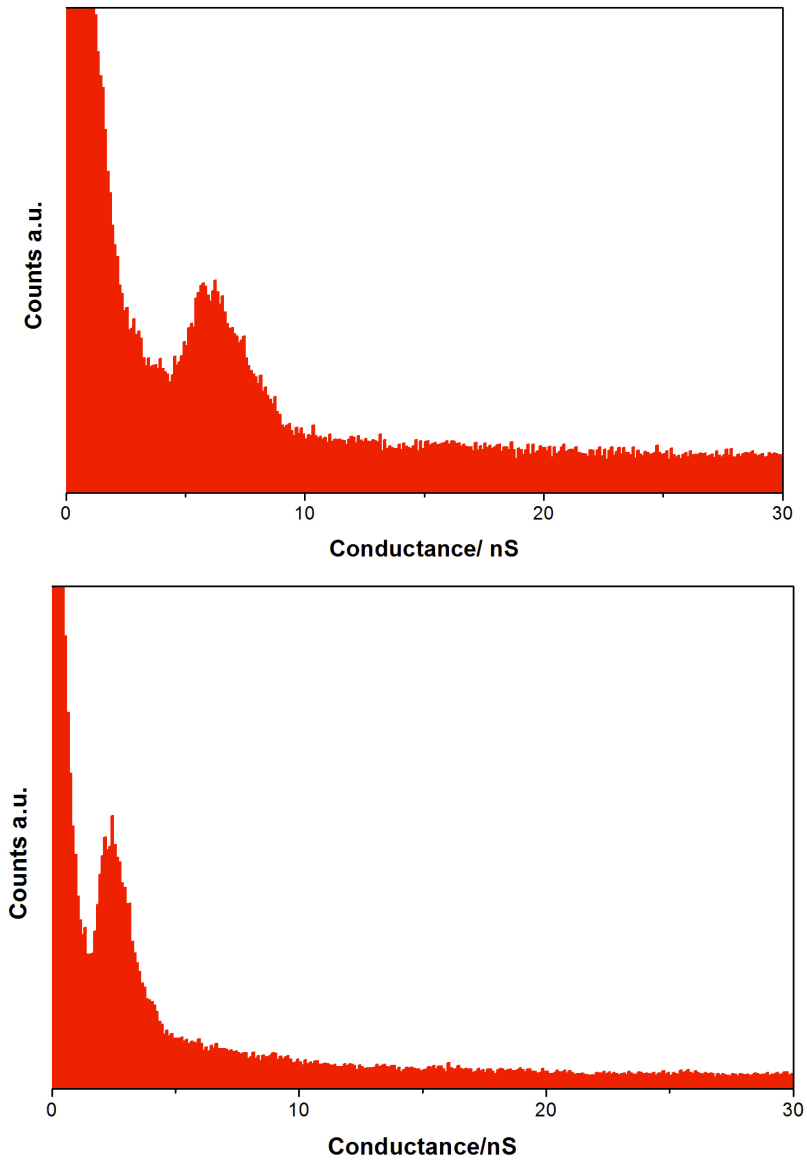

Figure 4-13. *Conductance histogram of **25** (top) and **26** (bottom) in mesitylene derived from the I(s) measurement (U_t = 0.6 V; I_0 = 20 nA for **25** (a)); U_t = 0.6 V; I_0 = 30 nA for **26** (b)) with conductance values (G = 6.11 ± 0.89 nS) and break-off distance of 1.80 nm for **25**; (G = 2.42 ± 0.44 nS) and break-off distance of 1.91 nm for **26**.*

More surprisingly the conductance of the platinum compound *trans*-Pt[C≡C{1,4-C_6H_4}C≡C$SiMe_3$]$_2$(PPh_3)$_2$ **25** (6.11 nS) is almost twice higher than the ruthenium analogue (Chart 4-2) (3.95 nS).[29] This result contrasts with the insulating behavior of platinum

acetylide against the conducting behavior of ruthenium acetylide described in the literature.[33,34] However, the two molecules studied by the different groups have both the thiol (derived from thioacetate) as an anchoring group. The conductance channels used by the thiols are the HOMO orbitals, and the different conductance channels of TMSE or pyridyl linkers could influence the conductance behavior.

In addition to the choice of linkers, the substitution on the phenyl ring seems to influence significantly the conductance of the organometallic complexes. For the platinum compound with hexyloxy side chains *trans*-Pt[C≡C{1,4-$C_6H_2(OC_6H_{13})_2$}C≡C$SiMe_3$]$_2$(PPh_3)$_2$ **26** the value (2.42 nS ± 0.44 nS) is lower than the analogue without the side chains **25** (6.11 nS ± 0.89 nS). This result starkly contrasts the negligible effect that such solubilizing groups play on the conductance of structurally related OAE all-organic molecules with thiol contacts.[44] In our case, the frontier orbital levels of the organometallic molecules might be more affected by the electro-donating effect of the alkoxy substituent than in the organic parents. Alternatively, the difference in conductance between **25** and **26** might be explained once more by contact to the PPh_3 ancillary ligand(s). This would be hindered by the hexyloxy chains in **26** which would then display lower conductance due to the longer contact distance (Si…Si) compared to **25** (PPh_3…Si or PPh_3-PPh_3) (Figure 4-14) which is in agreement with the break-off distance of the latter.

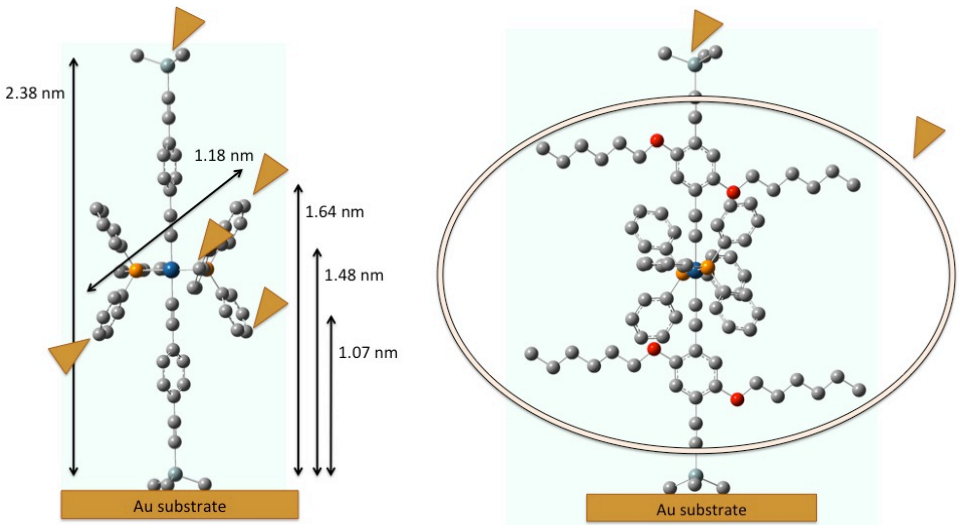

Figure 4-14. *Possible binding contacts for compound **25** (left) and compound **26** with the hexyloxy shell (right).*

4.8.2. Single molecule measurements of the organometallic molecules with pyridyl anchoring groups

To further explore the conductance behavior of platinum organometallic complexes, pyridyl-terminated analogues were studied. The conductance histograms obtained from the *I*(*s*) curves are shown in Figure 4-15 - 4-17. The length of the molecule obtained crystallographically for **27** (1.48 nm), **30** (2.86 nm), **33** (2.86 nm) and the additional Au-N bonds (ca. 0.2 nm).

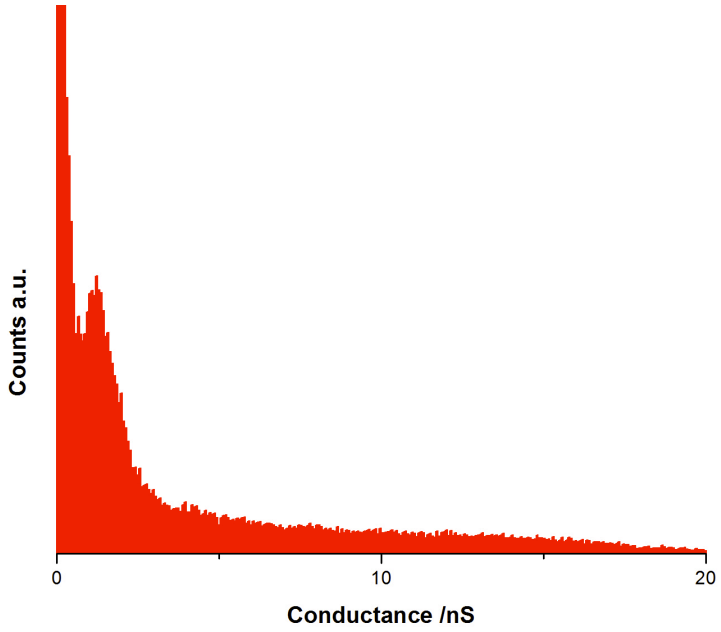

Figure 4-15. *Conductance histogram of **27** derived from the I(s) measurement with a conductance value (G = 1.35 ± 0.37 nS) and break-off distance of 1.47 nm (U_s = 0.6 V; I_0 = 10 nA).*

The conductance of **27** is lower (1.35 nS ± 0.37 nS; 1.7 × 10^{-5} ± 0.4 × 10^{-5} G_0) (Figure 4-15) than its organic homologue with phenyl instead of the metal (2.45 nS; 3.2 × 10^{-5} G_0),[32] which implies that the conductance is difficult to predict because a lot of parameters have to be considered. Indeed, the length of the organometallic molecule might influence the position and the distribution of the orbitals throughout the molecule.

A single conductance peak in the histogram of the ruthenium complex **30** is observed with data selection and gives a conductance value of 0.35 ± 0.1 nS (4.5 x 10^{-6} G_0) (Figure 4-16). This is much higher than the value of 0.015 nS (2.0 x 10^{-7} G_0) obtained for the similarly structured five-ring oligoarylene ethynylene OAE5 (*see* Chart 4-1). The

difference in conductance is certainly not the result of the slight shortening of the molecular length (2.86 nm for RuOPEPy **30**; 3.00 nm for the OAE5) and suggests input of the ruthenium metal in the organic core.

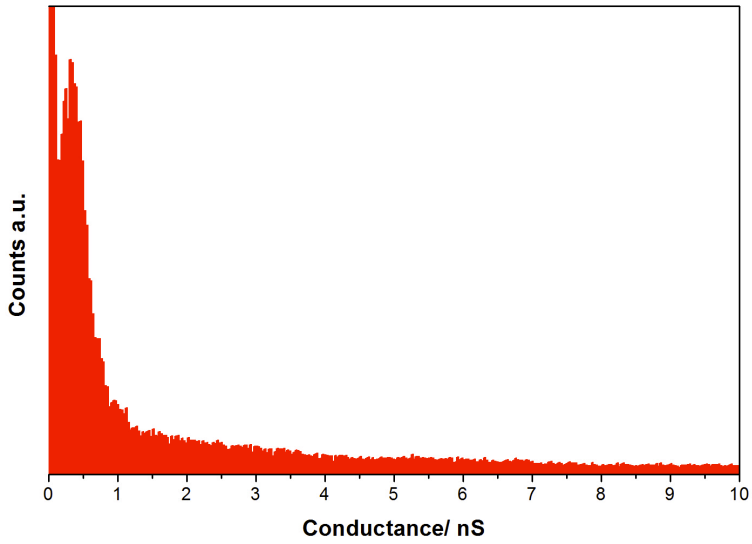

Figure 4-16. *Conductance histogram of **30** derived from the I(s) measurement with a conductance value (G = 0.35 ± 0.10 nS) and a break-off distance of 3.90 nm*

In contrast, in the absence of data selection, the platinum compound **33** gave a more complex series of overlapping conductance regions (Figure 4-17), consistent with different pyridine-gold contact geometries,[40] combined with possible contact through PPh_3 ancillary ligand and the pyridyl group. The data were then selected to give only the A-type contact which display a conductance value of ca. 0.81 ± 0.22 nS ($1 \times 10^{-5} \pm 0.28 \times 10^{-5}$ G_0).

Surprisingly, in contrast with the expectations based on Mayor's and Liu's work, the conductance of the two metal-OPE molecules (**30** and **33**) is comparable with a slight increase for the platinum-OPE **33** (as for the TMSE molecules, **25** and **26**). This surprising set of results, in which two different families of metal complexes were indicating Pt complexes to be more conductive than the Ru systems, prompted computational modeling, which was carried out in Professor Colin Lambert's group at Lancaster University.

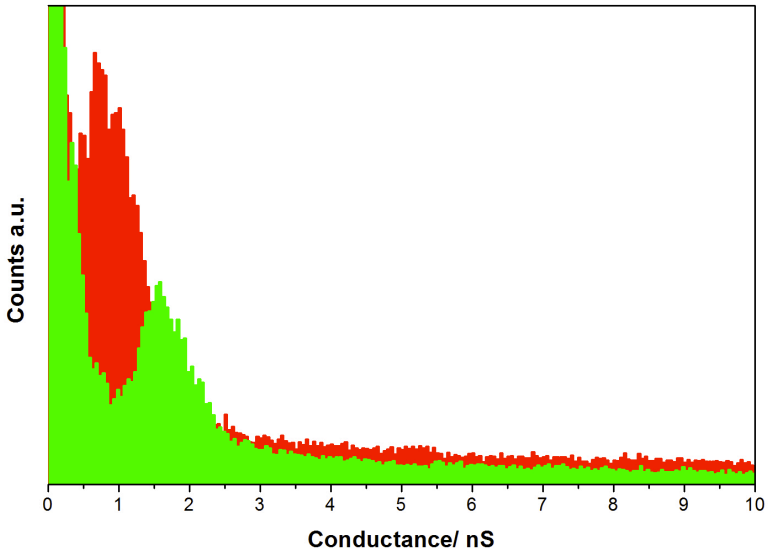

Figure 4-17. *Conductance histogram of **33** derived from the I(s) measurement with a conductance value (G = 0.81 ± 0.22 nS and 1.64 ± 0.24 nS) and a break-off distance of 2.90 and 2.60 nm. The red peak is the conductance from the A-type contact (high) and the green peak is the conductance from the B-type contact (medium)*

4.8.3. Single molecule measurement of the compound 39

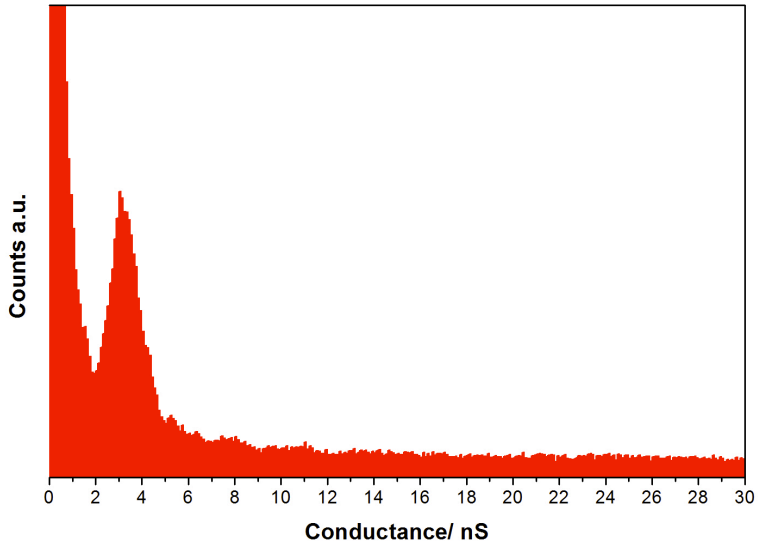

Figure 4-18. *Conductance histogram of **39** in mesitylene derived from the I(s) measurement (U_t = 0.6 V; I_0 = 30 nA) with a conductance value (G = 3.19 ± 0.62 nS) and a break-off distance of 1.66 nm*

The conductance for the compound **39** is high (3.19 ± 0.62 nS) and should result from the contact through the PPh_3 ancillary ligand, perpendicular to the molecule backbone. The high conductance is not so surprising because of the short distance between the two phenyl rings from PPh_3, estimated at 1.18 nm (*see* Figure 4-14). This data is interesting for future check test of binding contact through the phosphine ligands.

4.9. Quantum chemical modelling

The role of the metal atom within the molecular backbone was further investigated using computational methods. The preparation of complexes such as **30** and **33** without the hexyloxy side chains was not possible due to their insolubility; however the structurally simpler analogues **30´** and **33´** (Chart 4-3) were modeled using the same computational approaches to probe the influence of the structural modules on the overall junction behavior. The computational procedures are described in the experimental section.

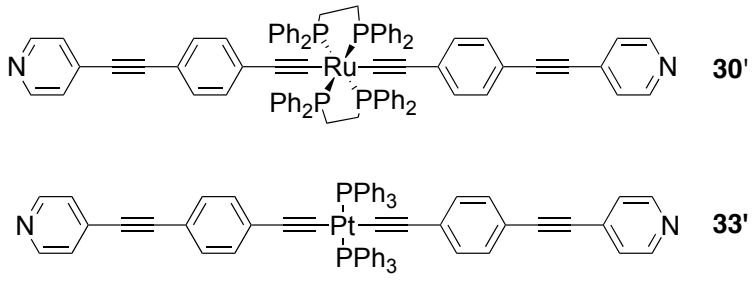

Chart 4-3. *Analogous molecules studied in this work under computational methods.*

Results for the electrical conductance and various geometrical features of the relaxed junctions are shown in Table 4-3. The data support the experimental observation of higher conductance of the pyridine contacted platinum complex **33** and the hexyloxy-free model **33´** compared to the ruthenium analogues **30** and **30´**. These results also show that the conductance of the molecules with hexyloxy groups are lower than that of the molecules without hexyloxy groups. This change can be explained by a combination of competing effects. First, the addition of these groups increases the size of the molecules and when the size of a quantum system is increased, energy levels typically decrease in value. On the

other hand, the hexyloxy groups donate electrons to the backbone which, due to electron-electron repulsion, tends to increase the energies of the molecular orbitals.

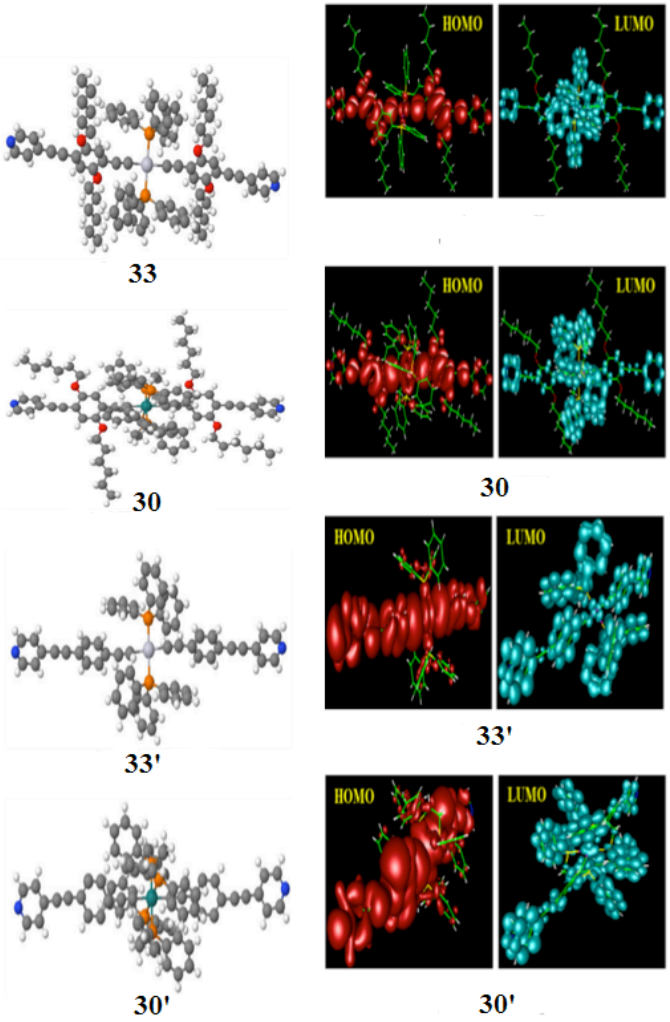

Figure 4-19. *The left-hand figures show the relaxed geometries of the isolated molecules. The right hand figures show isosurfaces of the HOMO (red) and LUMO (blue) of each molecule.*

These competing factors are reflected in the positions of resonances in the transmission curves shown in the top right pane (Figure 4-20). For the ruthenium systems **30** and **30´**, the bis(phosphine) co-ligands make the complexes relatively electron-rich, and further electron transfer or donation from the hexlyoxy substituents to the backbone is only Q = 0.73 electrons, leading to a net decrease in both the HOMO and the LUMO resonances of 0.2 eV. The addition of the hexyloxy moieties also causes **30** to adopt a more linear geometry compared with **30´**, which is slightly bent. The linear geometry increases the

distance between the anchor and the gold electrodes, resulting in a weaker coupling, a decrease in the widths of the HOMO and LUMO resonances and a further decrease in the conductance.

For the platinum complexes **33** and **33´**, the hexyloxy groups produce a rather large electron transfer to the backbone of Q = 1.76 electrons and therefore electron repulsion dominates, leading to a small (0.1 eV) increase in the LUMO resonance and a larger (0.45 eV) increase in the HOMO resonance, due to the larger weight of the HOMO on the hexyloxy groups, as shown by the isosurface plot (Figure 4-19). This leads to a decrease in the gap between the HOMO and the LUMO resonances and a slight decrease in conductance G due to the slight increase in the position of the LUMO.

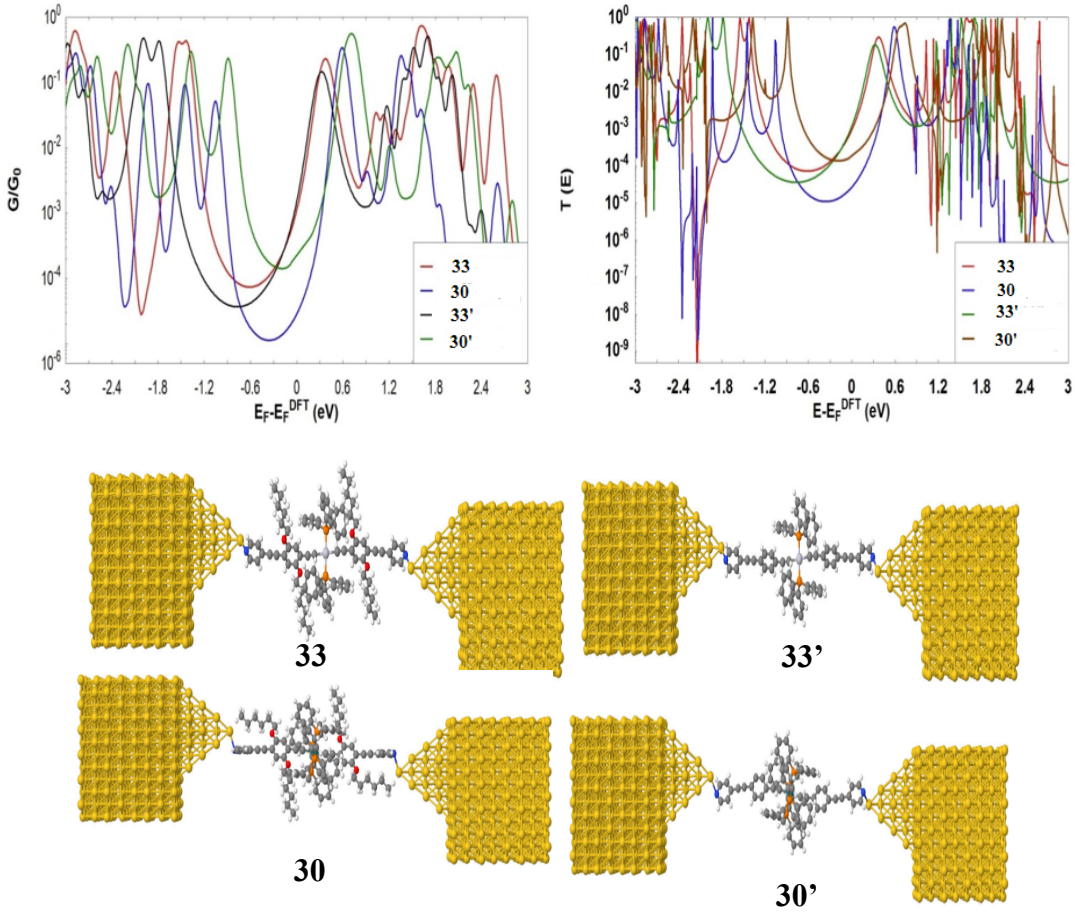

Figure 4-20. *The top-left-hand plots show the room-temperature conductance as a function of the Fermi energy for all pyridyl-based structures with and without hexyloxy groups for different metals (Pt and Ru). These conductances are obtained from the transmission coefficients T(E) shown in the top-right figure. The bottom panel shows the relaxed junctions.*

Table 4-3. *Results for the conductances and relaxed geometries of the Pt- and Ru-based molecules with pyridine anchors. d_{N-N} is the distance between centres of nitrogen atoms. X is the bond length between the top gold atoms of the pyramidal electrodes and anchor N atoms. Z is the theoretical electrode separation, which is defined as $z = d_{Au-Au}$-0.25 nm, where d_{Au-Au} is the centre to centre distance of the apex atoms of the two opposing gold pyramids in the relaxed structure, and 0.25 nm is the value of d_{Au-Au} when the conductance through the two contacting pyramids (the absence of a molecule) is G_0. For the latter, Q denotes the number of electrons transferred from the HX-group to the backbone (for an isolated molecule).*

Molecule	**Conductance**	**d_{Au-Au} (nm)**	**d_{N-N} (nm)**	**X (nm)**	**Z = dAu-Au-0.25 (nm)**	**Q**
30	10^{-4}	3.100	2.882	0.24	2.850	0.73
30´	$10^{-3.38}$	3.056	2.883	0.24	2.806	
33	$10^{-1.86}$	3.027	2.886	0.21	2.777	1.76
33´	$10^{-1.59}$	2.887	0.21	2.775	2.775	

In contrast to expectations drawn from past results with ruthenium[14,15,34,45] and platinum[33] complexes bearing sulfur-based surface contacts, our results show that the order of the conductance values, **33´** > **33** > **30´** > **30** follows the trend in the molecular lengths and arise primarily from a dominating contribution from LUMO-based conduction channels (Figure 4-21).

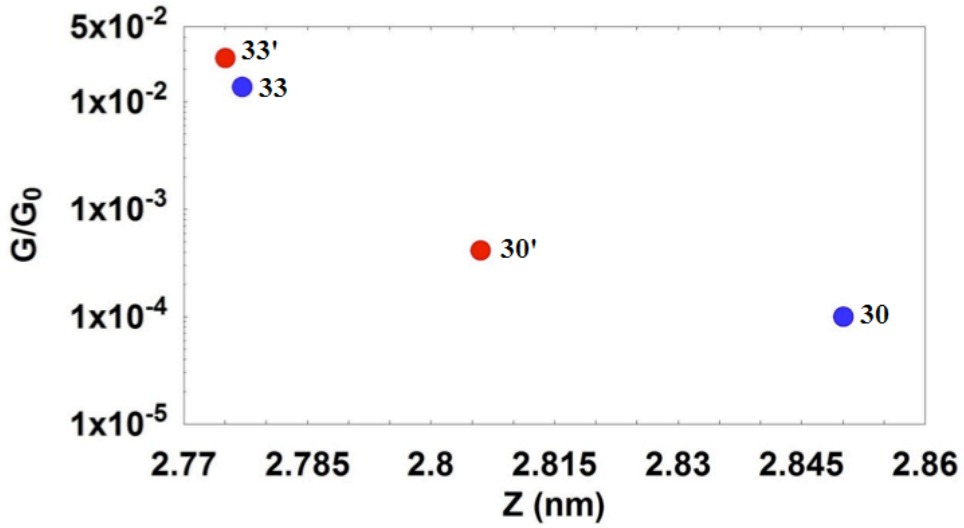

Figure 4-21. *A plot of the conductance versus theoretical electrode separation (Z) shown in Table 4-3 for Pt- and Ru-based molecules with pyridyl anchors, with and without hexyloxy groups.*

4.10. Conclusion

New metal-OPE molecules have been synthesized through the "on complex" Sonogashira cross-coupling route. The single molecule measurements gave a guideline for future design of organometallic molecule for molecular electronics. Indeed, the conductance can be tuned by the nature of the metal, the substituents attached to the organic core, the nature of the bridge and the anchor groups. The conductance is higher in the organometallic molecules bearing TMSE binding groups because of the proximity between the LUMO and the Fermi level. However, when the hexyloxy side chains are present (**26**), the conductance unexpectedly dropped. This may be due to electron repulsion which destabilizes the HOMO and LUMO levels, or possibly the backbone geometry being planarized which increases the distance between the gold electrodes (**30**). Indeed, DFT calculations showed that the metal-OPE molecule bearing pyridyl anchoring group is more linear when the hexyloxy side chains are present than when there is none. Moreover, Pt-OPE **33** displays a slightly higher conductance than the Ru-OPE **30** which can be explained by the alignment of the orbitals level relative to the Fermi level but also might arise from the different binding sites available inside the molecular backbone (e.g. PPh_3).

The phenyl ring of PPh_3 has been considered as a possible binding group (**39**). Contacts through the PPh_3…PPh_3 lead to a higher conductance due to the small intramolecular distance (≈ 1.18 nm). These different types of contacts available when no hexyloxy chains are present, suggest a future design of similar organometallic molecules with PPh_3 replaced by trialkylphosphine ancillary ligands, e.g. PEt_3.

Further studies are under investigation to explore various linker that use other conductance channels such as thiomethyl (**34**, **35**) and studies of metal-OPE charge transport with increasing length can be made from the future result of **38**.

CHAPTER 4

4.11. Experimental

4.11.1. General conditions

All reactions were carried out in oven-dried glassware under oxygen-free argon atmosphere using standard Schlenk techniques. HN^iPr_2, $HNEt_2$ were purified by distillation from KOH and Et_3N purified by distillation from $CaSO_4$; other reaction solvents were purified and dried using Innovative Technology SPS-400 and degassed before use. The compounds $[RuCl(dppe)_2]OTf$,[26] $PtCl_2(PPh_3)_2$,[46] 1-ethynyl-2,5-bis(hexyloxy)-4-(trimethylsilylethynyl)benzene[47], 1-ethynyl-4-(trimethylsilylethynyl)benzene[48] were prepared following previous literature methods. 4-ethynylpyridine was prepared by Dr Xiaotao Zhao using the literature route.[49] Other reagents were purchased commercially and used as received or prepared by variations of literature methods as described below. NMR spectra were recorded in deuterated solvent solutions on Bruker Avance 400 MHz and Varian VNMRS 700 MHz spectrometers and referenced against residual protio-solvent resonances ($CHCl_3$: ^1H 7.26 ppm, ^{13}C 77.00 ppm and CH_2Cl_2: ^1H 5.32 ppm, ^{13}C 53.84 ppm). In the NMR assignment, the phenyl ring associated with the dppe and PPh_3 are denoted Ph (subscript i for ipso, o for ortho, m for meta and p for para); Ar indicates any arylene group belonging to the alkynyl ligands, pyridine and thioanisole are replaced by C_5H_4N and C_6H_4SMe respectively.

Matrix-assisted laser desorption ionization (MALDI) mass spectra were recorded using an Autoflex II TOF/TOF mass spectrometer with a 337 nm laser. Electron ionisation mass spectra were recorded on a Thermoquest Trace or a Thermo-Finnigan DSQ. Infrared spectra were recorded on a Thermo 6700 spectrometer from CH_2Cl_2 solution in a cell fitted with CaF_2 windows. UV spectra were recorded on a Thermo Scientific evolution 220 UV-Vis spectrophotometer. Elemental analyses were performed on a CE-400 Elemental Analyzer. Infrared spectra were recorded on a Thermo 6700 spectrometer from CH_2Cl_2 solution in a cell fitted with CaF_2 windows. Electrochemical analyses were recorded using Emstat 2, Palm instruments BV electrochemical analyzer fitted with a three-electrode system consisting of a Pt disk as working electrode, auxiliary and reference electrode from solution in CH_2Cl_2 containing 0.1 M NBu_4PF_6.

CHAPTER 4

$Pt(PPh_3)_2(C{\equiv}CC{\equiv}CSiMe_3)_2$; 24[43]

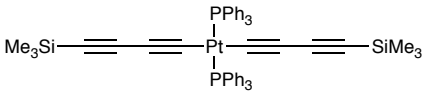

A suspension of *cis*-$Pt(PPh_3)_2Cl_2$ (79 mg, 0.10 mmol), $HC{\equiv}CC{\equiv}CSiMe_3$ (61 mg, 0.08 mL) and CuI (6 mg) in CH_2Cl_2 (5 mL) and $HNEt_2$ (15 mL) was stirred at room temperature for 3 h and then heated at 80 °C for 2 h. The resulting brown solution was dried and the residue was columned on neutral alumina using toluene as an eluent. The yellow solution was concentrated and addition of MeOH gave an off-white precipitate that was collected by filtration and dried in air. Yield: 45 mg, 47%. ^{1}H NMR ($CDCl_3$): 7.70 - 7.65 (m, 12H, Ph), 7.41-7.39 (m, 18H, Ph), 0.01 (s, 18H, Si*Me*$_3$) ppm. ^{31}P {H} NMR (162 MHz, $CDCl_3$): δ 17.4 (s, $J_{P\text{-}Pt}$ = 2572 Hz) ppm. IR (CH_2Cl_2): ν(C≡C) 2129 (s), ν(C≡CSiMe$_3$) 2186 (m) cm^{-1}. The NMR data were in accord with the literature.[43]

$Pt(PPh_3)_2(C{\equiv}C\text{-}C_6H_4\text{-}C{\equiv}C\text{-}SiMe_3)_2$; 25

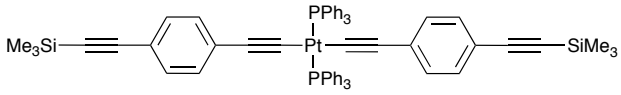

cis-$PtCl_2(PPh_3)_2$ (300 mg, 0.36 mmol), 1-ethynyl-4-(trimethylsilylethynyl)benzene (168 mg, 0.72 mmol) and CuI (6 mg, 0.03 mg) were added to a degassed solution of $HNEt_2$ (30 mL). The solution was refluxed for 3 h and the precipitate was collected by filtration and washed with MeOH to give a pale yellow powder. Yield: 340 mg, 85%. ^{1}H NMR (400 MHz, $CDCl_3$): δ 7.79 - 7.32 (m, 30H, Ph), 7.0 (d, J = 8.3 Hz, 4H, Ar), 6.17 (d, J = 8.3 Hz, 4H, Ar), 0.19 (s, 18H, Si*Me*$_3$). ^{31}P {H} NMR (162 MHz, $CDCl_3$): δ 17.7 (s, $J_{P\text{-}Pt}$ = 2626.7 Hz). ^{13}C {^{1}H} NMR (101 MHz, $CDCl_3$): δ 135.0 (t, J = 6.0 Hz, Ph_o), 131.1 (t, J = 30.9 Hz, Ph_i), 130.7 (H*C*$_{Ar}$), 130.6 (H*C*$_{Ar}$), 130.2 (*C*$_{Ar}$), 130.1 (Ph_p), 128.9, 127.8 (t, J = 5.5 Hz, Ph_m), 118.7, 113.4, 105.8, 94.0 (*C*≡), 0 (H_3C_{SiMe3}). IR (CH_2Cl_2): ν(C≡CSiMe$_3$) 2150, ν(C≡C) 2104 cm^{-1}. MS$^+$ (MALDI-TOF; m/z): 718.9 [M/2 + 2H]$^+$, 1114.2 [M + H]$^+$, 1957.3. Crystals suitable for X-ray study were obtained from CH_2Cl_2/MeOH. HR-(ESI$^+$)-MS: calcd for $C_{62}H_{56}P_2{}^{194}PtSi_2Na$ 1136.2944; found 1136.2985. Crystal data for **25**:

$C_{62}H_{56}P_2{}^{194}PtSi_2$, M = 1114.28, orthorhombic, space group Pbcn, a = 21.2751(3) Å, b = 13.91150(17) Å, c = 18.261(2) Å, β = 90.00 °, U = 5404.88(12) Å^3, F(000) = 2256, Z = 4, D_C = 1.369 mg/mm^3, μ = 2.737 mm^{-1}; 62222 reflections were collected , yielding 7526 unique data (R_{merg} = 0.0533). Final $wR_2(F^2)$ = 0.0657 for all data (307 refined parameters), conventional R_1 (F) = 0.0272 with I ≥ 2σ, GOF = 1.027.

$Pt(PPh_3)_2\{C{\equiv}CC_6H_2(OC_6H_{13})_2C{\equiv}C\text{-}SiMe_3\}_2$; 26

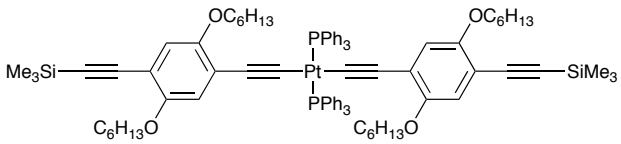

A solution of 1-ethynyl-2,5-bis(hexyloxy)-4-(trimethylsilylethynyl)benzene (48 mg, 0.12 mmol), *cis*-$Pt(PPh_3)_2Cl_2$ (50 mg, 0.06 mmol), CuI (1 mg) in $HNEt_2$ (5 mL), was refluxed overnight. The resulting solution was dried and the residue was purified on silica column chromatography with CH_2Cl_2/hexane (1:1 v/v) changing to pure CH_2Cl_2 to yield a yellow oily solid. The product was obtained as a yellow solid after a precipitation from CH_2Cl_2/MeOH. Yield: 30 mg, 33%. ^{1}H NMR (400 MHz, CD_2Cl_2): δ 7.84 - 7.78 (m, 12H, Ph), 7.38 - 7.29 (m, 18H, Ph), 6.60 (s, 2H, Ar), 5.68 (s, 2H, Ar), 3.63 (t, J = 6.5 Hz, 4H, OC*H*$_2$), 3.56 (t, J = 6.5 Hz, 4H, OC*H*$_2$), 1.72 - 1.65 (m, 4H, C*H*$_2$), 1.50 - 1.42 (m, 4H, C*H*$_2$), 1.37 - 1.33 (m, 12H, CH_2), 1.26 - 1.15 (m, 12H, C*H*$_2$), 0.93 - 0.86 (m, 12H, C*H*$_3$), 0.20 (s, 18H, Si*Me*$_3$) ppm. ^{31}P {H} NMR (162 MHz, $CDCl_3$): δ 17.58 (s, $J_{P\text{-}Pt}$ = 2645.8 Hz). ^{13}C {^{1}H} NMR (101 MHz, CD_2Cl_2): δ 154.2, 152.7 (O-*C*$_{Ar}$), 135.6 (t, J = 6.2 Hz, Ph$_o$), 131.6 (m, Ph$_i$), 130.7 (Ph$_p$), 128.1 (t, J = 5.3 Hz, Ph$_m$), 117.7, 117.2 (H*C*$_{Ar}$), 109.3, 102.6, 98.1 (*C*≡ or *C*$_{Ar}$), 70.0, 69.6 (O-*C*H$_2$), 32.0, 29.8, 29.5, 26.1, 25.9, 23.1, 23.0 (*C*H$_2$), 14.31, 14.29 (*C*H$_3$), -0.1 ($SiMe_3$). MS^+ (MALDI-TOF; m/z): 1514.6 $[M + H]^+$. IR (CH_2Cl_2): ν(C≡CSiMe$_3$) 2144 (m), ν(Pt-C≡) 2102 (m) cm^{-1}. HR-ESI$^+$-MS: *m/z* calcd for $C_{86}H_{104}O_4P_2PtSi_2H$ 1513.8940; found 1513.6693.

$Pt(PPh_3)_2(C{\equiv}C\text{-}C_6H_4N)_2$; 27[50]

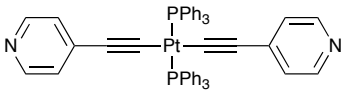

A solution of $HNEt_2$ (20 mL), *cis*-$Pt(PPh_3)_2Cl_2$ (197 mg, 0.25 mmol), 4-ethynylpyridine (50 mg, 0.5 mmol) and CuI (4 mg, 0.02 mmol) was heated at 50 °C overnight. The resulting white and cloudy solution was filtered and the solid was washed with MeOH. The product was obtained as a white solid. Yield: 59 mg, 25%. ^{1}H NMR ($CDCl_3$): δ 8.10 (d, J = 5.1 Hz, 4H, C_5H_4N), 7.79 - 7.73 (m, 12H, Ph), 7.44 - 7.35 (m, 18H, Ph), 6.13 - 6.12 (m, 4H, C_5H_4N) ppm. ^{31}P {H} NMR (162 MHz, $CDCl_3$): δ 18.8 (s, $J_{P\text{-}Pt}$ = 2601.2 Hz) ppm. ^{13}C {^{1}H} NMR (101 MHz, $CDCl_3$): δ 148.3 (HC_{C5H4N}), 134.9 (t, J = 6.5 Hz, Ph_o), 130.8 (t, J = 29.8 Hz, Ph_i), 130.5 (Ph_p), 128.0 (t, J= 5.4 Hz, Ph_m), 125.3 (C_{C5H4N}), 111.3, 100.0 (*C*≡) ppm, the other quaternary carbon is not visible. IR (CH_2Cl_2): 2984 (s); ν(Pt-C≡) 2112 (m); ν(C=N) 1587 (s) cm^{-1}. MS$^+$ (MALDI-TOF; m/z): 924.1 $[M + H]^+$. The data were consistent with the literature.[50]

5-Trimethylsilylethynyl-1,4-bishexyloxybenzene Similar procedure[25]

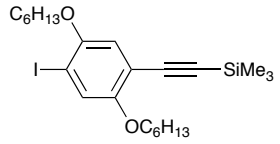

In a 250 mL Schlenk flask, a solution of 1,4-bis(hexyloxy)-2,5-diiodobenzene (6.0 g, 11 mmol), trimethylsilylacetylene (491 mg, 0.7 mL, 5 mmol), $PdCl_2(PPh_3)_2$ (140 mg, 0.2 mmol), CuI (38 mg, 0.2 mmol) in degassed dry NEt_3 (120 mL) was stirred overnight at room temperature. The solvent was removed and the residue purified on a silica column. Elution with hexane recovered unreacted 1,4-bis(hexyloxy)-2,5-diiodobenzene, followed by elution with CH_2Cl_2:hexane (1:9), which after evaporation produced a yellowish oil of the desired mono-alkyne. Yield: 1.88 g, 76%. ^{1}H NMR (400 MHz, $CDCl_3$): δ 7.25 (s, 1H, Ar); 6.83 (s, 1H, Ar); 3.95 - 3.92 (dt, J = 12.7 Hz, 6.4Hz, 4H, -OC*H*$_2$); 1.81 - 1.76 (m, 4H, C*H*$_2$); 1.52 - 1.48 (m, 4H, C*H*$_2$); 1.36 - 1.33 (m, 8H, C*H*$_2$); 0.93 - 0.88 (m, 6H, CH_2CH_3); 0.25 (s, 9H, Si*Me*$_3$) ppm. The NMR data were consistent with the literature.[25]

2-Triisopropylsilylethynyl-5-trimethylsilylethynyl-1,4-bishexyloxybenzene (Similar procedure[25])

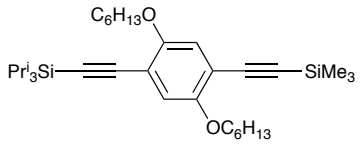

To a solution of TMS-C≡C$C_6H_2(OC_6H_{13})_2$-I (1.88 g, 3.8 mmol) in degassed NEt_3 (30 mL), TIPSA (638 mg, 0.78 mL, 3.5 mmol), $Pd(PPh_3)_4$ (219 mg, 0.19 mmol) and CuI (36 mg, 0.19 mmol) were added. The reaction mixture was stirred overnight at room temperature. The solvent was removed and the residue was purified by passage through a silica pad and elution by ethyl acetate (EtOAc):hexane (1:9) to give a yellow oil, which solidified on storage to give an off-white coloured solid. Yield: 1.30 g, 60%. ^{1}H NMR (400 MHz, $CDCl_3$): δ 6.88 (s, 1H, Ar), 6.87 (s, 1H, Ar), 3.97 - 3.91 (dt, J = 12.7, 6.4 Hz, 4H, -OCH_2), 1.82-1.72 (m, 4H, CH_2), 1.53 - 1.43 (m, 4H, CH_2), 1.35 - 1.30 (m, 8H, CH_2), 1.13 (s, 21H, SiPr^i_3), 0.92 - 0.88 (m, 6H, CH_2CH_3), 0.25 (s, 9H, SiMe_3) ppm. The NMR data were consistent with the literature.[25]

2-Triisopropylsilylethynyl-5-ethynyl-1,4-bishexyloxybenzene; I[25]

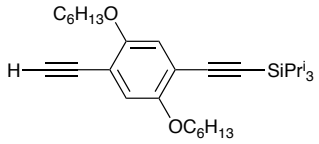

Potassium carbonate (298 mg, 2.16 mmol) was added to a solution of 2-triisopropylsilylethynyl-5-trimethylsilylethynyl-1,4-bis(hexyloxy)benzene (1.20 g, 2.16 mmol) in THF/MeOH (1:1) (160 mL). The solution was stirred for 2 h at room temperature before CH_2Cl_2 was added. The solution was washed with water, the organic layer was collected and dried over $MgSO_4$, before the solvent was removed to yield an orange solid, which was used without further purification. Yield: 950 mg, 91%. ^{1}H NMR (700 MHz, $CDCl_3$): δ 6.90 (d, J = 3.3 Hz, 2H, Ar), 3.98 (t, J = 6.5 Hz, 2H, -OCH_2), 3.92 (t, J = 6.5 Hz, 2H, -OCH_2), 3.31 (s, 1H, C≡C-*H*); 1.83 - 1.72 (m, 4H, CH_2), 1.49 - 1.44 (m, 4H, CH_2), 1.35 - 1.30 (m, 8H, CH_2), 1.13 (s, 21H, SiPr^i_3), 0.92 - 0.87 (m, 6H, CH_2CH_3) ppm.

CHAPTER 4

Trans-Ru(C≡C-(1,4-OC_6H_{13}-C_6H_4)-C≡C-$SiPr^i_3$)$_2$(dppe)$_2$; 28

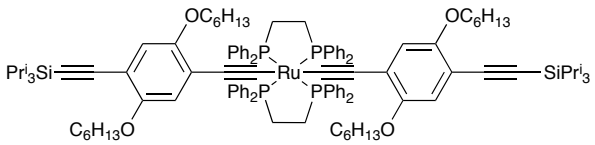

The complex salt [RuCl(dppe)$_2$]OTf (100 mg, 0.09 mmol) was added to a degassed solution of CH_2Cl_2 (4 mL) containing 1,8-diazabicyclo[5.4.0]undec-7-ene (DBU) (4 drops). The solution changed from red to orange with the addition of **I** (96 mg, 0.20 mmol). The reaction mixture was stirred for 1 h at room temperature before $TlBF_4$ (27 mg, 0.09 mmol) was added. After 20 min, the resulting solution had turned yellow in colour and formed a precipitate (TlCl). The precipitate was removed by filtration through a Millex syringe filter (Millipore) to give an orange solution, which was reduced to the minimum volume and methanol (5 mL) added. A yellow precipitate was obtained upon further concentration of the mixture. The product was collected by filtration, and dried in air to give **28** as a bright yellow solid. Yield: 131 mg, 76%. ^{1}H NMR (400 MHz, $CDCl_3$): δ 7.44 (m, 16H, Ph_o), 7.08 - 7.04 (m, 8H, Ph_p), 6.86 - 6.82 (m, 18H, (16H, Ph_m + 2H, Ar)), 5.86 (s, 2H, Ar), 3.84 (t, J = 6.9 Hz, 4H, O-CH_2), 3.64 (t, J = 6.4 Hz, 4H, O-CH_2), 2.89 (m, 8H, PCH_2CH_2P), 1.73 - 1.61 (m, 8H, CH_2), 1.48 - 1.46 (m, 4H, CH_2), 1.34 - 1.30 (m, 12H, CH_2), 1.18 (bs, 50H, (42H, SiPr^i_3 + 8H, CH_2), 0.92 (t, J = 7.0 Hz, 6H, CH_2CH_3), 0.81 (t, J = 7.0 Hz, 6H, CH_2CH_3) ppm. ^{31}P{^{1}H} NMR (162 MHz, $CDCl_3$): δ 52.07 (s) ppm. ^{13}C {^{1}H} NMR (101 MHz, $CDCl_3$): δ 154.3, 152.6 (-OC_{Ar}), 137.3 (t, J = 11.4 Hz, Ph_i), 134.1 (Ph), 128.3 (Ph), 126.8 (Ph); 121.8 (*C*≡ or C_{Ar}); 117.2, 115.2 (HC_{Ar}); 114.7, 106.5, 104.9, 93.2 (*C*≡ or C_{Ar}); 68.9 (-O*C*H$_2$), 68.7 (-O*C*H$_2$), 31.74 (P-*C*H$_2$) overlapping with *C*H$_2$, 31.69, 29.6, 27.5, 25.9, 25.8, 22.7, 22.6 (*C*H$_2$), 18.8 (H$_3C_{SiPr3}$), 14.1 (*C*H$_3$), 14.0 (*C*H$_3$), 11.5 (HC_{SiPr3}) ppm. IR (CH_2Cl_2): ν(C≡CSiPr^i_3) 2138 (m); ν(RuC≡C) 2050 (s) cm^{-1}. MS$^+$ (MALDI-TOF; *m/z*): 898.1 [Ru(dppe)$_2$]$^+$; 1861.9 [M + H]$^+$. HR-ESI$^+$-MS: *m/z* calcd for $C_{114}H_{146}O_4P_4{}^{96}RuSi_2$ 1856.8895; found 1856.8856.

***Trans*-Ru(C≡C-(1,4-OC_6H_{13}-C_6H_4)-C≡C-H)$_2$(dppe)$_2$; 29**

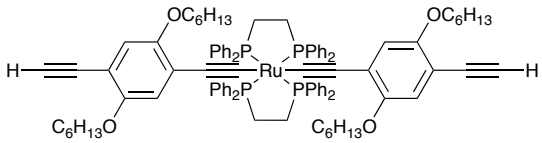

TBAF (1.0 M in THF) (0.24 mL, 0.24 mmol) was added to a solution of **28** (180 mg, 0.1 mmol) in THF (15 mL). The solution was stirred overnight at room temperature. The resulting mixture was dried and purified on a neutral alumina column eluted with CH_2Cl_2:hexane:NEt_3 (50:45:5) to give a yellow solid (100 mg, 60%). Crystals suitable for X-ray diffraction were grown by slow diffusion of MeOH into a CH_2Cl_2 solution of **29** containing 5% NEt_3. ^{1}H NMR (400 MHz, $CDCl_3$): δ 7.45 - 7.43 (m, 16H, Ph_o), 7.09 - 7.05 (m, 8H, Ph_p), 6.89 (s, 2H, Ar), 6.87 - 6.83 (m, 16H, Ph_m), 5.83 (s, 2H, Ar), 3.86 (t, J = 7.0 Hz, 4H, O-C*H*$_2$), 3.67 (t, J = 7.0 Hz, 4H, O-C*H*$_2$), 3.31 (s, 2H, C≡C-*H*), 2.93 - 2.89 (m, 8H, PC*H*$_2$C*H*$_2$P), 1.75 - 1.64 (m, 8H, C*H*$_2$), 1.43 - 1.41 (m, 4H, C*H*$_2$), 1.36 - 1.30 (m, 12H, C*H*$_2$), 1.23 - 1.20 (m, 8H, C*H*$_2$), 0.92 (t, J = 7.0 Hz, 6H, CH_2C*H*$_3$), 0.82 (t, J = 7.0 Hz, 6H, CH_2C*H*$_3$) ppm. ^{31}P NMR {^{1}H} NMR (162 MHz, $CDCl_3$): δ 51.85 (s) ppm. ^{13}C {^{1}H} NMR (101 MHz, $CDCl_3$): δ 154.0, 152.6 (-O*C*$_{Ar}$), 137.2 (t, J = 15.5 Hz, Ph_i), 134.1 (Ph), 128.4 (Ph), 126.9 (Ph), 122.3 (*C*≡ or *C*$_{Ar}$), 117.7, 115.3 (H*C*$_{Ar}$), 114.5, 104.9 (*C*≡ or *C*$_{Ar}$), 81.7 (H-*C*≡), 80.0 (*C*≡), 69.0 (-O*C*H$_2$), 68.9 (-O*C*H$_2$), 31.6 (P-*C*H$_2$), 31.5, 30.1, 29.5, 29.3, 25.8, 25.6, 22.64, 22.58 (*C*H$_2$), 14.05 (*C*H$_3$), 14.02 (*C*H$_3$) ppm, one quaternary ^{13}C≡ was not detected. MS$^+$ (MALDI-TOF; m/z): 898.1 [Ru(dppe)$_2$]$^+$, 1548.4 [M]$^+$. IR (CH_2Cl_2): ν(≡CH) 3301 (m); ν(RuC≡C) 2049 (s) cm^{-1}. HR-ESI$^+$-MS: *m/z* calcd for $C_{96}H_{106}O_4P_4Ru$ 1548.6113; found 1548.6082. Crystal data for **29**: $C_{96}H_{106}O_4P_4Ru.2CHCl_3$, M = 1787.49, triclinic, space group P-1, *a* = 12.35270(3) Å, *b* = 13.0518(3) Å, *c* = 15.0197(3) Å, *β* = 73.804(2) °, *U* = 2220.86(7) Å^3, F(000) = 934, Z = 1, D_C = 1.337 mg/mm^3, μ = 0.481 mm^{-1}; 36070 reflections were collected, yielding 12943 unique data (R_{merg} = 0.0398). Final $wR_2(F^2)$ = 0.1118 for all data (521 refined parameters), conventional R_1 (F) = 0.0457 with I ≥ 2σ, GOF = 1.034.

CHAPTER 4

Trans-Ru(C≡C-(1,4-OC_6H_{13}-C_6H_4)-C≡C-$C_6H_4N)_2(dppe)_2$; 30

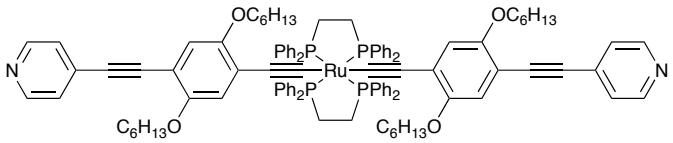

Compound **29** (120 mg, 0.077 mmol), 4-iodopyridine (39 mg, 0.19 mmol), $Pd(PPh_3)_4$ (4.6 mg, 0.004 mmol) and CuI (0.8 mg, 0.004 mmol) were added to a degassed solution of HN^iPr_2 (10 mL). The yellow solution was heated at 80 °C for 20 h, during which time the solution turned orange in colour. The precipitate which developed was removed by filtration and the solid was washed with methanol to remove ammonium salts, to give **30** as a yellow powder. Yield: 85 mg, 64%. Crystals suitable for X-ray diffraction were grown by slow diffusion of MeOH into a CH_2Cl_2 solution of **29** containing 5% NEt_3. ^{1}H NMR (400 MHz, CD_2Cl_2): δ 8.57 (d, J = 5.2 Hz, 4H, C_5H_4N), 7.52 - 7.40 (m, 16H, Ph_o), 7.37 (d, J = 5.2 Hz, 4H, C_5H_4N), 7.13 - 7.11 (m, 8H, Ph_p), 6.95 (s, 2H, Ar), 6.90 - 6.87 (m, 16H, Ph_m), 5.84 (s, 2H, Ar), 3.93 (t, J = 6.5 Hz, 4H, -OCH_2), 3.68 (t, J = 7.2 Hz, 4H, O-CH_2), 2.96 - 2.93 (m, 8H, PCH_2CH_2P), 1.79 - 1.74 (m, 8H, CH_2), 1.52 - 1.50 (m, 4H, CH_2), 1.38 - 1.36 (m, 12H, CH_2), 1.26 - 1.23 (m, 8H, CH_2), 0.94 - 0.92 (pseudo-t, 6H, CH_2CH_3), 0.84 - 0.82 (pseudo-t, 6H, CH_2CH_3) ppm. ^{31}P{^{1}H} NMR (162 MHz, CD_2Cl_2): δ 51.7 (s) ppm. ^{13}C{^{1}H} NMR (101 MHz, CD_2Cl_2): δ 154.3, 153.3 (-OC_{Ar}); 150.1 (HC_{C5H4N}), 137.7 (t, J = 10.9 Hz, Ph_i), 134.5 (Ph), 132.6 (C_{C5H4N}), 128.9 (Ph), 127.3 (Ph), 125.4 (HC_{C5H4N}), 123.3 (C≡ or C_{Ar}), 117.9, 114.9 (HC_{Ar}), 105.3 (C≡ or C_{Ar}), 93.2, 90.7 (C≡), 69.4, 69.3 (O-CH_2), 32.1 (P-CH_2), 32.0, 29.5, 29.4, 25.8, 22.7, 22.6 (CH_2), 13.9 (CH_3), 13.8 (CH_3) the other quaternary ^{13}C≡ were not detected. IR (CH_2Cl_2): ν(C≡CC_5H_4N) 2208 (m); ν(RuC≡C) 2044 (s) cm^{-1}. MS^+ (MALDI-TOF; *m/z*): 898.0, $[Ru(dppe)_2]^+$; 1702.6, $[M]^+$. HR-ESI^+-MS: *m/z* calcd for $C_{106}H_{112}N_2O_4P_4{}^{96}Ru$ 1697.6682; found 1697.6688. Anal. Calcd for $C_{106}H_{112}N_2O_4P_4Ru$: C, 74.76; H, 6.63; N, 1.64. Found: C, 74.66; H, 6.72; N, 1.70. Crystal data for **30**: $C_{106}H_{112}N_2O_4P_4Ru$, M = 1702.93, triclinic, space group P-1, *a* = 12.3676(7) Å, *b* = 12.9676(7) Å, *c* = 13.9333(8) Å, *β* = 83.489(2) °, *U* = 2181.4(2) $Å^3$, F(000) = 898, Z = 1, D_C = 1.296 mg/mm^3, μ = 0.309 mm^{-1}; 47816 reflections were collected, yielding 12134 unique data (R_{merg} = 0.0244). Final $wR_2(F^2)$ = 0.0952 for all data (531 refined parameters), conventional R_1 (F) = 0.0356 with I ≥ 2σ, GOF = 1.065.

***Trans*-Pt(C≡C-(1,4-OC_6H_{13}-C_6H_4)-C≡C-$SiPr^i_3$)$_2$(PPh_3)$_2$; 31**

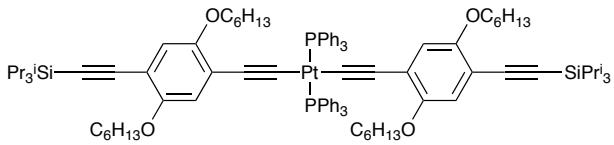

A mixture of **I** (250 mg, 0.52 mmol) and CuI (4 mg) was added to a solution of *cis*-$PtCl_2(PPh_3)_2$ (200 mg, 0.26 mmol) in dry and degassed $HNEt_2$ (20 mL). The orange reaction mixture was heated to 100 °C for 2 h. The solvent was removed and the remaining residue was purified on a silica column eluted by CH_2Cl_2. The resulting product was obtained as an amorphous orange solid. Yield: 320 mg, 73%. ^{1}H NMR (400 MHz, $CDCl_3$): δ 7.82 - 7.77 (m, 12H, Ph), 7.31 - 7.24 (m, 18H, Ph), 6.63 (s, 2H, Ar), 5.71 (s, 2H, Ar), 3.60 (t, J = 6.5 Hz, 4H, O-CH_2), 3.49 (t, J = 6.8 Hz, 4H, O-CH_2), 1.71 - 1.63 (m, 4H, CH_2), 1.46 - 1.39 (m, 4H, CH_2), 1.32 - 1.27 (m, 24H, CH_2), 1.10 (s, 42H, SiPr^i_3), 0.91 (t, J = 7.0 Hz, 6H, CH_2CH_3), 0.86 (t, J = 7.0 Hz, 6H, CH_2CH_3) ppm. ^{31}P{^{1}H} NMR (162 MHz, $CDCl_3$) : δ 17.43 (s, $J_{P\text{-}Pt}$ = 2654.12 Hz) ppm. ^{13}C{^{1}H} NMR (101 MHz, $CDCl_3$): δ 154.1, 152.2 (-OC_{Ar}), 135.3 (t, J = 6.0 Hz, Ph_o), 131.3 (t, J = 29.3 Hz, Ph_i), 130.1 (Ph_p), 127.6 (t, J = 5.4 Hz, Ph_m), 120.9 (*C*≡ or C_{Ar}), 118.9, 116.6 (HC_{Ar}), 109.1, 104.0, 93.8 (*C*≡ or C_{Ar}), 70.0, 68.9 (O-*C*H_2), 31.7, 31.6, 29.5, 29.2, 25.9, 25.5, 22.7, 22.6 (*C*H_2), 18.7 (H_3C_{SiPr3}), 14.1 (*C*H_3) (one visible), 11.4 (HC_{SiPr3}) ppm, the other quaternary ^{13}C≡ were not detected. IR (CH_2Cl_2): ν(C≡C$SiPr^i_3$) 2145 (m); ν(PtC≡C) 2103 (m) cm^{-1}. MS^+ (MALDI-TOF; *m/z*): 1682.5 $[M]^+$. HR-ESI^+-MS: *m/z* calcd for $C_{98}H_{128}O_4P_2{}^{194}PtSi_2$ 1682.8558; found 1682.8484.

***Trans*-Pt(C≡C-(1,4-OC_6H_{13}-C_6H_4)-C≡C-H)$_2$(PPh_3)$_2$; 32**

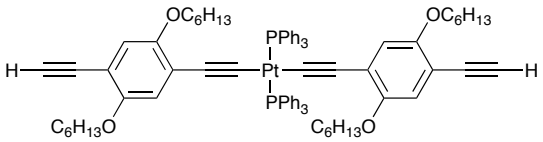

A solution of TBAF (1.0 M in THF) (0.38 mL, 0.38 mmol) was added to a solution of **31** (150 mg, 0.096 mmol) in THF (25 mL). The reaction mixture was stirred for 24 h at room temperature. The solvent was removed and the residue re-dissolved in CH_2Cl_2 and washed

sequentially with water, ammonium chloride (NH_4Cl) (aq.) and brine. The organic phase was dried ($MgSO_4$) and the solvent removed to give an amorphous yellow solid. The solid was purified on a short silica pad, eluting with 5% NEt_3 in CH_2Cl_2; compound **32** was obtained by precipitation in CH_2Cl_2/MeOH. Yield: 130 mg, 93%. ^{1}H NMR (400 MHz, $CDCl_3$): δ 7.83 - 7.78 (m, 12H, Ph), 7.32 - 7.25 (m, 18H, Ph); 6.65 (s, 2H, Ar), 5.74 (s, 2H, Ar), 3.64 (t, J = 7.0 Hz, 4H, O-C*H*$_2$), 3.48 (t, J = 7.0 Hz, 4H, O-C*H*$_2$), 3.19 (s, 2H, C≡CH), 1.73 - 1.66 (m, 4H, C*H*$_2$), 1.44 - 1.40 (m, 4H, C*H*$_2$), 1.34 - 1.13 (m, 24H, C*H*$_2$), 0.91 (t, J = 6.3 Hz, 6H, CH_2C*H*$_3$), 0.86 (t, J = 6.3 Hz, 6H, CH_2C*H*$_3$). ^{31}P{^{1}H} NMR (162 MHz, $CDCl_3$): δ 17.61 (s, $J_{P\text{-}Pt}$ = 2648.49 Hz) ppm. ^{13}C{^{1}H} NMR (101 MHz, $CDCl_3$): δ 153.9, 152.3 (-O*C*$_{Ar}$), 135.2 (t, J = 6.2 Hz, Ph$_o$), 131.2 (t, J = 29.3 Hz, Ph$_i$), 130.1 (Ph$_p$), 127.6 (t, J = 5.4 Hz, Ph$_m$), 121.3 (*C*$_{Ar}$ or *C*≡), 119.4 (t, J = 15.1 Hz, *C*$_\alpha$), 118.7, 116.9 (H*C*$_{Ar}$), 110.2, 107.6 (*C*$_{Ar}$ or *C*≡), 80.9 (H-*C*≡), 80.4 (*C*≡), 69.9, 69.2 (O-C*H*$_2$), 31.6, 29.2, 29.1, 25.6, 25.4, 22.61, 22.56 (*C*H$_2$), 14.1, 14.0 (*C*H$_3$) ppm. IR (CH_2Cl_2): ν(≡C-H) 3300 (w); ν(PtC≡C) 2098 (m) cm^{-1}. MS$^+$ (MALDI-TOF; *m/z*): 719.4 [Pt(PPh$_3$)$_2$]$^+$, 1371.1 [M + H]$^+$. HR-ESI$^+$-MS: *m/z* calcd for $C_{80}H_{88}O_4P_2{}^{194}Pt$ 1369.5863; found 1369.5836.

***Trans*-Pt(C≡C-(1,4-OC$_6$H$_{13}$-C$_6$H$_4$)-C≡C-C$_6$H$_4$N)$_2$(PPh$_3$)$_2$; 33**

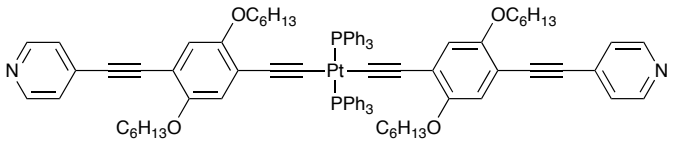

Compound **32** (90 mg, 0.064 mmol), 4-iodopyridine (30 mg, 0.15 mmol), Pd(PPh$_3$)$_4$ (4 mg, 0.003 mmol) and CuI (0.8 mg, 0.004 mmol) were added to a Schlenk flask charged with degassed NEt_3 (10 mL), and the reaction mixture was heated for 2 h at 100 °C. The solvent was removed from the yellow solution and the residue purified by column chromatography on silica eluting with CH_2Cl_2:hexane:NEt_3 (8.5:1.5:0.5) to give a yellow solid. The solid was dissolved in the minimum amount of CH_2Cl_2 and MeOH (5 mL) was added. Concentration of the solution caused **33** to precipitate. Yield : 30 mg, 30%. Crystals suitable for X-ray diffraction were grown by slow diffusion of MeOH into a CH_2Cl_2 solution of **33** containing 5% NEt_3. ^{1}H NMR (400 MHz, $CDCl_3$): δ 8.54 (pseudo-d, 4H, C_5H_4N), 7.83 - 7.81 (m, 12H, Ph), 7.33 - 7.26 (m, 22H, (18H, Ph + 4H, C_5H_4N), 6.69 (s,

2H, Ar), 5.78 (s, 2H, Ar), 3.68 (pseudo-t, 4H, O-CH_2), 3.53 (pseudo-t, 4H, O-CH_2), 1.76 - 1.72 (m, 4H, CH_2), 1.50 - 1.47 (m, 4H, CH_2), 1.38 - 1.16 (m, 24H, CH_2), 0.92 - 0.85 (m, 12H, CH_2CH_3) ppm. $^{31}P\{^1H\}$ NMR (162 MHz, $CDCl_3$): δ 17.67 (s, $J_{P\text{-}Pt}$ = 2643.5 Hz) ppm. $^{13}C\{^1H\}$ NMR (101 MHz, $CDCl_3$): δ 153.8, 152.5 (-OC_{Ar}); 149.5 (HC_{C5H4N}), 135.2 (t, J = 6.2 Hz, Ph_o), 131.2 (t, J = 29.1 Hz, Ph_i), 130.1 (Ph_p), 127.6 (t, J = 5.4 Hz, Ph_m), 125.3 (HC_{C5H4N}), 117.9, 116.9 (HC_{Ar}), 107.6 (*C*≡ or C_{Ar}), 92.0, 90.5, 69.9, 69.2 (*C*≡) 31.60, 31.57, 29.3, 29.1, 25.7, 25.4, 22.65, 22.56 (*C*H_2), 14.1, 14.0 (*C*H_3) ppm, other quaternary ^{13}C≡ were not seen,. IR (CH_2Cl_2): 2112 (m) ν(C≡CC_5H_4N); 2102 (s) ν(PtC≡C) cm^{-1}. MS^+ (MALDI-TOF; *m/z*): 1524.5 $[M]^+$. HR-ESI+-MS: *m/z* calcd for $C_{90}H_{95}N_2O_4P_2{}^{194}Pt$ 1523.6394; found 1523.6362. Anal. Calcd for $C_{90}H_{94}N_2O_4P_2Pt$: C, 70.89; H, 6.21; N, 1.84. Found: C, 70.72; H, 6.13; N, 1.93. Crystal data for **33**: $C_{90}H_{94}N_2O_4P_2Pt$, M = 1524.70, triclinic, space group P-1, *a* = 9.5706(4) Å, *b* = 13.1673(6) Å, *c* = 16.6608(9) Å, *β* = 86.786(4) °, *U* = 1880.29(16) $Å^3$, F(000) = 788, Z = 1, D_C = 1.347 mg/mm^3, μ = 1.962 mm^{-1}; 17913 reflections were collected, yielding 8632 unique data (R_{merg} = 0.0719). Final *w*$R_2(F^2)$ = 0.1048 for all data (450 refined parameters), conventional R_1 (F) = 0.0535 with I ≥ 2σ, GOF = 1.007.

Trans-Ru[C≡C{1,4-$C_6H_2(OC_6H_{13})_2$}C≡C(4-C_5H_4SMe)]$_2$(dppe)$_2$; 34

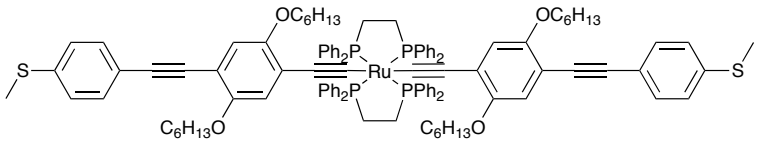

Compound **29** (40 mg, 0.026 mmol), 4-iodothioanisole (13 mg, 0.052 mmol), $Pd(PPh_3)_4$ (1.5 mg, 0.001 mmol) and CuI (0.2 mg, 0.001 mmol) were added to a degassed solution of NH^iPr_2 (5 mL). The yellow solution was heated at 80 °C for 24 h and the precipitate was removed by filtration. The crude solid was purified on a neutral alumina column eluted by CH_2Cl_2/5% NEt_3 to give a yellow powder after removing the solvent. Yield: 15 mg, 34%. ^1H NMR (700 MHz, CD_2Cl_2): δ 7.45 - 7.43 (m, 20H, Ph_o (16H) + C_6H_4SMe (4H)), 7.23 (d, J = 7.8 Hz, 4H, C_6H_4SMe), 7.10 (t, J = 7.4 Hz, 8H, Ph_p), 6.92 (s, 2H, Ar), 6.88 (t, J = 7.6 Hz, 16H, Ph_m), 5.85 (s, 2H, Ar), 3.92 (t, J = 6.9 Hz, 4H, OCH_2), 3.68 (t, J = 6.4 Hz, 4H, OCH_2), 2.93 (s, 6H, C_6H_4S*Me*), 1.78 - 1.69 (m, 8H, CH_2), 1.38 – 1.35 (m, 12H, CH_2), 1.26 - 1.20 (m, 12H, CH_2), 0.96 - 0.89 (t, J = 6.6 Hz, 6H, CH_2CH_3), 0.82 (t, J = 6.9 Hz, 6H, CH_3). ^{31}P NMR $\{^1H\}$ NMR (162 MHz, $CDCl_3$): δ 51.8 (s) ppm. ^{13}C $\{^1H\}$ NMR (700

MHz, $CDCl_3$): δ 153.9, 153.3 (O-C_{Ar}), 139.1, 137.8 (S-C_{Ar}), 134.5 (Ph), 131.8 (H$C_{C6H4SMe}$), 128.9 (Ph), 127.3, 126.3 (Ph), 122.2, 120.9 (C_{Ar}), 118.1, 114.8 (HC_{Ar}), 106.7, 92.8, 88.2 (C≡), 69.41, 69.36 (OCH_2), 32.09, 32.07, 30.0, 29.9, 26.2, 23.1, 23.0 (CH_2), 15.7 (SCH_3), 14.3, 14.2 (CH_3). MS^+ (MALDI-TOF; m/z): 898.1 $[Ru(dppe)_2]^+$, 1793.3 $[M + H]^+$. IR (CH_2Cl_2): 2055s ν(Ru-C≡) cm^{-1}. HR-ESI^+-MS: calcd for $C_{110}H_{118}O_4P_4RuS_2$ 1792.6495; found 1792.6510.

***Trans*-Pt[C≡C{1,4-$C_6H_2(OC_6H_{13})_2$}C≡C(4-C_5H_4SMe)]$_2$(PPh_3)$_2$; 35**

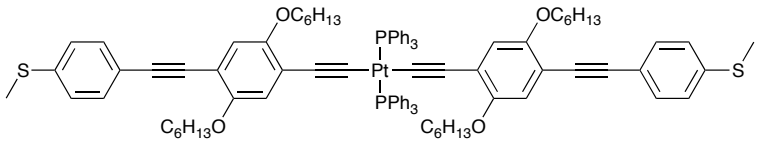

32 (90 mg, 0.064 mmol), 4-iodothioanisole (37.5 mg, 0.15 mmol), $Pd(PPh_3)_4$ (4 mg, 0.003 mmol) and CuI (1 mg) were added to a Schlenk flask charged with degassed HN^iPr_2 (8 mL), and the reaction mixture was heated for 2 h at 100 °C. The yellow solution was evaporated to dryness and the residue was purified on a silica column eluted by CH_2Cl_2:hexane (1 : 1 v/v) followed by pure CH_2Cl_2 to give yellow crystals. Yield: 17 mg, 17%. X-ray quality crystals were grown by slow diffusion in CH_2Cl_2/MeOH/5% NEt_3. ^1H NMR (600 MHz, $CDCl_3$) :δ 7.84 - 7.81 (m, 12H, Ph), 7.38 (d, J = 9.1 Hz, 4H, C_6H_4SMe), 7.33 - 7.27 (m, 18H, Ph), 7.17 (d, J = 9.1 Hz, 4H, C_6H_4SMe), 6.68 (s, 2H, Ar), 5.77 (s, 2H, Ar), 3.78 (t, J = 6.5 Hz, 4H, O-CH_2), 3.54 (t, J = 6.9 Hz, 4H, O-CH_2), 2.48 (s, 6H, SCH_3), 1.76 - 1.71 (m, 4H, CH_2), 1.51 - 1.47 (m, 4H, CH_2), 1.36 - 1.27 (m, 16H, CH_2), 1.21 - 1.14 (m, 8H, CH_2), 0.91 - 0.86 (m, 12H, CH_2CH_3) ppm. ^{31}P NMR {^1H} NMR (162 MHz, $CDCl_3$): δ 17.6 (s, J_{P-Pt} = 2653.1 Hz) ppm. ^{13}C {^1H} NMR (101 MHz, $CDCl_3$): δ 153.3, 152.5 (O-C_{Ar}), 138.4 (S-C_{Ar}), 135.3 (t, J = 6.2 Hz, Ph_o), 131.6 (H$C_{C6H4SMe}$), 131.3 (t, J = 29.2 Hz, Ph_i), 130.1 (Ph_p), 127.6 (t, J = 5.5 Hz, Ph_m), 125.9 (H$C_{C6H4SMe}$), 120.7, 120.5 (C_{Ar}), 117.7 , 117.2 (HC_{Ar}), 109.1, 92.9, 86.9 (C≡), 69.8, 69.2 (OCH_2), 31.64, 31.58, 29.4, 29.1, 25.8, 25.5, 22.7, 22.6 (CH_2), 15.5 (SCH_3), 14.12, 14.08 (CH_3) ppm. MS^+ (MALDI-TOF; m/z): 719.4 $[Pt(PPh_3)_2]^+$, 1614.3 $[M + H]^+$. IR (CH_2Cl_2): ν(Pt-C≡) 2104 (s) cm^{-1}. HR-(ESI^+)-MS: calcd for $C_{94}H_{100}O_4P_2PtS_2Na$ 1637.6107; found 1637.6124. Crystal data for **35**: $C_{94}H_{100}O_4P_2PtS_2$, M = 1614.89, triclinic, space group P2/n, a = 22.659(10) Å, b = 9.469(4) Å, c = 22.765(10) Å, β = 118.005(5) °, U = 4313(3) $Å^3$, F(000) = 1672, Z = 2, D_C = 1.244 mg/mm^3, μ = 1.622 mm^{-1}; 42922

reflections were collected, yielding 8352 unique data (R_{merg} = 0.2997). Final $wR_2(F^2)$ = 0.2517 for all data (371 refined parameters), conventional R_1 (F) = 0.0949 with I ≥ 2σ, GOF = 1.024.

Me_3Si-C≡C-$C_6H_2(OC_6H_{13})_2$-C≡C-$C_6H_2(OC_6H_{13})_2$-C≡C-$SiPr^i_3$[25]

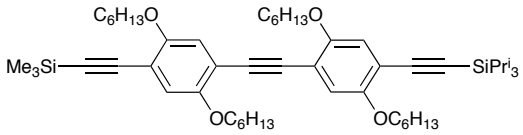

To a solution of 5-trimethylsilylethynyl-1,4-bis(hexyloxy)benzene (260 mg, 0.52 mmol) in dry and degassed NH^iPr_2 (15 mL) was added 5-iodo-1,4-bis(hexyloxy)benzene (250 mg, 0.52 mmol), $Pd(PPh_3)_4$ (58 mg, 0.05 mmol) and CuI (9 mg, 0.05 mmol). The reaction mixture was stirred at room temperature overnight and the solvent removed. The residue was purified on a silica column chromatography eluting with hexane/EtOAc (9.7:0.3 v/v) to give a yellow oil which crystallized on standing. Yield: 300 mg, 67%. ^{1}H NMR (400 MHz, $CDCl_3$): δ 6.95 (s, 1H, Ar), 6.93 (m, 3H, Ar), 4.03 - 3.92 (m, 8H, O-C*H*$_2$), 1.86 - 1.74 (m, 8H, O-C*H*$_2$) C*H*$_2$, 1.46 - 1.53 (m, 8H, C*H*$_2$), 1.36 - 1.30 (m, 16H, C*H*$_2$), 1.14 (m, 21H, Si*Pr$^i_3$*), 0.93 - 0.84 (m, 12H, CH_2CH_3), 0.26 (s, 9H, Si*Me*$_3$). ^{13}C{^{1}H} NMR (101 MHz, $CDCl_3$): δ 154.3, 154.2, 153.3, 153.2 (-OC_{Ar}), 117.9, 117.4, 117.02, 116.6 (HC_{Ar}), 114.6, 114.0, 113.6, 113.02, 101.2, 100.1, 96.5, 91.6, 91.2 (*C*≡ or C_{Ar}), 69.8, 69.6, 69.4, 69.3 (O-*C*H_2), 31.7, 31.62, 31.60, 29.4, 29.33, 29.30, 29.26, 25.9, 25.7, 25.6, 25.64, 22.6 (*C*H_2), 18.7 (H_3C_{SiPr3}), 14.1 (*C*H_3), 14.0 (*C*H_3), 11.4 (HC_{SiPr3}), -0.03 ($SiMe_3$). The NMR data were consistent with the literature.[25]

H-C≡C-$C_6H_2(OC_6H_{13})_2$-C≡C-$C_6H_2(OC_6H_{13})_2$-C≡C-$SiPr^i_3$; J[25]

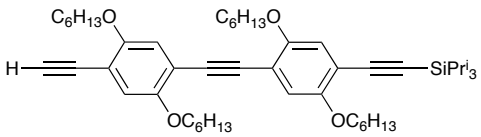

A solution of TMSC≡C{1,4-$C_6H_2(OC_6H_{13})_2$}C≡C{1,4-$C_6H_2(OC_6H_{13})_2$}C≡CTIPS (300 mg, 0.35 mmol) and K_2CO_3 (48 mg, 0.35 mmol) in MeOH/THF (1:1) (20 mL) was stirred at room temperature overnight. The mixture was poured into water, extracted with CH_2Cl_2 and the organic layer dried ($MgSO_4$) and concentrated. The residue was purified on a silica

chromatography column eluting with hexane/EtOAc (7.5:0.5 v/v) to give **J** as a waxy yellow solid. Yield: 229 mg, 83%. ^{1}H NMR (400 MHz, $CDCl_3$): δ 6.98 (s, 1H, Ar), 6.97 (s, 1H, Ar), 6.94 (s, 1H, Ar), 6.93 (s, 1H, Ar), 4.04 - 3.92 (m, 8H, O-C*H*$_2$), 3.34 (s, 1H, *H*-C≡), 1.84 - 1.75 (m, 8H, C*H*$_2$), 1.53 - 1.46 (m, 8H, C*H*$_2$), 1.37 - 1.28 (m, 16H, C*H*$_2$), 1.14 (s, 21H, Si*Pr*$^{i}_{3}$), 0.94 - 0.84 (m, 12H, CH_2CH_3). ^{13}C{^{1}H} NMR (101 MHz, $CDCl_3$): δ 154.3, 154.1, 153.3, 153.3 (-OC_{Ar}), 117.91, 117.89, 116.5, 115.0, 114.2, 114.1, 112.5 (HC_{Ar} or C_{Ar}), 103.0, 96.5, 91.6, 91.0, 82.2, 80.0 (*C*≡), 69.8, 69.7, 69.6, 69.2 (O-*C*H$_2$), 31.7, 31.61, 31.59, 31.53, 29.4, 29.3, 29.2, 29.1, 25.9, 25.64, 25.60, 22.62, 22.58 (*C*H$_2$), 18.7 (H_3C_{SiPr3}), 14.1, 14.0 (*C*H$_3$), 11.4 (HC_{SiPr3}). IR (CH_2Cl_2): ν(≡C-H) 3303 (br); 2959 (s); ν(≡C-Si^{i}Pr$_3$) 2148 (s); 2106 (m). The NMR data were consistent with the literature.[25]

***Trans*-Ru(C≡C-(1,4-OC$_6$H$_{13}$-C$_6$H$_4$)-C≡C-(1,4-OC$_6$H$_{13}$-C$_6$H$_4$)-C≡C-SiPr$^{i}_{3}$)$_2$(dppe)$_2$; 36**

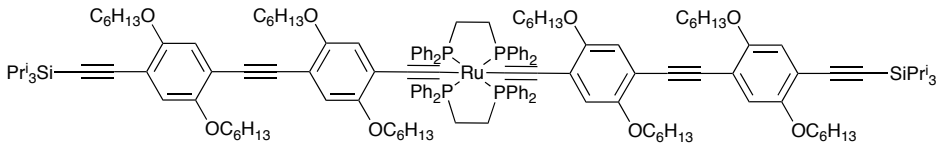

To a Schlenk flask containing [RuCl(dppe)$_2$]OTf (100 mg, 0.09 mmol) in dry and degassed CH_2Cl_2 (4 mL) was added **J** (149 mg, 0.19 mmol) and 4 drops of DBU. The reaction was stirred for 30 min before the addition of $TlBF_4$ (27 mg, 0.09 mmol). The yellow solution was stirred for a further 2 h and the mixture was filtered through a Millex syringe filter (Millipore) to remove the precipitated TlCl. The orange solution was reduced to the minimum volume and acetonitrile (10 mL) added. Further concentration of the solution resulted in formation of a yellow precipitate which was collected by filtration, and dried in air to give a bright yellow solid. Yield : 65 mg, 33%. ^{1}H NMR (400 MHz, CD_2Cl_2): δ 7.45 - 7.44 (m, 16H, Ph$_o$), 7.10 - 7.08 (m, 8H, Ph$_p$), 6.95 - 6.93 (m, 4H, Ar), 6.90 (s, 2H, Ar), 6.87 - 6.85 (m, 16H, Ph$_m$), 5.83 (s, 2H, Ar), 4.03 (t, J = 6.5 Hz, 4H, O-C*H*$_2$), 3.97 (t, J = 6.5 Hz, 4H, O-C*H*$_2$), 3.90 (t, J = 6.5 Hz, 4H, O-C*H*$_2$), 3.67 (t, J = 6.5 Hz, 4H, O-C*H*$_2$), 2.92 (m, 8H, PC*H*$_2$C*H*$_2$P), 1.91 - 1.69 (m, 16H, C*H*$_2$), 1.59 – 1.45 (m, 16H, *CH*$_2$), 1.40 - 1.33 (m, 32H, C*H*$_2$), 1.14 (s, 42H, Si*Pr*$^{i}_{3}$), 0.92 - 0.88 (m, 18H, CH_2CH_3), 0.81 - 0.79 (m, 6H, CH_2CH_3). ^{31}P{^{1}H} NMR (162 MHz, $CDCl_3$): δ 51.6 (s) ppm. ^{13}C{^{1}H} NMR (101 MHz, $CDCl_3$): δ 154.8, 152.8, 153.3 (-OC_{Ar}), 137.8 (m, Ph$_i$), 134.5, 128.9, 127.3, 122.4, 118.1,

116.7, 115.6, 115.5, 115.0, 113.4, 106.9, 103.7, 95.5, 93.8, 89.8, 77.9, 77.7, 77.6, 70.2, 70.2, 69.8, 69.4 (O-CH_2), 32.13, 32.10, 32.09, 32.07, 30.0, 29.9, 29.85, 29.81, 26.3, 26.3, 26.2, 26.1, 23.14, 23.11, 23.09, 23.06, 23.05, 18.92 (CH_2), 18.89 (H_3C_{SiPr3}), 14.30, 14.29, 14.2 (CH_3), 11.8 (HC_{SiPr3}).

***Trans*-Ru(C≡C-(1,4-OC_6H_{13}-C_6H_4)-C≡C-(1,4-OC_6H_{13}-C_6H_4)-C≡C-H)$_2$(dppe)$_2$; 37**

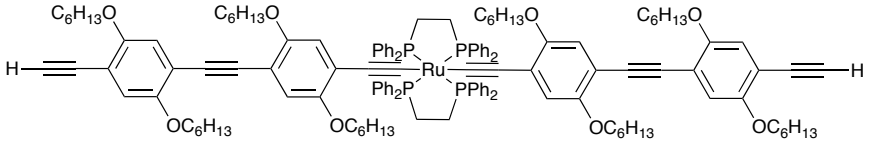

A suspension of **36** (60 mg, 0.025 mmol) and TBAF (1 M in THF) (0.06 mL, 0.062 mmol) in THF (6 mL) was stirred at room temperature overnight after which time the reaction was adjudged complete by TLC (silica using hexane/EtOAc (9.5:0.5 v/v)). The solvent was removed to give an orangy coloured oily solid, presumed to be **37**, which was used without further purification.

***Trans*-Ru(C≡C-(1,4-OC_6H_{13}-C_6H_4)-C≡C-(1,4-OC_6H_{13}-C_6H_4)-C≡C-C_6H_4N)$_2$(dppe)$_2$; 38**

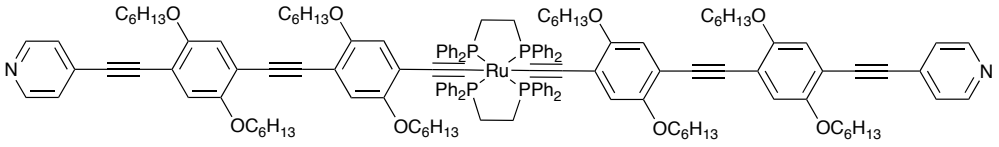

To a degassed and dry solution of THF (3 mL) and HN^iPr_2 (6 mL) was added **37** (60 mg, 0.03 mmol), 4-iodopyridine (13 mg, 0.06 mmol), $Pd(PPh_3)_4$ (5 mg, 0.003 mmol) and CuI (1 mg, 0.003 mmol). The reaction mixture was heated at 100 °C overnight after which time the solution was evaporated to dryness. The residue was re-dissolved in a minimum of CH_2Cl_2 and MeOH (5 mL) was added and the solution concentrated to precipitate the product. The precipitate was collected by filtration as an orange solid **38**. Yield: 30 mg, 43%. Crystals suitable for X-ray diffraction were grown by slow diffusion of Et_2O into a CH_2Cl_2. ^{1}H NMR (400 MHz, CD_2Cl_2): δ 8.40 (brs, 4H, C_5H_4N), 7.47 - 7.46 (m, 16H, Ph_o),

7.40 (brs, 4H, C_5H_4N), 7.12 - 7.10 (m, 8H, Ph_p), 7.06 (s, 2H, Ar), 7.05 (s, 2H, Ar), 6.93 (s, 2H, Ar), 6.90 - 6.88 (m, 16H, Ph_m), 5.85 (s, 2H, Ar), 4.09-4.05 (m, 8H, O-CH_2), 3.93 (t, J = 6.8 Hz, 4H, O-CH_2), 3.69 (t, J = 6.8 Hz, 4H, O-CH_2), 2.94 (brs, 8H, PCH_2CH_2P), 1.91 - 1.86 (m, 8H, CH_2), 1.78 - 1.76 (m, 4H, CH_2), 1.73 - 1.71 (m, 4H, CH_2), 1.58 - 1.56 (m, 4H, CH_2), 1.49-1.47 (m, 4H, CH_2), 1.46 - 1.35 (m, 32H, CH_2), 1.26 - 1.23 (m, 8H, CH_2), 0.94 - 0.90 (m, 18H, CH_2CH_3), 0.84 - 0.81 (m, 6H, CH_2CH_3). $^{31}P\{^1H\}$ NMR (162 MHz, $CDCl_3$): δ 51.6 (s) ppm. $^{13}C\{^1H\}$ NMR (101 MHz, $CDCl_3$): δ 154.6, 153.9, 153.5, 153.3, 150.2, 137.8 (m), 134.5, 128.9, 127.3, 125.6, 118.1, 117.5, 117.1, 116.8, 115.6, 115.0, 112.0, 106.7, 94.5, 89.7, 77.9, 77.7, 77.6, 70.2, 70.0, 69.4, 32.10, 32.09, 32.07, 32.0, 30.0, 29.9, 29.8, 26.3, 26.19, 26.17, 26.1, 23.15, 23.12, 23.09, 23.0, 14.3, 14.2. IR (CH_2Cl_2): ν(C≡CC_5H_4N) 2197 (br); ν(RuC≡C) 2047 (s) cm^{-1}. MS^+ (MALDI-TOF; *m/z*): 2304 $[M + H]^+$. Anal. Calcd for $C_{146}H_{168}N_2O_8P_4Ru$: C, 76.11; H, 7.35; N, 1.22. Found: C, 75.96; H, 7.49; N, 1.27. Crystal data for **38**: $C_{146}H_{168}N_2O_8P_4{}^{96}Ru.2C_4H_{10}O$, M = 2452.01, triclinic, space group P-1, *a* = 12.5576(10) Å, *b* = 17.0560(14) Å, *c* = 18.0172(14) Å, β = 105.504(2) °, *U* = 3458.6(5) $Å^3$, F(000) = 1310, Z = 1, D_C = 1.177 mg/mm^3, μ = 0.218 mm^{-1}; 55843 reflections were collected, yielding 15047 unique data (R_{merg} = 0.0.1518). Final $wR_2(F^2)$ = 0.2414 for all data (678 refined parameters), conventional R_1 (F) = 0.0898 with I ≥ 2σ, GOF = 0.968.

$Pt(PPh_3)_2\{C\equiv C\text{-}(4\text{-}C_6H_4{}^tBu)\}_2$; 39

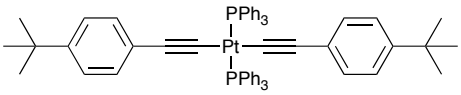

A mixture of *cis*-$Pt(PPh_3)_2Cl_2$ (100 mg, 0.13 mmol), 4-tert-butylphenylacetylene (45 mg, 0.05 mL, 0.28 mmol) and CuI (2 mg, 0.01 mmol) in HN^iPr_2 (10 mL) was stirred at room temperature overnight. The solution was filtered and the precipitate was washed with MeOH and dried to give an off-white solid. Yield: 92 mg, 69%. ^1H NMR ($CDCl_3$): δ 7.82 - 7.80 (m, 12H, Ph), 7.45 - 7.43 (m, 6H, Ph), 7.40 - 7.38 (m, 12H, Ph), 6.92 (d, J = 8.0 Hz, 4H, Ar), 6.19 (d, J = 8.0 Hz, 4H, Ar), 1.17 (s, 18H, CH_3) ppm. $^{31}P\{^1H\}$ NMR (162 MHz, $CDCl_3$): 18.6 (s, $J_{P\text{-}Pt}$ = 2661.6 Hz) ppm. $^{13}C\{^1H\}$ NMR (700 MHz, $CDCl_3$): δ 148.09 (C_{Ar}), 135.4 (t, J = 6.1 Hz, Ph_o), 132.0 (t, J = 28.3 Hz, Ph_i), 130.7 (Ph_p), 130.6 (HC_{Ar}), 128.25 (t, (J = 5.3 Hz), Ph_m), 124.6 (HC_{Ar}), 113.2, 109.7 (*C*≡), 34.6 (C_{tBu}), 31.3 (H_3C_{tBu})

ppm. IR (CH_2Cl_2): ν(PtC≡C) 2108 cm^{-1}. MS^+ (MALDI-TOF; m/z): 719.1 $[Pt(PPh_3)_2]^+$, 1033.3 $[M]^+$. HR-ESI^+-MS: *m/z* calcd for $C_{60}H_{56}P_2{}^{194}PtNa$ 1055.3383; found 1055.3459.

4.11.2. Computational methods

Before computing transport properties, all the molecules in this study were initially geometrically relaxed in isolation to yield the geometries shown in Figure 4-21. The geometrical optimizations were carried out using the DFT code SIESTA, with generalized gradient approximation method (PBE functional), double-zeta polarized basis set, 0.01 eV/A force tolerance and 250 Ry mesh cutoff. To compute the electrical conductance of these molecules, they were each placed between pyramidal gold electrodes and the molecules and first few layers of gold were again allowed to relax, to yield the structures shown in the lower panes of Figure 4-20. For each structure, the transmission coefficient *T(E)* describing the propagation of electrons of energy *E* from the left to the right electrode was calculated by first obtaining the corresponding Hamiltonian and overlap matrices using SIESTA,[51,52] and using the GOLLUM code[53] to compute *T(E)* via the relationship: $T(E) = Trace\{\Gamma_R(E)G^R(E)\Gamma_L(E)G^{R\dagger}(E)\}$ In this expression, $\Gamma_{L,R}(E) = i\left(\sum_{L,R}(E) - \sum_{L,R}{}^{\dagger}(E)\right)$ describes the level broadening due to the coupling between left (L) and right (R) electrodes and the central scattering region; $\sum_{L,R}(E)$ are the retarded self-energies associated with this coupling and $G^R = (ES - H - \sum_L - \sum_R)^{-1}$ is the retarded Green's function, where *H* is the Hamiltonian and *S* is the overlap matrix (both of them obtained from SIESTA). Finally, the room temperature electrical conductance G was computed from the formula $G = G_0 \int_{-\infty}^{\infty} dE\, T(E)(-\frac{df(E)}{dE})$ where $f(\mathrm{E}) = [e^{\beta(E-E_F)} + 1]^{-1}$ is the Fermi function, $\beta = 1/k_BT$, E_F is the Fermi energy and $G_0 = \left(\frac{2e^2}{h}\right)$ is the quantum of conductance. Since the quantity $(-\frac{df(E)}{dE})$ is a probability distribution peaked at $E=E_F$, with a width of order k_BT, the above expression shows that G/G_0 is obtained by averaging *T(E)* over an energy range of order k_BT in the vicinity of $E=E_F$. It is well-known that the Fermi energy E_F^{DFT} predicted by DFT is not usually reliable: therefore the left-hand panes of Figure 4-20 show plots of G/G_0 as a function of $E_F - E_F^{DFT}$. To determine E_F, the predicted values of all molecules were compared with the experimental values and a single common value of E_F was chosen which gave the closest overall agreement. This yielded a value of $E_F - E_F^{DFT} = 0.17$ eV, which is used in all theoretical results described here.

4.12. References

(1) Zhang, J.; Kuznetsov, A. M.; Medvedev, I. G.; Chi, Q.; Albrecht, T.; Jensen, P. S.; Ulstrup, J. *Chem. Rev.* **2008**, *108*, 2737.

(2) Nichols, R. J.; Haiss, W.; Higgins, S. J.; Leary, E.; Martin, S.; Bethell, D. *Phys. Chem. Chem. Phys.* **2010**, *12*, 2801.

(3) Kiguchi, M.; Kaneko, S. *Phys. Chem. Chem. Phys.* **2013**, *15*, 2253.

(4) Low, P. J. *Dalton Trans.* **2005**, *17*, 2821.

(5) Rigaut, S. *Dalton Trans.* **2013**, *42*, 15859.

(6) Park, J.; Pasupathy, A. N.; Goldsmith, J. I.; Chang, C.; Yaish, Y.; Petta, J. R.; Rinkoski, M.; Sethna, J. P.; Abruña, H. D.; McEuen, P. L.; Ralph, D. C. *Nature* **2002**, *417*, 722.

(7) Nesvorný, D.; Bottke, W. F., Jr; Dones, L.; Levison, H. F. *Nature* **2002**, *417*, 720.

(8) Albrecht, T.; Moth-Poulsen, K.; Christensen, J. B.; Guckian, A.; Bjørnholm, T.; Vos, J. G.; Ulstrup, J. *Faraday Discuss.* **2006**, *131*, 265.

(9) Ricci, A. M.; Calvo, E. J.; Martin, S.; Nichols, R. J. *J. Am. Chem. Soc.* **2010**, *132*, 2494.

(10) Ponce, J.; Arroyo, C. R.; Tatay, S.; Frisenda, R.; Gaviña, P.; Aravena, D.; Ruiz, E.; van der Zant, H. S. J.; Coronado, E. *J. Am. Chem. Soc.* **2014**, *136*, 8314.

(11) Li, J.-C.; Wu, J.-Z.; Gong, X. *J. Phys. Chem. Lett.* **2014**, *5*, 1017.

(12) Marqués-González, S.; Yufit, D. S.; Howard, J. A. K.; Martin, S.; Osorio, H. M.; García-Suárez, V. M.; Nichols, R. J.; Higgins, S. J.; Cea, P.; Low, P. J. *Dalton Trans.* **2013**, *42*, 338.

(13) Meng, F.; Hervault, Y.-M.; Shao, Q.; Hu, B.; Norel, L.; Rigaut, S. E. P.; Chen, X. *Nature Communications* **2014**, *5*, 3023.

(14) Luo, L.; Benameur, A.; Brignou, P.; Choi, S. H.; Rigaut, S.; Frisbie, C. D. *J. Phys. Chem. C* **2011**, *115*, 19955.

(15) Kim, B. S.; Beebe, J. M.; Olivier, C.; Rigaut, S.; Touchard, D.; Kushmerick, J. G.; Zhu, X. Y.; Frisbie, C. D. *J. Phys. Chem. C* **2007**, *111*, 7521.

(16) Wen, H.-M.; Yang, Y.; Zhou, X.-S.; Liu, J.-Y.; Zhang, D.-B.; Chen, Z.-B.; Wang, J.-Y.; Chen, Z.-N.; Tian, Z.-Q. *Chem. Sci.* **2013**, *4*, 2471.

(17) Hong, W.; Manrique, D. Z.; Moreno-García, P.; Gulcur, M.; Mishchenko, A.; Lambert, C. J.; Bryce, M. R.; Wandlowski, T. *J. Am. Chem. Soc.* **2012**, *134*, 2292.

(18) Martin, S.; Grace, I.; Bryce, M. R.; Wang, C.; Jitchati, R.; Batsanov, A. S.; Higgins, S. J.; Lambert, C. J.; Nichols, R. J. *J. Am. Chem. Soc.* **2010**, *132*, 9157.

(19) Park, Y. S.; Whalley, A. C.; Kamenetska, M.; Steigerwald, M. L.; Hybertsen, M. S.; Nuckolls, C.; Venkataraman, L. *J. Am. Chem. Soc.* **2007**, *129*, 15768.

(20) Kamenetska, M.; Quek, S. Y.; Whalley, A. C.; Steigerwald, M. L.; Choi, H. J.; Louie, S. G.; Nuckolls, C.; Hybertsen, M. S.; Neaton, J. B.; Venkataraman, L. *J. Am. Chem. Soc.* **2010**, *132*, 6817.

(21) Kim, T.; Vázquez, H.; Hybertsen, M. S.; Venkataraman, L. *Nano Lett.* **2013**, *13*, 3358.

(22) Saitner, M.; Eberle, F.; Baccus, J.; D'Olieslaeger, M.; Wagner, P.; Kolb, D. M.; Boyen, H.-G. *J. Phys. Chem. C* **2012**, *116*, 21810.

(23) Ren, T. *Chem. Rev.* **2008**, *108*, 4185

(24) Sonogashira, K.; Fujikura, Y.; Yatake, T.; Toyoshima, N.; Takahashi, S.; Hagihara, N. *Journal of Organometallic Chemistry* **1978**, *145*, 101.

(25) Wielopolski, M.; Atienza, C.; Clark, T.; Guldi, D. M.; Martín, N. *Chem. Eur. J.* **2008**, *14*, 6379.

(26) Fox, M. A.; Harris, J. E.; Heider, S.; Pérez-Gregorio, V.; Zakrzewska, M. E.;

Farmer, J. D.; Yufit, D. S.; Howard, J. A. K.; Low, P. J. *Journal of Organometallic Chemistry* **2009**, *694*, 2350.

(27) Vacher, A.; Benameur, A.; Ndiaye, C. M.; Touchard, D.; Rigaut, S. *Organometallics* **2009**, *28*, 6096.

(28) Rigaut, S.; Perruchon, J.; Le Pichon, L.; Touchard, D.; Dixneuf, P. H. *Journal of Organometallic Chemistry* **2003**, *670*, 37.

(29) Marqués-González, S.; Parthey, M.; Yufit, D. S.; Howard, J. A. K.; Kaupp, M.; Low, P. J. *Organometallics* **2014**, *33*, 4947.

(30) Sonogashira, K.; Yatake, T.; Tohda, Y.; Takahashi, S.; Hagihara, N. *J. Chem. Soc., Chem. Commun.* **1977**, *9*, 291.

(31) Sadowy, A. L.; Ferguson, M. J.; McDonald, R.; Tykwinski, R. R. *Organometallics* **2008**, *27*, 6321.

(32) Zhao, X.; Huang, C.; Gulcur, M.; Batsanov, A. S.; Baghernejad, M.; Hong, W.; Bryce, M. R.; Wandlowski, T. *Chem. Mater.* **2013**, *25*, 4340.

(33) Mayor, M.; Hanisch, von, C.; Weber, H.; Reichert, J.; Beckmann, D. *Angew. Chem. Int. Ed.* **2002**, *41*, 1183.

(34) Liu, K.; Wang, X.; Wang, F. *ACS Nano* **2008**, *2*, 2315.

(35) Khairul, W. M.; Fox, M. A.; Schauer, P. A.; Albesa-Jové, D.; Yufit, D. S.; Howard, J. A. K.; Low, P. J. *Inorganica Chimica Acta* **2011**, *374*, 461.

(36) Wuttke, E.; Pevny, F.; Hervault, Y.-M.; Norel, L.; Drescher, M.; Winter, R. F.; Rigaut, S. *Inorg. Chem.* **2012**, *51*, 1902.

(37) Vives, G.; Carella, A.; Sistach, S. P.; Launay, J.-P.; Rapenne, G. N. L. *New J. Chem.* **2006**, *30*, 1429.

(38) Vacher, A.; Barrière, F.; Camerel, F.; Bergamini, J.-F.; Roisnel, T.; Lorcy, D. *Dalton Trans.* **2013**, *42*, 383.

(39) Flatt, A. K.; Yao, Y.; Maya, F.; Tour, J. M. *J. Org. Chem.* **2004**, *69*, 1752.

(40) Wang, C.; Batsanov, A. S.; Bryce, M. R.; Martin, S.; Nichols, R. J.; Higgins, S. J.; García-Suárez, V. M.; Lambert, C. J. *J. Am. Chem. Soc.* **2009**, *131*, 15647.

(41) Moreno-García, P.; Gulcur, M.; Manrique, D. Z.; Pope, T.; Hong, W.; Kaliginedi, V.; Huang, C.; Batsanov, A. S.; Bryce, M. R.; Lambert, C.; Wandlowski, T. *J. Am. Chem. Soc.* **2013**, *135*, 12228.

(42) Haiss, W.; Van Zalinge, H.; Higgins, S. J.; Bethell, D.; Höbenreich, H.; Schiffrin, D. J.; Nichols, R. J. *J. Am. Chem. Soc.* **2003**, *125*, 15294.

(43) Peters, T. B.; Zheng, Q.; Stahl, J.; Bohling, J. C.; Arif, A. M.; Hampel, F.; Gladysz J. A. *Journal of Organometallic Chemistry* **2002**, *641*, 53.

(44) Huber, R.; González, M. T.; Wu, S.; Langer, M.; Grunder, S.; Horhoiu, V.; Mayor, M.; Bryce, M. R.; Wang, C.; Jitchati, R.; Schönenberger, C.; Calame, M. *J. Am. Chem. Soc.* **2008**, *130*, 1080.

(45) Mahapatro, A. K.; Ying, J.; Ren, T.; Janes, D. B. *Nano Lett.* **2008**, *8*, 2131.

(46) Bailar, J. C.; Itatani, H. *Inorg. Chem.* **1965**, 1618.

(47) Goeb, S.; Ziessel, R. Org. Lett, **2007**, *9*, 737.

(48) Zhou, C.-Z.; Liu, T.; Xu, J.-M.; Chen, Z.-K. *Macromolecules* **2003**, *36*, 1457.

(49) Ziessel, R; Suffert, J.; Youinou; M. T. *Journal of Organometallic Chemistry* **1996**, *61*, 6535.

(50) Li, X.; Zhao, X.; Zhang, J.; Zhao, Y. *Chem. Commun.* **2013**, *49*, 10004.

(51) Artacho, E.; Anglada, E.; Diéguez, O.; Gale, J. D.; García, A.; Junquera, J.; Martin, R. M.; Ordejón, P.; Pruneda, J. M.; Sánchez-Portal, D.; Soler, J. M. *J. Phys.: Condens. Matter* **2008**, *20*, 064208.

(52) Soler, J. M.; Artacho, E.; Gale, J. D.; García, A.; Junquera, J.; Ordejón, P.; Sánchez-Portal, D. *Journal of Physics: Condensed Matter* **2002**, *14*, 2745.

(53) Ferrer, J.; Lambert, C. J.; García-Suárez, V. M.; Manrique, D. Z.; Visontai, D.; Oroszlany, L.; Rodríguez-Ferradás, R.; Grace, I.; Bailey, S. W. D.; Gillemot, K.; Sadeghi, H.; Algharagholy, L. A. *New Journal of Physics* **2014**, *16*, 930029.

CHAPTER 5. CARBON RICH BIS-TERPYRIDINE MOLECULES

5.1. Abstract

When compared with metal bis(alkynyl) complexes, metallo-bis(terpyridine) complexes $[M(tpy)_2]^{n+}$ represent an alternative motif for use in single molecule electronics. Metal bis(alkynyl) complexes feature the metal centre directly conjugated within the extended –C≡C-M-C≡C– chain, whereas $[M(tpy)_2]^{n+}$ integrate the multi-functional properties of the metal coordination sphere within a direct metal-nitrogen bond. $[M(tpy)_2]^{n+}$ complexes offer a rich chemistry associated with both metal oxidation and ligand reduction processes; photophysical activity arises from the combination of MLCT transitions and associated photo- and thermal deactivation pathways; and magnetic properties arise from the well-defined, approximately octahedral metal coordination geometry. A series of ethynyl-functionalised 2,2′:6′,2″-terpyridine (tpy) ligands and cationic homoleptic $[M(tpy)_2]^{n+}$ complexes were designed and prepared from the perspective of single molecule measurements. The 4,4'-positions of the tpy ligand core were chosen for attachment of a conjugated alkyne or phenyleneethynylene 'linker' to incorporate trimethylsilylethynyl (TMSE) and pyridyl anchor groups. The metal complexes were realised by the addition of group 8 metals such as Ru(II) and Fe(II), which favour octahedral geometry, to solutions of the functionalised tpy ligands. Not so surprisingly, results from single molecule measurements on the metal complexes with 4'-phenyl-2,2':6',2"-terpyridine (phtpy) based cores showed lower conductance than those analogues in which the anchor group is more directly connected to the terpyridine through the cylindrically symmetrical alkynyl moiety. Indeed, the conductance value of [Ru(4′-[4-(trimethylsilylethynyl)phenyl]-2,2′:6′,2″-terpyridine)$_2$]$(PF_6)_2$ **M** was slightly lower compared to the value of [Ru(4′-(trimethylsilylethynyl)-2,2′:6′,2″-terpyridine)$_2$]$(PF_6)_2$ **N**. This result was attributed to the combination of the greater molecular length of **M** and also from the twist angle that exists between the phenyl and the tpy in **M** which led to reduced conjugation. Moreover, the different conformations available due to the existing twist angle are the origin of the broad histogram found for the molecule **M.** For this reason, the attention was subsequently turned to the preparation of tpy derivatives substituted at the 4-positions by π-conjugated oligoynes of increasing length.

5.2. Introduction

Some 80 years ago, Morgan and Burstall isolated what may be the first tpy complex after heating pyridine and iron trichloride at 340 °C in an autoclave for 36 h.[1] Tpy is an interesting oligopyridine tridentate building block in coordination chemistry due to its stability gained by the σ-donor/π-acceptor character of the dative metal-nitrogen bond. The strength of the $[M(tpy)_2]^{n+}$ system is due to the back donation ($d\rightarrow\pi^*$) of the metal-ligand bond and the strong chelate effect of the ligand. 4'-substituted tpy (X-tpy) reacts with M^{n+} octahedral metals to give $[M(X\text{-}tpy)_2]^{n+}$ which gives a rigid linear molecule (Chart 5-1).[2-4] Since the tpy discovery, the synthesis of the tpy ligands from Kröhnke synthesis,[5] from tpyCl, tpyOH[6], Ziessel's ethynyl-based systems[7] and derived complexes have advanced dramatically. Now, there are countless examples of tpy based ligands and complexes for most of the transition metals.[8-10] Varying the metal ions along with the electronic influence of the substituents in $[M(X\text{-}tpy)_2]^{n+}$ systems leads to different redox and photophysical properties with multiple potential applications.

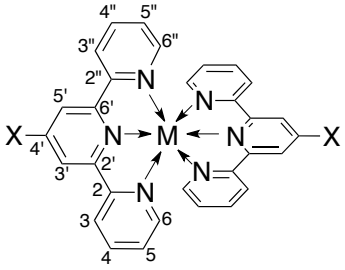

Chart 5-1. *(Distorted) octahedral complex of the 4'-X substituted 2,2':6',2"-terpyridine with the atom numbering scheme.*

More particularly, while the absorption spectra of $[M(X\text{-}tpy)_2]^{n+}$ species always display a LC band, the $[Fe(tpy)_2]^{2+}$ and $[Ru(tpy)_2]^{2+}$ analogues display a MLCT band at 450 nm and 550 nm, respectively, hence the interest in using these systems for photovoltaic devices,[11,12] dyes,[13] molecular probes and photochromic switches.[14] Moreover, these photophysical properties can be tuned by the introduction in the 4'-position of donor and acceptor properties. Examples of donor-tpy-acceptor include OPV-terpyridine-C_{60}[15] and ferrocene-terpyridine-methylviologen.[16] The substituents on the 4'-tpy position include groups that are suitable for anchoring to a metal surface, such as carboxylic acid to bind TiO_2 in solar cell applications[17] or 2,2'-bithiophene used for wiring purposes[18].

The charge transfer between two or three $[M(X\text{-}tpy)_2]^{n+}$ can be studied in so-called dyad or triad systems. For this reason, a heterobimetallic dyad $[Ru(tpy)_2]^{2+}$-bridge-$[Co(tpy)_2]^{2+}$ has been synthesized (Chart 5-2). Various bridges joining the two metal complexes can also be used to tune their photophysical properties,[16,19] and also appropriate substitution at the 4'-position can enhance the electronic communication.[20-22]

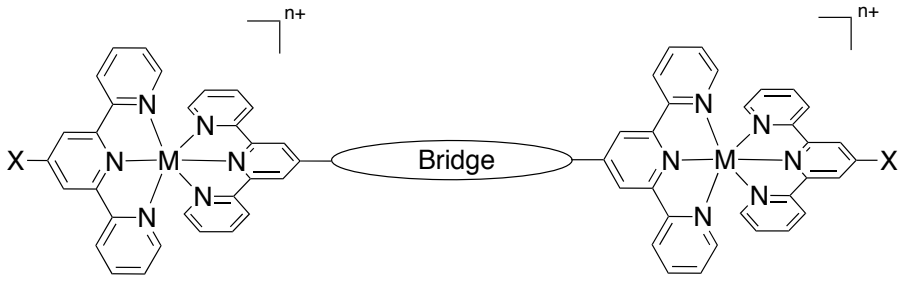

Chart 5-2. *Representation of a M[(X-tpy)$_2$]$^{n+}$ dyad separated by a conjugated bridge.*[19]

4'-phenyl-2,2':6',2"-terpyridine (phtpy) gives metal complexes $[M(phtpy)_2]^{n+}$ with better stability than tpy analogues.[23,24] Recently, the electron transfer in metalloterpyridines was explored in a donor-bridge-acceptor (D-B-A) fashion by using Au/mica surface and ferrocene as a donor. In this example, tpy/phtpy units were assembled step-wise with the anchoring unit (Figure 5-1, a) already attached to the electrode, bridging ligand (Figure 5-1, l) and terminal ligand (Figure 5-1, t).[25] The evaluation of the electron transfer in metalloterpyridines via thermodynamic analysis and electrochemistry indicates a favoured hopping mechanism (Figure 5-1, bottom) leading to long range electron transport. This example illustrates the ability of tpy/phtpy in the presence of a suitable metal to generate supramolecular architectures due to their well-defined geometries.[26-29]

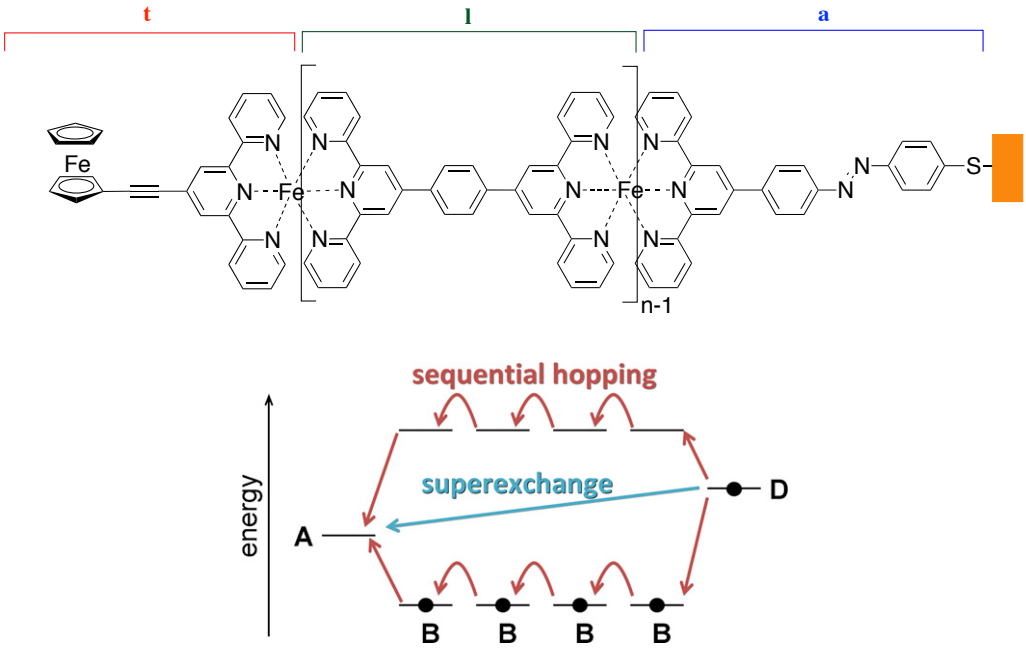

Figure 5-1. *Metalloterpyridine systems studied by Sakamoto et al. (top) and a schematic representation of hopping (hole transport through LUMO orbitals) versus superexchange or tunnelling (electron transport through the HOMO orbitals) from reference.* [25,30]

5.3. Synthetic consideration

Two approaches are well known for the synthesis of the terpyridines: a) ring closure especially employed for 4'-aryl substituted tpy (Kröhnke-type terpyridines);[5] b) Pd^0-catalyzed cross-coupling reactions[31,32] (Chart 5-3).

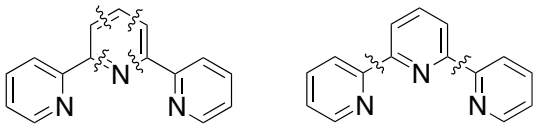

Chart 5-3. *Bond disconnections employed in the ring closure (Kröhnke-type terpyridine) (left) and Pd^0 cross-coupling approaches (right).*

On the other hand, phtpy derivatives are commonly obtained from the halogenated phtpy intermediates[24,26] and Pd cross-coupling reactions.[7]

In Chapters 2 and 4 the electrical behaviour of oligoyne series, metal-oligoynyl and metal-OPE was described. To explore other types of metal complexes featuring d-metal ions such as Fe, tpy and phtpy were suitable ligands to investigate. Consequently, the bis(terpyridine) ruthenium complex **40** was made from the on-complex Sonogashira reaction to avoid any deprotection of the trimethylsilyl termini due to the basic and alcoholic condition used for the metallation. In the future, this method will allow the addition of different alkyne substituents for different applications. It is worth noting that the "on complex" route is rarely applied, although some examples are found, such as the Suzuki reaction on $[Ru(phtpy)_2]^{2+}$.[32]

However, the usual synthetic route is used to synthesise bis(terpyridine) ruthenium **43** and bis(terpyridine) iron complex **47** due to the failure of the "on complex" strategy.

5.3.1. 4'-phenyl-2,2':6',2"-terpyridine derivatives

While the ring assembly can be really interesting for inserting different functionalization at the central and/or at the outer pyridine rings, in our case, the ring closure was preferred for the elaboration of 4'-(4-bromophenyl)-2,2':6',2"-terpyridine (Brphty).

Phtpy derivatives were prepared from Brphtpy (**K**), which was made in a one-pot reaction from two equivalents of 2-acetylpyridine and one equivalent of 4-bromobenzaldehyde via the Kröhnke reaction (Scheme 5-1).

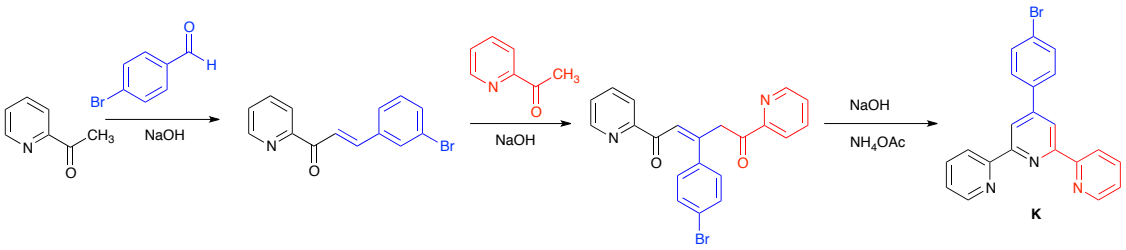

Scheme 5-1. *Kröhnke reaction for the formation of 4'-bromophenyl-2,2':6',2"-terpyridine **K**.*

The 1,5-diketone intermediate, prepared by aldol and Michael cascade reactions, is followed by a ring closure with ammonium acetate (NH_4OAc) to give Brphtpy **K**. The elaboration of homoleptic complexes $[M(X\text{-}tpy)_2]^{n+}$ necessitates the correct ratio between

ligand and metal centre, 2:1. In the case of M = Ru, the possible synthetic routes are the one-pot ruthenium trichloride ($RuCl_3$)/N-ethylmorpholine method,[33,34] or the route described by Rehahn[35] where $RuCl_3$ is de-chlorinated with $AgBF_4$ in acetone leading to a hexa-acetone ruthenium(III)•3$(BF_4)^-$ complex. Then, the loosely bound acetone ligands are displaced by the two tpy ligands and the ruthenium centre is reduced from Ru^{III} to Ru^{II}.

In this work, the key metal complex platform was bis[4'-(4-bromophenyl)-2,2':6,2"-terpyridine]ruthenium(II) tetrafluoroborate **L**, obtained in 54% yield over two steps following Rehahn's method.[36,37] Using the "on complex" route bis(4'-[4-(trimethylsilylethynyl)phenyl]-2,2':6',2''-terpyridine)ruthenium (II) tetrafluoroborate **40** was prepared in 10% yield by reaction between **L** and 2 equivalents of 1-ethynyl-4-(trimethylsilylethynyl)benzene followed by precipitation from CH_2Cl_2 solution upon addition of Et_2O (Scheme 5-2). IR spectroscopy showed clearly the $\nu(C{\equiv}CSiMe_3)$ stretching mode at 2153 cm^{-1}. The characteristic protons of the central pyridine ring are at low field (singlet at δ 9.50 ppm), because the ligands are orthogonal which leads to a deshielded environment. In addition, low-resolution MALDI-TOF mass spectrometry shows the peak of the molecular mass doubly charged with loss of one or two tetrafluoroborate anions.

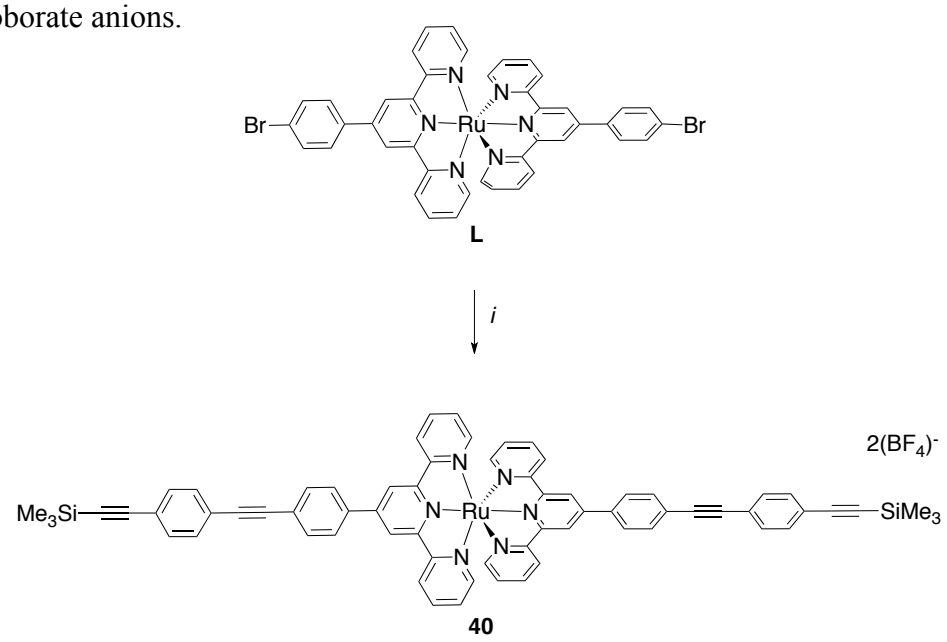

Scheme 5-2. *Preparation of Ru(II) bis-2,2':6,2"-terpyridine **40**. (i) 1-ethynyl-4-(trimethylsilylethynyl)benzene (2 eq), 20 mol% $PdCl_2(PPh_3)_2$, 40 mol% CuI in $MeCN/HNEt_2$ (2.5/1), reflux, overnight, 10%.*

Unfortunately, the single molecule measurements of the complex **40** were not obtained due to a lack of time. However, recent measurements of a similar molecule bearing the phtpy unit and TMSE as anchor group (**M**) gave a similar conductance (1.94 ± 0.65 nS) within the error range to the molecule **N** with the tpy unit (2.27 ± 0.73 nS) but more importantly slightly lower when considering the mean peak value and with narrower conductance distribution (Chart 5-4). Indeed, the insertion of the phenyl spacer in the molecule **M** allows a free rotation relative to the tpy plane leading to a range of conformation which is in agreement with the broader histogram observed. The two molecules **M** and **N** have been synthesized by Dr Ross Davidson in the Low and Beeby's groups, with single molecule conductance studies carried out in the Nichols' group at Liverpool. Therefore, the efforts were focussed on the elaboration of metalloterpyridine systems which contain just tpy as subunit.

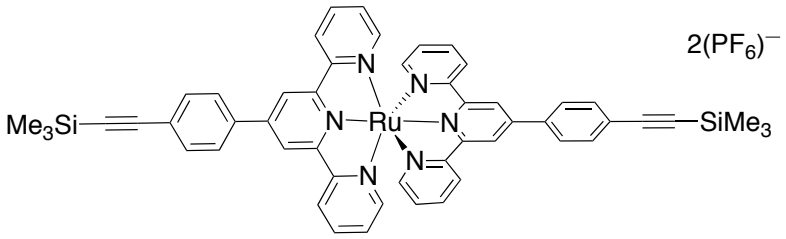

M

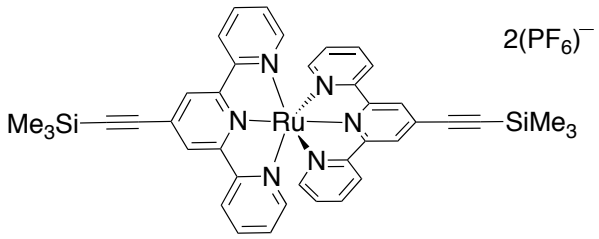

N

Chart 5-4. *Bis(terpyridyl)Ru(II) molecules **M** and **N** synthesized by Dr Ross Davidson.*

5.3.2. 2,2':6',2"-terpyridine derivatives

Guided by the conclusions extracted from single molecule measurement of the complexes **M** and **N**, the project was focussed on the synthesis of $[M(tpy)_2]^{n+}$ complexes similar to the molecule **N** to complete the series by increasing the length of the alkyne connected in 4'-position of tpy. In addition to the length dependence, using metals with

different redox potentials, charge density and size were explored to see their influence on the conductance data. Preliminary results from the STM measurements in Liverpool on $[M(tpy)_2]^{n+}$ complex featuring different metals and linkers, synthesized by Dr Ross Davidson, suggest that the trend of conductance values depends not only on the metal but also on the linker (*see* Chapter 4). Therefore, iron and ruthenium were explored in this chapter and the linker TMSE was chosen for its facile incorporation into the molecule and for its clear conductance histogram.

Sonogashira reaction "on complex" was tried on bis(4'-(4-bromo)-2,2':6',2"-terpyridine) ruthenium(II) hexafluorophosphate $[Ru(Brphtpy)_2]^{2+}$ with TMSB (**F**) in a mixture 2/1 MeCN/HN^iPr_2, but no evidence for any reaction was observed: the purification of the reaction mixture returned only the starting material (Scheme 5-3). Thus, as an alternative route 4'-(trimethylsilylbutadiynyl)-2,2':6',2"-terpyridine (TMSBtpy) **41** was prepared and converted into $[Fe(TMSBtpy)_2]^{2+}$ (**42**) and $[Ru(TMSBtpy)_2]^{2+}$ (**43**) by direct complexation reaction of $(FeBF_4)_2.6H_2O$ and $RuCl_3.nH_2O$ respectively, with two equivalents of the ligand **41** (Scheme 5-5).

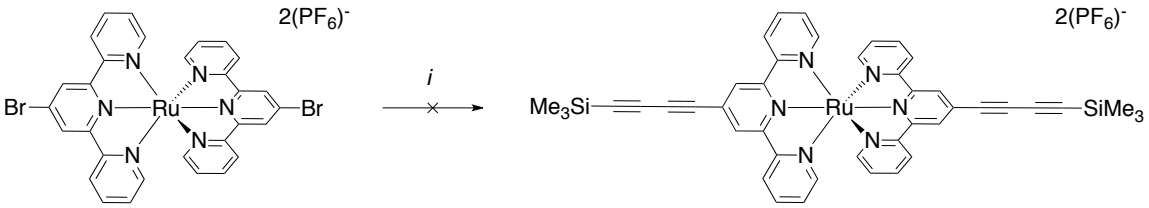

Scheme 5-3. *Attempted Sonogashira reaction between $[Ru(Brphtpy)_2]^{2+}$ and TMSB (**F**). (i) **F** (4 eq), 5 mol% $Pd(PPh_3)_4$, 5 mol% CuI in MeCN/HN^iPr_2 (2:1 v/v), 100°C, overnight.*

Surprisingly the ligand **41** was not obtained from the reaction between 4'-(trifluoromethylsulfonyloxy)-2,2':6',2"-terpyridine (TpyOTf) **O** and **F**, as described in the literature for the synthesis of 4'-(trimethylsilylethynyl)-2,2':6',2"- terpyridine[38] using various palladium catalysts ($Pd(PPh_3)_4$, $Pd(PPh_3)_2Cl_2$ and $Pd_2(C_6H_4CN)_2Cl_2$ + $P(tBu)_3$). Instead, the starting material tpyOTf was recovered. A possible explanation of this unreactivity might be the decomposition of the $Pd(PPh_3)_4$ catalyst with the generated triflate anion ^-OTf which leads to the formation of $[Pd(PPh_3)_2{}^-OTf]$. Similar decomposition of the palladium catalyst has been reported during Suzuki reactions between an aryl triflate and an organoboron (Scheme 5-4) to give a phosphonium salt.[39] To

prevent the decomposition, lithium bromide was used to convert the cationic palladium(II) to organopalladium(II) bromide.

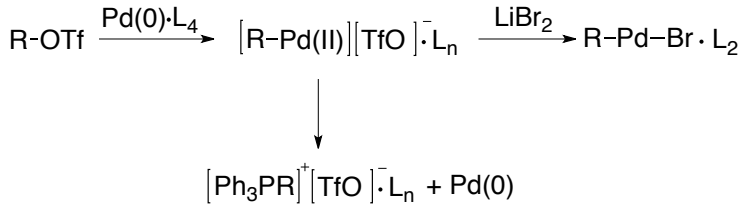

Scheme 5-4. *Possible decomposition of the catalyst $Pd(PPh_3)_4$ in presence of triflate anion.*[39]

Therefore, tpyOTf was brominated to give 4'-bromo-2,2':6',2"-terpyridine (TpyBr) **P**, which was cross-coupled with **F** to give the ligand **41** (Scheme 5-5) which was successfully obtained after 2 days. The extended reaction time was necessary to consume entirely the starting material **P**, as judged by Thin Layer Chromatography (TLC). The temperature employed for the preparation of **41** is chosen carefully to keep TMSB in the reaction mixture. The pure product was obtained in 72% yield after column chromatography on neutral alumina and a single crystal suitable for X-ray determination was grown from the eluent (hexane/EtOAc). The tpy ligand **41** was characterized by ^{1}H NMR, ^{13}C NMR, low and high-resolution ES-MS, IR spectroscopies and elemental analysis. The four quaternary carbons were clearly seen at δ_C 93.1, 87.2, 78.2, 74.1 ppm in the ^{13}C NMR spectrum and the $SiMe_3$ group was at δ_H 0.26 ppm in the ^{1}H NMR spectrum.

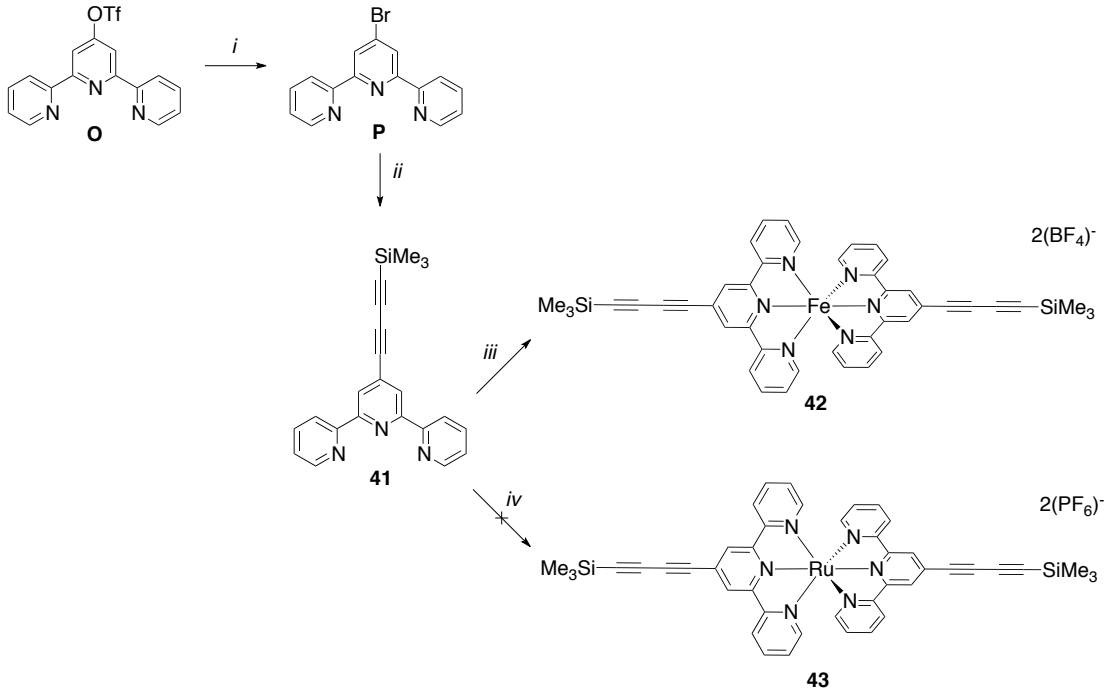

Scheme 5-5. *Synthetic routes for the formation of the bis(terpyridyl) metal complexes **42** and **43**. (i) CH_3COOH, HBr, 120 °C, overnight; (ii) **F** (2 eq), 10 mol% $Pd(PPh_3)_4$, 5 mol% CuI in NEt_3/THF, 50 °C, 2 h and 90 °C, 2 days; (iii) $Fe(BF_4)_2.6H_2O$ (0.46 eq) in CH_2Cl_2/MeOH (v/v 3/1), rt, 30 min; (iv) a) $RuCl_3.nH_2O$ (0.5 eq), 2 drops of 4-ethylmorpholine in MeOH, reflux, 6h.*

Subsequently, the complexation of 2.3 equivalents of **41** and $(FeBF_4)_2.6H_2O$ rapidly gave the bis(terpyridine) complex **42**, which was isolated by extraction of the crude material in hexane and the purple solid was filtered to remove the excess ligand **41** (Scheme 5-5). The structure of **42** was confidently assigned by a combination of ^{1}H NMR, ^{13}C NMR and IR spectroscopies, and low and high-resolution ES-MS spectrometry. The characteristic peak of the dicationic parent ion was found in ES-MS (382.84 [M + H^+]/2) and the complexation was confirmed by the desheilded singlet corresponding to the protons of the central pyridine ring.

However, because of the deviation observed twice from the expected CHN percentages for **42** (calcd C, 56.43; H, 4.09; N, 8.97 and found C, 49.02; H, 3,26; N, 7.80), column chromatography was used in an attempt to purify **42** after an anion exchange with ammonium hexafluorophosphate. However, this led to a partial removal of the

trimethylsilyl groups resulting in an inseparable mixture of the deprotected **42'** and **42** (Chart 5-5). The deprotection might be due to the alcoholic and basic eluent MeCN/MeOH used for the purification generating a nucleophilic methoxide which is known to remove TMS protecting groups (Figure 5-2).

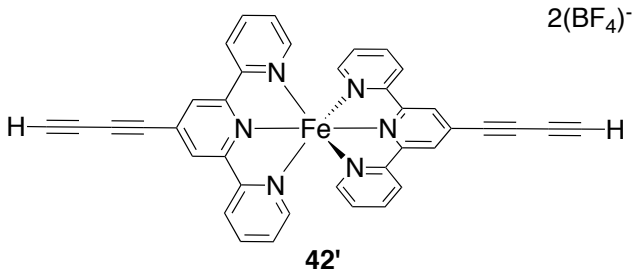

42'

Chart 5-5. *Deprotected compound **42'** obtained after the purification of **42**.*

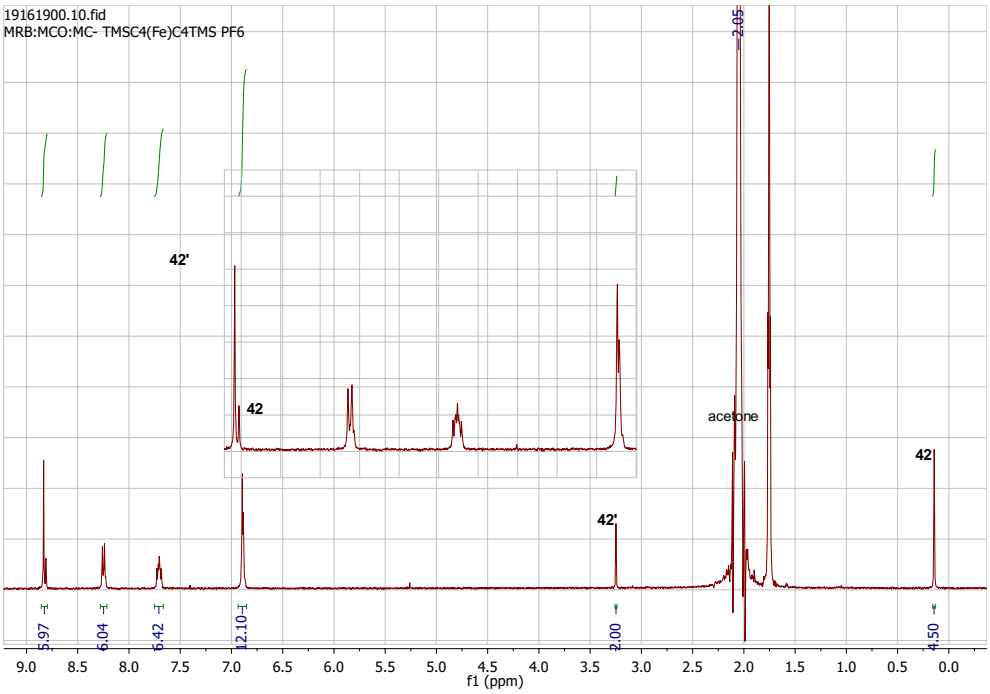

Figure 5-2. *^{1}HNMR of the mixture of compound **42** and the desilylated compound **42'** after attempted purification of **42**.*

Similarly, the synthesis of the ruthenium complex **43** was realised from the reaction between 2.1 equivalents of **41** and $RuCl_3.nH_2O$ under $RuCl_3$/N-ethylmorpholine conditions in MeOH, followed by an anion exchange with the addition of ammonium hexafluorophosphate (NH_4PF_6). However, once again, the mixture of protected **43** and deprotected **43'** were obtained before the purification on an alumina pad eluted by

DCM/5% NEt_3. Therefore, the characterization of pure **43** was not possible (Figure 5-3). Nevertheless, taking advantage of the formation of the mixture of **43'** and **43**, the idea was to fully deprotect **43** with KF in MeCN/MeOH to give exclusively **43'** which was not isolated. In fact, after trial to purify the compound **43'** in order to use it for the next step involving the Sonogashira reaction with 4-iodopyridine, an interesting compound (**44**) was obtained (Scheme 5-6). Compound **44** was characterized only by X-ray crystallography. Further studies on this reaction were outside the scope of our work.

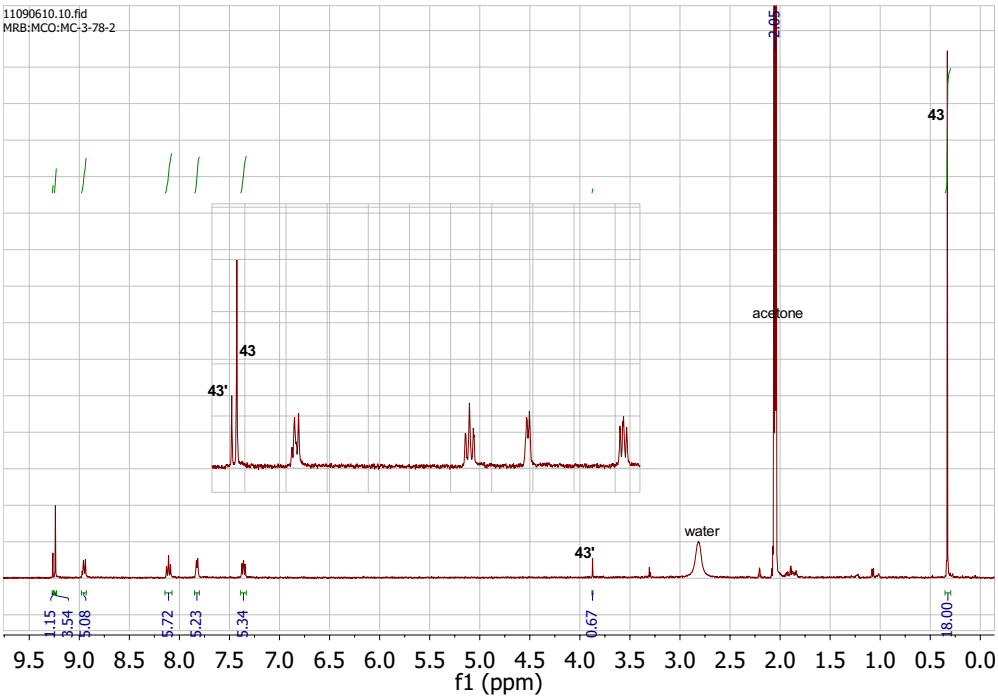

Figure 5-3. *^{1}HNMR of the mixture of compound **43** and the desilylated compound **43'** after attempted purification of **43**.*

Compound **44** may arise from nucleophilic attack of the triethylamine contained in the chromatography eluent mixture (CH_2Cl_2/MeCN/5% NEt_3). This amine addition on the C_δ can be explained by the withdrawing effect of the metal on the carbon chain. Jung and Buszek described a similar reaction between alkenylammonium tetrafluoroborate salts with activated acetylenes in a *trans* position.[40] Recently, Wang et al. showed nucleophilic additions of a primary or secondary amine to the electron-deficient multiple bond of ethynylcobalticinium hexafluorophosphate.[41]

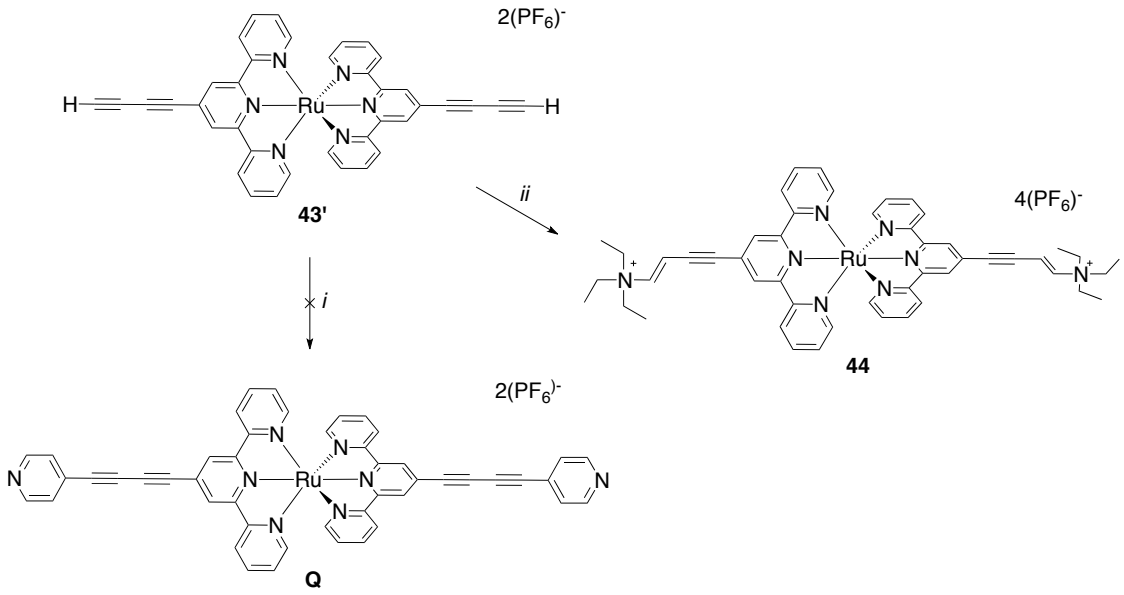

Scheme 5-6. *Attempted "on complex" Sonogashira reaction*; *(i) 4-iodopyridine (2.1 eq),* 5 mol% $Pd(PPh_3)_4$ and 10 mol% CuI in 2/1 $MeCN/HNEt_2$ *and conversion of* ***43'*** *to* ***44*** *after (ii) purification on neutral alumina CH_2Cl_2/ MeCN/5% NEt_3 as eluent.*

At that stage, it was realised that a better approach to the elaboration of the bis(terpyridine) metal complexes was by using a suitable tpy ligand featuring the pyridine anchoring group. Moreover, due to the ease of obtaining bis(terpyridine) iron complexes, we turned to the homolog of molecule **Q** but with the iron metal centre instead. Then, 4'-(pyridylbutadiyne)-2,2':6',2"-terpyridine (tpyC4Py) **46** was synthesized in 2 steps: a) desilylation of tpyTMSB **41** to give 4'-butadiynyl-2,2':6',2"-terpyridine (tpyC4H) **45**; b) Sonogashira reaction with 4-iodopyridine (Scheme 5-7). The identity of the tpy ligands **45** and **46** was confirmed by ^1H NMR, ^{13}C NMR spectroscopy, and low and high resolution mass spectrometry.

Therefore, the bis(terpyridyl)iron complex **47** bearing pyridyl instead of TMSE anchor groups was prepared in 56% yield using the same conditions as for **42** (Scheme 5-7). Complex **47** was characterized by elemental analysis, ^1H NMR, ^{13}C NMR and IR spectroscopies, and low and high resolution mass spectrometry. The mass data displays the expected doubly charged ion (386.14 $[M]^{2+}$). Nevertheless, the bis(terpyridyl) compound **47** is less soluble than the compound **42** with $SiMe_3$ groups.

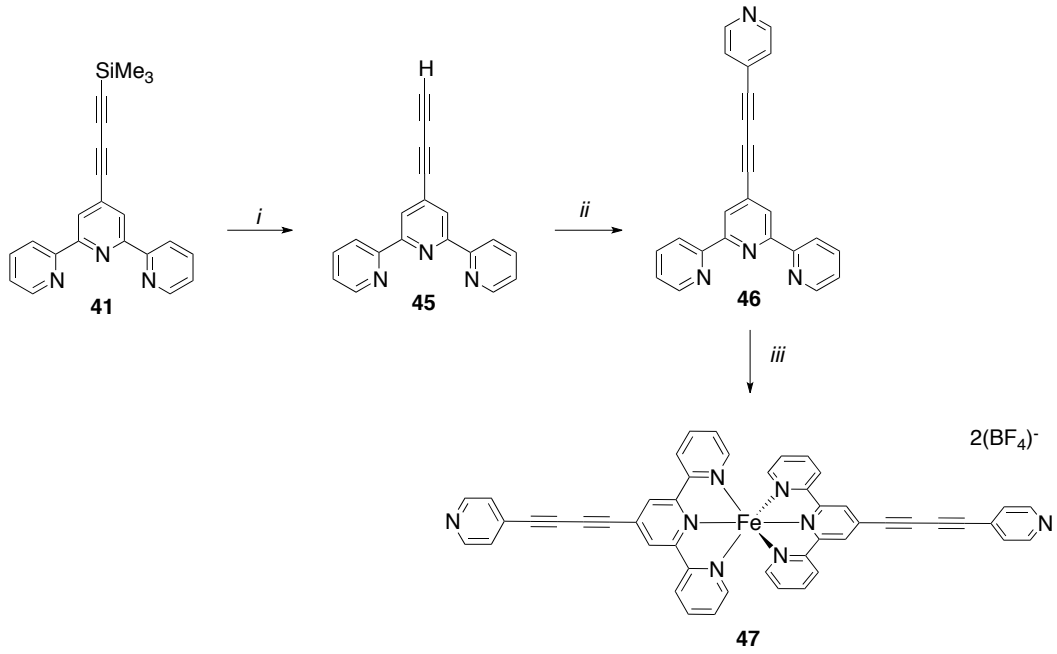

Scheme 5-7. *Synthetic route to the bis(terpyridyl) metal complex **47**. (i) KF (1.2 eq) in MeOH/THF, overnight, rt, 40%; (ii) 4-iodopyridine (1.2 eq), 5 mol% $Pd(PPh_3)_4$, 5 mol% CuI in THF/HN^iPr_2 (1.5:1 v/v), rt, overnight, 59%; (iii) 0.48 eq $Fe(BF_4)_2.6H_2O$ in CH_2Cl_2/MeOH (3.3/1 v/v), rt, 30 min, 56%.*

5.4. Electrochemical measurements

The solution cyclic voltammetric data are in Table 5-1.

Table 5-1: *Redox potentials for the complexes **40**, **42** and **47** in 0.1 M NBu_4PF_6 in acetonitrile with Pt dot working electrode. Potentials of Fe(II) at scan rate 0.6 V/s and Ru(II) at scan rate 1 V/s were referenced against $FeCp^*_2/[FeCp^*_2]^+$ = - 0.53 V vs $FeCp_2/[FeCp_2]^+$. [b]Reversible process $E_{1/2}$*

	M^{III}/M^{II}	Terpyridine based reduction	
	$E_{pa}(1)$	$E_{pa}(2)$	$E_{pa}(3)$
40	0.91	- 1.37	- 1.80
42	0.84[b]	-1.39	×
47	0.74[b]	- 1.58	- 1.88

All the bis(terpyridyl) complexes display a metal-centred oxidation and one or two reductions based on the terpyridine ligands. The metal-centred oxidation is reversible for the iron species (**42** and **47**) supported by the linear dependence of i_p versus $\nu^{1/2}$ or, irreversible for the ruthenium molecule (**40**) (Appendix B, Figure B-1 - B-4). The poor quality of the oxidation and reduction waves is probably due to the complexes' poor solubility in acetonitrile. Alternative solvents were not investigated due to the very limited amount of samples available. Moreover, the irreversibility of the reduction of the terpyridine ligands was predicted, knowing that the butadiyne unit is not electrochemically stable. The solubility increases when the pyridyl group is replaced by trimethylsilyl group which can be seen with the better distinction of the oxidation and reduction waves in the cyclic voltammogram of **42** (Appendix B, Figure B-2). The HOMO level of the compound **42** can be estimated at 5.43 V and the LUMO at 3.61 V using the formula: $E_{HOMO} = E_{ox}^{on} + 4.8$ and $E_{LUMO} = E_{red}^{on} + 4.8$. The differential pulse data shed light on the electron processes occurring in the oxidation/reduction of the bis(terpyridyl)metal complexes **40**, **42** and **47**. For example, in the case of the compound **40**, the metal-centred oxidation wave was not easy to observe, but with the differential pulse, it is visible.

5.5. Molecular structures

Single crystals suitable for X-ray diffraction were obtained for the terpyridine ligand **41** and bis(terpyridyl) ruthenium complex **44**. Plots of these molecules are given in Figures 5-7 – 5-8. In **41** the carbon chain displays alternation of short-long bond lengths with triple bonds 1.202(3) - 1.208(3) Å and single bonds ca. 1.378(3) - 1.430(2) Å. For the complex **44**, the distorted octahedral geometry is in agreement with related bis(terpyridyl) ruthenium complexes.[10,42] The angles Ru(1)-N(3)-N(1), N(4)-Ru(1)-N(6) are 157.62(12) ° and 157.88(17) °, respectively, and the angle N(2)-Ru(1)-N(5) is 179.21(16) °. The bond lengths are Ru(1)-N(5) 1.975(4) Å to Ru(1)-N(4) 2.078 (4) Å. The carbon chains show the characteristic lengths with the triple bond shorter (C(16) - C(17) 1.186(7) Å) than the double bond (C(18) - C(19) 1.320(8) Å). The ethylene bonds are both trans, which is why the torsion angle between C(17)-C(18)-C(19)-N(7) is -0.31 ° and the angle between C(43)-C(44)-N(8) is 128.9(12).

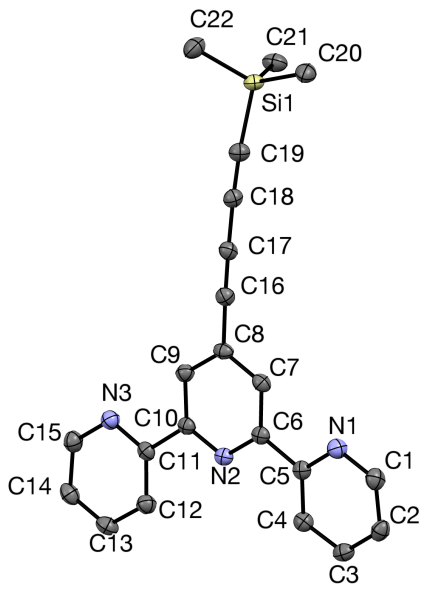

Figure 5-7. *Molecular structure of **41** showing the atom labelling scheme with thermal ellipsoids plotted at 50%.*

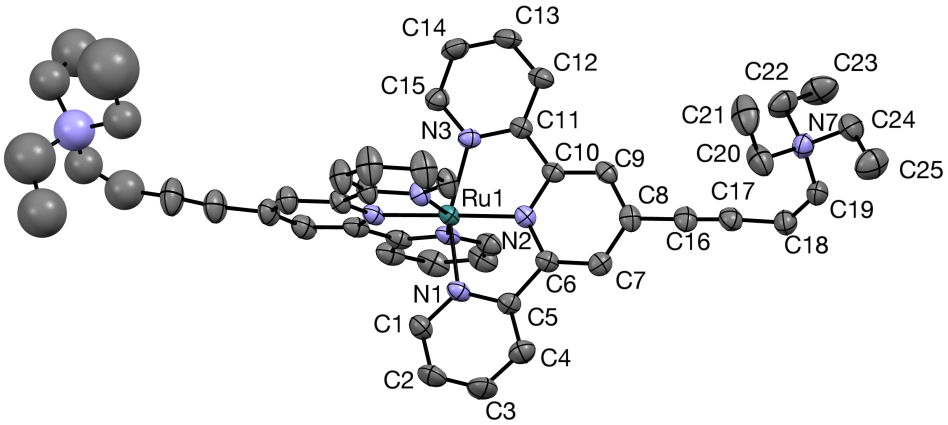

Figure 5-8. *Molecular structure of **44** showing the atom labelling scheme with thermal ellipsoids plotted at 50%. The disorder has been omitted for clarity.*

5.6. Conclusion

A new synthetic approach has facilitated the elaboration of carbon rich butadiynyl terpyridine ligands such as **41**, **45** and **46**. However, the stability of these compounds is a drawback and the length limit has probably been reached due to increasing insolubility when with increased molecular length. The instability of the bis(terpyridyl) compounds **43'** and **47** is shown by the high reactivity with triethylamine (**44**) and the irreversibility of the terpyridine-based reductions. The addition of hexyloxy chains (*see* Chapter 4) could enhance solubility even if the molecular conductance might be affected, depending of the molecular orbital levels relative to the gold Fermi level. The electrochemical data for two different anchor groups, pyridyl and TMSE, suggests that the iron complex with TMSE **42** should behave better especially due its good solubility and the LUMO level (3.61 eV) being not far from the gold work function (4.3 eV). STM measurement of the two bis(terpyridyl) compounds **42** and **47** are under investigation. Future work could be to connect 1,4-bis(ethynyl)benzene to the terpyridine core, to improve stability and keep a good conductance value. Thus, the length of the molecule can be increased by the addition of arylbutadiyne and the use of thiomethyl linker could be a nice comparison with the bis(terpyridines) containing pyridyl linker.

5.7. Experimental

5.7.1. General conditions

$HNEt_2$, HN^iPr_2 were purified by distillation from KOH and NEt_3 was purified by distillation from $CaSO_4$, other reaction solvents were purified and dried using Innovative Technology SPS-400 and degassed before use. Bis[4′-(p-bromophenyl)-2,2′:6′,2″-terpyridine]ruthenium-(II) Tetrafluoroborate **L**,[36] 1-ethynyl-4-(trimethylsilylethynyl)benzene[43] and 4'-trifluoromethylsulfonyloxy-2,2':6',2"-terpyridine[44] were prepared following the literature methods. The synthesis of TMSB (**F**) is described in Chapter 2. Other reagents were purchased commercially and used as received. NMR spectra were recorded in deuterated solvent solutions on Bruker Avance 400 MHz and Varian VNMRS 700 MHz spectrometers and referenced against residual protio-solvent resonances ($CDCl_3$: ^{1}H 7.26 ppm, ^{13}C 77.00 ppm; dmso: ^{1}H 2.50 ppm, ^{13}C 39.52 ppm; $(CD_3)_2CO$: ^{1}H 2.05 ppm, ^{13}C 29.84 and 206.26 ppm; CD_3CN: ^{1}H 1.94 ppm, ^{13}C 1.32 and 118.26 ppm).

Matrix-assisted laser desorption ionization (MALDI) mass spectra were recorded using an Autoflex II TOF/TOF mass spectrometer with a 337 nm laser. Electron ionisation mass spectra were recorded on a Thermoquest Trace or a Thermo-Finnigan DSQ. Infrared spectra were recorded on a Thermo 6700 spectrometer from CH_2Cl_2 or MeCN solution in a cell fitted with CaF_2 windows. Infrared spectra were recorded on a Thermo 6700 spectrometer from CH_2Cl_2 solution in a cell fitted with CaF_2 windows. Electrochemical analyses were recorded using Emstat2 Palm instruments BV electrochemical analyzer fitted with a three-electrode system consisting of a Pt disk as working electrode, auxiliary and reference electrode from solution in CH_2Cl_2 containing 0.1 M NBu_4PF_6. Melting points were determined in an open-ended capillaries using Stuart Scientific SMP40 melting point apparatus at ramping rate of 2 °C/min. Elemental analyses were performed on a CE-400 Elemental Analyzer. Elemental analyses were performed on a CE-400 Elemental Analyzer. Single-crystal X-ray data were collected at 120(2) K on a Bruker SMART CCD 6000 (fine-focus sealed tube, graphite-monochromator).

Bis(4'-[4-(Trimethylsilylethynyl)phenyl]-2,2':6',2''-terpyridine)ruthenium(II) Tetrafluoroborate; 40

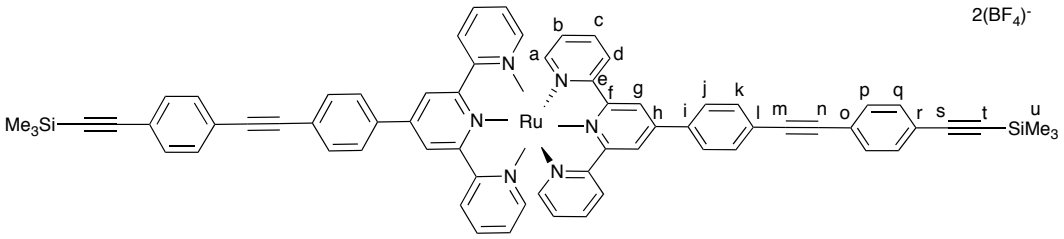

To a degassed solution of MeCN (35 mL) and $HNEt_2$ (14 mL) was added **L** (195 mg, 0.22 mmol), 1-ethynyl-4-(trimethylsilylethynyl)benzene (0.10 g, 0.44 mmol), $PdCl_2(PPh_3)_2$ (0.01 g, 0.02 mmol) and CuI (0.08 g, 0.04 mmol). The red suspension was heated overnight at reflux and was then allowed to cool to room temperature. The mixture was collected by filtration and washed with MeCN to remove any salts. The red filtrate was evaporated to dryness and the residue was re-dissolved in the minimum amount of CH_2Cl_2. Et_2O was added dropwise to cause precipitation. The precipitate was collected by filtration and washed with MeOH to give a purple solid. Yield: 0.028 g, 10%. ^{1}H NMR (100 MHz, $(CD_3)_2CO$): δ 9.53 (s, 4H, g), 9.11 (d, J = 8.1 Hz, 4H, d), 8.47 (d, J = 8.0 Hz, 4H, a), 8.12 (t, J = 7.8 Hz, 4H, c), 7.93 (d, J = 7.9 Hz, 4H, j/k), 7.85 (d, J = 5.4 Hz, 4H, j/k), 7.64 (d, J = 8.0 Hz, 4H, p/q), 7.57 (d, J = 8.0 Hz, 4H, p/q), 7.26 (t, J = 6.7 Hz, 4H, b), 0.24 (s, 18H, u) ppm. ^{13}C NMR {^{1}H} (101 MHz, dmso): δ 158.0, 155.1, 152.2, 138.1, 136.3 (j/k), 132.4, 132.0, 131.7 (p/q), 127.9, 127.7, 124.9, 121.0, 97.6, 91.3, - 0.1 (u) ppm, the other quaternary carbon was not seen. IR (CH_2Cl_2): 3062 (s); ν(C≡CSiMe$_3$) 2153 (m); 1675 (s); 1620 (s) cm^{-1}. MS (MALDI-TOF; m/z): 1111.3 [M - $(BF_4)_2$]$^+$, 1199.3 [M - BF_4]$^+$.

4'-bromo-2,2':6',2"-terpyridine; P

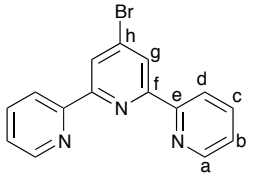

A solution of **O** (1.00 g, 2.62 mmol) in acetic acid (25 mL) and hydrobromic acid (20 mL) was heated to 120 °C overnight. The mixture was poured into water (60 mL) and sodium

bicarbonate was added until the solution was neutralized. The resulting solution was extracted with $CHCl_3$ and the organic fractions were dried over $MgSO_4$. The solvent was removed and the product was purified on a neutral alumina column using hexane/EtOAc (5:5 v/v). Product **P** was obtained as a white solid (570 mg, 68%). ^{1}H NMR (400 MHz, $CDCl_3$): δ 8.71 (d, J = 4.8 Hz, 2H, a), 8.66 (s, 2H, g), 8.59 (d, J = 8.0 Hz, 2H, d), 7.87 (t, J = 8.0 Hz, 2H, c), 7.36 (m, 2H, b) ppm. The NMR data were consistent with the literature.[30]

4'-(trimethylsilylbutadiynyl)-2,2'-6',2"-terpyridine; 41

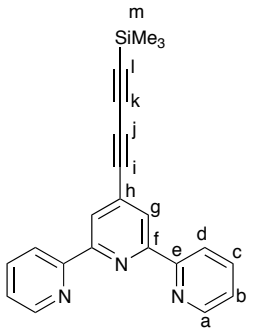

To an oven dried Schlenk flask containing a solution of **P** (0.10 g, 0.32 mmol) in dry and degassed NEt_3 (3 mL) and THF (4 mL) was added **F** (0.08 g, 0.09 mL, 0.64 mmol), $Pd(PPh_3)_4$ (0.04 g, 0.03 mmol) and CuI (0.003 g, 0.02 mmol). The solution was heated at 50 °C for 2 h and then at 90 °C for 2 days. The mixture was evaporated and purified on a neutral alumina column using hexane/EtOAc (10:1 v/v) to give a brown oil which solidified. Yield: 0.08 g, 72%. ^{1}H NMR (400 MHz, $CDCl_3$): δ 8.72 (d, J = 4.9 Hz, 2H, a), 8.60 (d, J = 8.0 Hz, 2H, d), 8.53 (s, 2H, g), 7.88 (t, J = 7.7 Hz, 2H, c), 7.37 (d, J = 7.6 Hz, 2H, b), 0.26 (s, 9H, m) ppm. ^{13}C NMR $\{^1$H$\}$ (101 MHz, $CDCl_3$): δ 155.4, 155.1, 149.0 (a), 137.2 (c), 131.8, 124.2 (b), 123.7 (g), 121.3 (d), 93.1, 87.2, 78.2, 74.1 (i/j/k/l), - 0.48 (m) ppm. IR (CH_2Cl_2): ν(C≡CSiMe$_3$) 2105 (br); 1601 (br); 1582 (s); 1567 (br); 1542 (br); 1469 (m); 1392 (m). MS (ES^+; m/z): 353.96 [M] 100%. Anal. Calcd for $C_{22}H_{19}N_3Si$: C, 74.75; H, 5.42; N, 11.89; Found C, 74.67; H, 5.50; N, 11.75. mp: 149.1 – 150.6 °C. Crystal data for **41**: $C_{22}H_{19}N_3Si$, M = 353.49, monoclinic, space group $P2_1/n$, a = 10.3446(7) Å, b = 11.2438(7) Å, c = 16.4242(11) Å, β = 97.067(2) °, U = 1895.8(2) Å^3, F(000) = 744, Z = 4, D_C = 1.238 mg/mm^3, μ = 0.134 mm^{-1}; 32572 reflections were collected , yielding 4575 unique data (R_{merg} = 0.0914). Final $wR_2(F^2)$ = 0.1694 for all data (311 refined parameters), conventional R_1 (F) = 0.0674 with I ≥ 2σ, GOF = 1.109.

Bis(4'-[4-(Trimethylsilylbutadiynyl]-2,2':6',2''-terpyridine)iron(II) Tetrafluoroborate; 42

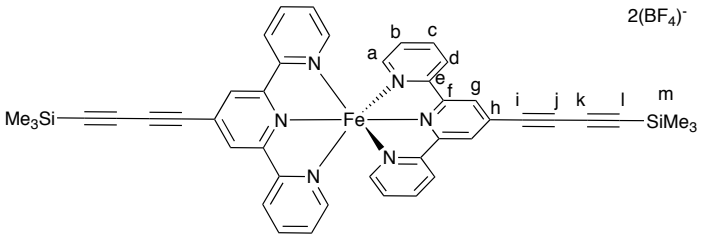

A suspension of **41** (0.10 g, 0.03 mmol) and $Fe(BF_4)_2.6H_2O$ (0.04 g, 0.13 mmol) in CH_2Cl_2 (10 mL), MeOH (3 mL) was stirred at room temperature for 30 min. The solvent was removed by reduced pressure and the solids were extracted with hexane to remove the excess of ligand, filtered and washed with Et_2O to give a purple solid. Yield: 100 mg, 85%. ^1H NMR (400 MHz, dmso-d_6): δ 9.51 (s, 4H, g), 8.81 (d, J = 8.1 Hz, 4H, d), 8.01 (t, J = 7.8 Hz, 4H, c), 7.25 (d, J = 5.6 Hz, 4H, a), 7.17 (t, J = 6.7 Hz, 4H, b), 0.33 (s, 18H, m). ^{13}C NMR $\{^1H\}$ (700 MHz, CD_3CN): δ 161.1, 158.0, 154.0, 140.0, 131.4, 128.7, 127.0, 125.1, 97.9, 86.9, 81.8, 73.8 (i/j/k/l), - 0.7 (m). IR (CH_2Cl_2): 3622 (br); 3540 (br); 1658 (s). MS (ES^+; m/z): 382.84 $[M + H^+]^{2+}$ 100%. HR-ESI^+-MS: m/z calcd for $C_{44}H_{38}B_2F_8FeN_6Si_2^{2-}$ 381.1024; found 381.0957.

4'-(buta-1,3-diynyl)-2,2':6',2"-terpyridine; 45

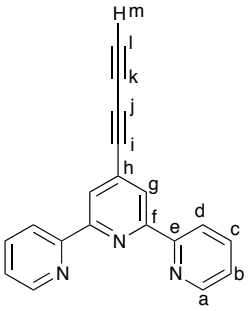

To a solution of 4'-(trimethylsilylbutadiynyl)-2,2'-6',2"-terpyridine **41** (310 mg, 0.88 mmol) in MeOH/THF (20 mL, 1:1 v/v) was added potassium fluoride (61 mg, 1.05 mmol). The reaction mixture was stirred at room temperature overnight. The solution was evaporated to dryness and the residue was purified on a neutral alumina column using

hexane/EtOAc (9:1 v/v) as an eluent to give a brown solid. Yield: 100 mg, 40%. ^{1}H NMR (400 MHz, $CDCl_3$): δ 8.71 (d, J = 4.8 Hz, 2H, a), 8.60 (d, J = 7.9 Hz, 2H, d), 8.56 (s, 2H, g), 7.88 (t, J = 7.7 Hz, 2H, c), 7.37 (d, J = 4.8 Hz, 2H, b), 2.58 (s, 1H, m). ^{13}C NMR {^{1}H} (700 MHz, $CDCl_3$): δ 155.7, 155.2, 149.2 (a), 137.0 (c), 131.3, 124.2 (b), 123.7, 121.2 (d), 73.03, 72.9, 67.6 (i/j/k/l). IR (CH_2Cl_2): ν(≡C-H) 3291 (s); 1584 (s); 1570 (m); 1468 (m); 1393 (m). MS (ES^+; m/z): 281.91 [M] 100%. HR-ESI^+-MS: *m/z* calcd for $C_{19}H_{11}N_3H$ 282.1035; found: 282.1031.

4'-[4-(buta-1,3-diynyl)pyridine]-2,2':6',2"-terpyridine; 46

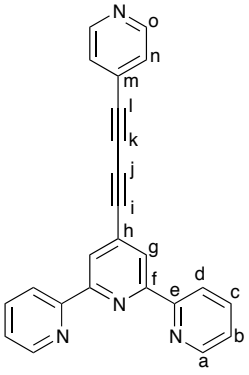

In a 50 mL Schlenk flask containing a solution of degassed anhydrous THF (20 mL) and HN^iPr_2 (15 mL) was added **45** (225 mg, 0.80 mmol), 4-iodopyridine (197 mg, 0.96 mmol), $Pd(PPh_3)_4$ (45 mg, 0.04 mmol) and CuI (8.5 mg, 0.04 mmol). The reaction mixture was stirred at room temperature overnight and the solution was dried and re-dissolved in CH_2Cl_2 to filter the salts. The filtrate was concentrated to the minimum volume and MeCN was added to precipitate the product which was obtained as a grey solid. Yield: 170 mg, 59%. ^{1}H NMR (600 MHz, $CDCl_3$): δ 8.67 (d, J = 4.8 Hz, 2H, a), 8.60 (d, J = 6.0 Hz, 2H, o), 8.55 (t, J = 7.9 Hz, 2H, d), 8.53 (s, 2H, g), 7.83 (t, J = 7.7 Hz, 2H, c), 7.36 (d, J = 6.0 Hz, 2H, n), 7.32 (d, J = 4.8 Hz, 2H, b). ^{13}C NMR {^{1}H} (700 MHz, $CDCl_3$): δ 156.7, 155.1, 149.7 (o), 149.1 (a), 136.9 (c), 131.1, 129.6, 126.1 (n), 124.1 (b), 123.3 (g), 121.1 (d), 81.1, 79.7, 77.5, 76.7 (i/j/k/l). IR (CH_2Cl_2): 1602 (br); 1583 (s); 1568 (m); 1541 (br); 1469 (m); 1393 (m). MS (ES^+; m/z): 360.18 [M + $2H^+$] 100%. HR-ESI^+-MS: *m/z* calcd for $C_{24}H_{14}N_3H$ 359.1298; found: 359.1297. mp: 149.7 – 151.2 °C.

Bis(4'-[4-(buta-1,3-diynyl)pyridine]-2,2':6',2''-terpyridine)iron(II) Tetrafluoroborate; 47

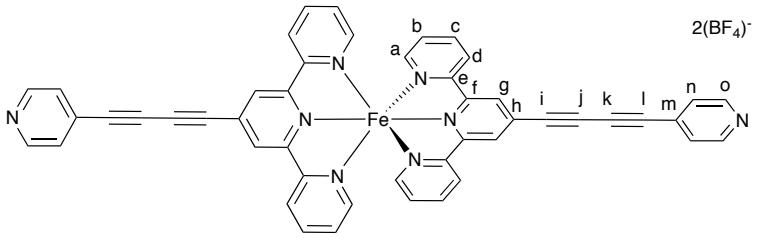

To a solution of **46** (75 mg, 0.21 mmol) in CH_2Cl_2 (10 mL) and MeOH (3 mL) was added $Fe(BF_4)_2.6H_2O$ (35 mg, 0.1 mmol). The purple solution was stirred at room temperature for 30 min and then dried. The residue was washed with hexane, dried and washed again with a small amount of CH_2Cl_2 to give a purple solid (53 mg, 56%). ^{1}H NMR (700 MHz, CD_3CN): δ 9.06 (s, 4H, g), 8.72 (d, J = 5.7 Hz, 4H, o), 8.47 (d, J = 7.8 Hz, 4H, d), 7.91(t, J = 8.2 Hz, 4H, c), 7.62 (d, J = 5.8 Hz, 4H, n), 7.12 - 7.09 (m, 8H, b). ^{13}C NMR $\{^1$H$\}$ (700 MHz, $CDCl_3$): δ 161.2, 157.9, 154.0, 150.9, 140.1, 131.0, 129.5, 128.7, 127.2, 126.8, 125.2, 83.5, 80.7, 80.3, 76.8 (i/j/k/l). IR (CH_2Cl_2): 3622 (br); 3543 (br); 1634 (s). MS (ES^+; m/z): 387.17 $[M + H^+]^{2+}$ 100%. HR-ESI^+-MS: m/z calcd for $C_{48}H_{28}B_2F_8FeN_8^{2-}$ 386.0894; found 386.0850. Anal. Calcd for $C_{48}H_{28}B_2F_8FeN_8^{2-}$: C, 60.93; H, 2.98; N, 11.84. Found: C, 60.88; H, 2.92; N, 11.77.

5.8. References

(1) Morgan, G.; Burstall, F. H. *J. Chem. Soc.* **1937**, *347*, 1649.

(2) Constable, E. C. *J. Chem. Soc., Dalton Trans.* **1985**, *12*, 2687.

(3) Schubert, U. S.; Hofmeier, H.; Newkome, G. R. *Modern terpyridine chemistry*; Wiley-VCH, Ed.; Weinheim; **2006**.

(4) Constable, E. C. *Advances in Inorganic Chemistry* **1986**, *30*, 69.

(5) Kröhnke, F. *Synthesis* **1976**, *1*, 1.

(6) Constable, E. C.; Ward, M. D. *J. Chem. Soc., Dalton Trans.* **1990**, *4*, 1405.

(7) Groshenny, V.; Romero, F. M.; Ziessel, R. *J. Org. Chem.* **2012**, *62*, 1491.

(8) Constable, E. C. *Chem. Soc. Rev.* **2007**, *36*, 246.

(9) Hofmeier, H.; Schubert, U. S. *Chem. Soc. Rev.* **2004**, *33*, 373.

(10) *Terpyridine-based Materials: For Catalytic, Optoelectronic and Life Science Applications*; Schubert, U. S.; Winter, A.; Newkome, G. R., Eds.; Wiley-VCH; Weinheim; **2014**.

(11) O'Regan, B.; Grätzel, M. *Nature* **1991**, *353*, 737.

(12) Kalyanasundaram, K.; Grätzel, M. *Coordination Chemistry Reviews* **1998**, *77*, 347.

(13) Shklover, V.; Nazeeruddin, M. K.; Grätzel, M.; Ovchinnikov, Y. E. *Appl. Organometal. Chem.* **2002**, *16*, 635.

(14) Zhong, Y.-W.; Vila, N.; Henderson, J. C.; Abruña, H. D. *Inorg. Chem.* **2009**, *48*, 991–999.

(15) El-ghayoury, A.; Schenning, A.; van Hal, P. A.; Weidl, C. H.; van Dongen, J.; Janssen, R.; Schubert, U. S.; Meijer, E. W. *Thin Solid Films* **2002**, *403*, 97.

(16) Sauvage, J.-P.; Collin, J.-P.; Chambron, J.-C.; Guillerez, S.; Coudret, C. *Chem. Rev.* **1994**, 993.

(17) Jin, G. J.; Chen, G.; Xia, J. L.; Yin, J.; Yu, G.-A.; Liu, S. H. *Transition Met Chem* **2011**, *36*, 611.

(18) Constable, E. C.; Figgemeier, E.; Housecroft, C. E.; Medlycott, E. A.; Neuburger, M.; Schaffner, S.; Reymann, S. *Polyhedron* **2008**, *27*, 3601.

(19) Harriman, A.; Khatyr, A.; Ziessel, R.; Benniston, A. C. *Angew. Chem. Int. Ed.* **2000**, *39*, 4287.

(20) Barigelletti, F.; Flamigni, L. *Chem. Soc. Rev.* **2000**, *29*, 1.

(21) Constable, E. C.; Housecroft, C. E.; Kokatam, S. L.; Medlycott, E. A.; Zampese, J. A. *Inorganic Chemistry Communications* **2010**, *13*, 457.

(22) Murphy, F. A.; Draper, S. M. *J. Org. Chem.* **2010**, *75*, 1862.

(23) Constable, E. C.; Lewis, J.; Liptrot, M. C. *Inorganica Chimica Acta* **2000**, *178*, 47.

(24) Han, F. S.; Higuchi, M.; Kurth, D. G. *Org. Lett.* **2007**, *9*, 559.

(25) Sakamoto, R.; Katagiri, S.; Maeda, H.; Nishihara, H. *Coordination Chemistry Reviews* **2013**, *257*, 1493.

(26) Eryazici, I.; Farha, O. K.; Compton, O. C.; Stern, C.; Hupp, J. T.; Nguyen, S. T. *Dalton Trans.* **2011**, *40*, 9189.

(27) Winter, A.; Friebe, C.; Hager, M. D.; Schubert, U. S. *Macromol. Rapid Commun.* **2008**, *29*, 1679.

(28) Li, S.; Moorefield, C. N.; Wang, P.; Shreiner, C. D.; Newkome, G. R. *Eur. J. Org. Chem.* **2008**, *19*, 3328.

(29) Dumur, F.; Mayer, C. R.; Dumas, E.; Marrot, J.; Sécheresse, F. *Tetrahedron Letters* **2007**, *48*, 4143.

(30) Katagiri, S.; Sakamoto, R.; Maeda, H.; Nishimori, Y.; Kurita, T.; Nishihara, H. *Chem. Eur. J.* **2013**, *19*, 5088.

(31) Fallahpour, R.-A.; Neuburger, M.; Zehnder, M. *New J. Chem.* **1999**, *23*, 53.

(32) Aspley, C. J.; Williams, J. A. G. *New J. Chem.* **2001**, *25*, 1136.

(33) Constable, E.; Housecroft, C.; Johnston, L.; Armspach, D.; Neuburger, M.; Zehnder, M. *Polyhedron* **2001**, *20*, 483.

(34) Maestri, M.; Armaroli, N.; Balzani, V.; Constable, E. C.; Cargill Thompson, A. M. W. *Inorg. Chem.* **1995**, *34*, 2759.

(35) Kelch, S.; Rehahn, M. *Macromolecules* **1997**, *30*, 6185.

(36) Duprez, V.; Biancardo, M.; Spanggaard, H.; Krebs, F. C. *Macromolecules* **2005**, *38*, 10436.

(37) Kelch, S.; Rehahn, M. *Macromolecules* **1999**, *32*, 5818.

(38) Mishra, A.; Mena-Osteritz, E.; Bäuerle, P. *Beilstein J. Org. Chem.* **2013**, *9*, 866.

(39) Miyaura, N.; Suzuki, A. *Chem. Rev.* **1995**, *95*, 2457.

(40) Jung, M. E.; Buszek, K. R. *J. Am. Chem. Soc.* **1998**, *110*, 3965.

(41) Wang, Y.; Rapakousiou, A.; Latouche, C.; Daran, J.-C.; Singh, A.; Ledoux-Rak, I.; Ruiz, J.; Saillard, J.-Y.; Astruc, D. *Chem. Commun.* **2013**, *49*, 5862.

(42) Siebert, R.; Schlütter, F.; Winter, A.; Presselt, M.; Görls, H.; Schubert, U. S.; Dietzek, B.; Popp, J. *Cent.Eur.J.Chem.* **2011**, *9*, 990.

(43) Goeb, S.; Ziessel, R. *Org. Lett.* **2007**, *9*, 737.

(44) Holbrey, J. D.; Tiddy, G. J. T.; Bruce, D. W. *J. Chem. Soc., Dalton Trans.* **1995**, *11*, 1769.

APPENDIX A

A-1. Single molecule conductance measurements

An Agilent STM running Picoscan 5.3.3 software was used for all single molecule conductance measurements which were performed at room temperature in mesitylene or in trichlorobenzene (TCB) solutions. Molecular ad-layers were formed on Au(111) substrates. These substrates were produced from commercially available gold on glass samples with a chromium adhesive layer (Arrandee) which were flame annealed immediately prior to use. Flame annealing involved heating the gold slide until it looks a slight orange hue. It was then kept in this state for approximately 30 s, but care was taken to ensure that the sample did not overheat. Molecular adsorption was achieved by adding the gold slide to a 0.2 ml solution of 1×10^{-4} M of the target molecule in either mesitylene or trichlorobenzene. Gold STM tips were fabricated from 0.25 mm Au wire (99.99%) which was freshly electrochemically etched for each experiment at +7 V in a mixture of ethanol (50%) and HCl (50%).

Electrical measurements were performed using an STM and the *I*(*s*) method. In brief, this method involves the repeated formation and cleavage of molecular bridges generally formed between gold contacts (an Au STM tip and an Au substrate). In the *I*(*s*) technique the electrical conductance of the junction is measured as the molecule is fully extended in the gap between STM-tip and substrate as the tip is rapidly retracted. Current steps are seen in the retraction process which are taken to be characteristic of the cleavage of Au | molecule(s) | Au electrical junctions. These current-distance curves are repeatedly measured and they are then plotted in a conductance histogram. In this work we have performed *I*(*s*) scans from the position defined by the set-point values of tunnelling current (I_0) and tunnelling voltage (U_t) to a distance of + 4 nm with a scan rate of 20 nm s^{-1}. The voltage to length conversion factor of the STM was calibrated using images of Au(111) monatomic steps (0.235 nm height). The set point values applied to ensure the formation of contacts and the bias voltage applied depend on the analyte.

The experiments were performed employing an Agilent STM controlled using Picoscan 4.19 software. The STM tips were freshly prepared for each experiment by etching a Au wire (99.99%) in a HCl:EtOH (50 v/v) solution at 2.4 V. The gold-on-glass substrates employed were purchased from Arrandee, Schroeer, Germany. The substrates were flame

annealed with a butane flame immediately before use. This thermal treatment is known to generate atomically flat terraces on the Au(111) substrate. The substrates were immersed in low concentration solutions (~10^{-5} M, $CHCl_3$) of the target molecule for ~30 seconds. The low concentrations and short immersion times were chosen to promote a low surface coverage of the gold substrate, consequently promoting single molecule events instead of molecular aggregates. After adsorption, the sample was rinsed thoroughly with $CHCl_3$ and blown dry in a stream of N_2 gas.

Appendix B

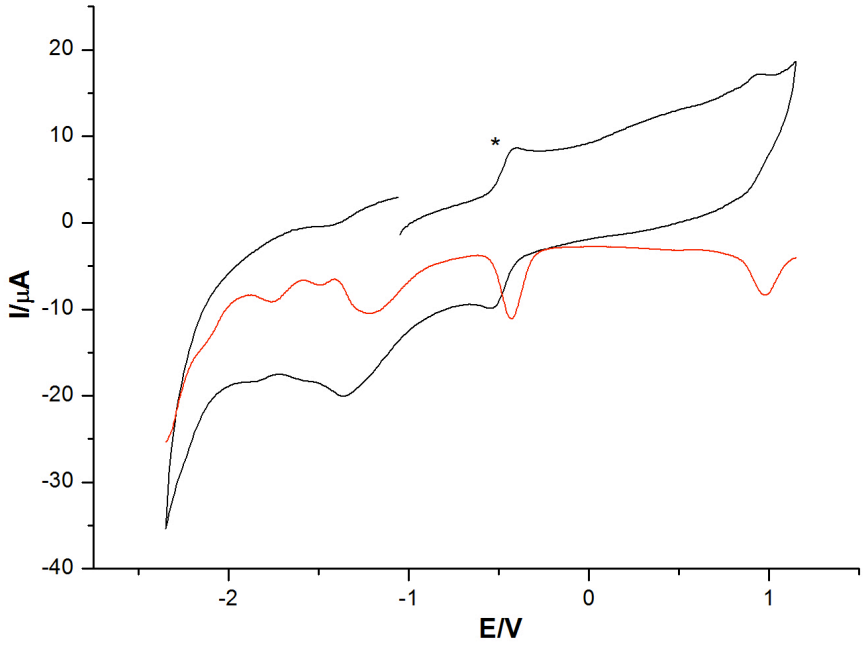

Figure B-1 *Cyclic and differencial pulse voltammograms (ν = 0.04 V/s) of compound **40**. The internal decamethylferrocene is shown with an asterisk. Experimental conditions are given in table 5-1 (see Chapter 5).*

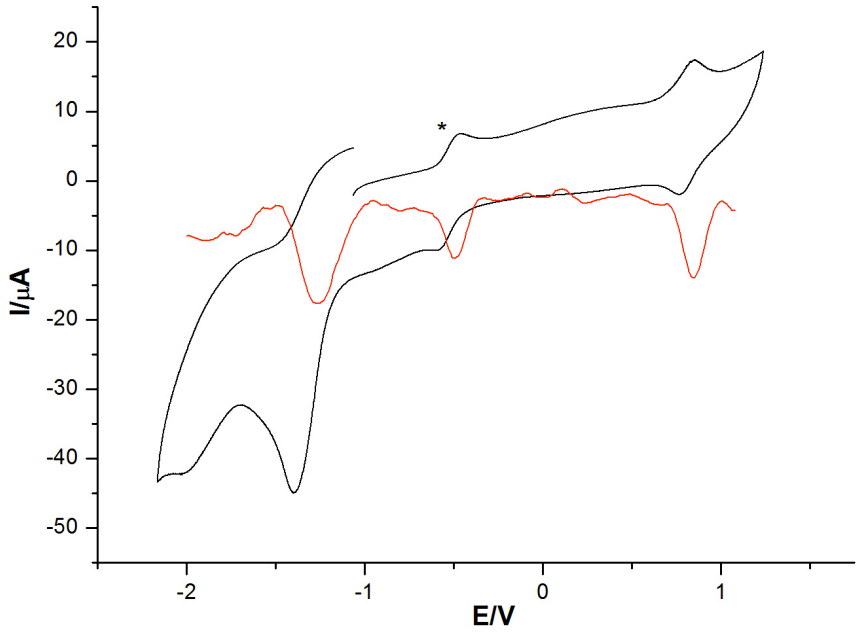

Figure B-2. *Cyclic and differential pulse voltammograms (ν = 0.04 V/s) of compound **42**. The internal decamethylferrocene is shown with an asterisk. Experimental conditions are given in table 5-1 (see Chapter 5)*

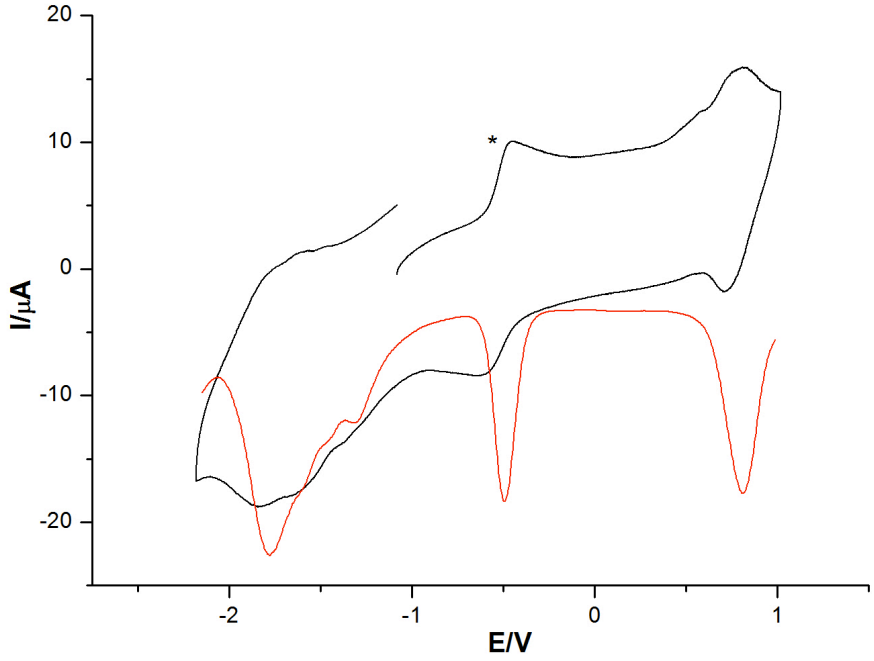

Figure B-3. *Cyclic and differential pulse voltammograms (ν = 0.04 V/s) of compound **47**. The internal decamethylferrocene is shown with an asterisk. Experimental conditions are given in table 5-1 (see Chapter 5)*

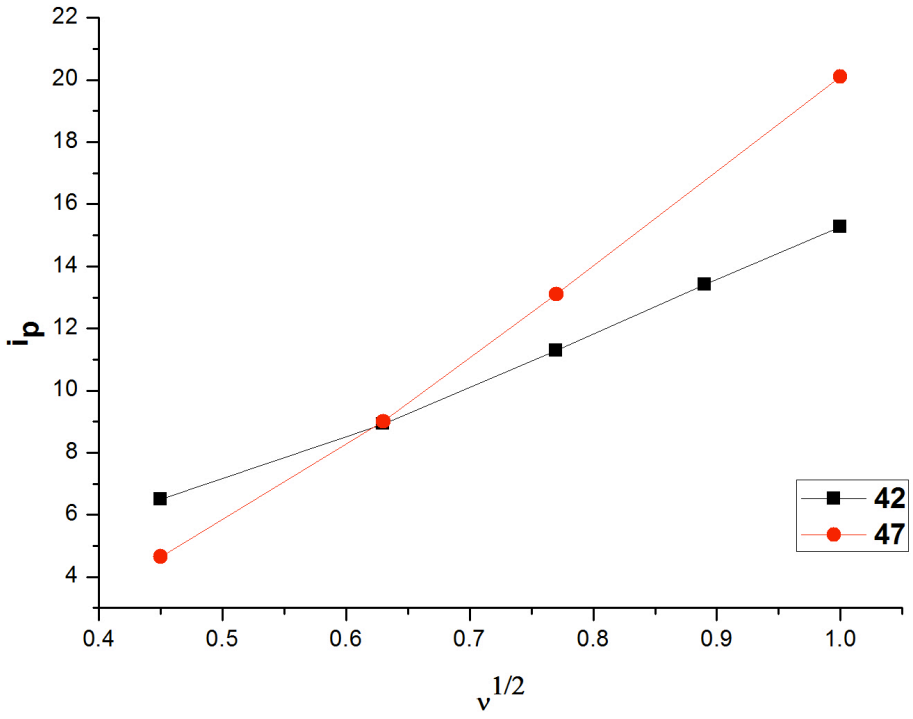

Figure B-4. Graphical representation of the peak current (i_p) versus $\nu^{1/2}$ *for compounds **42** and **47**.*